

SILICONE RESINS AND THEIR COMPOSITES

by

Yuhong Wu

M.S., Materials Science
Dartmouth College, Hanover, 1997

B.S., Materials Science
Shanghai Jiaotong University, Shanghai, 1994

Submitted to the Department of Materials Science and Engineering
in Partial Fulfillment of the Requirements for the Degree of

DOCTOR OF PHILOSOPHY
in Materials Science
at the

Massachusetts Institute of Technology

September 2003

© 2003 Massachusetts Institute of Technology
All rights reserved

The author hereby grants to MIT permission to reproduce and to
distribute publicly paper and electronic copies of this thesis document in whole or in part.

Signature of author

Department of Materials Science and Engineering
June 18, 2003

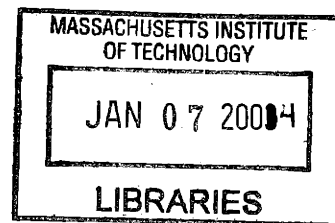
Certified by

Frederick J. McGarry
Professor of Polymer Engineering and Civil Engineering
Thesis Supervisor

Accepted by

Harry L. Tuller
Professor of Ceramics and Electronic Materials
Chair, Departmental Committee on Graduate Students

ARCHIVES



Silicone Resins and Their Composites

by
Yuhong Wu

Submitted to the Department of Materials Science and Engineering
on June 18, 2003 in partial fulfillment of the requirements for the Degree of
Doctor of Philosophy in Materials Science

ABSTRACT

Addition cure (X1-2672) and condensation cure (4-3136) silicone resins have been studied for their mechanical property change with temperature. Properties include maximum flexural stress, flexural modulus and fracture toughness K_{Ic} . Temperature effect on mechanical properties of addition cure resin is substantial and also depends on the crosslinkers used. Generally the maximum stress and flexural modulus decrease with temperature, and the dependence upon crosslinkers in addition cure resin is obvious. Fracture toughness data of addition cure silicone resins have a peaking behavior with the peak appearing $\sim 58-101^{\circ}\text{C}$ (depending on the crosslinker) below their glass transition temperatures. This can be explained by the competing effect between network mobility and rigidity of the silicone polymer. Rate effect on fracture toughness of silylphenylene crosslinked 2672 has also been studied. It is concluded that the temperature effect on such a system is more dominant compared to the rate effect. The condensation resins also experience decrease in modulus and strength but the toughness changes little with temperature. This is due to its tight network structure.

Silylphenylene crosslinked addition cure resin (2672B) and the toughened condensation cure resin (3136T) were used to make silicone fiberglass laminates. They have been successfully processed with a vacuum bagging technique. Silicone resin composites are proved to be thermally stable, moisture resistant and fire resistant. However, they have weak strength and modulus. Their temperature dependence of mechanical properties is also big and results in poor property retention at high temperatures.

2672B was used to produce hybrid composites with an organic resin – vinyl ester. The processes of curing the hybrid composites in both sequential cure and co-cure methods prove to be successful. The hybrid composites are stronger and their property retention at elevated temperatures is improved compared to silicone resin composites. They also have improved moisture resistance, thermal stability and fire resistance over vinyl ester composites. The co-cured V/B 8/4 structure has excellent strength and rigidity and also extraordinary property retention at high temperatures, which can be explained by the chemical reaction at the silicone resin and vinyl ester resin interface. The hybrid composites prove to be successful in having balanced mechanical and environmental properties.

Thesis Supervisor: Frederick J. McGarry
Title: Professor of Polymer Engineering and Civil Engineering

Acknowledgements

The author of this thesis has many acknowledgements to make for everything made possible in this research work.

To my personal Savior - Jesus Christ - for His unfailing love, mercy and grace that I experienced throughout the grad school years at MIT. May all the glory and thanks be to God.

To Professor F. J. McGarry, for his guidance throughout the research work and for his patience and encouragement during the course of this research, especially when things didn't turn out well. For his continuous support and care during these years.

To my thesis committee members Professors Samuel M. Allen and David Roylance, for their willingness to serve on my committee, their valuable inputs regarding the thesis, and their kindness as to accommodating my presentation schedules.

To Dow Corning for all the funding support these years. To researchers there for all their help throughout the project: Rocky Zhu, Dimi Katsoulis, John Keryk, Liz McQuiston, and many unnamed others. Special thanks to Rocky and Dimi for reading and editing this thesis.

To researchers at DMSE labs for their help with using the equipment. To Yinlin Xie - for her help, encouragement and friendship. To Tim McClure, Don Galler, Toby Bashaw, and Libby Shaw for all their help and patience. To John Kane in TELAC for his help with the composite work.

To all the people who have greatly helped with the machining work of the project - which is very important and essential as to making apparatus, testing fixture and all the test samples. Steve Rudolph, Fred Cote and MIT Central Machine Shop. Special thanks to Steve and Fred for all the nice conversations, their patience and great help.

To administrative people at DMSE and MIT: Diane Rose, Marj Joss, Kathy Farrel, Angelita Mireles, Jenna Picceri, Gloria Landahl, Ann Jacoby, Steve Malley and Dwayne Daughtry.

To my group mates and fellow students at MIT who made my life here interesting and memorable. Group mates Zhongtao Li, Darin Spain, Rizwan Gul, Andrew Satorius and Manish Deopura. Special thanks to Andrew for taking responsibilities in the lab so I could concentrate on writing in the past few months. To friends Ching-yin Hong, Pimpa Limthongkul, and Esther Ku: for all the conversations, encouragement and delicious dinners together.

To my husband Kang Liu, for all his love during the good and bad times. For the long hours he spent on the road driving back and forth between Boston and NJ. For his trust in me and his special care and love. To my parents Gengyi Wu and Wenyu Hu, and my mother-in-law Jinmei Yang in China, for their “long distant” love, support and care. To my brother-in-law Jie Liang and sister-in-law Fang Liu, my brother Jianlin Wu and my sister-in-law Saini Yang. I am blessed with their love and care.

To dear brothers and sisters and friends at Boston Chinese Bible Study Group and those at Chinese Bible Church of Greater Boston and Emeth Chapel – for their fellowship, prayer and love in Christ. Special thanks to Richard Perng for correcting the grammar mistakes in this thesis. To my prayer partners: Joyce Chen and Renee Shih. To Pastor Tzu-Kun Chuang and Mrs. Chuang for all their care, sharing and prayer.

For the foolishness of God is wiser than man's wisdom,
And the weakness of God is stronger than man's strength.

- 1 Corinthians 1:25 (NIV)

Table of Contents

Title page	1
Abstract	2
Acknowledgements	3
Table of contents	6
Table of figures	9
Table of tables	15
Introduction and scope of research	17
Part I Mechanical properties of silicone resins	21
CHAPTER 1. Background information	21
1.1 Fracture mechanics of polymers	21
1.2 Temperature and rate effects on mechanical behavior of polymers	24
1.2.1 Temperature and rate effect on yielding	24
1.2.2 Temperature and rate effect on fracture	28
CHAPTER 2. Materials and experiments	35
2.1 Materials	35
2.1.1 Dow Corning X1-2672 addition cure resin	35
2.1.2 Crosslinkers and catalyst for X1-2672	35
2.1.3 Dow Corning 4-3136 condensation cure resin	37
2.1.4 Catalyst for 4-3136	38
2.2 Experimental procedures	38
2.2.1 Curing procedure for X1-2672	38
2.2.2 Curing procedure for 4-3136	39
2.2.3 Dynamic mechanical analysis	39
2.2.4 Thermogravimetric analysis	39
2.2.5 Mechanical testing	39
2.2.6 Scanning electron microscope analysis	42
CHAPTER 3. Temperature and rate effects on silicone resin mechanical properties	45
3.1 Mechanical testing results of Dow Corning X1-2672 addition cure resin	45
3.1.1 B100 system – temperature effect	45
3.1.2 B100 system – rate effect	46
3.1.3 DP system – temperature effect	47
3.1.3.1 D100	47
3.1.3.2 DP73	48
3.1.3.3 DP55	49
3.1.3.4 DP37	50
3.1.3.5 P100	51
3.1.4 DMA (Tan δ vs. T) and fracture toughness (K_{Ic} vs. T)	52
3.1.5 Plastic zone size and activation energy calculation	53
3.1.6 Summary of data analysis	54

3.2	Mechanical testing results of Dow Corning 4-3136 condensation cure resin ..	84
3.3	SEM analysis of fracture surfaces.....	90
3.3.1	Addition cure resin.....	93
3.3.1.1	B100.....	93
3.3.1.2	D100.....	97
3.3.1.3	DP73	101
3.3.1.4	DP55	104
3.3.1.5	DP37	106
3.3.2	Condensation cure resin.....	109
3.3.3	Summary.....	114
3.4	Conclusion and proposed mechanism.....	115
Part II Silicone resin composites and hybrid composites		118
CHAPTER 4. Background and scope of research		118
4.1	Composites.....	118
4.1.1	Polymer composites.....	118
4.1.2	Mechanics of composites.....	122
4.1.2.1	Uni-directional composites.....	122
4.1.2.2	Mechanics of a lamina (single-ply).....	123
4.1.2.3	Mechanics of a laminate composite.....	124
4.1.2.4	Sandwich beam stress analysis	127
4.1.2.5	Interlaminar shear stress	128
4.1.3	Environmental effects	131
4.1.3.1	Moisture absorption	131
4.1.3.2	Elevated temperature	133
4.1.3.3	Fire performance.....	134
4.2	Silicone resin composites.....	137
4.3	Scope of composite research.....	139
CHAPTER 5. Silicone and hybrid composites - experimental		144
5.1	Materials and properties.....	144
5.1.1	Matrix materials	144
5.1.1.1	Addition cure silicone resin 2672B.....	144
5.1.1.2	Condensation cure silicone resin 3136T	145
5.1.1.3	Vinyl ester resin	146
5.1.1.4	Summary of matrix material abbreviations.....	147
5.1.2	Reinforcement materials - woven fiberglass fabric	147
5.2	Laminate fabrication procedures.....	149
5.2.1	Fabrication procedure of 2672B/fiberglass laminates	150
5.2.2	Fabrication procedure of 3136T/fiberglass laminates.....	151
5.2.3	Fabrication procedure of vinyl ester/fiberglass laminates	151
5.2.4	Fabrication procedure of (vinyl ester+2672B)/fiberglass hybrid laminates.....	152
5.2.4.1	Sequential cure.....	152
5.2.4.2	Co-cure.....	153
5.2.5	Summary.....	154
5.3	Characterization methods.....	156

5.3.1	Resin weight content measurement	156
5.3.2	Dynamic mechanical analysis.....	158
5.3.3	Flexural property test.....	158
5.3.4	Short beam shear test.....	159
5.3.5	Thermal aging property test.....	160
5.3.6	Thermogrametric analysis.....	160
5.3.7	Moisture absorption test.....	161
5.3.8	Fire property test.....	162
5.3.9	Scanning electron microscope analysis	162
CHAPTER 6. Silicone and hybrid composites – results and discussion		164
6.1	Mechanical properties.....	164
6.1.1	Flexural properties at room temperature.....	164
6.1.1.1	3136T composite.....	164
6.1.1.2	2672B composite	165
6.1.1.3	Vinyl ester composite	165
6.1.1.4	VB hybrid composite	166
6.1.1.5	Summary.....	167
6.1.2	Flexural properties at elevated temperatures	171
6.1.2.1	3136T composite.....	171
6.1.2.2	2672B composite	172
6.1.2.3	Vinyl ester composite	174
6.1.2.4	VB hybrid composite	175
6.1.2.5	Summary.....	181
6.1.3	SEM analysis of flexural samples.....	183
6.1.4	Interlaminar shear strength	185
6.2	Environmental effects.....	187
6.2.1	Moisture absorption	187
6.2.2	Thermal aging properties	193
6.2.2.1	Weight loss.....	193
6.2.2.2	Flexural property retention	197
6.2.2.3	Thermogravimetric analysis.....	202
6.2.3	Fire performance.....	204
6.3	DMA and proposed explanation.....	206
6.4	Summary.....	213
CHAPTER 7. Conclusions.....		217
CHAPTER 8. Future work.....		219
Appendix A. Load-displacement curves and results of fracture toughness tests of silicone resins		221

Table of Figures

Chapter 2

Figure 2-1 Sketch of low temperature testing setup on Instron 4500 with an Instron environmental chamber.....	42
Figure 2-2 Sketch of SEM analysis of broken notched samples.	43

Chapter 3

Figure 3-1 Flexural modulus vs. temperature for silylphenylene (B) crosslinked X1-2672 (B100).	61
Figure 3-2 Maximum flexural stress change with temperature for silylphenylene (B) crosslinked X1-2672 (B100).	61
Figure 3-3 Maximum flexural strain change with temperature for silylphenylene (B) crosslinked X1-2672 (B100).	62
Figure 3-4 Fracture toughness change with temperature for silylphenylene (B) crosslinked X1-2672 (B100).	62
Figure 3-5 Plots of fracture toughness versus Log (rate) at different temperatures for the silylphenylene crosslinked X1-2672 (B100).	63
Figure 3-6 Plots of fracture toughness versus temperature at different rates for the silylphenylene crosslinked X1-2672 (B100).	63
Figure 3-7 Flexural modulus change with temperature for hexamethyltrisiloxane (D) crosslinked X1-2672 (D100).	64
Figure 3-8 Maximum flexural stress change with temperature for hexamethyltrisiloxane (D) crosslinked X1-2672 (D100).	64
Figure 3-9 Maximum flexural strain change with temperature for hexamethyltrisiloxane (D) crosslinked X1-2672 (D100).	65
Figure 3-10 Fracture toughness change with temperature for hexamethyltrisiloxane (D) crosslinked X1-2672 (D100).	65
Figure 3-11 Flexural modulus change with temperature for hexamethyltrisiloxane (D)/diphenylsilane (P) crosslinked X1-2672 (DP73).	66
Figure 3-12 Maximum flexural stress change with temperature for hexamethyltrisiloxane (D) / diphenylsilane (P) crosslinked X1-2672 (DP73).	66
Figure 3-13 Maximum flexural strain change with temperature for hexamethyltrisiloxane (D) / diphenylsilane (P) crosslinked X1-2672 (DP73).	67
Figure 3-14 Fracture toughness change with temperature for hexamethyltrisiloxane (D) / diphenylsilane (P) crosslinked X1-2672 (DP73).	67
Figure 3-15 Flexural modulus change with temperature for hexamethyltrisiloxane (D) / diphenylsilane (P) crosslinked X1-2672 (DP55).	68
Figure 3-16 Maximum flexural stress change with temperature for hexamethyltrisiloxane (D) /diphenylsilane (P) crosslinked X1-2672 (DP55).	68
Figure 3-17 Maximum flexural strain change with temperature for hexamethyltrisiloxane (D) / diphenylsilane (P) crosslinked X1-2672 (DP55).	69
Figure 3-18 Fracture toughness change with temperature for hexamethyltrisiloxane (D) / diphenylsilane (P) crosslinked X1-2672 (DP55).	69
Figure 3-19 Flexural modulus change with temperature for hexamethyltrisiloxane (D)/diphenylsilane (P) crosslinked X1-2672 (DP37).	70

Figure 3-20 Maximum flexural stress change with temperature for hexamethyltrisiloxane (D)/diphenylsilane (P) crosslinked X1-2672 (DP37).	70
Figure 3-21 Maximum flexural strain change with temperature for hexamethyltrisiloxane (D)/diphenylsilane (P) crosslinked X1-2672 (DP37).	71
Figure 3-22 Fracture toughness change with temperature for hexamethyltrisiloxane (D) / diphenylsilane (P) crosslinked X1-2672 (DP37).	71
Figure 3-23 Flexural modulus change with temperature for diphenylsilane (P) crosslinked X1-2672 (P100).	72
Figure 3-24 Maximum flexural stress change with temperature for diphenylsilane (P) crosslinked X1-2672 (P100).	72
Figure 3-25 Maximum flexural strain change with temperature for diphenylsilane (P) crosslinked X1-2672 (P100).	73
Figure 3-26 Fracture toughness change with temperature for diphenylsilane (P) crosslinked X1-2672 (P100).	73
Figure 3-27 Summary of flexural modulus vs. temperature for DP and B100 systems. ..	74
Figure 3-28 Summary of maximum flexural stress vs. temperature for DP and B100. ...	74
Figure 3-29 Summary of maximum flexural strain vs. temperature for DP and B100 systems.	75
Figure 3-30 Summary of fracture toughness vs. temperature for DP and B100 systems. 75	75
Figure 3-31 DMA Tan δ & fracture toughness of B100 vs. temperature.	76
Figure 3-32 DMA Tan δ & fracture toughness of D100 vs. temperature.	76
Figure 3-33 DMA Tan δ & fracture toughness of DP73 vs. temperature.	77
Figure 3-34 DMA Tan δ & fracture toughness of DP55 vs. temperature.	77
Figure 3-35 DMA Tan δ & fracture toughness of DP37 vs. temperature.	78
Figure 3-36 DMA Tan δ & fracture toughness of P100 vs. temperature.	78
Figure 3-37 Log (Rp) vs. T – B100, D100, DP37, DP55, DP73 and P100.	79
Figure 3-38 Log (Rp) vs. 1/T – B100, D100, DP37, DP55, DP73 and P100.	79
Figure 3-39 B100 – load displacement curves of fracture toughness testing at 40°C.	80
Figure 3-40 B100 – load displacement curves of fracture toughness testing at 60°C.	80
Figure 3-41 D100– load displacement curves of fracture toughness testing at RT.	81
Figure 3-42 D100– load displacement curves of fracture toughness testing at 40°C.	81
Figure 3-43 DP73– load displacement curves of fracture toughness testing at 40°C.	82
Figure 3-44 DP73– load displacement curves of fracture toughness testing at 60°C.	82
Figure 3-45 DP55– load displacement curves of fracture toughness testing at 60°C.	83
Figure 3-46 DP37– load displacement curves of fracture toughness testing at 60°C.	83
Figure 3-47 Flexural modulus change with temperature for both toughened (with 10% KPE) and untoughened 4-3136 resins.	87
Figure 3-48 Maximum flexural stress change with temperature for both toughened (with 10% KPE) and untoughened 4-3136 resins.	87
Figure 3-49 Maximum flexural strain change with temperature for both toughened (with 10% KPE) and untoughened 4-3136 resins.	88
Figure 3-50 Fracture toughness change with temperature for both toughened (with 10% KPE) and untoughened 4-3136 resins.	88
Figure 3-51 Tan Delta plot from DMA of 3136U resin (data provided by Rocky Zhu). .	89
Figure 3-52 Storage modulus plot from DMA of 3136U (data provided by Rocky Zhu).89	89

Figure 3-53 SEM micrograph of a B100 SENB sample tested at room temperature (average K_{Ic} value is $1.03 \text{ MPa m}^{1/2}$). (150x) (crack propagating direction \rightarrow).....	94
Figure 3-54 SEM micrograph of a B100 SENB sample tested at 40°C (average K_{Ic} value is $0.96 \text{ MPa m}^{1/2}$). (150x) (crack propagating direction \rightarrow).....	94
Figure 3-55 SEM micrograph of a B100 SENB sample tested at 60°C (average K_{Ic} value is $0.71 \text{ MPa m}^{1/2}$). (150x) (crack propagating direction \rightarrow).....	95
Figure 3-56 SEM micrograph of a B100 SENB sample tested at 0°C (average K_{Ic} value is $0.72 \text{ MPa m}^{1/2}$). (150x) (crack propagating direction \rightarrow).....	95
Figure 3-57 SEM micrograph of a B100 SENB sample tested at -20°C (average K_{Ic} value is $0.46 \text{ MPa m}^{1/2}$). (150x) (crack propagating direction \rightarrow).....	96
Figure 3-58 SEM micrograph of a B100 SENB sample tested at -40°C (average K_{Ic} value is $0.37 \text{ MPa m}^{1/2}$). (150x) (crack propagating direction \rightarrow).....	96
Figure 3-59 Summary of fracture surfaces of D100 K_{Ic} samples tested at different temperatures. (crack propagating direction \rightarrow).....	100
Figure 3-60 Summary of DP73 fracture surfaces of K_{Ic} tests at different temperatures. (crack propagating direction \rightarrow).....	103
Figure 3-61 Fracture surfaces of a DP55 K_{Ic} sample tested at 60°C . (crack propagating direction \rightarrow).....	105
Figure 3-62 Fracture surfaces of DP37 K_{Ic} samples tested at different temperatures. (crack propagating direction \rightarrow).....	108
Figure 3-63 Fracture surfaces of 3136T K_{Ic} samples: (a) 20°C & (b) 40°C with same toughness $0.39 \text{ MPa m}^{1/2}$. (crack propagating direction \rightarrow).....	110
Figure 3-64 Fracture surfaces of 3136T K_{Ic} samples: (a) 20°C ($0.39 \text{ MPa m}^{1/2}$) & (b) 60°C ($0.34 \text{ MPa m}^{1/2}$). (crack propagating direction \rightarrow).....	111
Figure 3-65 Fractograph of the rough band in 3136U K_{Ic} samples tested at 20°C . (crack propagating direction \rightarrow).....	112
Figure 3-66 Fractograph of 3136U K_{Ic} sample tested at 60°C . (crack propagating direction \rightarrow).....	112
Figure 3-67 Fractograph of 3136U K_{Ic} sample tested at 80°C . (crack propagating direction \rightarrow).....	113
 Chapter 4	
Figure 4-1 Eight harness satin weave pattern of woven fiberglass textile.....	120
Figure 4-2 Illustration of a uni-directional fiber composite under load.....	122
Figure 4-3 Construction of a laminate from laminas [5].	125
Figure 4-4 Construction of a sandwich beam with skin and core materials.	127
Figure 4-5 Shear stress in a short beam shear test specimen. (a) near the support points; (b) near the midspan; (c) ideal parabolic shear stress [5].	129
 Chapter 5	
Figure 5-1 Viscosity profile of 2672B solventless resin with heating rate of $3.1^\circ\text{F}/\text{min}$	145
Figure 5-2 Typical set-up for curing composites in the hot press.....	155
Figure 5-3 Illustration of hybrid laminates of two resin matrices: vinyl ester and silicone 2627B.	155

Chapter 6

Figure 6-1 Summary of room temperature maximum flexural stress of T, B, V and VB composites.....	170
Figure 6-2 Summary of room temperature flexural modulus of T, B, V and VB composites.....	170
Figure 6-3 Flexural property retention versus temperature for 3136T composite.....	171
Figure 6-4 Flexural property retention versus temperature for 2672B composite.....	173
Figure 6-5 Flexural property retention versus temperature for vinyl ester composite. ..	174
Figure 6-6 Flexural property retention versus temperature for sequential cured V/B 6/6 hybrid composite.....	177
Figure 6-7 Flexural property retention versus temperature for co-cured V/B 6/6 hybrid composite.	177
Figure 6-8 Flexural property retention versus temperature for sequential cured V/B 8/4 hybrid composite.....	178
Figure 6-9 Flexural property retention versus temperature for co-cured V/B 8/4 hybrid composite.	178
Figure 6-10 Summary flexural modulus versus temperature for VB hybrid composites.	180
Figure 6-11 Summary of maximum flexural stress versus temperature for VB hybrid composites.....	180
Figure 6-12 Summary of flexural modulus retention vs. temperature for V, B and V/B 8/4 co-cured composites.....	182
Figure 6-13 Summary of maximum flexural stress retention vs. temperature for V, B and V/B 8/4 co-cured composites.....	182
Figure 6-14 SEM micrograph of vinyl ester composite after flexural test.	183
Figure 6-15 SEM micrograph of 2672B composite after flexural test.	184
Figure 6-16 SEM micrograph of V/B 8/4 co-cured hybrid composite – near the tensile side of the specimen.....	184
Figure 6-17 SEM micrograph of V/B 8/4 co-cured hybrid composite after flexural test – near the center of the specimen.....	185
Figure 6-18 Moisture content vs. time ^{1/2} in V, B, and VB hybrid laminates (with non-sealed edges) at 49.7% R.H.	190
Figure 6-19 Moisture content vs. time ^{1/2} in V, B, and VB hybrid laminates (with non-sealed edges) at 100% R.H.	190
Figure 6-20 Moisture content vs. time ^{1/2} in V, B, and VB hybrid laminates of sealed edges at 49.7% R.H.....	191
Figure 6-21 Moisture content vs. time ^{1/2} in V, B, and VB hybrid laminates of sealed edges at 100% R.H.....	191
Figure 6-22 Moisture content vs. time ^{1/2} in vinyl ester, 2672B and 3136T resins at both 100% and 49.7% R.H.....	192
Figure 6-23 Moisture absorption induced strain of 2672B resin. (Data from Dow Corning Corp.)	192
Figure 6-24 Weight loss vs. aging temperature for V, B, and V/B 8/4 co-cured composites after aging for 10 hours.....	194

Figure 6-25 Weight loss vs. aging temperature for V, B, and V/B 8/4 co-cured composites after aging for 100 hours.....	195
Figure 6-26 Weight loss vs. aging temperature for V, B, and V/B 8/4 co-cured composites after aging for 1000 hours.....	195
Figure 6-27 Flexural modulus change vs. aging temperature for V, B, and VB composites after aging for 10 hours.....	199
Figure 6-28 Flexural modulus change vs. aging temperature for V, B, and VB composites after aging for 100 hours.....	199
Figure 6-29 Flexural modulus change vs. aging temperature for V, B, and VB composites after aging for 1000 hours.....	200
Figure 6-30 Maximum flexural stress change vs. aging temperature for V, B and VB composites after aging for 10 hours.....	200
Figure 6-31 Maximum flexural stress change vs. aging temperature for V, B, and VB composites after aging for 100 hours.....	201
Figure 6-32 Maximum flexural stress change vs. aging temperature for V, B, and VB composites after aging for 1000 hours.....	201
Figure 6-33 TGA of vinyl ester, 2627B and 3136T resins.....	203
Figure 6-34 TGA of vinyl ester composite, 2672B composite and V/B hybrid composite.....	203
Figure 6-35 DMA of 2672B composite.....	209
Figure 6-36 DMA of vinyl ester composite.....	209
Figure 6-37 DMA of co-cured V/B 8/4 composite.....	210
Figure 6-38 DMA graph overlay of V, B and VB composites.....	210
Figure 6-39 Illustration of reactive groups at the interface of vinyl ester resin and addition cure silicone resin inside the hybrid composites.....	211
Figure 6-40 Storage modulus of vinyl ester resins VS and VL and hybrid composites VB1 and VB2.....	212
Figure 6-41 Tan δ of vinyl ester resins VS and VL and hybrid composites VB1 and VB2.....	212

Appendix

Figure A - 1 Fracture toughness test results of B100 at -40°C.....	222
Figure A - 2 Fracture toughness test results of B100 at -20°C.....	222
Figure A - 3 Fracture toughness test results of B100 at 0°C.....	223
Figure A - 4 Fracture toughness test results of B100 at 20°C.....	223
Figure A - 5 Fracture toughness test results of B100 at 40°C.....	224
Figure A - 6 Fracture toughness test results of B100 at 60°C.....	224
Figure A - 7 Fracture toughness test results of D100 at -60°C.....	225
Figure A - 8 Fracture toughness test results of D100 at -40°C.....	225
Figure A - 9 Fracture toughness test results of D100 at -20°C.....	226
Figure A - 10 Fracture toughness test results of D100 at 0°C.....	226
Figure A - 11 Fracture toughness test results of D100 at 20°C.....	227
Figure A - 12 Fracture toughness test results of D100 at 40°C.....	227
Figure A - 13 Fracture toughness test results of DP73 at -40°C.....	228
Figure A - 14 Fracture toughness test results of DP73 at -20°C.....	228
Figure A - 15 Fracture toughness test results of DP73 at 0°C.....	229

Figure A - 16 Fracture toughness test results of DP73 at 20°C.....	229
Figure A - 17 Fracture toughness test results of DP73 at 40°C.....	230
Figure A - 18 Fracture toughness test results of DP73 at 60°C.....	231
Figure A - 19 Fracture toughness test results of DP55 at -40°C.....	232
Figure A - 20 Fracture toughness test results of DP55 at -20°C.....	233
Figure A - 21 Fracture toughness test results of DP55 at 0°C.....	233
Figure A - 22 Fracture toughness test results of DP55 at 20°C.....	234
Figure A - 23 Fracture toughness test results of DP55 at 40°C.....	235
Figure A - 24 Fracture toughness test results of DP55 at 60°C.....	236
Figure A - 25 Fracture toughness test results of DP37 at -40°C.....	238
Figure A - 26 Fracture toughness test results of DP37 at -20°C.....	238
Figure A - 27 Fracture toughness test results of DP37 at 0°C.....	239
Figure A - 28 Fracture toughness test results of DP37 at 20°C.....	239
Figure A - 29 Fracture toughness test results of DP37 at 40°C.....	240
Figure A - 30 Fracture toughness test results of DP37 at 60°C.....	240
Figure A - 31 Fracture toughness test results of P100 at -40°C.....	241
Figure A - 32 Fracture toughness test results of P100 at -20°C.....	241
Figure A - 33 Fracture toughness test results of P100 at 0°C.....	242
Figure A - 34 Fracture toughness test results of P100 at 20°C.....	242
Figure A - 35 Fracture toughness test results of P100 at 40°C.....	243
Figure A - 36 Fracture toughness test results of P100 at 60°C.....	243
Figure A - 37 Fracture toughness test results of toughened 3136 (3136T) at -40°C.....	244
Figure A - 38 Fracture toughness test results of toughened 3136 (3136T) at -20°C.....	244
Figure A - 39 Fracture toughness test results of toughened 3136 (3136T) at 0°C.....	245
Figure A - 40 Fracture toughness test results of toughened 3136 (3136T) at 20°C.....	245
Figure A - 41 Fracture toughness test results of toughened 3136 (3136T) at 40°C.....	246
Figure A - 42 Fracture toughness test results of toughened 3136 (3136T) at 60°C.....	246
Figure A - 43 Fracture toughness test results of un-toughened 3136 (3136U) at -40°C.....	247
Figure A - 44 Fracture toughness test results of un-toughened 3136 (3136U) at -20°C.....	247
Figure A - 45 Fracture toughness test results of un-toughened 3136 (3136U) at 0°C.....	248
Figure A - 46 Fracture toughness test results of un-toughened 3136 (3136U) at 20°C.....	248
Figure A - 47 Fracture toughness test results of un-toughened 3136 (3136U) at 40°C.....	249
Figure A - 48 Fracture toughness test results of un-toughened 3136 (3136U) at 60°C.....	249
Figure A - 49 Fracture toughness test results of un-toughened 3136 (3136U) at 80°C.....	250

Table of Tables

Chapter 3

Table 3-1 Mechanical properties of silylphenylene (B) crosslinked X1-2672 resin (B100) as a result of varying testing temperature.	57
Table 3-2 A summary of temperature and rate effects on fracture toughness of the silylphenylene crosslinked X1-2672 (B100).	57
Table 3-3 Mechanical properties of hexamethyltrisiloxane (D) crosslinked X1-2672 (D100) as a result of varying testing temperature.	58
Table 3-4 Mechanical properties of hexamethyltrisiloxane (D) /diphenylsilane (P) crosslinked X1-2672 (DP73) as a result of varying testing temperature.	58
Table 3-5 Mechanical properties of hexamethyltrisiloxane (D) /diphenylsilane (P) crosslinked x1-2672 (DP55) as a result of varying testing temperature.	59
Table 3-6 Mechanical properties of hexamethyltrisiloxane (D) /diphenylsilane (P) crosslinked X1-2672 (DP37) as a result of varying testing temperature.	59
Table 3-7 Mechanical properties of diphenylsilane (P) crosslinked X1-2672 (P100) as a result of varying testing temperature.	60
Table 3-8. Toughness curve peak and DMA Tan δ peak summary.	60
Table 3-9 Activation energy calculation – B100, D100, DP37, DP55, DP73 and P100..	60
Table 3-10 Mechanical properties of toughened 4-3136 at different temperatures.	86
Table 3-11 Mechanical properties of untoughened 4-3136 at different temperatures.	86
Table 3-12 Summary of load-displacement curves in K_{Ic} tests for different crosslinked 2672 resins. (K_{Ic} is in $MPa\ m^{1/2}$ and data points with * do not meet the test validity criterion of $P_{max}/P_q \leq 1.1$.)	91
Table 3-13 Summary of load-displacement curves in K_{Ic} tests for 3136 resins. (K_{Ic} is in $MPa\ m^{1/2}$.)	92

Chapter 5

Table 5-1 Typical properties of addition cure silicone resin 2672B.	144
Table 5-2 Typical properties of condensation cure resin 3136T.	146
Table 5-3 Typical properties of Derakane Momentum 470-300 vinyl ester resin.	146
Table 5-4 Specifications of fiberglass fabric used in laminate fabrication.	148
Table 5-5 A comparison between resin content obtained by ignition loss method and by weight.	157
Table 5-6 Calculated volume content of composites with different matrix materials.	157

Chapter 6

Table 6-1 Mechanical properties of 3136T laminate at room temperature.	165
Table 6-2 Mechanical properties of 2672B laminates at room temperature.	165
Table 6-3 Mechanical properties of vinyl ester laminate at room temperature.	166
Table 6-4 Mechanical properties of VB hybrid laminates at room temperature.	167
Table 6-5 Summary of silicone resin properties, both used as the matrix materials for composites.	169
Table 6-6 Flexural properties at different temperatures for 3136T composite.	172
Table 6-7 Flexural properties of 2672B composite at different temperatures.	173
Table 6-8 Flexural properties of vinyl ester composite at different temperatures.	175

Table 6-9 Properties of V/B 6/6 composites, sequential cured and co-cured, at different temperatures..... 179

Table 6-10 Properties of V/B 8/4 composites, sequential cured and co-cured, at different temperatures..... 179

Table 6-11 Short beam strength of vinyl ester, silicone and hybrid composites. 186

Table 6-12 Summary of moisture absorption test results of all composites. 189

Table 6-13 Summary of weight loss of composites subject to thermal aging. VB stands for V/B 8/4 co-cured hybrid composite. 196

Table 6-14 OSU test results of vinyl ester, silicone and hybrid resin composites..... 204

Table 6-15 Cone calorimetry test results of vinyl ester and silicone resin composites. . 205

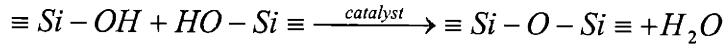
Introduction and scope of research

Silicone polymers are a group of polymers possessing the characteristic siloxane (Si-O) backbone. As rigid and brittle materials possessing the T ($\text{SiO}_{3/2}$) or Q ($\text{SiO}_{4/2}$) structures, silicone resins find applications in electronic, automotive and aerospace industries due to their moisture resistance, chemical resistance and thermal and oxidative stability. These properties mainly come from the unique characteristics of the Si-O bond. Si-O-Si bond has high bond energy, long bond length, large bond angle, and is inert to oxygen. These characteristics lead to the flexibility of silicone chains and weak interchain reactions. Thus, silicone resins have low T_g , weak mechanical properties, thermal stability, and oxidation resistance. Organic groups like methyl group on the siloxane backbone also help to shield the Si-O bond and thus lead to its moisture resistance. The brittleness and comparatively low strength among other thermoset resins are mostly attributed to the high crosslink density, weak interchain reaction and network structure of silicone resins. These limit some of the applications of silicone resins in industries.

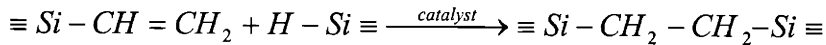
In recent years, successful cooperative research work have involved Dow Corning Corporation and MIT researchers to improve silicone resin mechanical properties for more applications and to achieve more understanding of the resin properties and structures. These have set the ground work for this thesis, where mechanical property evaluation of silicone resins at high temperature and their applications as matrix materials for composites are carried out.

Dow Corning has been playing a big role in the silicone resin industry and has developed many new silicone materials for different applications. Two major Dow Corning silicone resins studied at MIT are: condensation cure resin 4-3136 and addition cure resin X1-2672. Condensation cure resin 4-3136 has the formula of $(\text{PhSiO}_{3/2})_{0.40}(\text{MeSiO}_{3/2})_{0.45}(\text{Ph}_2\text{SiO})_{0.10}(\text{PhMeSiO})_{0.05}$. Addition cure resin X1-2672 has the empirical formula of $(\text{PhSiO}_{3/2})_{0.75}(\text{ViMe}_2\text{SiO}_{1/2})_{0.25}$. The experimental work in these materials proved to be successful and brought out many publications and patents.

Curing of the condensation resin is by reaction between silanol ends:



Curing reaction of the addition cure resin is by reaction of Si-H present in the crosslinker with the vinyl group in the resin:



Zhu et al. have studied the condensation cure resin and tried to incorporate PDMS rubber into the network to increase its toughness [1-7]. This is done by two methods: Phase I toughening of short PDMS chain to increase network mobility, Phase II toughening of forming rubber particles as sources of more plastic deformation within matrix. Both methods successfully induce network flow and deformation and thus lead to higher toughness. With Phase I toughening, the fracture toughness is increased from 0.25 MPa m^{1/2} to ~0.45 MPa m^{1/2}. The best Phase I toughening effect is obtained with 10% KPE (functional PDMS of a degree of polymerization of 57 with triethoxy silyl end group), which gives the best combination of fracture toughness and strength of the resin. On the basis of Phase I toughening and combined with Phase II toughening, the fracture toughness is increased to 0.55 MPa m^{1/2}.

Many have studied the Dow Corning addition cure resin X1-2672 to toughen it as well [8-18]. Spence has studied the effect of incorporating PDMS rubber into the X1-2672 network crosslinked with trifunctional phenyltris(dimethylsiloxy)silane and tetrafunctional tetrakis(dimethylsiloxy)silane [17]. She has found that silane terminated rubber has more effect on the mechanical properties of X1-2672 than the vinyl terminated one. With 12% silane terminated rubber (DP_n=4) addition and curing with trifunctional crosslinker phenyltris(dimethylsiloxy)silane, fracture toughness of the resin is increased to ~0.55 MPa m^{1/2} from 0.3 MPa m^{1/2}. Li has also worked with toughening the addition cure silicone resin and tried to incorporate various crosslinkers and a combination of those into the resin network [12, 13]. New crosslinkers he used include hexamethyltrisiloxane and diphenylsilane. A combination of 70% hexamethyltrisiloxane and 30% diphenylsilane results in a toughness of 0.72 MPa m^{1/2}. The crosslinker with the best toughening effect in X1-2672 has been discovered at Dow Corning [18].

1,4-bis(dimethylsilyl)benzene has been synthesized and used as a crosslinker in the addition cure resin. This results in a toughness of $1.08 \text{ MPa m}^{1/2}$. The guideline in this work is to get a combined flexible (with low crosslinking density) and rigid structure into the network. The former is achieved by using the di-functional crosslinker and the latter is realized by a rigid backbone structure of phenyl ring presence. On the basis of the silylphenylene modified X1-2672, Zhu et al. has been able to toughen the addition cure resin further to the range of $1.8 \text{ MPa m}^{1/2}$ by incorporating colloidal silica particles into the resin matrix [8]. The resultant toughness is comparable to the commercial epoxy resins and thus the research work achieves a big step in making it possible to commercialize the silicone resin.

The condensation resin has volatile by-products and also needs relatively higher curing temperatures. In order to produce sound and bubble/void free bulk samples, the curing cycle has to be very long and thus is relatively difficult to implement [1]. On the other hand, the addition cure resin has no volatile by-product, has comparatively good stability and also is relatively easy to cure. The addition cure resin also offers a solventless potential by replacing solvent with a crosslinker. All these lead to better application possibilities for the addition cure resin.

Because of its low dielectric constant, silicones as common dielectrics in the microelectronic or electronic industry also draw attention of researchers from that field. Spain has studied the mechanical properties of 4-3136 resin and methyl T silicone resins as thin film materials by modified edge lift off test [19, 20]. He has found that the thin film toughness measured by the edge lift-off test method is comparable to that of the bulk material. This offers a fast and easy way of measuring fracture toughness of silicone resins without casting the bulk material. A family of polyorganosiloxane resins has also been developed by being blended with other silicone or organic resins. With appropriate processing techniques and cure chemistry, higher nonvolatile content silicone resins with desired film performance have been achieved [21].

Although much more understandings of the silicone resin properties have been achieved and many applications of silicone resins are explored, work remains to

characterize the resins and also to use them in different fields. Because of its thermal stability, one area of research interests in silicone resins is to characterize how the mechanical behavior of these toughened and un-toughened resins changes at temperatures beyond room temperature. This information will be useful to find out if there are any other applications at high temperatures that we can explore. Regarding application, one field is the composite area where these toughened resins can be used as a matrix material to take advantage of their thermal, oxidation, and moisture resistance.

The scope of the thesis is to understand the resin mechanical behavior at different temperatures and to explore their applications as matrix materials in composite applications. The first part of the thesis will focus on the mechanical behavior and mechanisms of silicone resins at temperatures other than room temperature. Due to the thermal stability and oxidation resistance of silicones, there have been research interests in identifying mechanical behavior changes at elevated temperatures and in understanding the mechanisms associated with the changes. Then in the second part, silicone resins are used as matrix materials for fiberglass composites. The first step involves processing silicone resin composites and also characterizing their properties including mechanical, thermal, and environmental properties. A further step is then taken to process silicone resin / organic resin (vinyl ester) hybrid composites, which uses two resins as matrix materials with silicone resin as the skin and the organic resin as the core. This is to achieve balanced mechanical properties and environmental properties by taking advantage of the environmental properties of silicone resins and the mechanical properties of vinyl ester resin.

Part I Mechanical properties of silicone resins

CHAPTER 1. Background information

1.1 Fracture mechanics of polymers

Fracture in polymers involves the breakage of either primary covalent bonds or secondary bonds like van der Waals bonds. Which type of breakage occurs is generally considered to be dependent upon the types of polymers and testing conditions. For thermoset resins, it is believed that primary covalent bond breakage is usually attributed to fracture [22]. A material often fractures at a stress much lower than its theoretical bond strength, because of the presence of defects and cracks inside. This makes it useful to study the behavior of such a material, which leads to fracture mechanics studies.

Fracture mechanics is a way of analyzing stress-strain field in front of a crack tip and it derives the criteria of crack stability by an energy balance consideration. Intensive treatments of the subject can be found in references [22, 23]. Griffith's treatment of isotropic brittle materials containing an elliptical crack of length $2a$ has been used widely to quantify this criterion [24]. The critical stress level for a crack to propagate in such a material is given by:

$$\sigma_f = \left(\frac{2E\gamma}{\pi a} \right)^{1/2} \quad \text{Equation 1-1}$$

where γ is the surface energy of the material and E is the modulus.

Such an equation also applies to brittle solids like glassy polymers, except for modifying the surface free energy term γ with G_c , where G_c is the fracture energy, i.e. the total amount of energy dissipated during crack growth, and is defined as the energy required to form a unit area of the crack. The reason is because glassy polymer fracture often involves a large amount of plastic deformation in front of the crack tip and can not be treated the same as a real brittle solid.

$$\sigma_f = \left(\frac{EGc}{\pi a} \right)^{1/2} \quad \text{Equation 1-2}$$

Stress intensity factor concept is based on the crack tip stress state analysis and is used to characterize the crack tip stress field. At the critical applied stress level σ_f , crack propagation occurs and this critical value of the stress intensity factor is called the fracture toughness and expressed as:

$$Kc = \sigma_f \times f\left(\frac{a}{b}\right) \times a^{1/2} \quad \text{Equation 1-3}$$

where a is the initial crack length, b is the specimen width, and $f(a/b)$ is a geometrical correction factor. This is the basis of the experimental measurements of fracture toughness in a material. Experimentally, fracture toughness can be measured on a single edge notched bending specimen under plane strain stress state [25].

Although it is clear that for thermoset resins plastic deformation must take place in front of crack tip during crack growth and propagation, it is very difficult to directly observe and to prove the presence of the crack tip plastic zone by experiment. In epoxy resins, work has been done to use the crack slow growth region, the area after the crack arrest line, to define the plastic zone [26]. But still direct observation is difficult. Calculation of the plastic zone size can be quantified by knowing the fracture toughness and yield stress of the material.

In considering localized plastic deformation in front of the crack tip, the size of the plastic zone radius is generally given in the form of yield strength (σ_y) and fracture toughness of the material (K_I) [22]:

$$r_y = \frac{1}{6\pi} \left(\frac{K_I}{\sigma_y} \right)^2 \quad \text{Equation 1-4}$$

For polymer materials, modification was made according to Dugdale line plastic zone model because the plastic zone shape ahead of a crack tip is considered a line zone. The final presentation of the length of the plastic zone ahead of a crack tip is:

$$R = \frac{\pi}{8} \left(\frac{K_I}{\sigma_y} \right)^2 \quad \text{Equation 1-5}$$

Fracture surfaces of the thermoset polymers are relatively featureless. Their characteristics depend highly upon the structure of the polymer and also testing conditions. There are three crack propagation modes observed in mostly studied epoxies. A stable brittle propagation with relatively featureless fracture surface often occurs in relatively brittle material and at low temperatures. An unstable brittle propagation unique to the epoxy resins features crack arrest lines and smooth featureless fracture area. The crack arrest lines result from the stopping of crack propagation, and the featureless area is associated with the brittle behavior of stable brittle crack propagation. This is the so-called stick/slip mode of crack propagation [27-29]. The reason is the crack initiation K_c value is higher than the stable growth and arrest values. One explanation is the effect of crack tip blunting and thus the resultant higher initiation K_c value. The third mode is the stable ductile propagation which tends to be observed at high temperatures [30, 31]. Features of this type of fracture surface often include a ridged structure running parallel to the crack propagating direction.

Experimental observations of crack propagation in thermoset polymers have found that an unstable stick/slip manner is usually characteristic, where the load displacement curves demonstrate a sawtooth shape with crack growth undergoes a propagation-arrest-propagation-arrest pattern [32, 33]. This pattern is explained by crack-tip blunting which causes the discontinuous propagation. Broutman and McGarry have employed a cleavage test to measure the fracture surface work of glassy polymers [33]. They find that the fracture surface work of Plexiglas II and polystyrene decrease with increasing temperature. The fracture surface appeared rough at low temperature and smooth at elevated temperature. Williams has found that stable brittle crack growth in

thermosets is similar to what is seen in PMMA and generally thermosets are slightly viscoelastic [23].

1.2 Temperature and rate effects on mechanical behavior of polymers

Temperature affects both deformation and fracture of polymers. Because of the viscoelasticity of polymers, temperature effects on mechanical behavior of polymers are more distinct and complex compared to those on metals and ceramics. The deformation and fracture behavior of a polymer is usually manifested through parameters like strength, plasticity and fracture toughness. Temperature effects on mechanical properties of polymers have been mainly concerned with the flow characteristics of the network and chains. Apparently, the temperature affects the strength behavior including the shear yielding stress – which is one major parameter from the flow. It is also generally believed that the temperature effect on mechanical properties of glassy polymers is more distinguished compared to the effect caused by rate change and environmental effects.

Studies on temperature and rate effects on mechanical properties of polymer materials including strength and toughness have found that results are much material dependent. Explanations of the behavior are material specific and there is no general theory obtained so far. Major polymer systems studied include PMMA, polycarbonate, epoxies, and other glassy polymers. The most studied thermoset resin is epoxy.

1.2.1 TEMPERATURE AND RATE EFFECT ON YIELDING

According to Williams [23], because thermoset resins often possess a strong and three-dimensional network structure from crosslinking, there is little thermal softening of the structure so they behave mostly like glasses. However, it is generally believed that even in brittle solids as thermoset polymers, localized plastic deformation in front of a crack tip takes place before bonds actually break. Because experimental observations of crazing in front of crack tips in thermoset polymers were rare, shear yielding is believed to be the main mechanism of crack tip localized energy dissipation in highly crosslinked network polymers like thermoset resins. Researchers have observed that a high degree crosslinking in epoxy would lead to the disappearing of crazing and visible shear bands

[34]. So yielding behavior is important in understanding mechanical properties of thermosets. Through studying the yielding behavior of an epoxy resin, it is found that its yielding is very similar to the un-crosslinked thermoplastics like polystyrene, which can be explained by Argon's yielding theory [35]. It also has been found that the amount of post-yielding plastic deformation in thermosets is substantially smaller than that in thermoplastics. The lack of post-yielding deformation is believed to be one of the main reasons for brittleness in thermosets.

Classical continuum mechanics has developed a few famous criteria in characterizing failure of homogeneous and isotropic material [36, 37]. One of the criteria is the Coulomb yield criterion, which states that the critical shear stress τ^* accompanying the shear deformation in any plane is proportional to the normal stress σ_n applied to that plane:

$$\tau^* = \tau_0 + \mu\sigma_n \quad \text{Equation 1-6}$$

where τ_0 is a constant related to the cohesion of material. This criteria, although quantify the shear deformation stress, does not take account into variables like time and temperature.

Microscopically, the viscoelastic nature of yielding behavior of polymer is quantified by the Eyring theory, which assumes an activated-rate process involving the overcome of an energy barrier ΔE . It is generally accepted that the yield stress decreases with temperature and yet increases with strain rate in glassy polymers. The Eyring theory correlates the applied stress σ with the strain rate $\dot{\epsilon}$ as:

$$\dot{\epsilon} = A_E \exp\left(-\frac{(\Delta E^* - \nu^*|\sigma|)}{RT}\right) \quad \text{Equation 1-7}$$

where A_E is a constant, R is the gas constant, ΔE^* is the potential energy barrier, T is the temperature and ν^* is the activation volume.

Rearranging the equation will give the relationship between yield stress σ_y and temperature and strain rate as:

$$|\sigma_y| = \frac{\Delta E^*}{v^*} + \frac{RT}{v^*} \ln\left(\frac{\dot{\epsilon}}{A_E}\right) \quad \text{Equation 1-8}$$

Because of thermal fluctuations, the kinetic or thermal energy of an atom or molecule varies, which provides a possibility of overcoming the barrier ΔE^* . Applied stress has the effect of reducing the energy barrier. Temperature increase also has the effect of lowering the barrier, making the yielding flow easier.

Due to the complexity of long chain molecular motions in polymers, microscopic mechanisms of shear yielding in polymers are more complicated than the dislocation model proposed in metals. One model is Argon's double kink model which proposes that yield occurs by thermally activated production of local molecular kinks. At absolute zero, this model predicts that the yield stress is only dependent on the shear modulus and Poisson's ratio. Between absolute zero and near glass transition temperature, the theory also incorporates the temperature, pressure, and strain rate dependence of the yield stress [35, 38, 39].

Based upon the theory that a polymer molecule changes from *cis* to *trans* conformation at yielding, Wu has proposed a semi-empirical relationship between shear yield stress and molecular parameters related to molecular structure: glass transition temperature, cohesive energy density, and characteristic ratio [40]. The relationship between shear yield stress τ_y (which is defined by the Von Mises yielding criterion) and these parameters is given by:

$$\frac{\tau_y}{\delta^2(T_g - T)} = 2.51 \times 10^{-4} \times C_\infty \quad \text{Equation 1-9}$$

where δ^2 is the cohesive energy density, C_∞ is the characteristic ratio, T_g is the glass transition temperature and T is the testing temperature. This equation accounts for the

intermolecular effect on shear yielding, which is reflected in both δ^2 and $(T_g - T)$ terms. It also includes the intramolecular effect, which is expressed in C_∞ - a measure of intrinsic molecular rigidity related to the conformational changeability.

Modifications to the Wu equation above have been made by Yamamoto and Furukawa to better characterize the temperature dependence of the shear yield stress [41]. The new relationship includes a term representing the effective moving unit of a polymer. The reason is that with the same amount of free volume the conformational change becomes more difficult as the effective moving unit getting larger.

$$\tau_y = A_1 C_\infty \delta^2 (T_g - T) (V_w / n_v)^{1/3} + A_2 \quad \text{Equation 1-10}$$

where V_w is the van der waal volume of a repeat unit and N_v is the statistical skeletal unit number in a repeat unit. The modified relationship shows good agreement with their experimental data from testing polystyrene, polycarbonate, PMMA, poly vinyl chloride and other glassy polymers.

Macroscopically, strength of polymers, including yield stress and ultimate stress, generally decreases with temperature [42]. This also applies to other material categories like metals and ceramics. The most general explanation of the process is due to the effect of thermal energy, which enhances deformation of the material. Under such condition, the material often undergoes changes from brittle stress-strain curves to curves that show substantial deformation.

Pink and Campbell have studied the tensile behavior of an epoxy resin [43]. The testing temperature ranges from -196°C to 108°C . Linear stress strain curves were observed at temperatures below 27°C , with the highest fracture stress reached at -196°C . At temperatures above room temperature, the stress strain curves start to bend over and show plastic deformation. At 33°C and 50°C , the material demonstrate both comparatively high ultimate strength and a small amount of plastic deformation. At 90°C and 108°C , the ultimate strength drop dramatically and yet the strains reach over 4%. In addition, Young's modulus of the resin also decreases with temperature, showing a

smaller resistance to load with increasing temperature. This behavior is typical of thermoset resins, which are often brittle at room temperature but demonstrate ductility at higher temperature.

Harismendy et al. have studied the strain rate and temperature effects on the mechanical behavior of two epoxy mixtures with different crosslink densities [44]. They have found that both flexural modulus and flexural strength are affected by the temperature greatly for two epoxies. The behavior is similar to that shown by the storage modulus and can be explained by the relaxational changes in these materials. The higher crosslinked epoxy exhibits lower flexural modulus and strength at the temperature range of above 10°C. The rate effect on the flexural modulus at room temperature is not big, the curve remains flat and the less crosslinked epoxy shows a higher modulus value. The room temperature flexural strength increases slightly for both epoxies with testing rate, with still the less crosslinked epoxy showing bigger values. These phenomena have been attributed to a ω relaxation between 40°C and 100°C which is unique to the more crosslinked epoxy. The relaxation can be related to the local motions of chains in the high crosslinked region due to a free volume increase. Their experiments suggest that testing temperature is an important factor in flexural properties of the epoxy resin studied and its effect is more obvious than that of the rate.

1.2.2 TEMPERATURE AND RATE EFFECT ON FRACTURE

In glassy polymers (including both thermosets and thermoplastics), the effect of temperature on fracture toughness can experience a monotonic increase or decrease, a constant, and a peaking mode with temperature. The effect is also material specific and different microscopic mechanisms contribute to the results.

Studying glassy polymers like Nylon, Polyacetal, PVC and Polyethylene, Hashemi and Williams [42] have found that their fracture toughness changes with temperature can be described by three different distinct regions: brittle, semi-brittle and ductile. These three modes are believed to be existent in thermosets too. These fracture modes are closely related to the load-displacement curve shapes during the single edge notched bending tests for fracture toughness. In the brittle mode, the load-displacement

curves behave linearly before breakage occurs. In the semi-brittle region, small non-linear part in the load-displacement curves is observed. In the ductile mode, distinguished non-linear curves are observed. The non-linear portion of the curve is believed to be related to the plastic deformation occurring at the crack tip during loading. The fracture toughness values of rubber modified PVC show a peak in the semi-brittle region, with both the brittle and the ductile side having lower values.

Testing both unmodified and rubber modified epoxy resins in the range of -60°C \rightarrow 60°C [45], Kinloch et al. have found that rubber modified epoxy demonstrate an enhanced temperature dependence in toughness. Crack propagation mode goes from stable brittle growth to unstable stick-slip growth to ductile tearing with temperature increase. With the unmodified epoxy, the ductile tearing mode at higher temperature is not observed, and its toughness is less temperature dependent. They have also found that the occurrence of three crack propagation modes would depend on the yield stress of the epoxy. Increasing yield stress has led to the transition from ductile tearing to brittle unstable to brittle stable crack growth.

By varying the testing rate and temperature in epoxy resins, it has been observed that the critical intensity factor for initiation of the crack decreases with increasing testing rate [22, 46]. When changing testing temperature, crack propagation is continuous at low temperatures but becomes unstable at high temperatures. The critical stress intensity factor of initiation drops with temperature and yet that of crack arresting increases with temperature. This has been attributed to the viscoelasticity of epoxy resins. A decrease in rate and an increase in temperature will promote the stick-slip crack propagation mode, which suggests the material becomes tougher.

In both rubber-modified and un-modified epoxy resins (epoxy resin with piperidine hardener and CTBN rubber), the compressive strength decreases with temperature in the region of -80°C \rightarrow 160°C [47-49]. The fracture energy increases monotonically in the range of -80°C \sim 60°C . The rate effect is characterized by: a decrease in rate is equivalent to an increase in temperature.

Cardwell and Yee have studied the rate and temperature effects on fracture toughness of a rubber modified DGEBA epoxy resin by three-point bending toughness testing [50]. The rubber modified epoxy has a bigger sensitivity to temperature change and its load-displacement curves appear non-linear at temperatures close to its T_g . The fracture toughness increases with decreasing testing rate and increasing temperature, accompanied by observed shear plasticity at the crack tip. On the other hand, un-modified epoxy shows no strong dependence on the rate and temperature. By using time-temperature superposition, they calculate that the apparent activation energy for the toughening process is $\sim 22.9 \text{ kcal mol}^{-1}$. It is concluded that fracture toughness dependence upon the testing rate and temperature is generally determined by the yielding process of the matrix. The second phase rubber particles promote shear yielding in front of the crack tip, which is the main mechanism of toughening the epoxy.

The strain rate is found to affect both the crack stability and the fracture energy G_c in the double cantilever beam test of epoxy resin [30]. The critical strain energy release rate decreases from 10^3 J/m^2 to about 10^2 J/m^2 when the crosshead speed increases for 10 fold. This can be qualitatively explained by the relaxation and crack blunting process at the crack tip which also correlates well with the crack stability. A big loading rate would result in less time available for crack tip relaxation. Thus crack tip would remain sharp and stable propagation occurs. On the other hand, slow loading would give rise to unstable crack propagation and crack arrest would happen before re-initiation. The same phenomena have also been observed by Selby and Miller [51].

In studying pure and modified epoxies, Low and Mai [52] have found that G_{Ic} from compact tension test increases monotonically with temperature for both epoxies. The reason lies in the increasing amount of crack tip blunting when the yield stress decreases with increasing temperature. This so-called “plastic blunting” at slow strain rate is used to explain G_{Ic} increase with temperature. As to the rate effect, the rubber modified epoxies are less dependent on strain rates than the pure epoxies.

In summary, both temperature and rate affect mechanical properties of polymers greatly. Although there is no general mechanism or theory accounting for the mechanical

behavior change with temperature and rate, including changes in fracture toughness and fracture mechanisms, previous on epoxies and other glassy polymers are important to gain further understanding of the subject.

References:

1. Zhu B. *Toughening of rigid silicone resins*, in *Department of Materials Science and Engineering*. 1997 (September), Massachusetts Institute of Technology: Cambridge, MA.
2. Zhu B, Katsoulis DE, Keryk JR. *Toughening of rigid silicone resins*. ABSTR PAP AM CHEM S, 1998. **226**(100-PMSE Part 2).
3. Zhu B, Katsoulis DE, Keryk JR, McGarry FJ, Li Z. *Fracture toughness and toughening of silicone resins*. in *33rd Organosilicone Symposium*. 2000. Saginaw, MI.
4. Zhu B, Katsoulis DE, Zank GA, McGarry FJ. *Mechanical properties and toughening of a polymethylsilsesquioxane network*. in *Materials Research Society Symposium Proceedings*. 2000.
5. Zhu B, Katsoulis DE, Keryk JR, McGarry FJ. *Toughening of rigid silicone resins*. *Polymeric Materials Science and Engineering*, 1998. **70**: 192-193.
6. Zhu B, Katsoulis DE, Keryk JR, McGarry FJ. *Toughening of a polysilsesquioxane network by homogeneous incorporation of polydimethylsiloxane segments*. *Polymer*, 2000. **41**(20): 7559-7573.
7. Katsoulis DE, Keryk JR, McGarry FJ, Zhu B. *Rubber-modified rigid silicone resins, toughened compositions and composites*, in *US patent 5,830,950*. 2000.
8. Zhu B, Katsoulis DE, Keryk JR, Bergstrom DF, Kwan KS, McGarry FJ, Li Z. *Hydrosilyation cured silicone resin containing colloidal silica and a process for producing the same*, in *US patent application 10/091,685*. 2002.
9. Zhu B, Katsoulis DE. *Development of tough silicone resin*. in *33rd International SAMPE Technical Conferences*. 2001. Seattle, WA.
10. Zhu B. *Silicone composition and cured silicone product*. US patent 6509423, 2003.
11. Katsoulis DE, Li Z, McGarry FJ, Nguyen BT, Zhu B. *Silsesquioxane resin with high strength and fracture toughness and method for the preparation thereof*. 2001, US patent 6,310,146.
12. Li Z. *High fracture toughness and high modulus silicone resins*, in *Department of Materials Science*. 2000, Massachusetts Institute of Technology: Cambridge, MA.
13. Li Z, McGarry FJ, Zhu B, Keryk JR, Katsoulis DE. *Effect of crosslinkers on the mechanical properties of addition cure phenylsilsesquioxanes*. *Polymer Preprint (American Chemical Society)*, 2001. **42**: 113.
14. Zhu B, Katsoulis DE, Keryk JR, Kwan KS, McGarry FJ, Li Z. *High fracture toughness hydrosilyation cured silicone resin*, in *US patent application 10/092,055*. 2002.
15. Zhu B, Katsoulis DE, Keryk JR, McGarry FJ, Li Z. *Hydrosilyation cured silicone resins obtained by fractionation*, in *US Patent application 10/091,678*. 2002.
16. Zhu B, Katsoulis DE, Nguyen BT, Keryk JR, McGarry FJ. *A new route to silicone resins of high fracture toughness: poly(silarylene and silalkylene silsesquioxane) networks*. *International SAMPE technical conference*, 2001. **33**: 697-708.
17. Spence DC. *Silicone resin studies*, in *Department of Materials Science*. 1996 (September), Massachusetts Institute of Technology: Cambridge, MA.

18. Zhu B, Nguyen BT, Katsoulis DE. *A tough addition cure silicone resin based on phenyl silsesquioxane crosslinked with silphenylene*. Dow Corning Technical Report, 2000. **2000-I0000-48291**.
19. Spain DR. *Fracture toughness measurements of thin film silicone polymers using the modified edge lift-off test*, in *Department of Materials Science*. 2000 (September), Massachusetts Institute of Technology: Cambridge, MA.
20. Zhu B, Katsoulis DE, Keryk JR, Spain D, Wu Y, McGarry FJ. *Fracture toughness of thin siloxane resin films measured by mELT*. International SAMPE Symposium and Exhibition, 2002. **47**: 1711-1721.
21. Finzel WA. *High solids polyorganosiloxane polymers for high temperature applications*. Journal of Coatings Technology, 1992. **64**(809): 47-50.
22. Kinloch AJ, Young RJ. *Fracture behavior of polymers*. London: Applied Science Publishers, 1983.
23. Williams JG. *Fracture mechanics of polymers*: Ellis Horwood Limited, 1984.
24. Griffith AA. Phil. Trans. Roy. Soc. (London), 1920. **A221**: 163-198.
25. ASTM Standard. *Standard test methods for plane-strain fracture toughness and strain energy release rate of plastic materials*. D5045-96.
26. Phillips DD, Scott JM, Jones M. Journal of Materials Science, 1979. **13**: 1609.
27. Yamini S, Young RJ. Polymer, 1977. **18**: 1075.
28. Yamini S, Young RJ. Journal of Materials Science, 1979. **14**(1609).
29. Young RJ. in *Developments in polymer fracture*, EH Andrews, Editor. 1980, Applied Science Publishers Ltd.: London. p. 183.
30. Cherry BW, Thomson KW. *Crack stability and strain rate dependence of G_c in epoxy resin*. Journal of Materials Science, 1981. **16**: 1925.
31. Kinloch AJ, Williams JG. Journal of Materials Science, 1980. **15**: 987.
32. Mostovoy S, Ripling EJ. Journal of Applied Polymer Science, 1966. **10**: 1351.
33. Broutman LJ, McGarry FJ. *Fracture surface work measurements on glassy polymers by a cleavage technique. I. Effects of temperature*. Journal of Applied Polymer Science, 1965. **9**: 589-608.
34. van den Boogaart A. *Physical basis of yield and fracture*. London: Institute of Physics, 1966. 167.
35. Argon AS. Philosophical Magazine, 1973. **28**: 839.
36. Kausch HH. *Polymer fracture*. Berlin: Springer-Verlag, 1978.
37. Hertzberg RW. *Deformation and fracture mechanics of engineering materials*. New York: John Wiley, 1976.
38. Argon AS, Bessonov MI. Polymer Engineering and Science, 1977. **17**: 174.
39. Argon AS, Bessonov MI. Philosophical Magazine, 1977. **35**: 917.
40. Wu S. Polymer Engineering and Science, 1990. **30**: 753.
41. Yamamoto T, Furukawa H. *Relationship between molecular structure and deformation-fracture mechanism of amorphous polymers: 1. shear yield stress*. Polymer, 1995. **36**(12): 2389-2392.
42. Hashemi S, Williams JG. *Effect of temperature on the fracture behavior of polymers*. in *Polymers at low temperatures: 20th Jan. 1987*,. 1987. City Conference Center, London.
43. Pink E, Campbell JD. Materials Science and Engineering, 1974. **15**: 187.

44. Harismendy I, Miner R, Valea A, Llano-Ponte R, Mujika F, Mondragon I. *Strain rate and temperature effects on the mechanical behavior of epoxy mixtures with different crosslink densities*. Polymer, 1997. **38**(22): 5573-5577.
45. Kinloch AJ, Shaw SJ, Todd DA, Hunston DL. Polymer, 1983. **24**: 1341-1354, 1355-1363.
46. Pennings AJ, Meihuizen KE. in *Ultra-high Modulus Polymers*, A Ciferri, Ward IM, Editors. 1979, Applied Sciences Publishers Ltd.: London. p. 117.
47. Kinloch AJ. *Relationships between the microstructure and fracture behavior of rubber toughened thermosetting polymers*, in *Rubber toughened plastics*, CK Riew, Editor. 1989, American Chemical Society: Washington DC. p. 67-92.
48. Hunston DL, Kinloch AJ, Shaw SJ, Wang SS. in *Adhesive joints*, KL Mittal, Editor. 1984, Plenum: New York. p. 789.
49. Kinloch AJ, Hunston DL. Journal of Materials Science Letters, 1987. **6**: 137.
50. Cardwell BJ, Yee AF. *Rate and temperature effects on the fracture toughness of a rubber-modified epoxy*. Polymer, 1993. **34**(8): 1695-1701.
51. Selby K, Miller LE. Journal of Materials Science, 1975. **10**: 12-24.
52. Low I, Mai Y. *Rate and temperature effects on crack blunting mechanisms in pure and modified epoxies*. Journal of Materials Science, 1989. **24**: 1634-1644.

CHAPTER 2. Materials and experiments

2.1 Materials

2.1.1 DOW CORNING X1-2672 ADDITION CURE RESIN

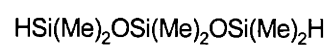
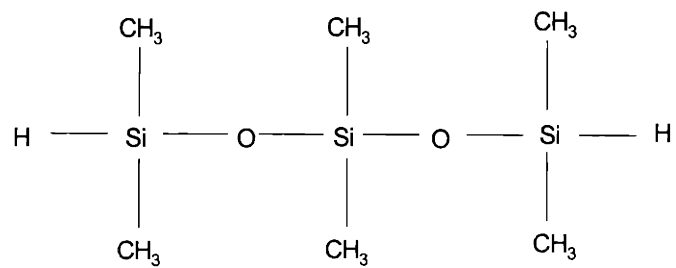
The lot numbers of the Dow Corning experimental X1-2672 resin (with the empirical formula $(\text{PhSiO}_{3/2})_{0.75}(\text{ViMe}_2\text{SiO}_{1/2})_{0.25}$), a vinyl dimethylsiloxy terminated phenylsilsesquioxane resin, are: PE#03700007 and #03700008. They were carried in toluene with the resin weight content around 60%. The weight content of the resin solution was measured by weighing differences between as-arrived resins and the ones that have been dried at $\sim 90^\circ\text{C}$ for 24 to 48 hours. The final weight was taken down when there was no substantial weight loss within a weighing period of ~ 4 hours.

2.1.2 CROSSLINKERS AND CATALYST FOR X1-2672

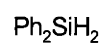
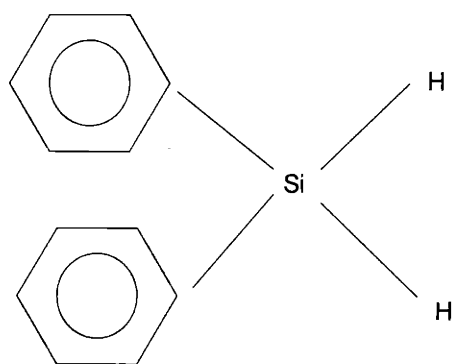
The crosslinkers used for curing x1-2672 resin are listed below. They are commercially available from Gelest Inc.

The controlled molar ratio of the silicon hydrogen group in the crosslinker to silicon vinyl group in the resin was 1.1:1. Resin and crosslinker(s) were mixed with a good agitation and yet as slow as possible by Teflon stirring bars or stirring rods. This was to ensure good mixing and yet minimize bringing air into the resin mixture.

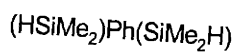
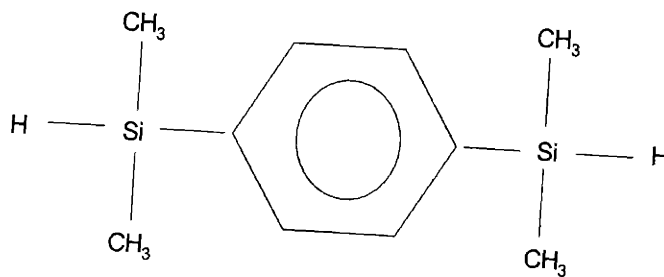
The catalyst was a Pt IV catalyst carried in toluene solution. The nominal weight concentration of the catalyst to the resin solid weight was controlled at 1 ppm for the silylphenylene and hexamethyltrisiloxane crosslinked resin and at 30 ppm for other crosslinked systems containing diphenylsilane due to its low reactivity. Mixing of the catalyst was carried out in the same careful fashion as described above after the resin and the crosslinker(s) were fully mixed.



1,1,3,3,5,5 – hexamethyltrisiloxane (MW 208.48)



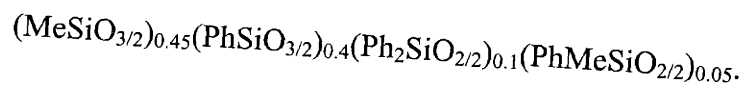
diphenylsilane , MW 184.31



1,4-bis(dimethylsilyl)benzene (or silylphenylene) (MW194.42)

2.1.3 DOW CORNING 4-3136 CONDENSATION CURE RESIN

This resin has been named 4-3136 initially and is now called 233 and its empirical formula is:



The flake resin was shipped in a solid state. It was dissolved in toluene before making sample castings. The toughened version of the resin was developed by Zhu from MIT [1]. Small short chain PDMS was used to toughen the resin and increased the toughness from ~ 0.25 to $\sim 0.45 \text{ MPa m}^{1/2}$ by adding 10% KPE (PDMS with ethoxy end and the degree polymerization is 55). This toughened resin appeared to have the best combination of mechanical properties and is hereafter named 3136T. The toughened resin used in this thesis work was synthesized at a Dow Corning lab and shipped to MIT in a toluene solution.

2.1.4 CATALYST FOR 4-3136

The catalyst used for curing 4-3136 was Dow Corning Catalyst Y-177[®]. It is a mixture of 7% zinc octoate, 3% choline 2-ethylhexanoate in 47% *n*-butyl alcohol, 30% toluene, and 12% Stoddart solvent [2]. The concentration is kept at 0.05 wt% for resin castings.

2.2 Experimental procedures

2.2.1 CURING PROCEDURE FOR X1-2672

After mixing resin with the crosslinker(s) and the right amount of Pt IV catalyst, the mixture was degassed in a vacuum oven without heat for about 20-30 minutes. The vacuum level was controlled so that the gas bubble could form and break, and yet it did not produce much agitation/bubbling/boiling motion within the mixture. This is a critical step to avoid void formation in the final casting. Care and patience was needed to ensure the completion of this step.

Cure was done in an air circulating oven, and the curing cycle for all x1-2672 castings was: 85°C x 24 hours, 150°C x 24 hours, and 200°C for 24 hours. Castings were cooled along with the furnace from 200°C to room temperature and removed from the Teflon coated mold. More complete details regarding the curing can be found in Li's thesis [3].

Buckling of the final casting plate was always noticed. The degree of buckling varies between castings but it was common that the center of the plate was always higher than the edges. This produced some difficulties in the next machining step of the samples. Care has to be taken when cutting and milling samples from these cast plates. Otherwise, breakage could occur during machining.

2.2.2 CURING PROCEDURE FOR 4-3136

Both toughened (with 10% KPE) and un-toughened resins were mixed with 0.05 wt% of the catalyst. The mixture was poured into a Teflon mold and degassed inside a heated (~60-70°C) vacuum oven to remove toluene and trapped air. Then it was placed into the oven for cure under the cycle recommended in Dr. Zhu's thesis: 70°C x 24hrs, 75°C x 24hrs, 80°C x 24hrs, 85°C x 24hrs, 90°C x 24hrs, 95°C x 48hrs, 110°C x 24hrs, 120°C x 24hrs, 130°C x 48hrs, 150°C x 4hrs, 175°C x 4hrs, 200°C x 12hrs, 230°C x 6hrs, and 260°C x 8hrs. More details of the casting procedure are available in Zhu's thesis [1].

2.2.3 DYNAMIC MECHANICAL ANALYSIS

DMA analysis was performed on a Dynamic Mechanical Rheology Station DMS200 from Seiko Inc. Tested specimens had rectangular cross-sections of a dimension 0.5 mm x 4 mm, the clamping distance was 20 mm. The data was collected at a frequency of 1 Hz, and temperature range was -150°C ~350°C with a rate of 2°C/min. The samples were loaded in tension mode, with a nitrogen atmosphere by flowing N₂ at 200 ml/min. Some samples failed before the end of the ramping temperature but enough useful data for analysis were collected in such cases.

2.2.4 THERMOGRAVIMETRIC ANALYSIS

Thermogravimetric analysis was done on a Texas Instrument TGA7. Sample weight was about 10-20 mg. The testing temperature range was 20 to 800°C, and the heating rate was 10°C/min. Gas flow rate was at 20 ml/min. Tests were done in air and data were collected in a computer controlled program.

2.2.5 MECHANICAL TESTING

Flexural samples and fracture toughness samples were made by standard machining tools. A band saw was first used to trim the edges and cut samples into smaller dimensions. Then a milling machine was used to machine samples down to the right thickness. Final samples were ground with SiC papers or polished with alumina polishing

solution. Samples were conditioned at room temperature for two days before being tested on an Instron 4505 machine.

Flexural tests were performed according to ASTM standard D790 [4]. The size for the samples was 12.7 mm x 2.5 mm x 51 mm and the span was 38 mm (0.5" x 0.1" x 2" and 1.5" span). Final flexural samples were polished with 0.3 μm alumina polishing solution to eliminate surface defects from grinding. The loading rate was at 1 mm/min (0.04 inch/min).

Fracture toughness measurements were performed according to ASTM standard D5045-96 [5]. Based on the stress intensity factor concept outlined in Chapter 1, critical stress intensity factor value is taken as the mode I fracture toughness. Three-point bending tests on single edge notched bending samples were performed. The fracture toughness is calculated by:

$$K_{Ic} = \frac{La^{1/2}}{bt} \left[1.99 - 0.41(a/b) + 18.7(a/b)^2 - 38.48(a/b)^3 + 53.85(a/b)^4 \right] \text{Equation 2-1}$$

where L is load at failure, a is the initial crack length, b is the specimen width, and t is specimen thickness.

Because of the sensitivity of fracture toughness to testing details in single edge notched bending, care was taken during every step of sample preparation and testing to make sure that the results were valid. There are a few points worth mentioning. The first is the plane strain state. To ensure that the test-obtained critical value of the stress intensity factor is a material property, the plane strain state requirement must be met by using a sample with enough thickness. Otherwise, the K_c obtained might be higher since K_c in a plane stress state is always higher than that in a plane strain state. This is not difficult because the plane strain state requires a sample thickness of less than 3 mm and our test sample has a thickness of 4.8 mm. Second is that the pre-crack sharpness has to be ensured because the presence of a relatively blunt crack will yield higher fracture toughness values. The sharp crack was produced by using a liquid nitrogen cooled razor blade to tap natural cracks in front of the saw-cut notches and also by producing enough

travel of the sharp crack in front of the notch front. The crack length to width ratio was controlled to meet the requirement of $0.45 < a/b < 0.55$. Extreme care was also taken when measuring the crack length after the sample was broken.

Fracture toughness sample dimension was 9.5 mm x 4.8 mm x 51 mm (0.375" x 0.19" x 2") with notch length of 2.5 mm. The span length was 38 mm. The loading rate was 10 mm/min (0.4 inch/min). There were other tests performed at different rates of 100 mm/min and 1 mm/min and those will be noted otherwise. All samples were polished with SiC paper (finest grit size 4000) with water-cooling.

For both flexural tests and fracture toughness tests done at temperatures other than room temperature, an Instron environmental chamber 3111 was used. Typically, testing at elevated temperatures was performed by heating the sample to the test temperature and held for 30 minutes before applying the force. For low temperature testing below room temperature, a typical holding time was 15-20 minutes. In this case, the Instron environmental chamber was still used, but the testing temperature was controlled by a setup outside the Instron box (Figure 2-1). From the thermocouple signal, the thermal controller energizes the cryogenic valve and thus controls the flow amount of liquid N₂ into the Instron chamber. The whole apparatus used stainless steel tubing and fittings to minimize low temperature embrittlement of the setup.

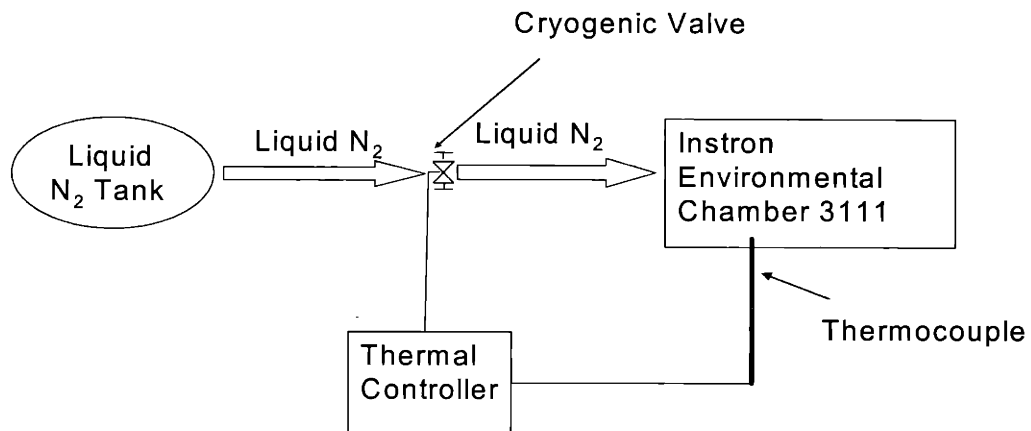


Figure 2-1 Sketch of low temperature testing setup on Instron 4500 with an Instron environmental chamber.

2.2.6 SCANNING ELECTRON MICROSCOPE ANALYSIS

SEM analysis was performed on a Leo-438VP machine (Leo Electron Microscopy Ltd.) at MIT. The acceleration voltage was set at 20 KV. A Variable Pressure Mode, which involves the back-scattered detector, was used for observing fracture surface. This required no gold coating on plastic sample surfaces to make them conductive. Broken samples were mounted onto aluminum holders with graphite tape, and micrographs were taken on different samples as indicated below in Figure 2-2.

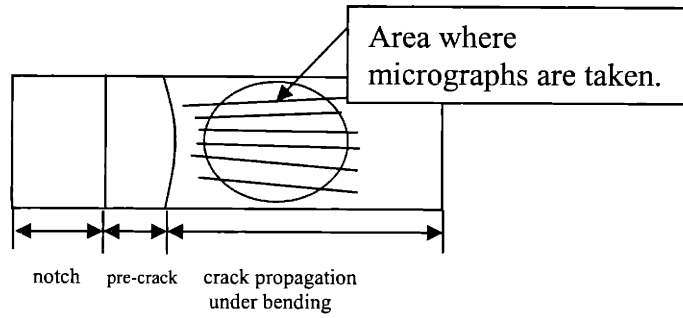


Figure 2-2 Sketch of SEM analysis of broken notched samples.

References:

1. Zhu B. *Toughening of rigid silicone resins*, in *Department of Materials Science and Engineering*. 1997 (September), Massachusetts Institute of Technology: Cambridge, MA.
2. Zhu B, Katsoulis DE, Keryk JR, McGarry FJ. *Toughening of a polysilsesquioxane network by homogeneous incorporation of polydimethylsiloxane segments*. *Polymer*, 2000. **41**(20): 7559-7573.
3. Li Z. *High fracture toughness and high modulus silicone resins*, in *Department of Materials Science*. 2000, Massachusetts Institute of Technology: Cambridge, MA.
4. *Standard test methods for flexural properties of unreinforced and reinforced plastics and electrical insulating materials, ASTM standard D790-92*. Annual Book of ASTM Standards, 1992. **Vol. 08.01**.
5. *Standard test methods for plane-strain fracture toughness and strain energy release rate of plastic materials, ASTM standard D5045-96*. Annual Book of ASTM Standards, 1996. **Vol. 08.03**.

CHAPTER 3. Temperature and rate effects on silicone resin mechanical properties

From three-point bending tests, results of flexural stress, modulus and strain were obtained. From the single edge notched bending tests, K_{Ic} data were obtained. These are presented and discussed in this section. Generally maximum flexural strain data exhibit a greater scattering because it is not an actual material property, but more or less dependent upon the testing condition. However, the data are still useful in presenting the trend of how deformation changes with temperatures.

3.1 Mechanical testing results of Dow Corning X1-2672 addition cure resin

As mentioned in the previous chapter, this resin has been used to make bubble free, defect free castings. Three-point bending tests were performed on them under different temperatures. 2672 resins crosslinked with D, P, DP and B are studied. For the DP system, variations in combination of the crosslinkers are: D100 (100%D), DP37 (30%D, 70%P), DP55 (50%D, 50%P), DP73 (70%D, 30%P) and P100 (100%P). With the B100 (100%B) system, effect of rate variation is studied too. The results are summarized and discussed in this section.

3.1.1 B100 SYSTEM – TEMPERATURE EFFECT

The B100 is the toughest system among all. It has both high strength and high toughness. The effect of testing temperature on its maximum flexural stress, strain, modulus and K_{Ic} is shown in Table 3-1 and Figure 3-1 through Figure 3-4. It is clear that both maximum flexural stress and flexural modulus decrease with temperature and the maximum flexural strain increases with temperature. Using room temperature properties as references, the flexural modulus increases 20% at -40°C and decreases 42% at 60°C . The maximum stress increases 57% at -40°C and decreases 53% at 60°C . Changes in maximum flexural strain are less dramatic: -24% at -40°C and +17% at 60°C . The fracture toughness, however, peaks at about room temperature. This is clearly seen from Figure 3-4, where the curve reaches its maximum near room temperature. At both

temperature extreme ends, toughness values drop; but with a bigger magnitude of -64% at -40°C.

From Table 3-1, it is observed that the P_{max}/P_q ratio at 60°C is slightly bigger than the test validity upper limit of 1.1. This is due to the non-linearity present in the load-displacement curves of the toughness testing (Figure 3-40). The semi-brittle behavior is already seen during test at 40°C (Figure 3-39) but the P_{max}/P_q criterion is still met under this temperature. Although the test validity is slightly off at 60°C, we can still say that the trend of toughness decreasing with temperature can be established at temperatures above 20°C.

The behavior of B100 toughness with temperature can be approximated as an asymmetric parabola. The high temperature end illustrates a gradual decrease, while the low temperature end has a steep slope. For B100, the increased mobility of the network at high temperatures enhances its plasticity, and this effect alone should increase the fracture toughness value. However, at the same time, B100 experiences a moderate loss of rigidity and strength due to thermal softening, which cancels out the network mobility effect. The final result is that loss of rigidity becomes dominant and there is a moderate drop in the toughness value above 20°C. At temperatures below room temperature, the network mobility is hindered and there is not much chain movement involved. This contributes to its brittleness. Although the polymer is stronger and more rigid under these temperatures, the decrease in the network mobility seems to be the key controlling factor. Thus, the overall toughness drops even more substantially compared to the high temperature end.

3.1.2 B100 SYSTEM – RATE EFFECT

The rate effect on the B100 fracture toughness has also been studied. In addition to the normal crosshead moving rate at 10 mm/min, the fracture toughness of B100 has been tested under the loading rates of 1 mm/min and 100 mm/min. The summary of all data is presented in Table 3-2. Plotting the fracture toughness versus the Log of testing rate in Figure 3-5 shows that the sensitivity of toughness to the loading rate is different at

different temperatures. From the experimental data, at 0°C and 60°C, testing rate has the biggest effect on toughness.

From Figure 3-6, the effect of temperatures on toughness exhibits similar trends even under different loading rates. At loading rates of both 1 mm/min and 100 mm/min, toughness curves present lower values compared to that under 10 mm/min. The loading rate of 100 mm/min has a bigger effect on the drop of K_{Ic} values, and the peaking temperature of the curve also shifts slightly to the higher end. However, the effect of rate is not conclusive. One reason could be that although tests were done at constant loading rates, the single edge notched bending test is not a test that can control the crack propagation rate. The instability in the crack front during bending makes it impossible to keep the rate of crack propagation at a constant level. Another reason could be that at temperatures higher than 40°C, we see big data variations accompanied by $P_{max}/P_q > 1.1$, which suggests the test does not meet the validity criterion. The dynamic effect of increasing rate has made it difficult to keep the test valid, and thus has brought some errors into the data.

3.1.3 DP SYSTEM – TEMPERATURE EFFECT

3.1.3.1 D100

The D100 system has the lowest rigidity but the biggest flexural deformation among all systems. This is well associated with the molecular structure of the crosslinker. Hexamethyltrisiloxane is a di-functional crosslinker, with soft and flexible backbone due to its lack of bulky groups. Theoretically, this is a low crosslinked system because the di-functional crosslinkers are the least effective in forming crosslinking points. D100 also has the lowest glass transition temperature, about 66°C from the $\text{Tan } \delta$ plot in Figure 3-32. From Table 3-3, it is clear that the stress and modulus decrease with temperature. Both flexural modulus and maximum flexural stress values drop about 10 folds from –40°C to 60°C. Its modulus and strength at 40°C decrease about 60-70% of the RT values, however, at –60°C they increase about 220%-240%. The maximum flexural strain shows an increase with temperature, and the relative increase at 60°C to RT is 16%. However,

its toughness has a unique pattern of going up at temperatures below RT, and it stays almost unchanged at -40°C and -60°C .

For this system, the dramatic increase in rigidity and strength below 0°C is unique. This seems to compensate for the minor loss of plastic deformation within the frozen network, which still demonstrates enough mobility at the low temperatures, and result in a high toughness at temperatures below 0°C . On the other hand, flexural modulus drop at 40°C is big and results in a moderate drop in toughness. Temperature effect on the strength and modulus of D100 is more substantial compared to that in B100. This effect, combined with the deformation characteristic of di-functional crosslinker, has been the main source of toughness.

The plastic zone size calculation also verifies that D100 experiences bigger plastic deformation in general, even at temperatures below RT. If we compare values of D100 values with those of B100 at same temperatures, we see big differences at temperatures below 20°C (last columns in Table 3-1 and Table 3-3). If we take into account of the difference between glass transition temperatures of D100 ($\sim 66^{\circ}\text{C}$) and B100 ($\sim 88^{\circ}\text{C}$), we can compare values at temperatures with the same magnitude below T_g , say comparing the value at -40°C in B100 with that at -60°C in D100 and so on. We see that the differences still exist until 0°C . Apparently there is still enough amount of deformation occurring in the D100 network even at low temperatures.

From the load-displacement curves, we see that non-linearity signifying a semi-brittle behavior starts to appear at 20°C , which only appears in other systems at a temperature higher than RT, say 40°C or 60°C . (Figure 3-41 and Figure 3-42)

3.1.3.2 DP73

In DP73 part of the hexamethyl crosslinker is substituted with a more rigid crosslinker P – diphenylsilane, which has two phenyl rings on the side chain and is also difunctional. In DP73 there is 70%D and 30%P. The diphenylsilane crosslinker adds some rigidity to DP73, and the D crosslinker provides network flexibility. This results in its high toughness of $0.75 \text{ MPa m}^{1/2}$ at room temperature.

Compared to D100, DP73 is stronger and more rigid at all temperatures. Table 3-4 shows the temperature effect on its flexural properties. At -40°C, increase in the maximum flexural stress is about 90% and flexural modulus increase is about 50% relative to their RT values. At 60°C they lose about 80% of the RT values. Compared to D100, DP73 shows a similar change of strength and modulus in relation to temperature, with the exception that its increase in stress and modulus is not as dramatic at the low temperature region. Figure 3-11 through Figure 3-13 show plots of flexural properties vs. temperature.

From Figure 3-14 we see the toughness drops at temperatures both below and above RT, and it peaks around 10°C. The toughness vs. temperature curve is similar to that of B100, but not that of D100. Compared to D100, DP73 has higher toughness at temperatures above 0°C. We see that the drop at the high temperature end is comparably bigger and causes the parabola to have a skewed shape. However, it is noted that the P_{max}/P_q value is 1.573 at 60°C, so the K_{Ic} value at 60°C is not valid (See Figure 3-44). The non-linearity is observed starting at 40°C (Figure 3-43) but becomes substantial at 60°C. Even without the data point at 60°C, we can still establish the trend of toughness dropping at temperatures above RT. The toughness sensitivity to temperature is about the same at both high temperatures and low temperatures.

Replacing 30% D crosslinker with P results in a very different toughness behavior at low temperatures. The hindrance from the phenyl rings on the side chains provides enough resistance force to the deforming of polymer network at low temperatures, even with the accompanying flexibility offered from the D crosslinker. The network mobility is greatly decreased, so the overall result is a toughness drop of 50% at -40°C.

3.1.3.3 DP55

DP55 has the same amount of diphenylsilane and hexamethyl crosslinkers in it. The results are shown in Figure 3-15 to Figure 3-18. Compared to D100 and DP73, the modulus and stress drop with temperature shows a similar trend. DP55 also has higher stress and modulus than both D100 and DP73 at all temperatures, which can be explained by the presence of higher content of P crosslinker. Using room temperature value as a

reference, the relative percentages of changes in stress and modulus at -40°C and +60°C are all slightly smaller compared to those of DP73.

The toughness curve of DP55 has a flatter shape than that of the DP73. Interestingly, its toughness at 0°C, 20°C and 40°C are almost the same – at a value around 0.64MPa m^{1/2}. Its toughness at temperatures below 40°C are lower than those of DP73, but its toughness values at 40°C and 60°C are greater. The toughness peaking temperature also moves to a higher temperature, ~20°C. Compared to the RT toughness value, the relative percentage change at -40°C is -52%, this is about the same compared to that of DP73. The relative percentage change at 60°C is -31%, a slightly smaller magnitude compared to that of DP73.

All P_{max}/P_q values are within the 1.1 limit, so all toughness tests are valid. At 60°C, we see slightly bent-over load-displacement curves showing small non-linearity. In this case, data points with P_{max}/P_q greater than 1.1 are discarded. (See Figure 3-45)

3.1.3.4 DP37

DP37 has 70% diphenylsilane and 30% hexamethyltrisiloxane. The results are presented in Figure 3-19 through Figure 3-22. Due to the presence of a major part of the P crosslinker, DP37 is the most rigid among all DP combinations. The relative changes in modulus and strength to their RT values are even smaller when compared with DP55 and DP73. From -40°C to 60°C, there is only a 2-3 fold drop in strength and modulus. This could be explained by the higher P content in the resin network, which contributes to the rigidity and strength of the network.

The toughness curve in Figure 3-22 shows an even flatter shape compared to DP73 and DP55. Compared to DP55, the relative change to RT toughness value is about the same (-53%) at -40°C, but it is in a small magnitude of -20% at 60°C. Toughness values are also lower than those of DP55 almost at all temperatures. The toughness curve peaks at ~30°C, which also moves a higher temperature. Toughness tests at all temperatures meet the criterion of $P_{max}/P_q < 1.1$. Even at 60°C, the load displacement curves of DP37 show brittle behavior (Figure 3-46).

3.1.3.5 P100

P100 is crosslinked only with diphenylsilane. Undoubtedly, this is the strongest system among D100, DP systems and B100, which exhibits highest maximum flexural stress. The modulus and maximum stress vs. temperature are described in Figure 3-23 and Figure 3-24, respectively. Because the system is relatively brittle compared to other DP series, there are bigger variations in the data obtained. This is due to the fact that brittleness causes samples to become more sensitive to scratches and defects, and thus to be more subjected to pre-mature breakage during loading. Generally, its room temperature strength and modulus is comparable to other DP systems at -40°C, suggesting the P100 network is very rigid even at room temperature. The phenyl rings on the crosslinker pose much resistance on the movement of the network.

The toughness of P100 at room temperature is the lowest, largely due to its limited network mobility from the diphenylsilane crosslinker. P100 toughness generally has lowest values at all temperatures and the flattest shape compared with other DP systems. Its change with temperature is also small (Figure 3-26). It is noted that toughness stays almost the same at $0.44 \pm 0.03 \text{ MPa m}^{1/2}$ at temperatures of 0°C, 20°C, 40°C and 60°C (Table 3-7), which shifts the toughness vs. temperature curve to a peak of higher temperature $\sim 35^\circ\text{C}$.

The diphenylsilane crosslinker brings in many phenyl side groups into the network. This results in more hindrance to the mobility of chains, which contributes to low deformation ability and thus small maximum strain. This also explains for the brittleness at RT. Even with increasing temperature, the resistance to the chain mobility is still high enough for the resin to have a low toughness. We see the proof from a very small increase ($\sim 2\%$) in the maximum flexural strain from -40°C to 60°C (Figure 3-25). In addition, plastic zone size at 40°C and 60°C remains small. These all suggest that the network mobility is greatly reduced in P100. However, the overall toughness does not drop much at 60°C due to the compensation effect of the rigidity of the network.

All P100 load-displacement curves of the toughness tests demonstrate pure brittle behavior with $P_{max}/P_q = 1$.

3.1.4 DMA (TAN δ VS. T) AND FRACTURE TOUGHNESS (K_{IC} VS. T)

Plots of Tan δ curves in Dynamic Mechanical Analysis and toughness with temperature for both DP series and B100 are shown in Figure 3-31 through Figure 3-36. As P crosslinker concentration increases (from DP73 to DP37), the Tan δ peak temperature shifts to the higher temperature end. At the same time, the peaking temperature of the toughness curve moves to a higher temperature, as discussed in previous sections.

If we list out the two peak temperatures and compare them as in Table 3-8, we see that except D100, all other systems fall into the same difference range – about $62\pm 4^\circ\text{C}$. The toughness peak always occurs at about 62°C below the Tan δ peak, thus it is closely associated with the glass transition temperature of the polymers. The molecular motions inside the polymer network at $\sim 62^\circ\text{C}$ below the glass transition temperature seem to be at its best when contributing to the toughness. At this temperature, molecules still have some mobility and also enough rigidity to achieve relatively high toughness. Above this they will lose too much rigidity and below this they will lose mobility, thus resins appear brittle under both situations.

The exception of D100 suggests that D100 is different in molecular structure and deformation mechanism. Its toughness peaks at a much lower temperature, $\sim 100^\circ\text{C}$ below its glass transition temperature. The D100 network is very flexible and deformable, which can be explained by the difunctional and long molecule crosslinker. At -40°C and -60°C , the network is still mobile and deformable at the same time of the network rigidity increase, this has resulted in its high toughness at these low temperatures.

3.1.5 PLASTIC ZONE SIZE AND ACTIVATION ENERGY CALCULATION

Using the fracture toughness and flexural strength data obtained in previous sections, the plane strain plastic zone size R_p has been estimated by [1]:

$$R_p = \frac{1}{6\pi} \cdot \left(\frac{K_q}{\sigma} \right)^2 \quad \text{Equation 3-1}$$

where σ is the maximum flexural stress and K_q is fracture toughness. The maximum flexural stress is used here instead of the yield stress as an approximation. The numbers are listed in the last column in Table 3-1 and Table 3-3 through Table 3-7.

A plot of $\text{Log}(R_p)$ vs. T of B100 and DP series is shown in Figure 3-37, and a plot of $\text{Log}(R_p)$ vs. $1/T$ is shown in Figure 3-38. Figure 3-37 clearly shows that the plane strain plastic zone size increases monotonically with temperatures for almost all systems. One exception occurs in DP73 tested at 60°C, which might be from the invalidity of the test. The trend of increase can be explained by larger plastic flow at higher temperatures.

At the same time, we can fit $\text{Log}(R_p)$ vs. $1/T$ with linear correlation (Figure 3-38). All fit equations have a form of

$$y = a \cdot e^{-bx} \quad (y \text{ is } R_p \text{ and } x \text{ is } 1/T) \quad \text{Equation 3-2}$$

and rewriting this will yield

$$\text{Log}(R_p) = \text{Log}(a) - b \times \frac{1}{T} \quad \text{Equation 3-3}$$

where $-b$ is the slope of the curve.

From the fitting equations shown in the figure, we can see that most systems can be grouped into one category – with slope varying from -2500 to -3200 . D100 falls out of this group because its slope is much smaller ~ -1400 .

From the activation energy theory of a thermally assisted process [2], we have:

$$Rp \propto e^{-\frac{Q}{RT}} \quad \text{Equation 3-4}$$

where Q is the apparent activation energy of the process. From the slopes of curves, we can calculate the apparent activation energy Q of the plastic zone deforming process. Values of calculated Q are listed in Table 3-9. We see that DP's and B100 have about the same apparent activation energy, but D100 has a much smaller value. D100 also has the biggest plastic zone size among all systems studied. This is due to the easiness and big magnitude of plastic deformation in the material, which involves more flow and ductility.

3.1.6 SUMMARY OF DATA ANALYSIS

Summary of flexural properties vs. temperature for D100, DP, P100 and B100 are presented in Figure 3-27 through Figure 3-30.

For DP systems:

- 1) D100 is unique in having highest flexural strain and lowest flexural strength and modulus over all temperature range. Its flexural modulus change over all temperatures is the most dramatic and results in the steepest modulus vs. temperature curve.
- 2) D100 is also unique in its fracture toughness change vs. temperature. The curve reaches a maximum point at -35°C . Its toughness at 0°C , -20°C , -40°C and -60°C remains almost the same at $0.72 \pm 0.03 \text{ MPa m}^{1/2}$, which is the highest value in the testing temperature range.
- 3) The behavior of D100 is attributed to its molecular structure of the di-functional crosslinker with no bulky groups, which gives rise to its high deformation ability and weak strength and stiffness. The deformation is even big at -40°C and -60°C , over 100°C below its T_g .

- 4) P100 is the strongest and most brittle system among all, with maximum flexural stress and modulus curves in the highest positions and its fracture toughness curve in the lowest. The toughness didn't change much with temperature, resulting in a flat shape of the toughness vs. temperature curve.
- 5) P100's stiffness and brittleness can also be explained by its molecular structure. P crosslinker has two phenyl groups on the side chain. It is also a short molecule, and reduces the network mobility when crosslinked into the network. These phenyl groups present a great obstacle to the network chain mobility.
- 6) Combination of DP crosslinker results in systems behaving more similar to the P100 than to the D100, which means the effect of the P crosslinker, particularly from its molecular structure, is dominant.
- 7) Comparing D100, DP73, DP55, DP37 and P100 in increasing P crosslinker content, we see that maximum flexural stress and modulus curves of DP series sit in between those D100 and P100. The bigger the P crosslinker content, the more rigid and stronger the system becomes. The relative changes to RT values at both -40°C and 60°C also become smaller with increasing P content.
- 8) Comparing DP73, DP55, DP37 and P100 in increasing P crosslinker content, the fracture toughness vs. temperature curves flattens. DP73 is more sensitive to temperature changes than DP37 and DP55. As P content increases, the relative decrease in toughness at the high temperature end also becomes smaller.
- 9) For D, DP's and P, fracture toughness vs. temperature curves all undergo maximum points at certain peaking temperatures. This temperature shifts to a higher value with increasing P content.

For B100:

- 10) B100 is moderately strong and stiff, with strength and modulus values closer to DP55 and DP37. They also experience has the least change with temperature, leading to curves with smaller slope.
- 11) B100 has the highest fracture toughness at temperatures above 0°C, but its value decreases substantially at temperatures below 0°C. B100 demonstrates a higher sensitivity to temperature change, especially at low temperatures. Its toughness peaking temperature is around 30°C.
- 12) Compared to P, B crosslinker has phenyl groups positioned on the backbone, not on the side chain. B also brings in fewer phenyl groups into the network compared to P. The backbone phenyl groups provide rigidity, but their hindrance to chain movement is low. Thus, B100 offers a better balance of rigidity and deformation ability of the network structure, which results in its high toughness.

Finally:

- 13) Tan δ peak and toughness peak difference analyses proves that these two temperatures are closely related. A common difference value of $62^{\circ}\text{C}\pm 4^{\circ}\text{C}$ is found in most crosslinked systems, except that such a value is 100°C in D100.
- 14) Plastic zone analysis proves that D100 has the biggest plastic zone size over all temperatures, and D100 also has the smallest apparent activation energy obtained from the plastic zone calculation. Other DP, P and B systems have close values of the apparent activation energy.
- 15) Both peaking temperature and plastic zone analyses prove that D100 is unique among other P, DP and B systems in its network deformation ability. The molecular structure of D explains for its network deforming mechanism.

Table 3-1 Mechanical properties of silylphenylene (B) crosslinked X1-2672 resin (B100) as a result of varying testing temperature.

Temp.	Maximum flexural stress (MPa)		Maximum flexural strain (%)		Flexural Modulus (GPa)		K_{Ic} (MPa m ^{1/2})		P_{max}/P_q	Plastic zone size (μ m)
	Ave	Stdev	Ave	Stdev	Ave	Stdev	Ave	Stdev	Ave	Ave
-40°C	72.40	±6.55	5.47	±0.64	1.96	±0.12	0.37	±0.04	1	1.39
-20°C	67.89	±5.52	7.6	±1.67	1.90	±0.04	0.46	±0.04	1	2.44
0°C	62.16	±1.67	7.65	±0.22	1.77	±0.03	0.72	±0.05	1	7.12
20°C	46.17	±1.27	7.23	±0.28	1.63	±0.06	1.03	±0.06	1.038	26.4
40°C	35.58	±0.96	7.4	±0.60	1.32	±0.03	0.96	±0.02	1.108	38.62
60°C	21.83	±0.92	8.49	±0.95	0.94	±0.08	0.71	±0.02	1.238	56.14

Table 3-2 A summary of temperature and rate effects on fracture toughness of the silylphenylene crosslinked X1-2672 (B100).

Temp	-40°C			-20°C			0°C			
	Rate	K_q (MPa m ^{1/2})	P_{max}/P_q	K_{max} (MPa m ^{1/2})	K_q (MPa m ^{1/2})	P_{max}/P_q	K_{max} (MPa m ^{1/2})	K_q (MPa m ^{1/2})	P_{max}/P_q	K_{max} (MPa m ^{1/2})
-40°C	1 mm/min	0.369	1.000	0.369	0.371	1.000	0.371	0.697	1.000	0.697
	stdev	0.035		0.035	0.025		0.025	0.053		0.053
-20°C	10 mm/min	0.366	1.000	0.366	0.455	1.000	0.455	0.716	1.000	0.716
	stdev	0.036		0.036	0.041		0.041	0.049		0.049
0°C	100 mm/min	0.300	1.000	0.300	0.303	1.000	0.303	0.331	1.000	0.331
	stdev	0.019		0.019	0.041		0.041	0.034		0.034

Temp	20°C			40°C			60°C			
	Rate	K_q (MPa m ^{1/2})	P_{max}/P_q	K_{max} (MPa m ^{1/2})	K_q (MPa m ^{1/2})	P_{max}/P_q	K_{max} (MPa m ^{1/2})	K_q (MPa m ^{1/2})	P_{max}/P_q	K_{max} (MPa m ^{1/2})
20°C	1 mm/min	1.050	1.142	1.213	0.886	1.316	1.158	0.512	1.570	0.794
	stdev	0.040		0.072	0.064		0.060	0.096		0.074
40°C	10 mm/min	1.038	1.029	1.038	0.907	1.108	0.907	0.706	1.239	0.875
	stdev	0.027		0.027	0.111		0.111	0.023		0.023
60°C	100 mm/min	0.936	1.000	0.936	0.880	1.280	1.077	0.418	2.045	0.843
	stdev	0.068		0.068	0.205		0.059	0.072		0.099

Table 3-3 Mechanical properties of hexamethyltrisiloxane (D) crosslinked X1-2672 (D100) as a result of varying testing temperature.

Temp.	Maximum flexural stress (MPa)		Maximum flexural strain (%)		Flexural Modulus (GPa)		K _{Ic} (MPa m ^{1/2})		P _{max} /P _q	Plastic zone size (μm)
	Ave	Stdev	Ave	Stdev	Ave	Stdev	Ave	Stdev	Ave	Ave
-60°C	71.55	±2.40	9.51	±0.40	1.77	±0.07	0.75	±0.06	1	5.83
-40°C	52.05	±1.33	8.87	±0.87	1.29	±0.06	0.75	±0.07	1	11.02
-20°C	41.47	±3.37	10.83	±0.52	1.15	±0.12	0.69	±0.04	1	14.69
0°C	31.44	±1.46	10.22	±0.40	0.83	±0.08	0.72	±0.05	1.047	27.83
20°C	22.20	±0.52	10.4	±1.10	0.52	±0.03	0.54	±0.03	1.172	31.4
40°C	8.78	±0.26	12.11	±0.26	0.14	±0.00	0.28	±0.02	1.177	53.91

Table 3-4 Mechanical properties of hexamethyltrisiloxane (D) /diphenylsilane (P) crosslinked X1-2672 (DP73) as a result of varying testing temperature.

Temp.	Maximum flexural stress (MPa)		Maximum flexural strain (%)		Flexural Modulus (GPa)		K _{Ic} (MPa m ^{1/2})		P _{max} /P _q	Plastic zone size (μm)
	Ave	Stdev	Ave	Stdev	Ave	Stdev	Ave	Stdev	Ave	Ave
-40°C	63.84	±2.59	7.83	±0.84	1.59	±0.06	0.36	±0.07	1.022	1.69
-20°C	53.68	±0.77	9.27	±1.10	1.51	±0.03	0.65	±0.05	1	7.78
0°C	46.43	±0.66	8.02	±0.21	1.34	±0.03	0.78	±0.04	1	14.97
20°C	33.34	±0.85	9.48	±1.10	1.07	±0.01	0.75	±0.02	1.106	26.84
40°C	17.41	±0.39	8.94	±0.55	0.63	±0.05	0.54	±0.07	1.199	51.05
60°C	7.32	±0.58	9.66	±0.52	0.17	±0.02	0.19	±0.01	1.573	35.75

Table 3-5 Mechanical properties of hexamethyltrisiloxane (D) /diphenylsilane (P) crosslinked x1-2672 (DP55) as a result of varying testing temperature.

Temp.	Maximum flexural stress (MPa)		Maximum flexural strain (%)		Flexural Modulus (GPa)		K _{Ic} (MPa m ^{1/2})		P _{max} /P _q Ave	Plastic zone size (μm) Ave
	Ave	Stdev	Ave	Stdev	Ave	Stdev	Ave	Stdev		
-40°C	73.63	±5.18	5.54	±0.91	1.86	±0.09	0.3	±0.03	1	0.88
-20°C	68.30	±2.59	7.89	±0.62	1.63	±0.03	0.5	±0.02	1	2.84
0°C	56.48	±2.14	7.11	±0.74	1.57	±0.06	0.64	±0.04	1	6.81
20°C	42.35	±1.41	7.44	±1.45	1.36	±0.03	0.62	±0.04	1	11.37
40°C	29.41	±1.75	9.54	±0.68	0.98	±0.08	0.64	±0.07	1.038	25.12
60°C	17.00	±2.55	9.78	±0.50	0.50	±0.07	0.43	±0.02	1.08	33.93

Table 3-6 Mechanical properties of hexamethyltrisiloxane (D) /diphenylsilane (P) crosslinked X1-2672 (DP37) as a result of varying testing temperature.

Temp.	Maximum flexural stress (MPa)		Maximum flexural strain (%)		Flexural Modulus (GPa)		K _{Ic} (MPa m ^{1/2})		P _{max} /P _q Ave	Plastic zone size (μm) Ave
	Ave	Stdev	Ave	Stdev	Ave	Stdev	Ave	Stdev		
-40°C	82.69	±3.31	6.65	±0.74	2.04	±0.04	0.28	±0.02	1	0.61
-20°C	71.29	±4.57	6.51	±1.85	1.93	±0.10	0.44	±0.03	1	2.02
0°C	68.14	±1.13	8.05	±1.23	1.75	±0.04	0.49	±0.05	1	2.74
20°C	44.45	±0.86	7.64	±0.81	1.61	±0.01	0.59	±0.01	1	9.35
40°C	35.33	±0.34	7.8	±0.25	1.28	±0.04	0.57	±0.04	1	13.81
60°C	23.16	±1.22	8.62	±0.71	0.77	±0.03	0.47	±0.03	1.08	21.84

Table 3-7 Mechanical properties of diphenylsilane (P) crosslinked X1-2672 (P100) as a result of varying testing temperature.

Temp.	Maximum flexural stress (MPa)		Maximum flexural strain (%)		Flexural Modulus (GPa)		K _{Ic} (MPa m ^{1/2})		P _{max} /P _q	Plastic zone size (μm)
	Ave	Stdev	Ave	Stdev	Ave	Stdev	Ave	Stdev	Ave	Ave
-40°C	91.95	±0.37	6.5	±0.35	2.30	±0.09	0.26	±0.01	1	0.42
-20°C	79.57	±0.92	6.33	±0.14	2.23	±0.06	0.26	±0.03	1	0.57
0°C	73.87	±5.10	6.01	±0.00	2.25	±0.26	0.44	±0.02	1	1.88
20°C	70.23	±3.24	7.27	±0.66	2.09	±0.11	0.47	±0.03	1	2.38
40°C	44.66	±3.01	7.5	±2.17	1.42	±0.06	0.44	±0.02	1	5.15
60°C	30.46	±0.09	8.38	±0.85	0.96	±0.01	0.41	±0.01	1	9.61

Table 3-8. Toughness curve peak and DMA Tan δ peak summary.

	toughness peak temperature °C	DMA Tanδ peak temperature °C	temperature difference DMA peak - toughness peak °C
B100	30	88	58
D100	-35	66	101
DP73	10	73	63
DP55	20	80	60
DP37	30	90	60
P100	35	101	66

Table 3-9 Activation energy calculation – B100, D100, DP37, DP55, DP73 and P100.

System	Fit equations	Intercept	Q/R	Q(J/mol)
B100	Log(R _p) = Log(0.8072) -3135.7 * (1/T)	-0.09	3135.7	26070.21
D100	Log(R _p) = Log(0.0046) -1423.5 * (1/T)	-2.34	1423.5	11834.98
DP37	Log(R _p) = Log(0.099) -2781.6 * (1/T)	-1.00	2781.6	23126.22
DP55	Log(R _p) = Log(0.1972) -2841.2 * (1/T)	-0.71	2841.2	23621.74
DP73	Log(R _p) = Log(0.1028) -2470.6 * (1/T)	-0.99	2470.6	20540.57
P100	Log(R _p) = Log(0.014) -2476.8 * (1/T)	-1.85	2476.8	20592.12

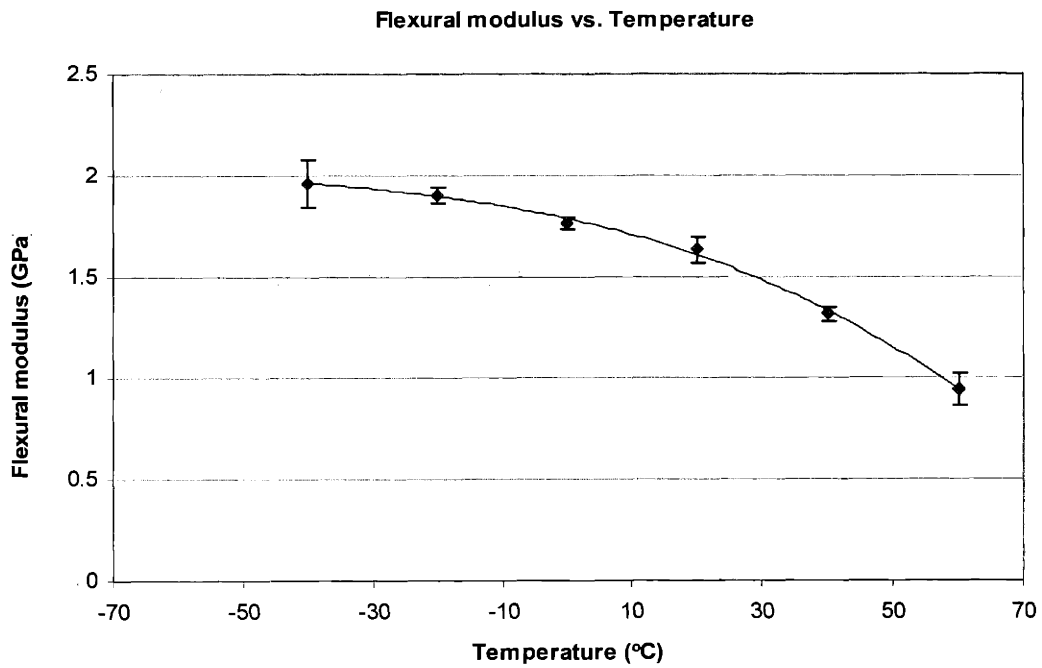


Figure 3-1 Flexural modulus vs. temperature for silylphenylene (B) crosslinked X1-2672 (B100).

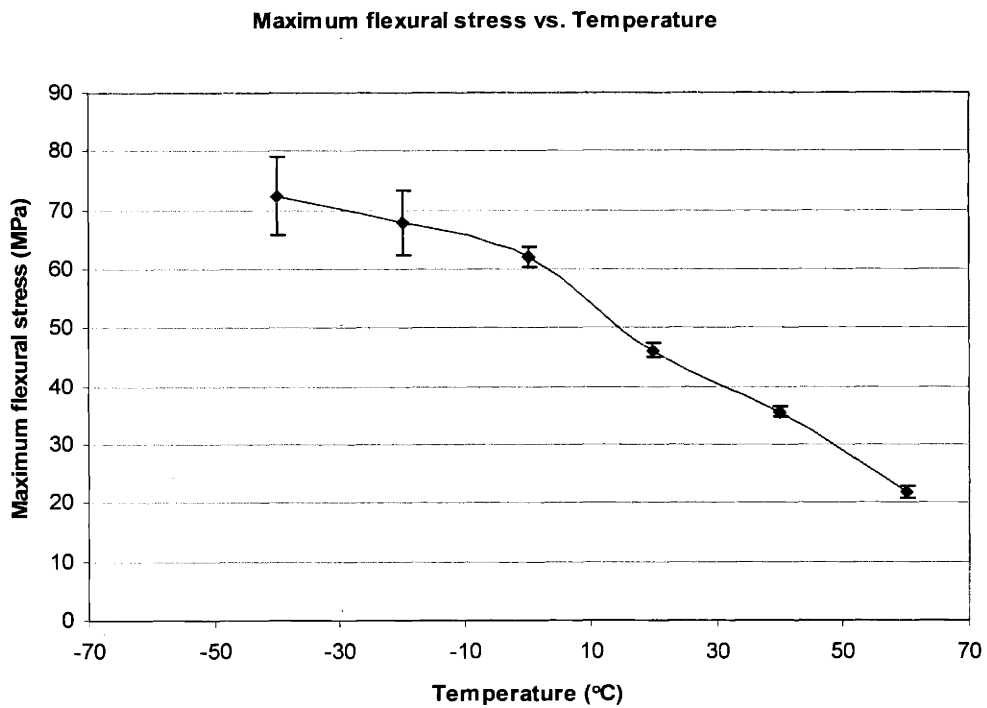


Figure 3-2 Maximum flexural stress change with temperature for silylphenylene (B) crosslinked X1-2672 (B100).

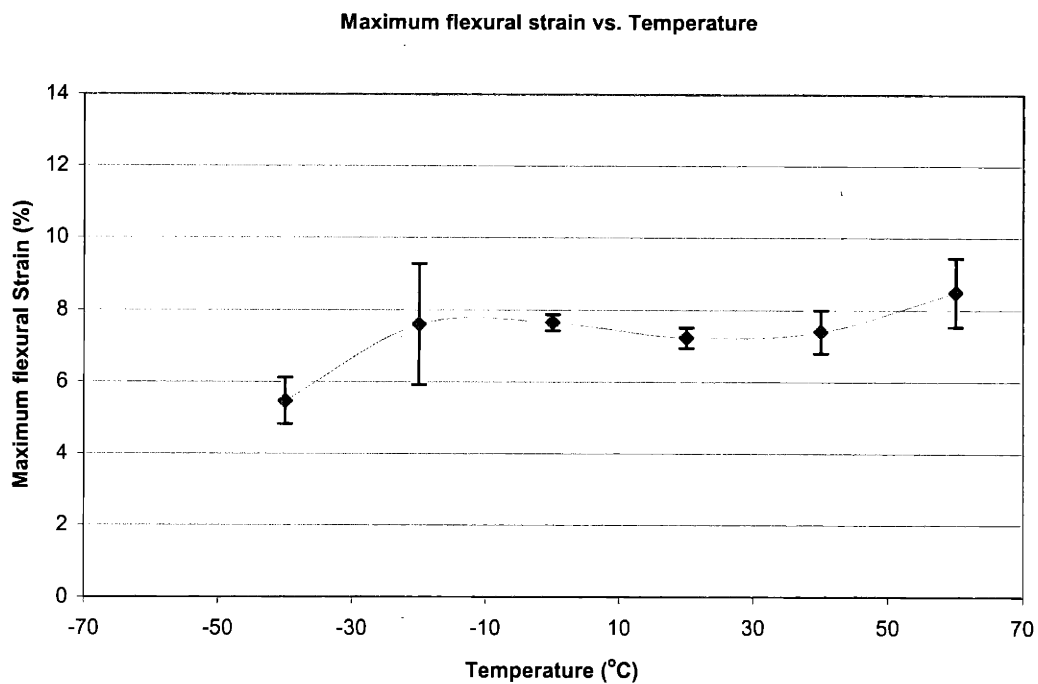


Figure 3-3 Maximum flexural strain change with temperature for silylphenylene (B) crosslinked X1-2672 (B100).

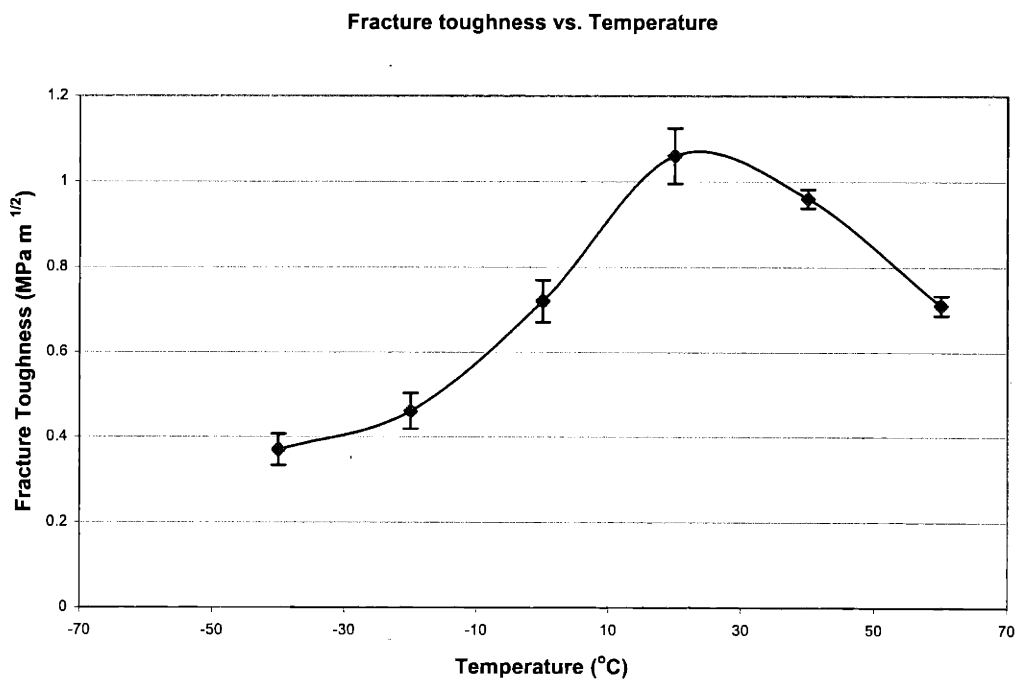


Figure 3-4 Fracture toughness change with temperature for silylphenylene (B) crosslinked X1-2672 (B100).

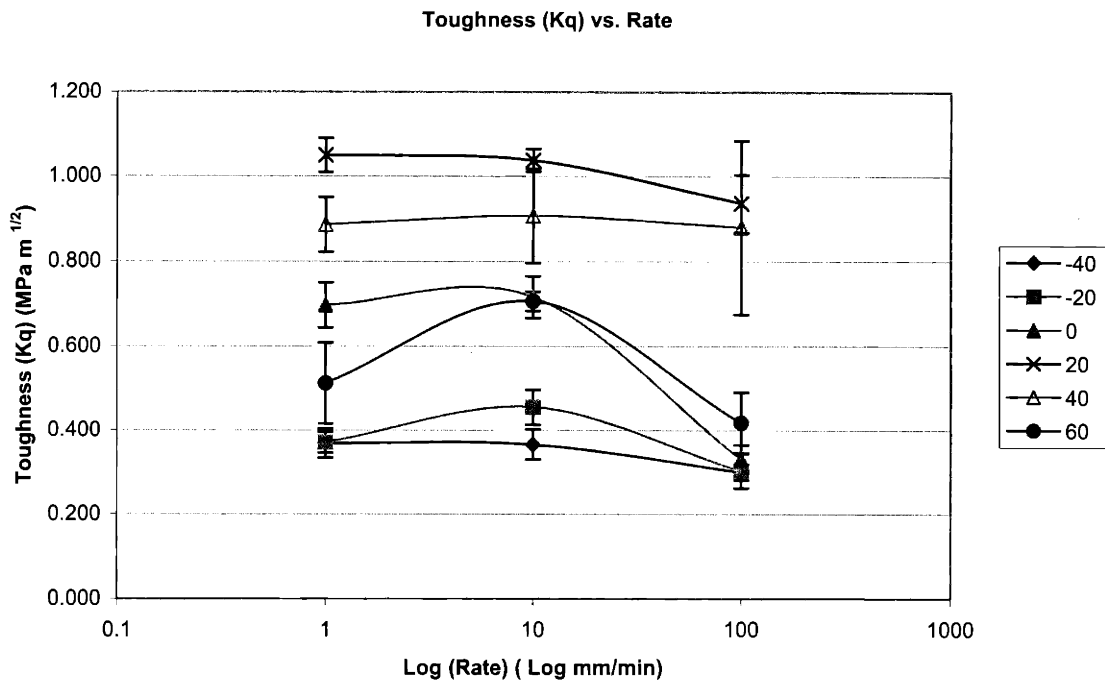


Figure 3-5 Plots of fracture toughness versus Log (rate) at different temperatures for the silylphenylene crosslinked X1-2672 (B100).

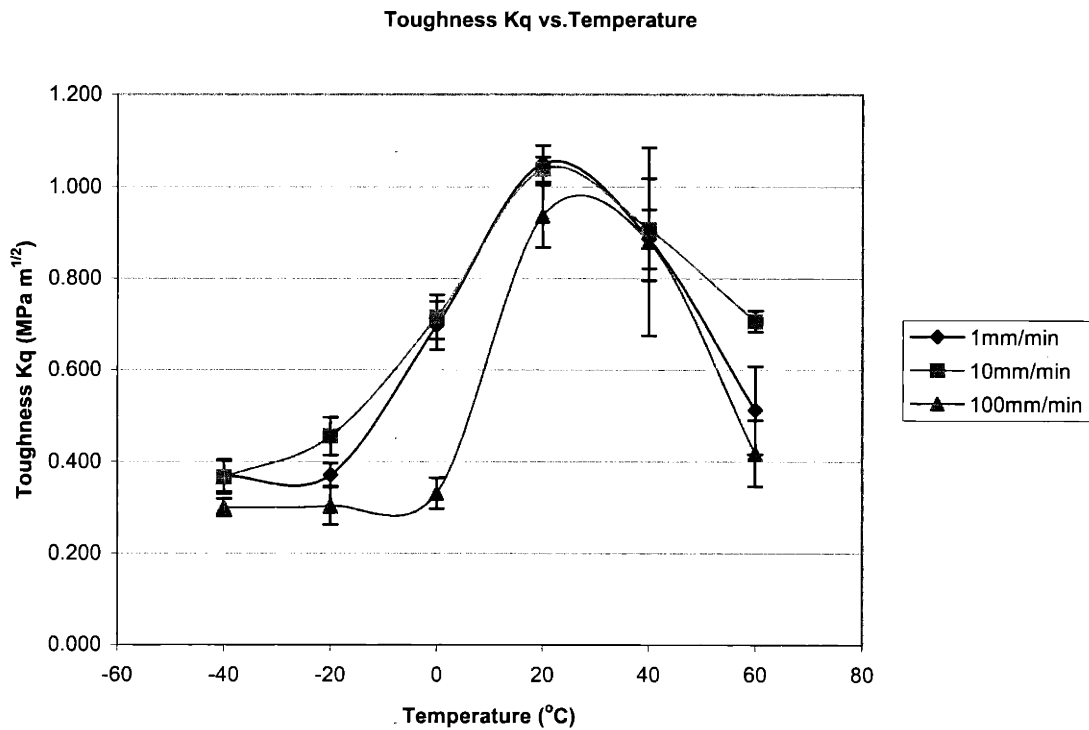


Figure 3-6 Plots of fracture toughness versus temperature at different rates for the silylphenylene crosslinked X1-2672 (B100).

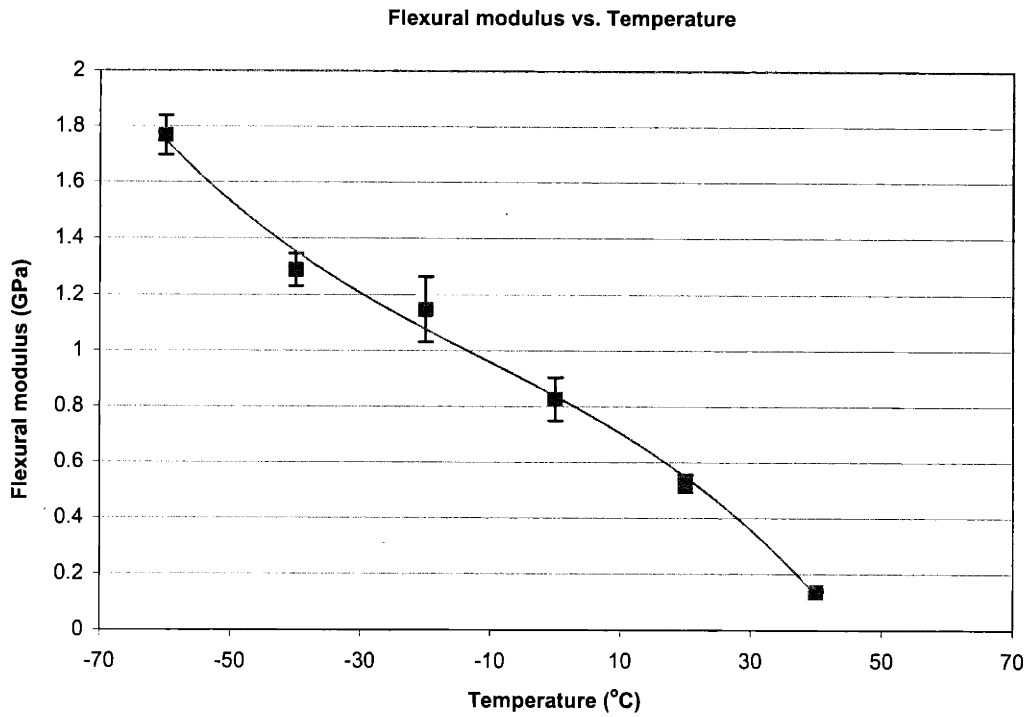


Figure 3-7 Flexural modulus change with temperature for hexamethyltrisiloxane (D) crosslinked X1-2672 (D100).

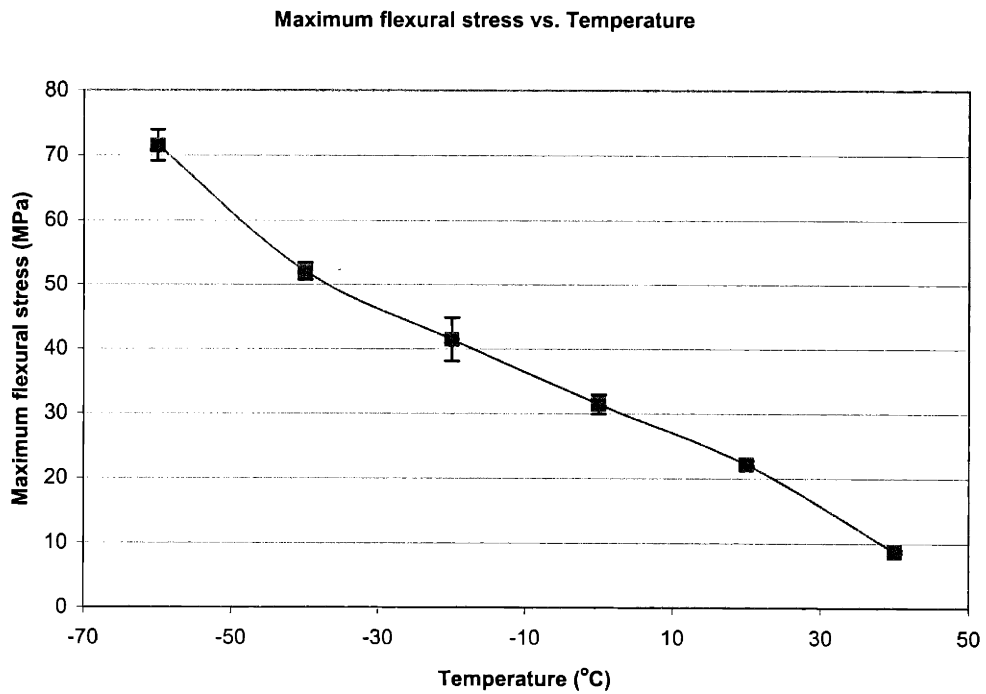


Figure 3-8 Maximum flexural stress change with temperature for hexamethyltrisiloxane (D) crosslinked X1-2672 (D100).

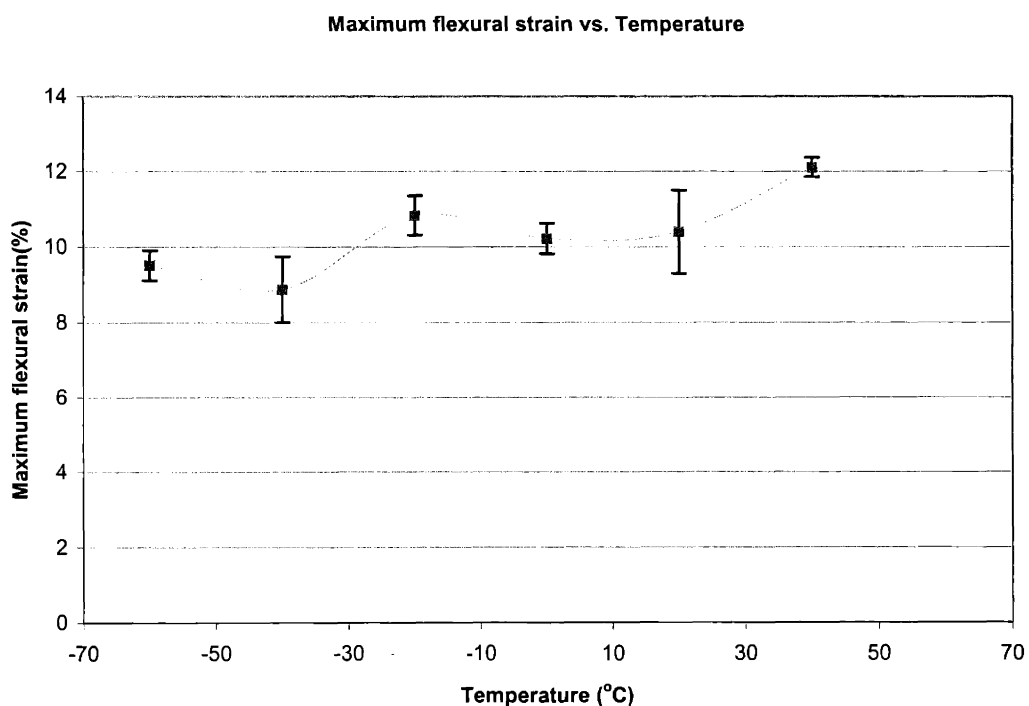


Figure 3-9 Maximum flexural strain change with temperature for hexamethyltrisiloxane (D) crosslinked X1-2672 (D100).

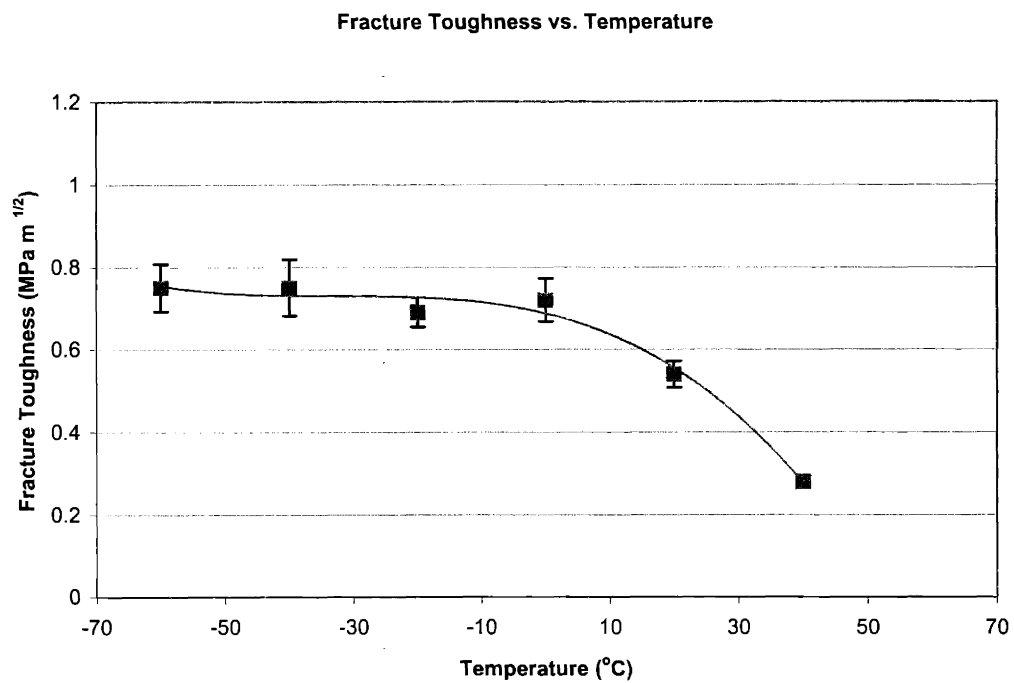


Figure 3-10 Fracture toughness change with temperature for hexamethyltrisiloxane (D) crosslinked X1-2672 (D100).

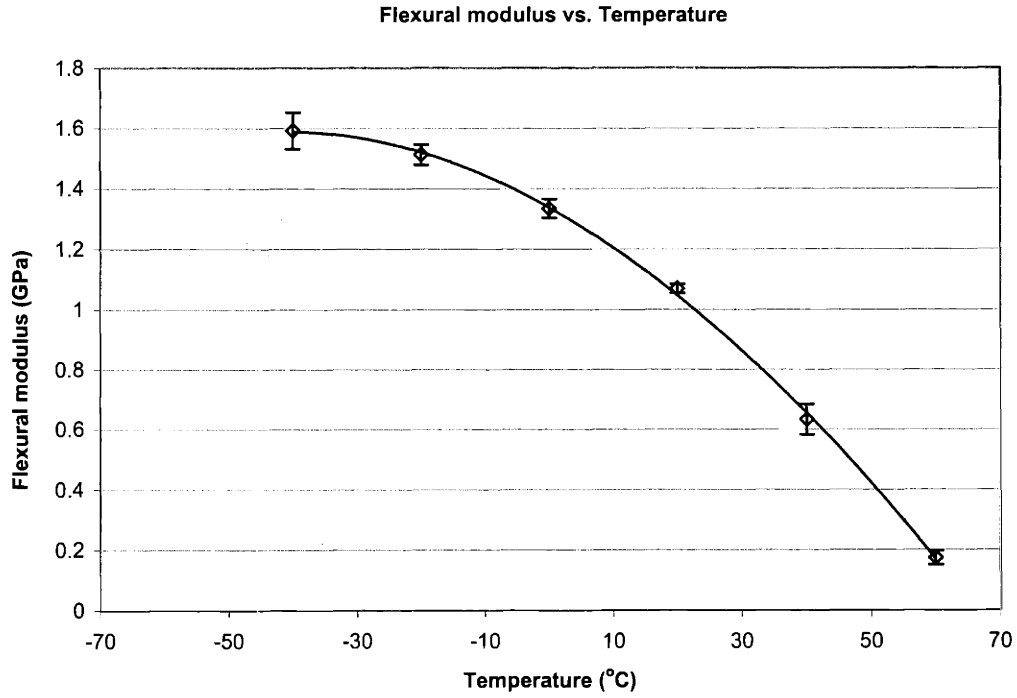


Figure 3-11 Flexural modulus change with temperature for hexamethyltrisiloxane (D)/diphenylsilane (P) crosslinked X1-2672 (DP73).

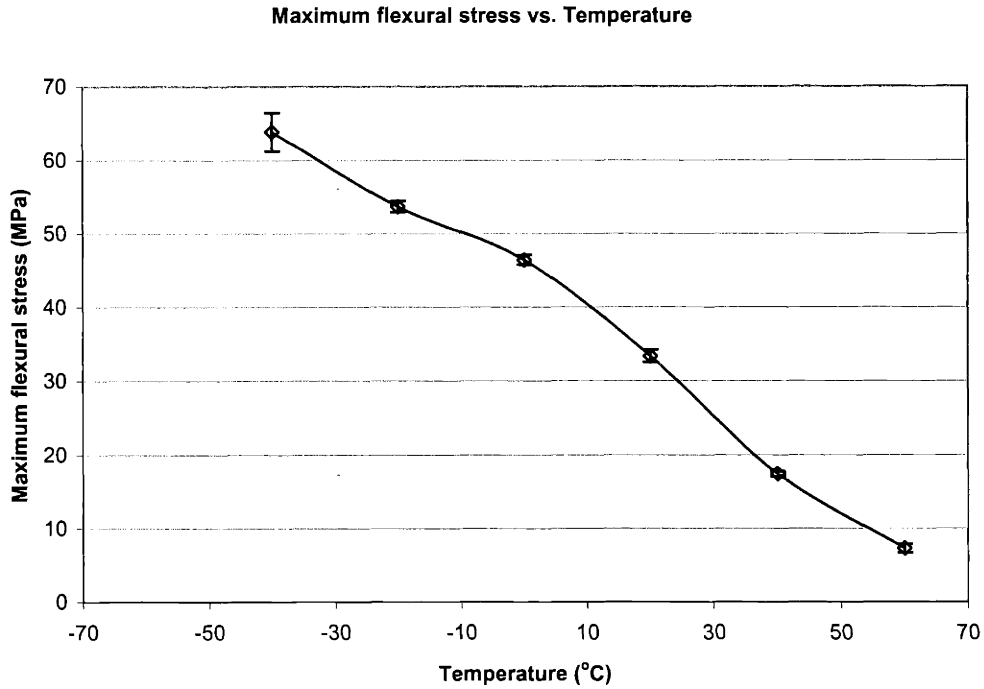


Figure 3-12 Maximum flexural stress change with temperature for hexamethyltrisiloxane (D) / diphenylsilane (P) crosslinked X1-2672 (DP73).

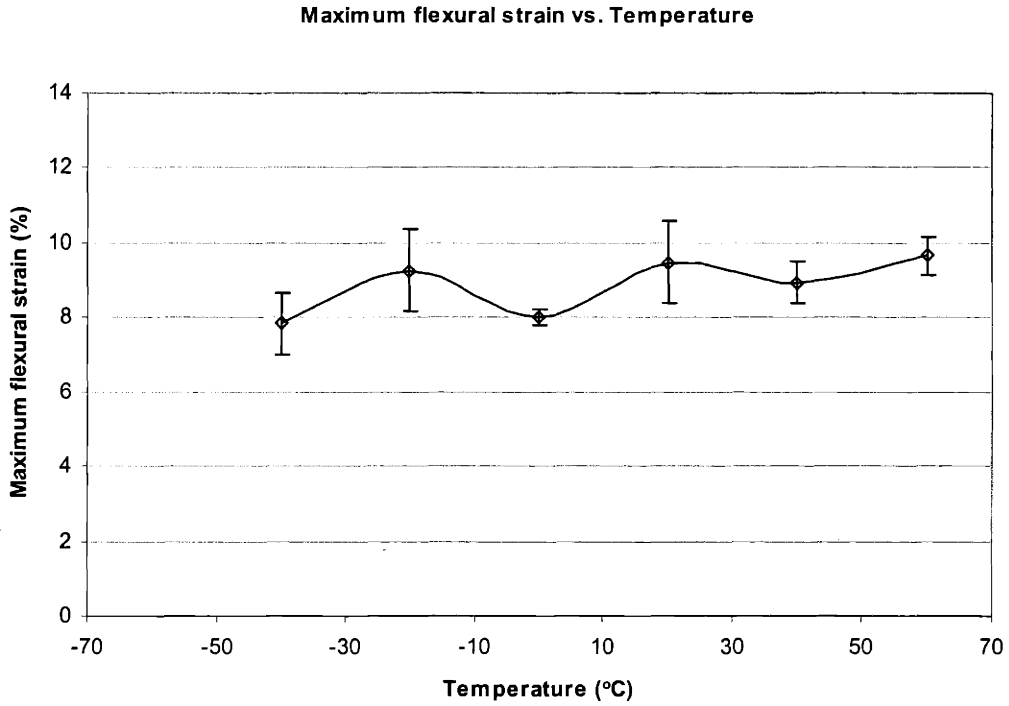


Figure 3-13 Maximum flexural strain change with temperature for hexamethyltrisiloxane (D) / diphenylsilane (P) crosslinked X1-2672 (DP73).

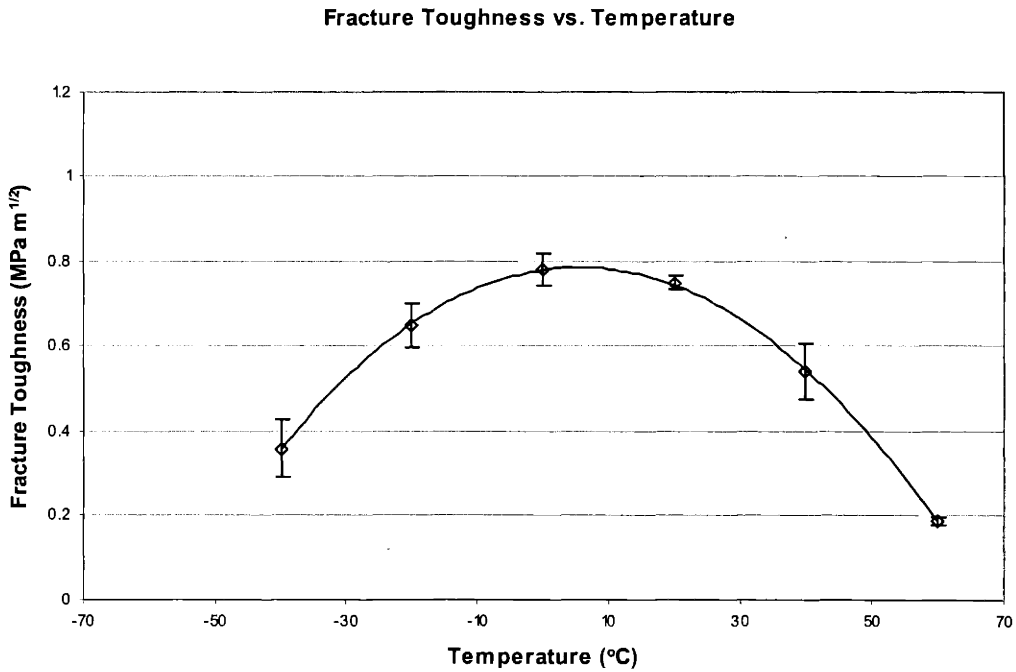


Figure 3-14 Fracture toughness change with temperature for hexamethyltrisiloxane (D) / diphenylsilane (P) crosslinked X1-2672 (DP73).

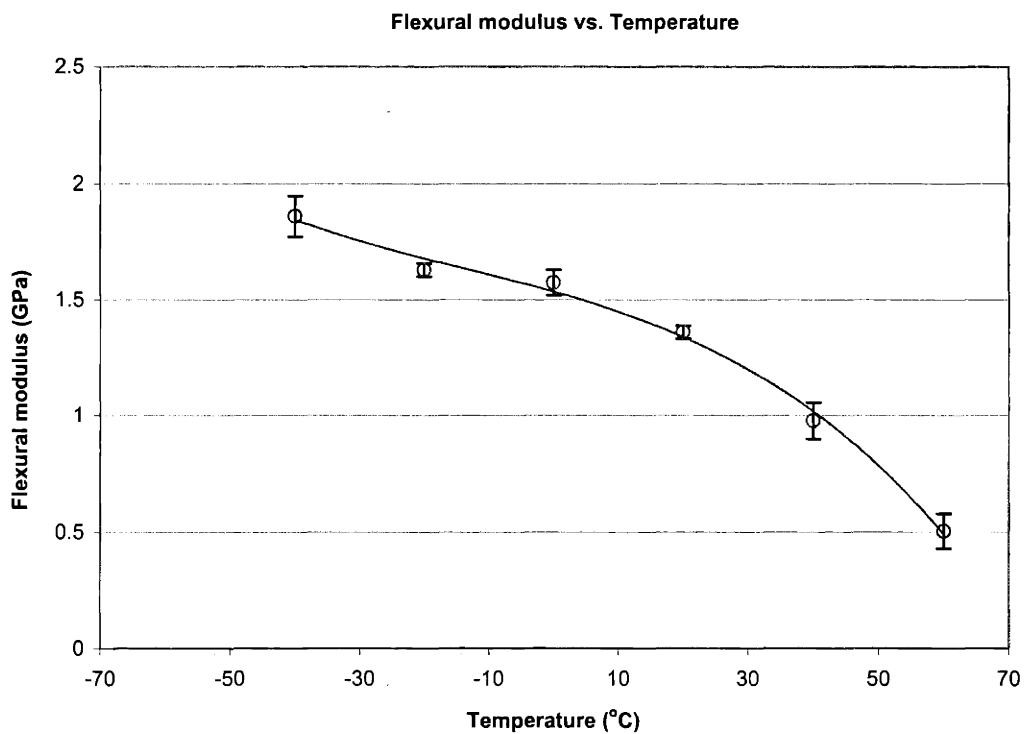


Figure 3-15 Flexural modulus change with temperature for hexamethyltrisiloxane (D) / diphenylsilane (P) crosslinked X1-2672 (DP55).

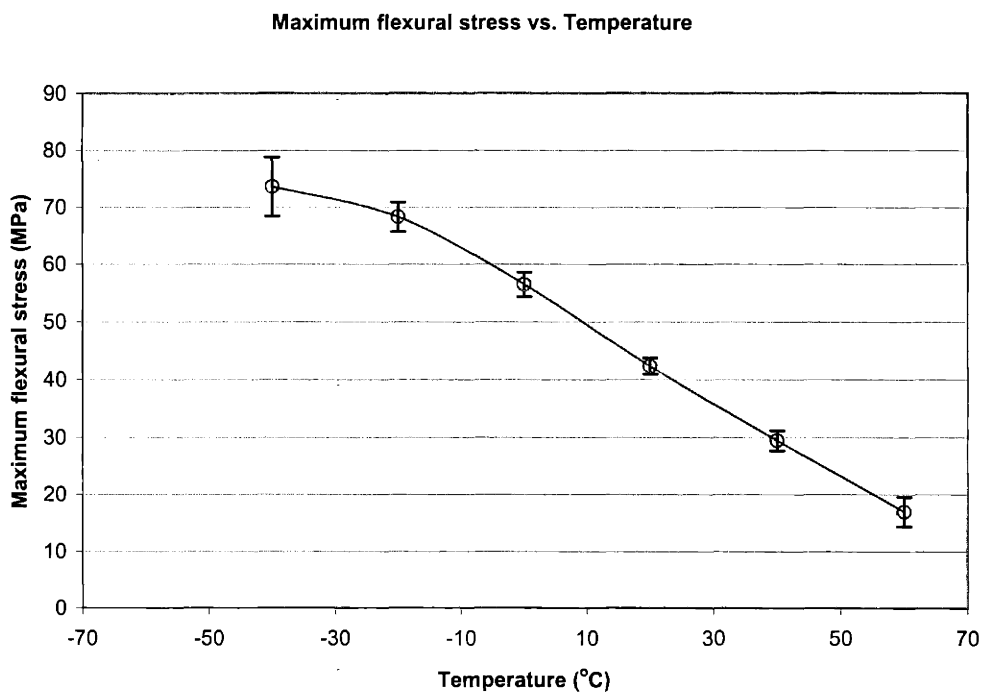


Figure 3-16 Maximum flexural stress change with temperature for hexamethyltrisiloxane (D) / diphenylsilane (P) crosslinked X1-2672 (DP55).

Maximum flexural strain vs. Temperature

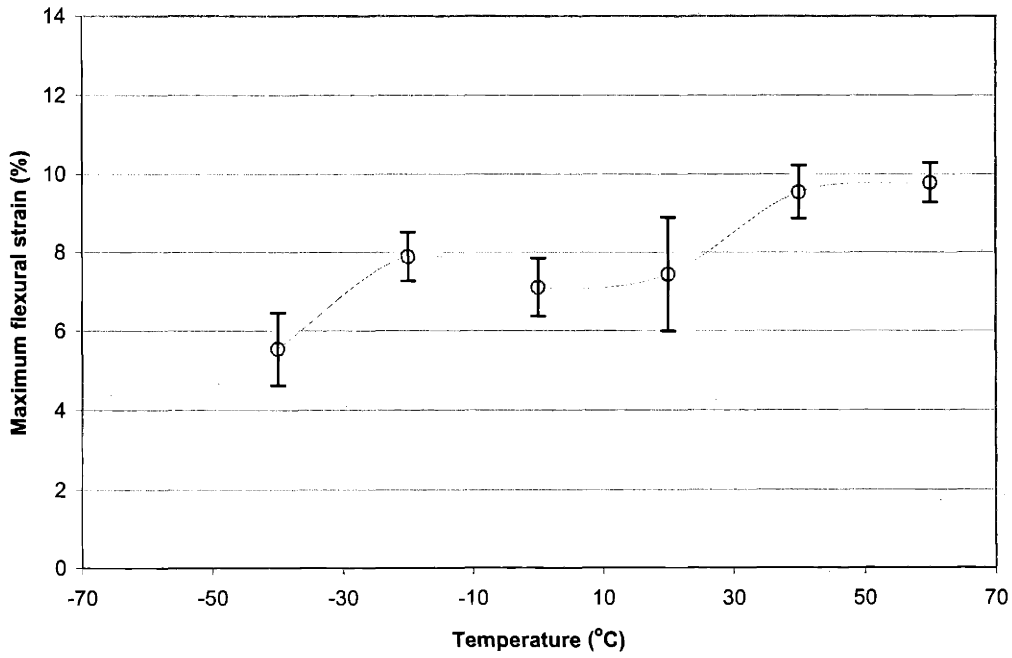


Figure 3-17 Maximum flexural strain change with temperature for hexamethyltrisiloxane (D) / diphenylsilane (P) crosslinked X1-2672 (DP55).

Fracture Toughness vs. Temperature

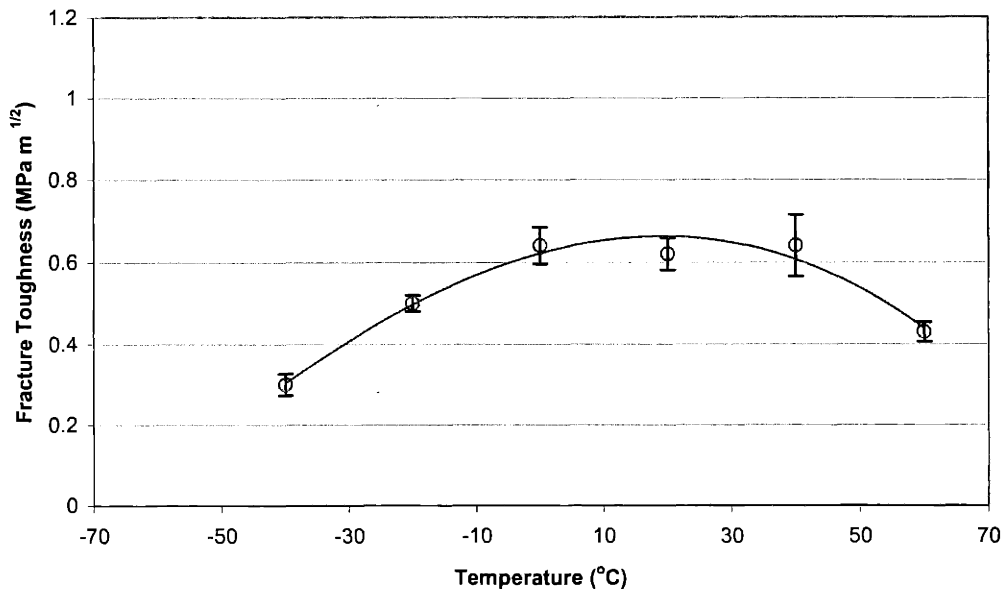


Figure 3-18 Fracture toughness change with temperature for hexamethyltrisiloxane (D) / diphenylsilane (P) crosslinked X1-2672 (DP55).

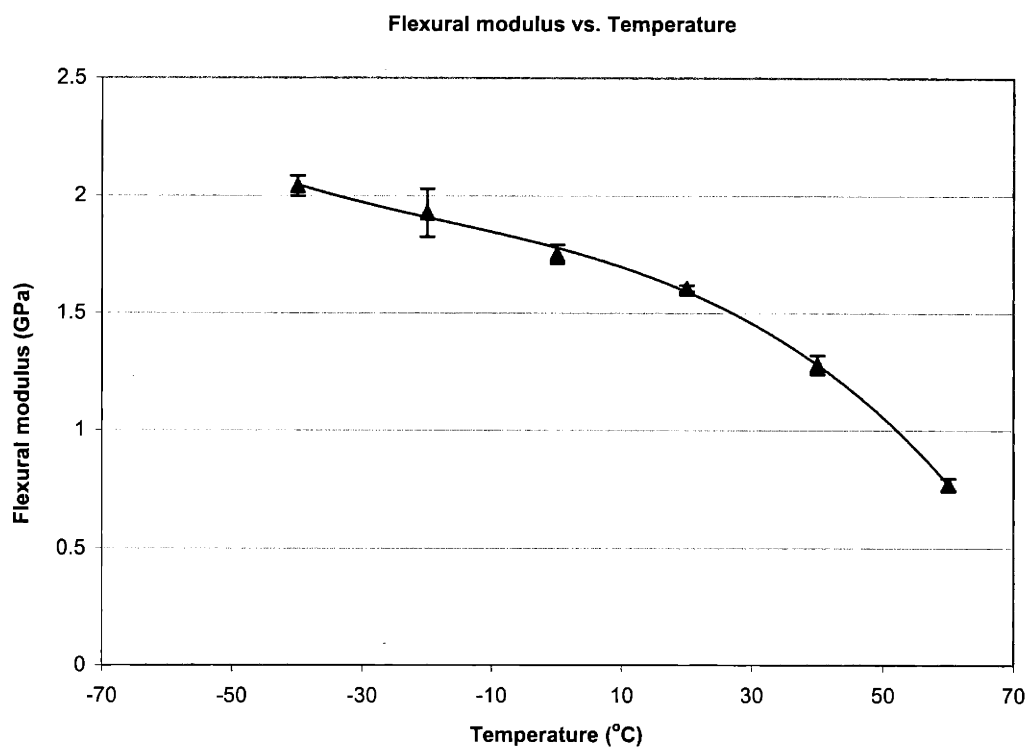


Figure 3-19 Flexural modulus change with temperature for hexamethyltrisiloxane (D)/diphenylsilane (P) crosslinked X1-2672 (DP37).

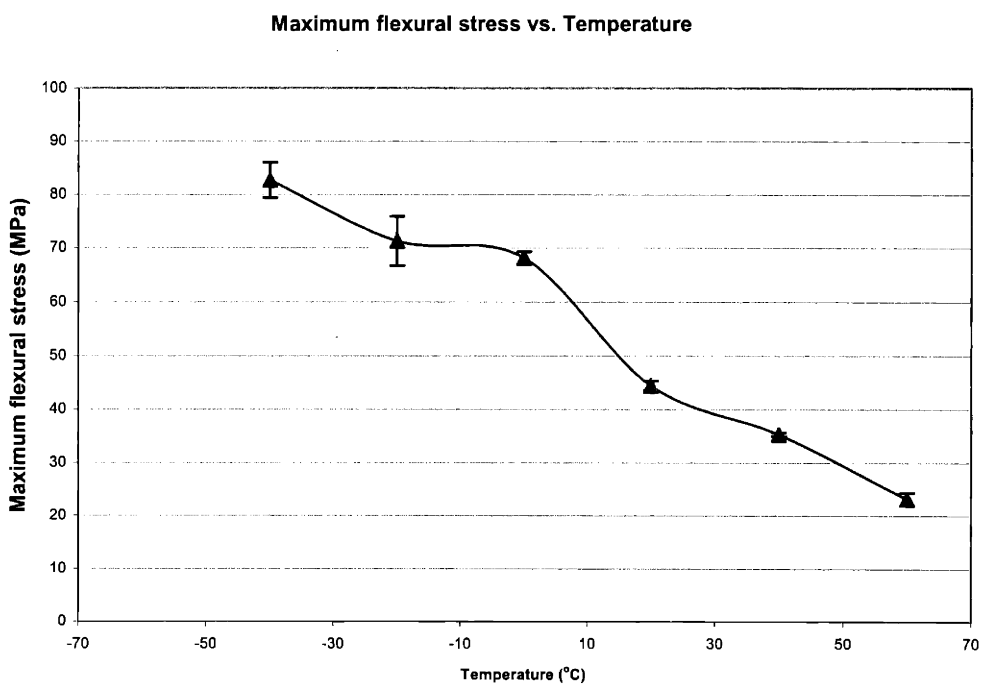


Figure 3-20 Maximum flexural stress change with temperature for hexamethyltrisiloxane (D)/diphenylsilane (P) crosslinked X1-2672 (DP37).

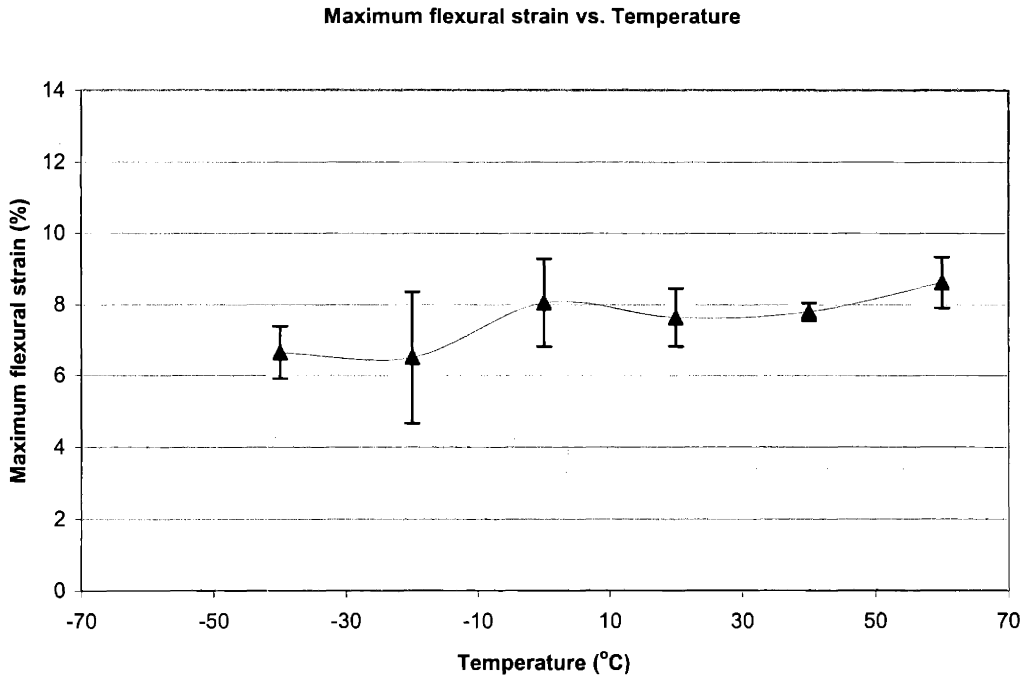


Figure 3-21 Maximum flexural strain change with temperature for hexamethyltrisiloxane (D)/diphenylsilane (P) crosslinked X1-2672 (DP37).

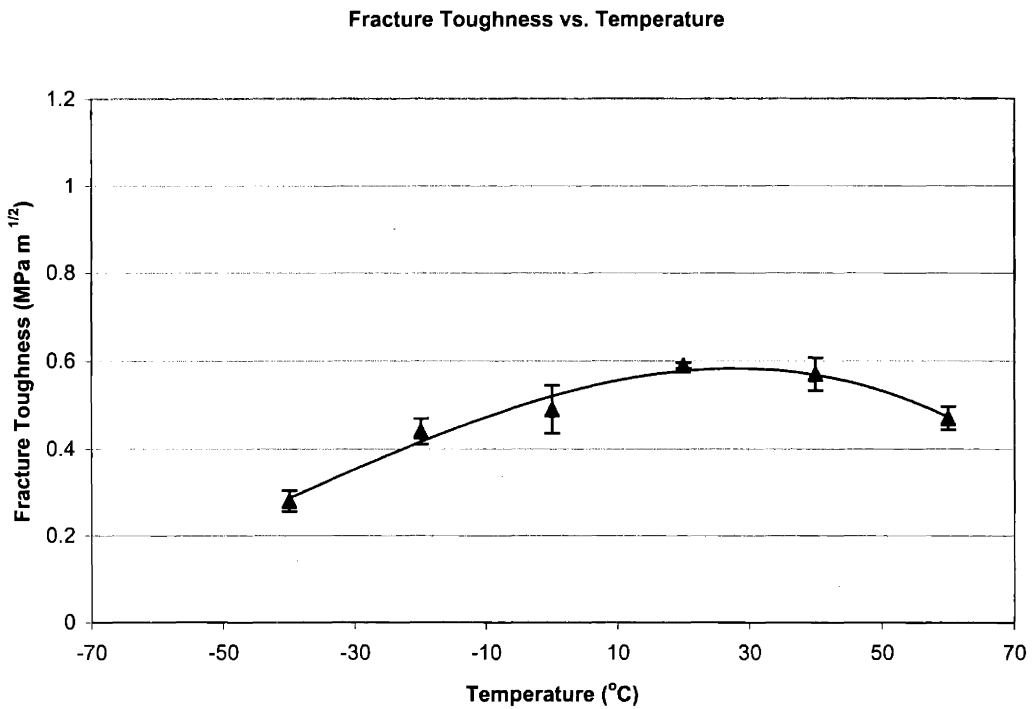


Figure 3-22 Fracture toughness change with temperature for hexamethyltrisiloxane (D) / diphenylsilane (P) crosslinked X1-2672 (DP37).

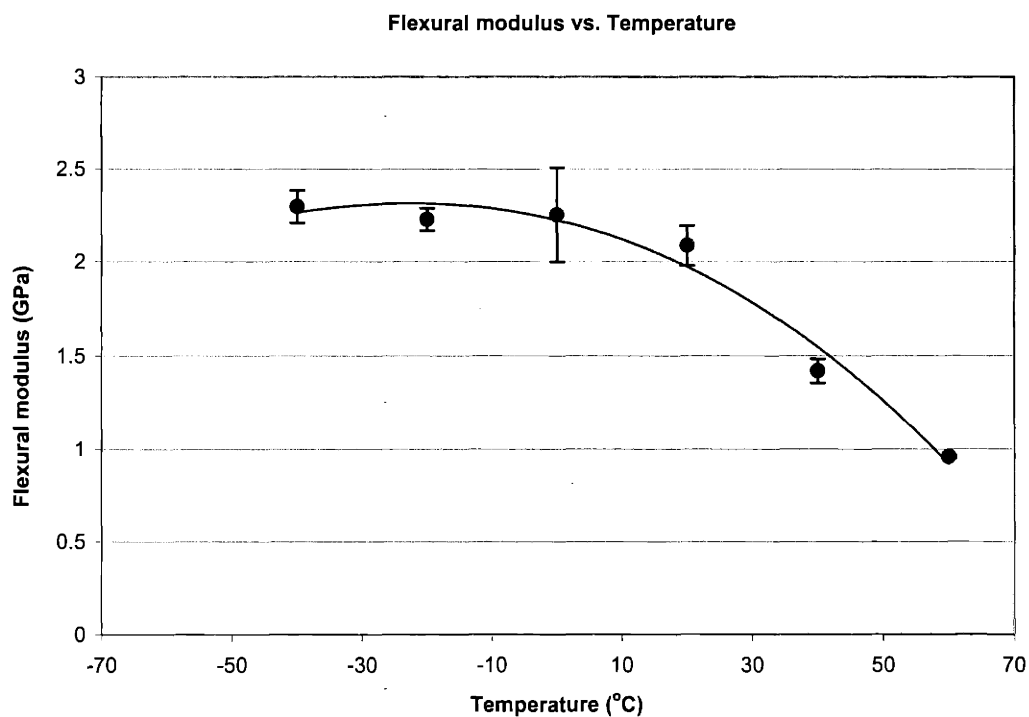


Figure 3-23 Flexural modulus change with temperature for diphenylsilane (P) crosslinked X1-2672 (P100).

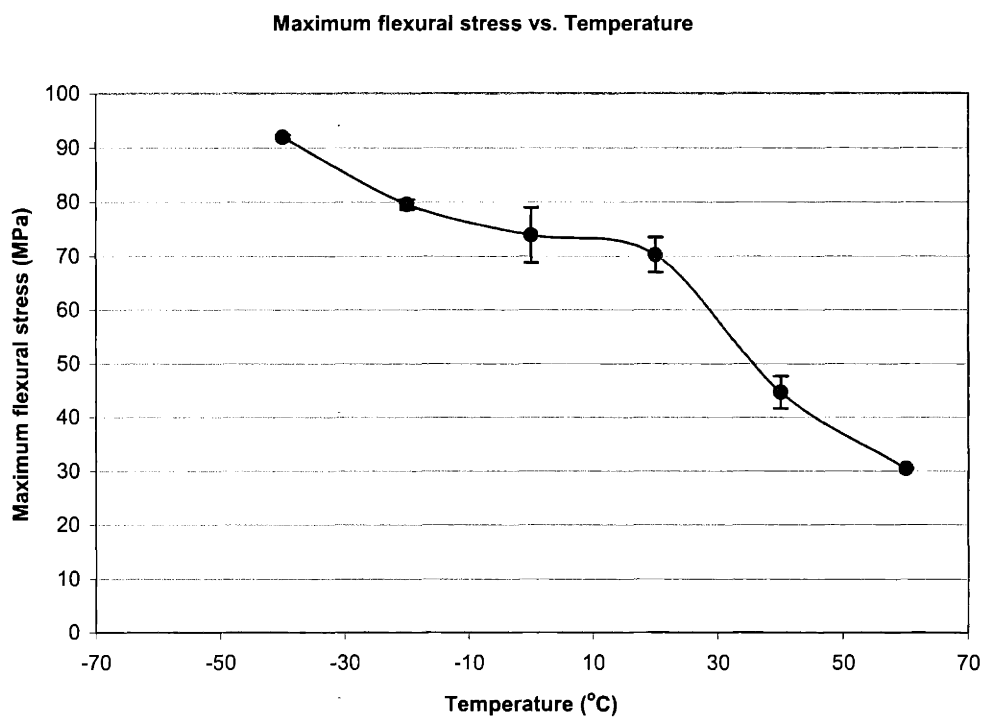


Figure 3-24 Maximum flexural stress change with temperature for diphenylsilane (P) crosslinked X1-2672 (P100).

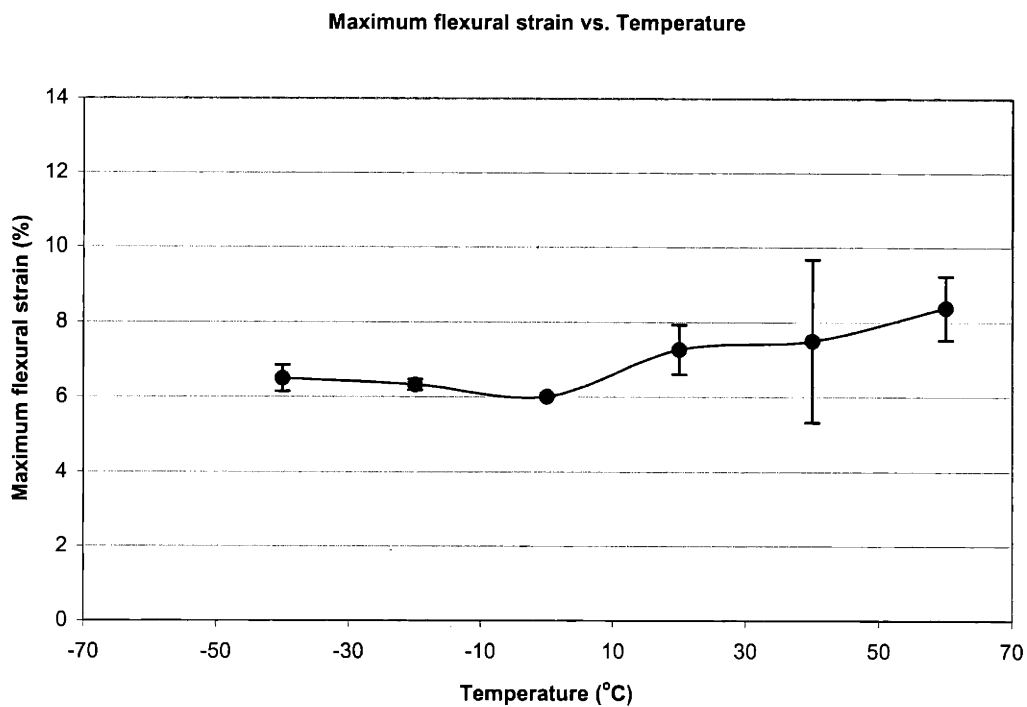


Figure 3-25 Maximum flexural strain change with temperature for diphenylsilane (P) crosslinked X1-2672 (P100).

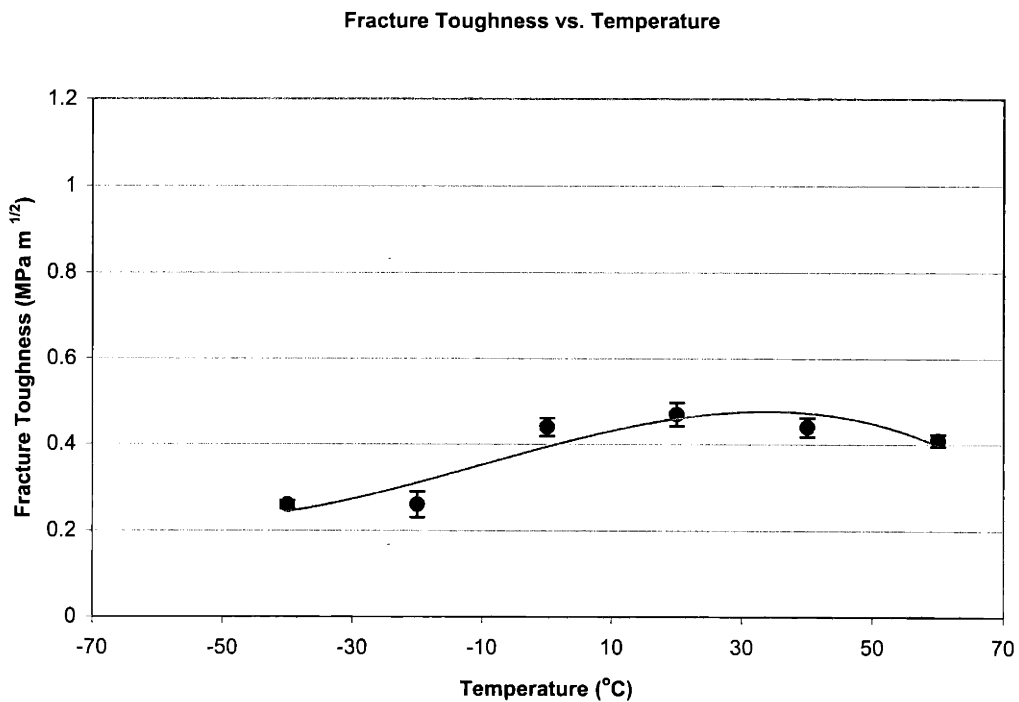


Figure 3-26 Fracture toughness change with temperature for diphenylsilane (P) crosslinked X1-2672 (P100).

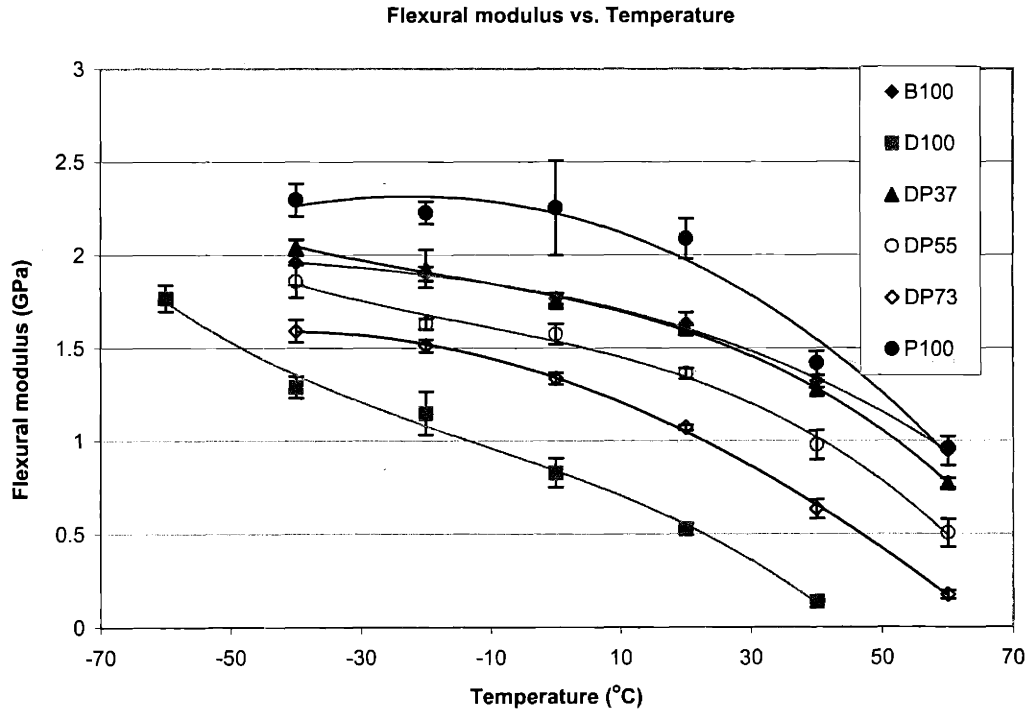


Figure 3-27 Summary of flexural modulus vs. temperature for DP and B100 systems.

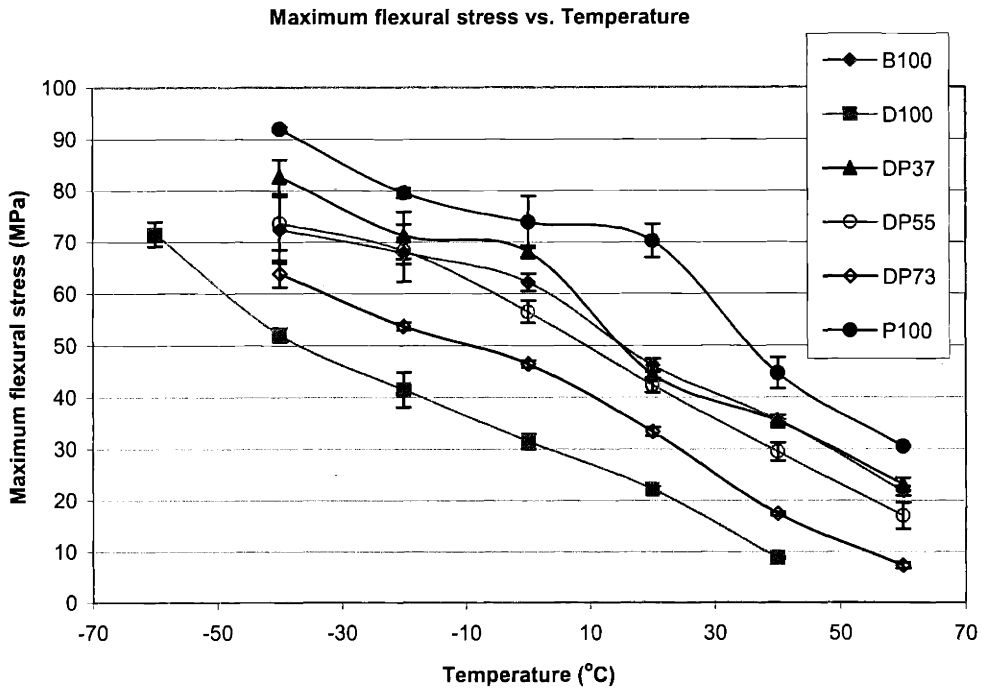


Figure 3-28 Summary of maximum flexural stress vs. temperature for DP and B100.

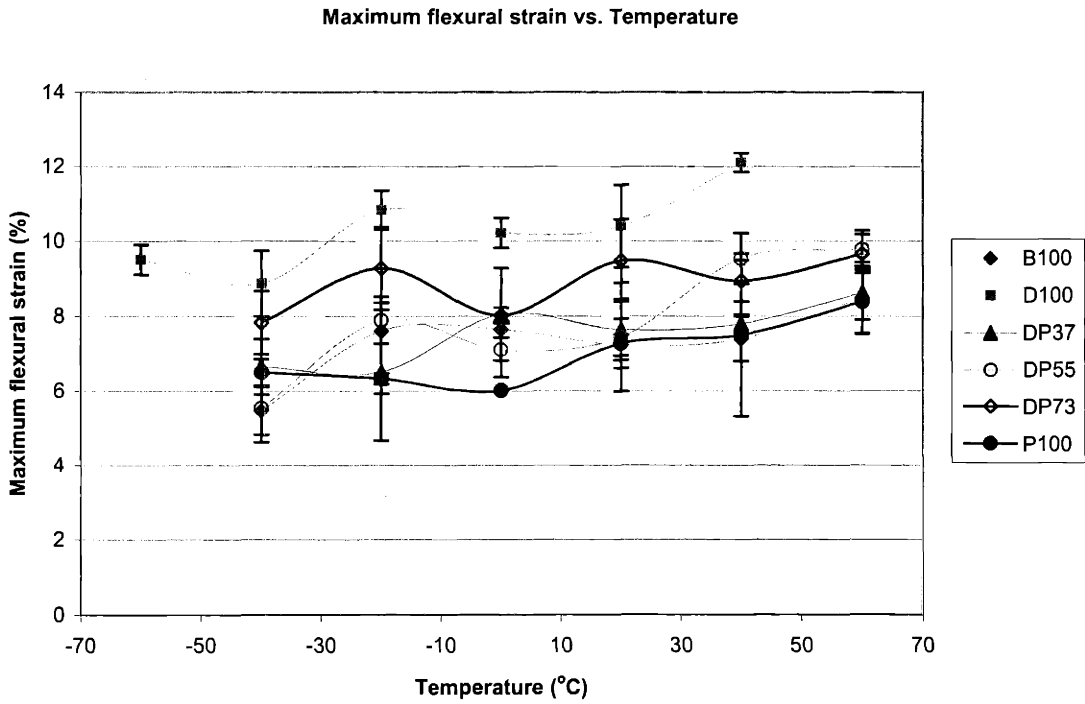


Figure 3-29 Summary of maximum flexural strain vs. temperature for DP and B100 systems.

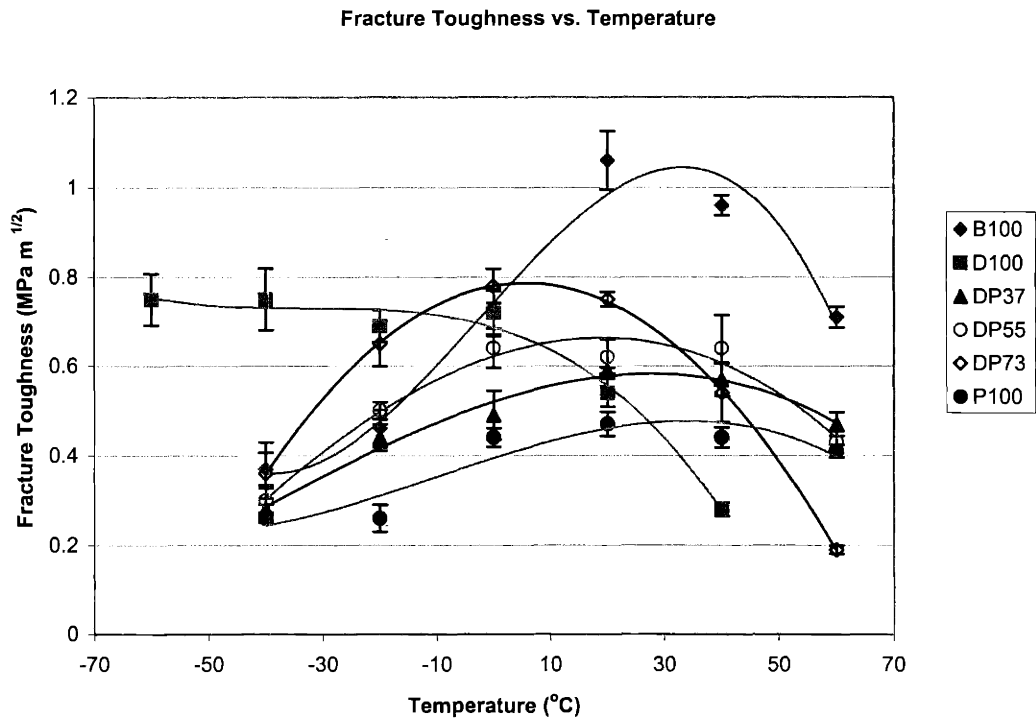


Figure 3-30 Summary of fracture toughness vs. temperature for DP and B100 systems.

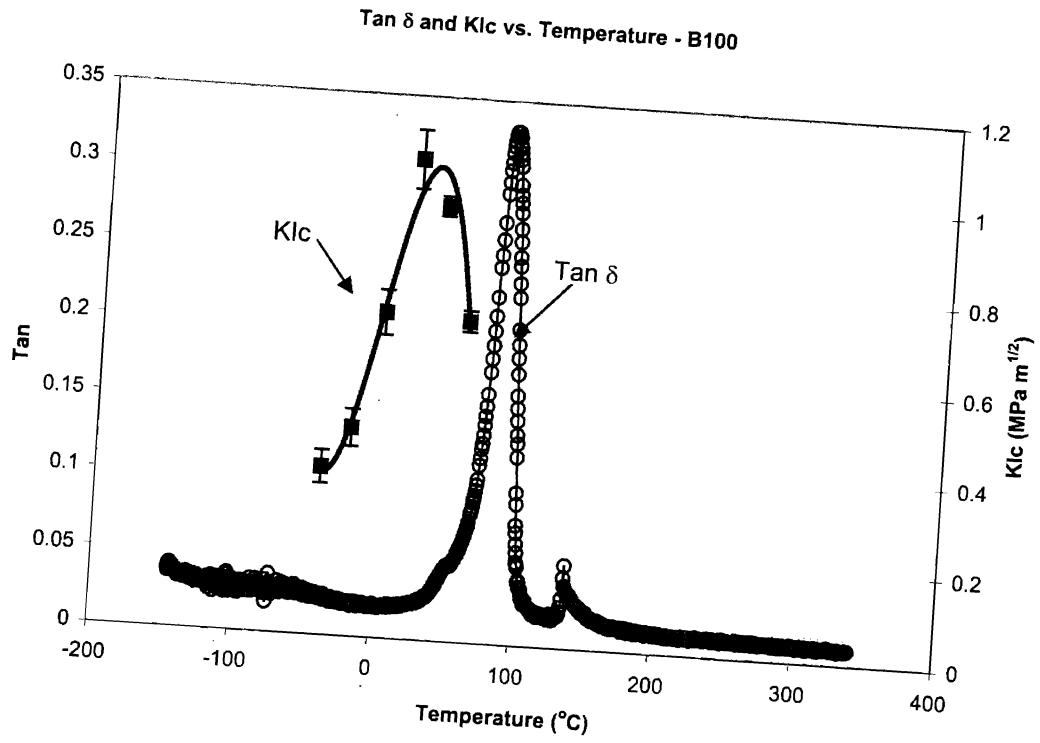


Figure 3-31 DMA Tan δ & fracture toughness of B100 vs. temperature.

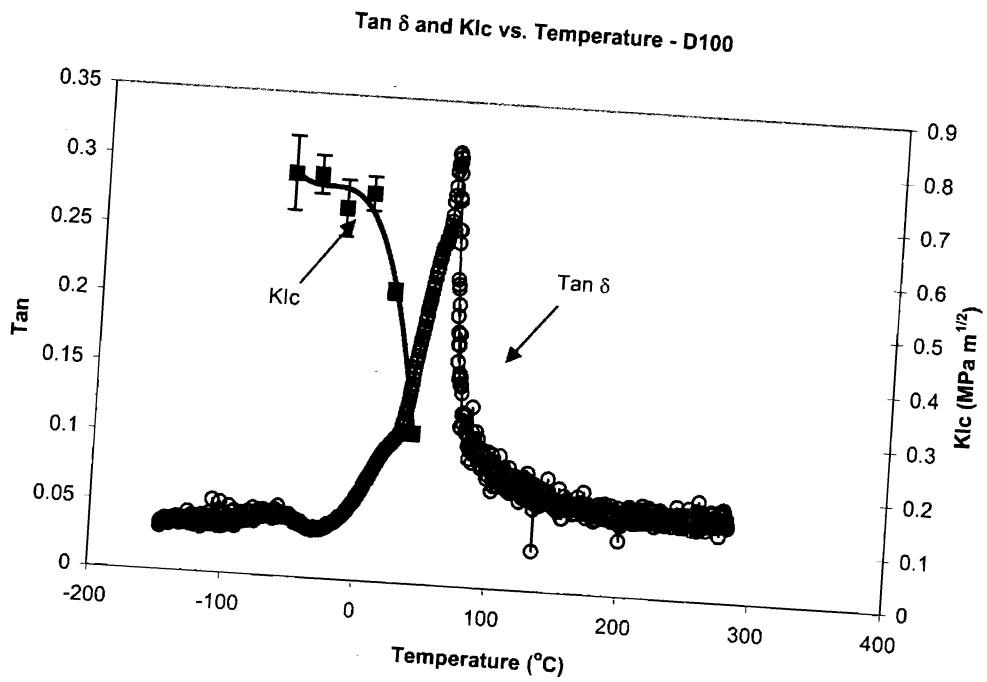


Figure 3-32 DMA Tan δ & fracture toughness of D100 vs. temperature.

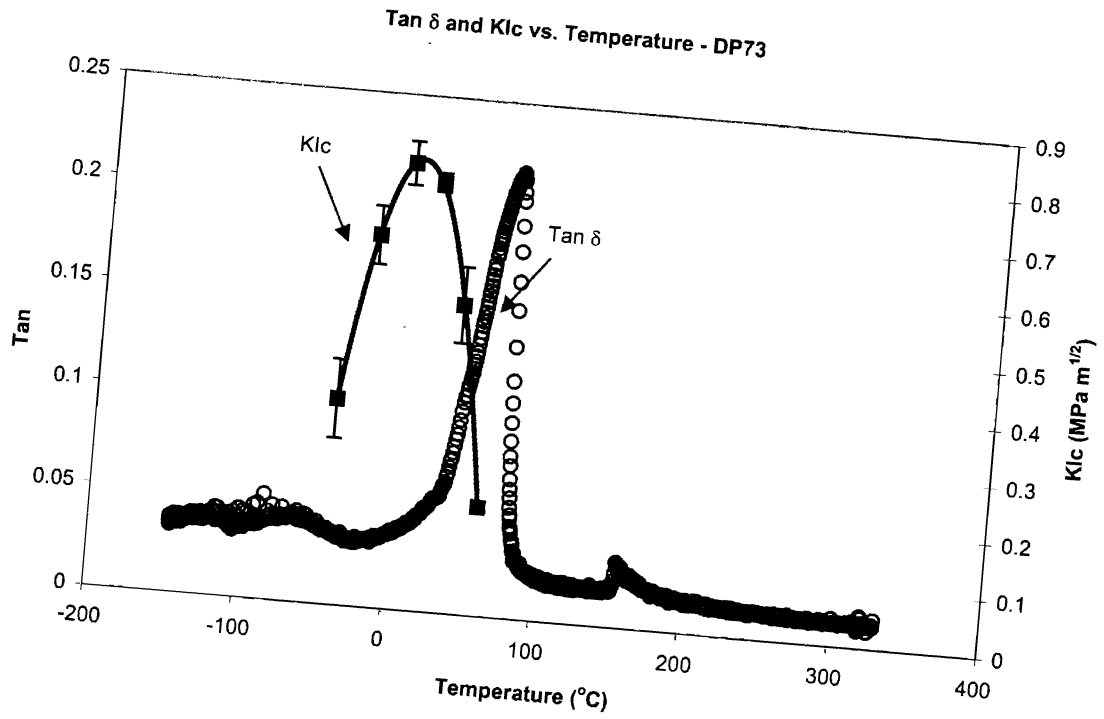


Figure 3-33 DMA Tan δ & fracture toughness of DP73 vs. temperature.

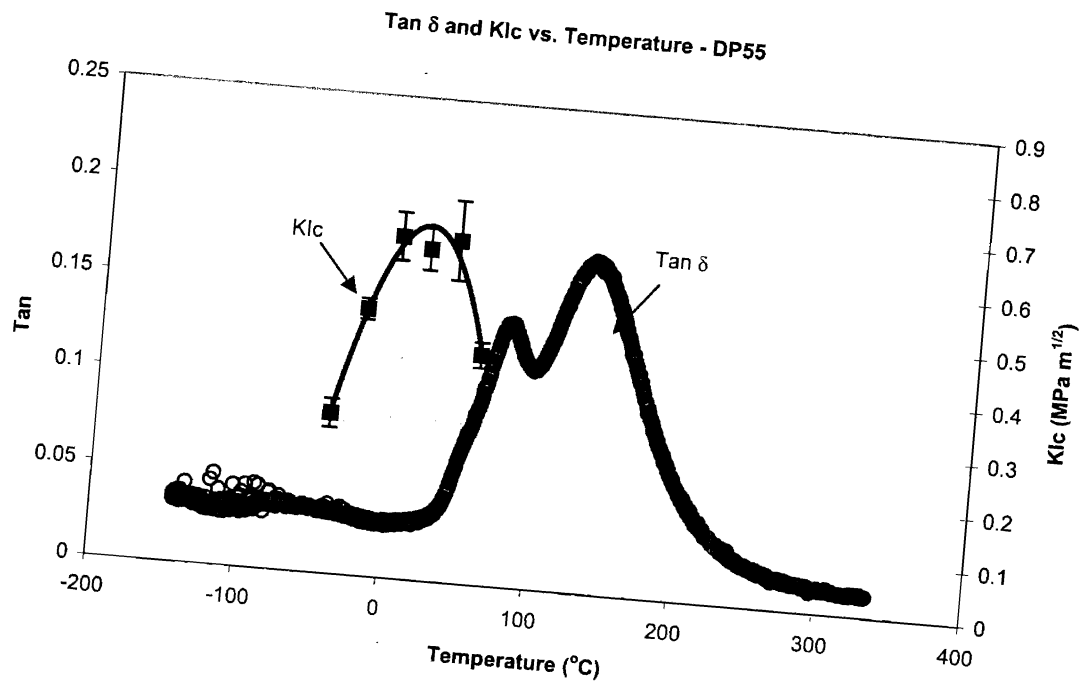


Figure 3-34 DMA Tan δ & fracture toughness of DP55 vs. temperature.

Tan δ and K_{Ic} vs. Temperature - DP37

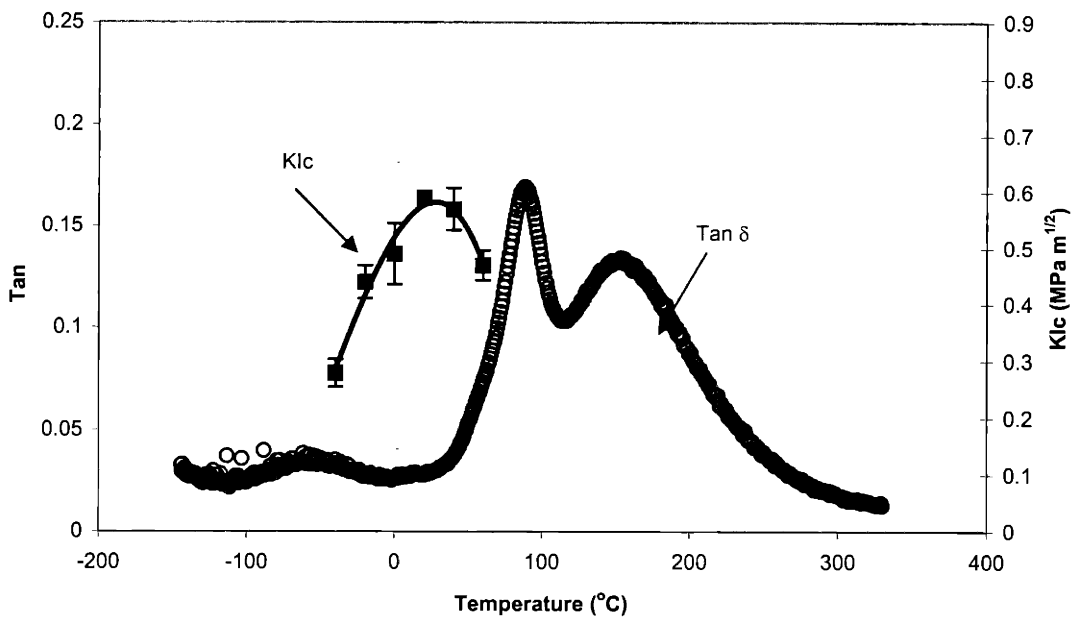


Figure 3-35 DMA Tan δ & fracture toughness of DP37 vs. temperature.

Tan δ and K_{Ic} vs. Temperature - P100

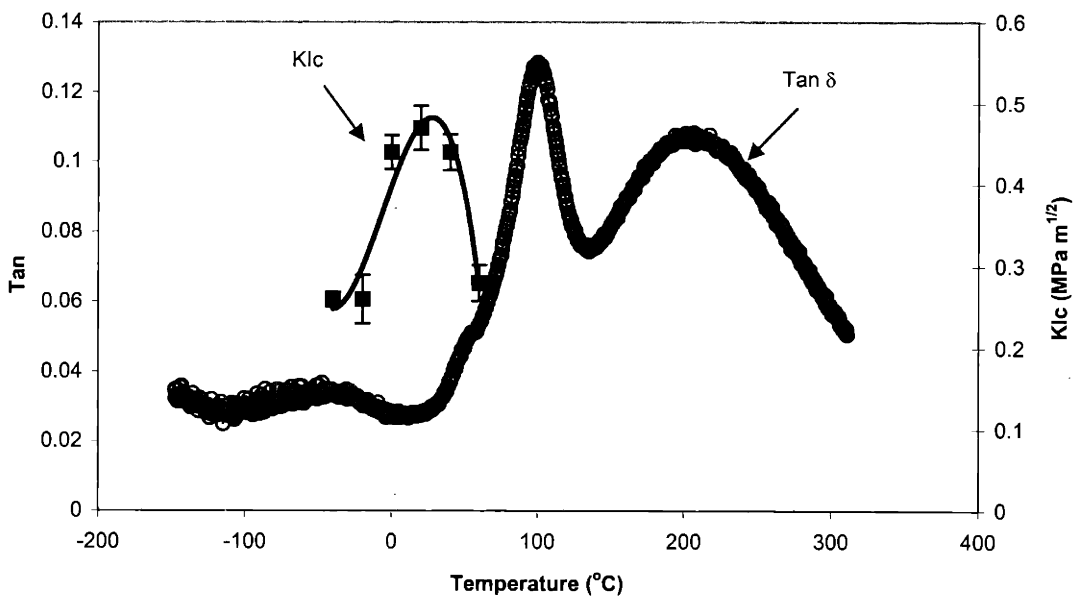


Figure 3-36 DMA Tan δ & fracture toughness of P100 vs. temperature.

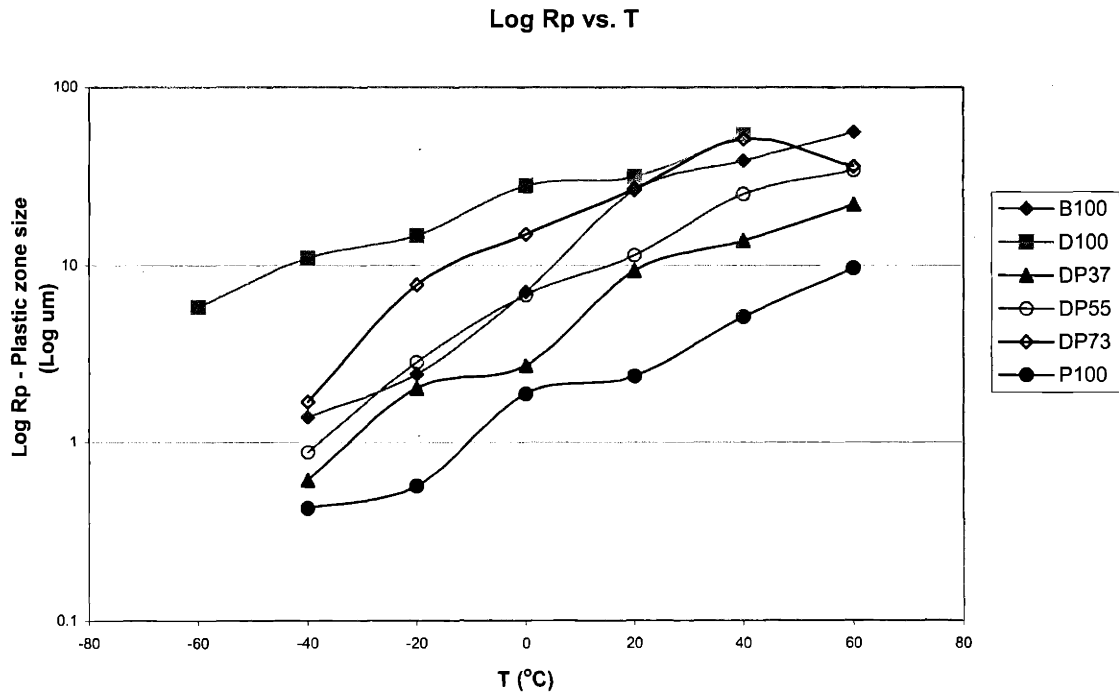


Figure 3-37 Log (Rp) vs. T – B100, D100, DP37, DP55, DP73 and P100.

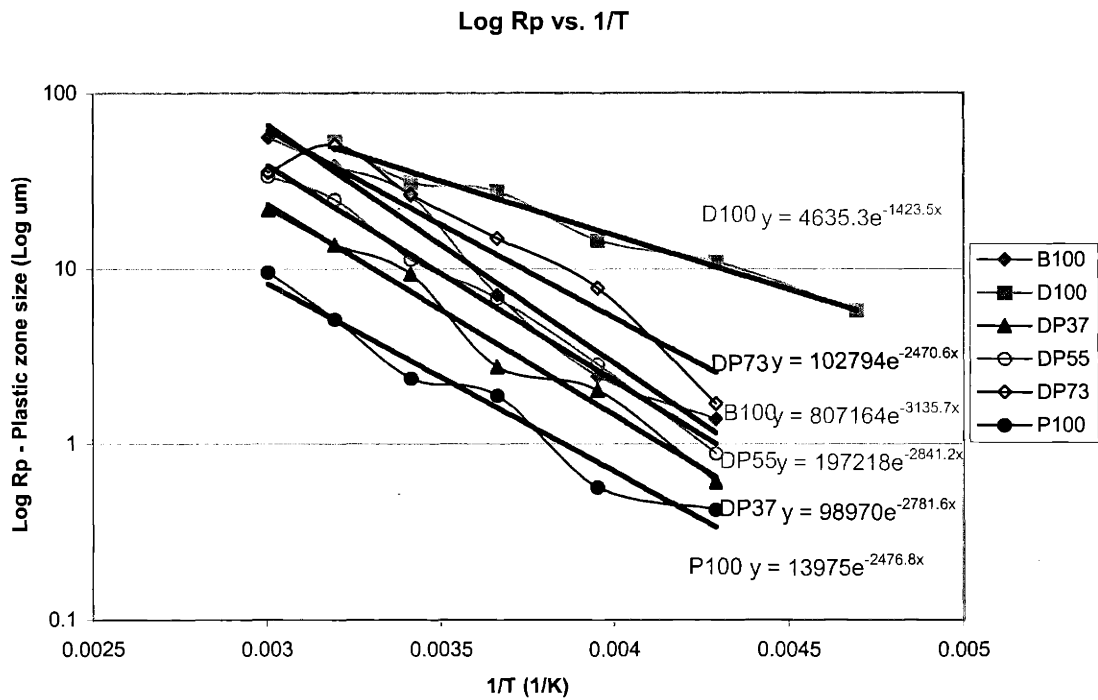


Figure 3-38 Log (Rp) vs. 1/T – B100, D100, DP37, DP55, DP73 and P100.

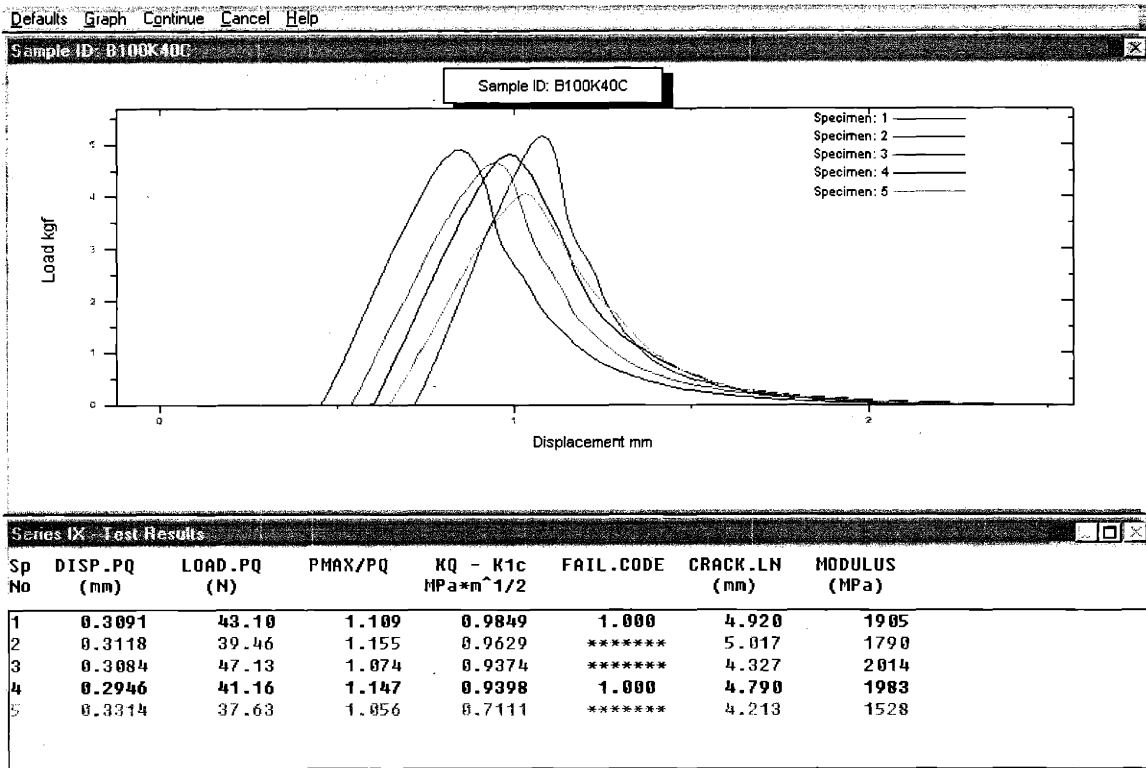


Figure 3-39 B100 – load displacement curves of fracture toughness testing at 40°C.

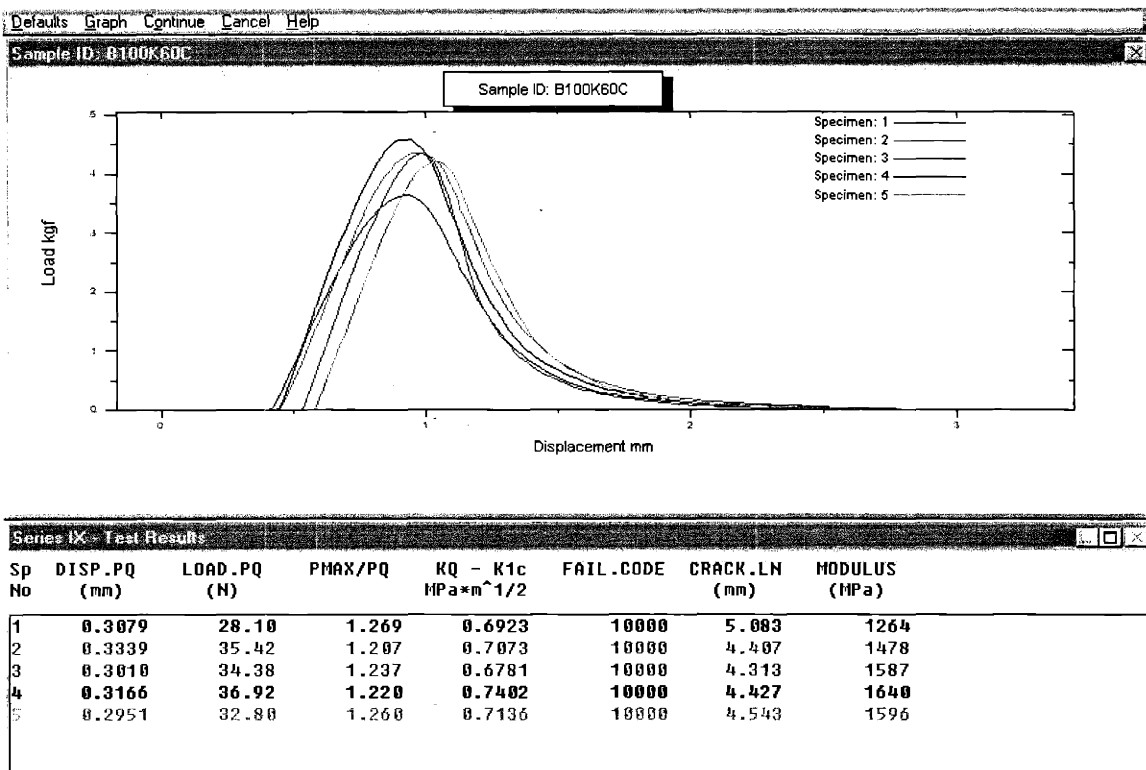


Figure 3-40 B100 – load displacement curves of fracture toughness testing at 60°C.

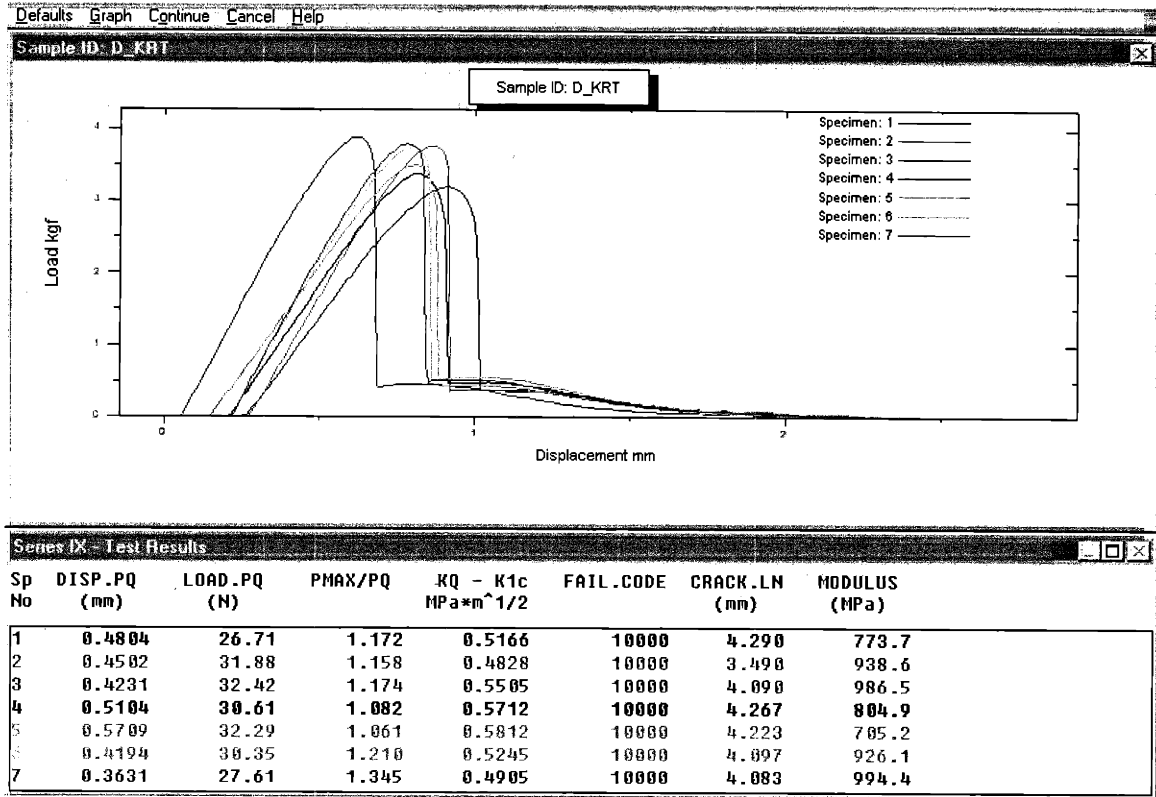


Figure 3-41 D100- load displacement curves of fracture toughness testing at RT.

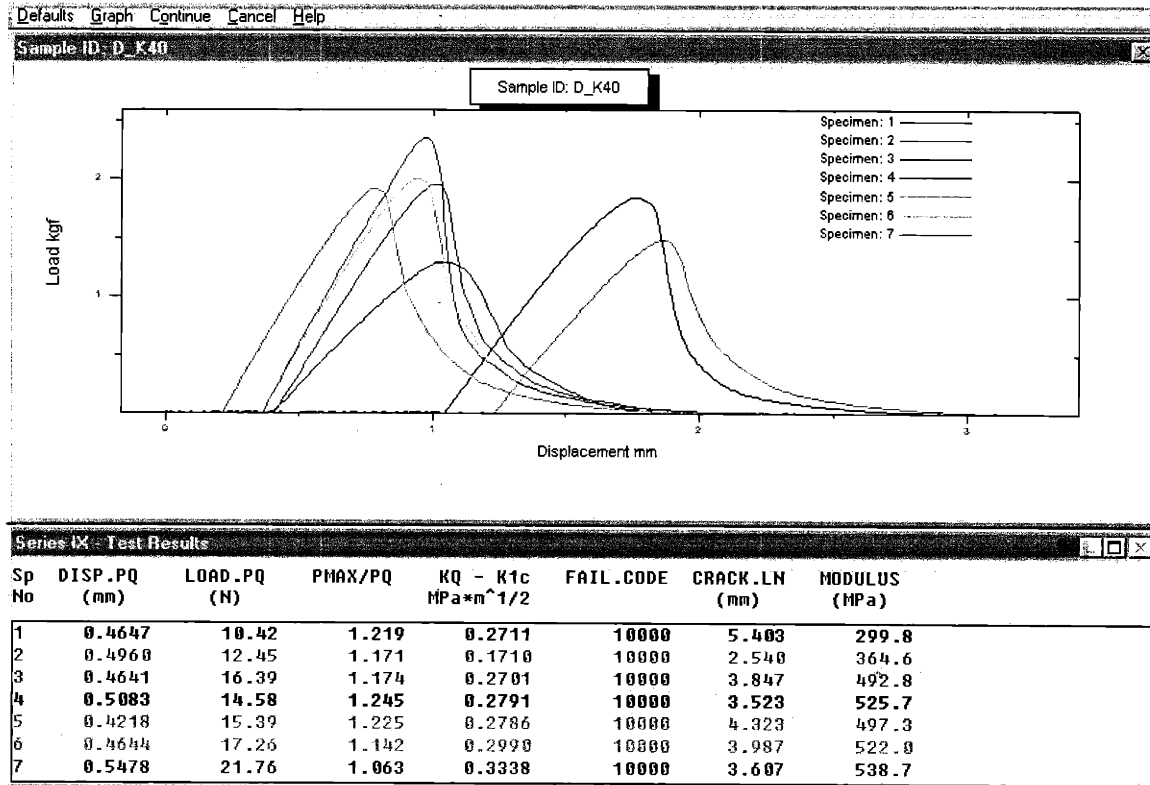


Figure 3-42 D100- load displacement curves of fracture toughness testing at 40°C.

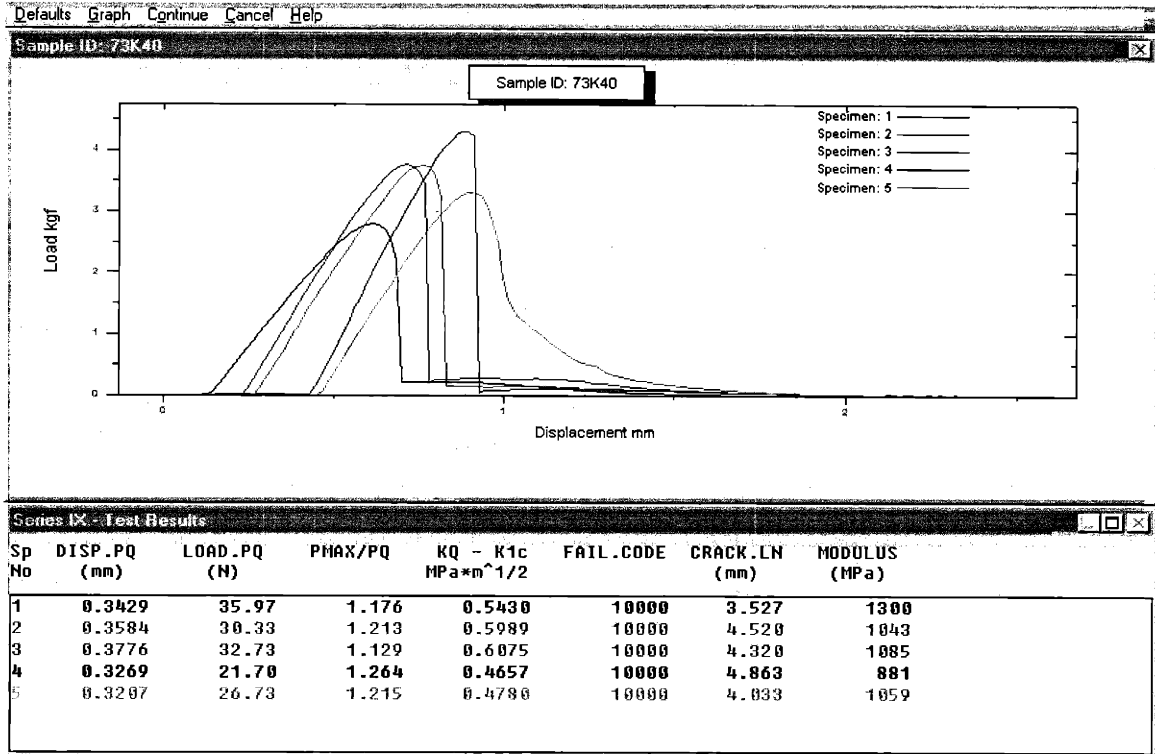


Figure 3-43 DP73— load displacement curves of fracture toughness testing at 40°C.

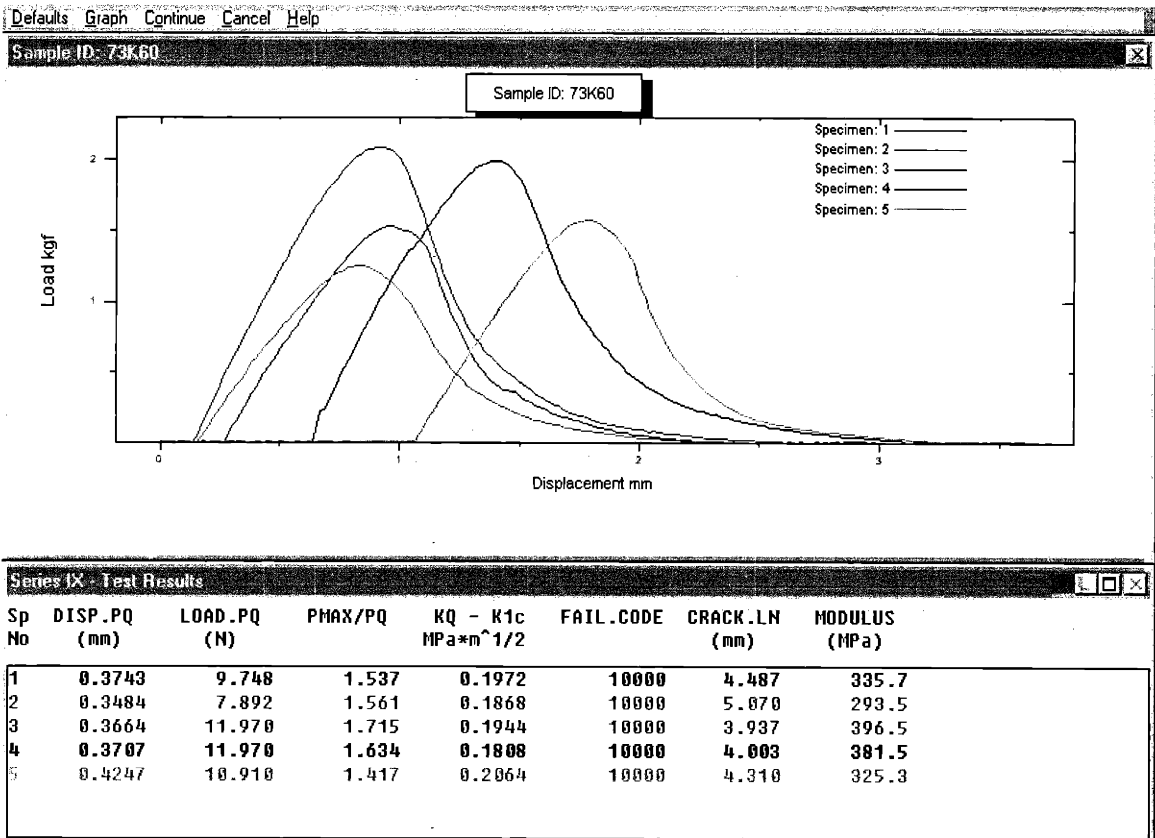


Figure 3-44 DP73— load displacement curves of fracture toughness testing at 60°C.

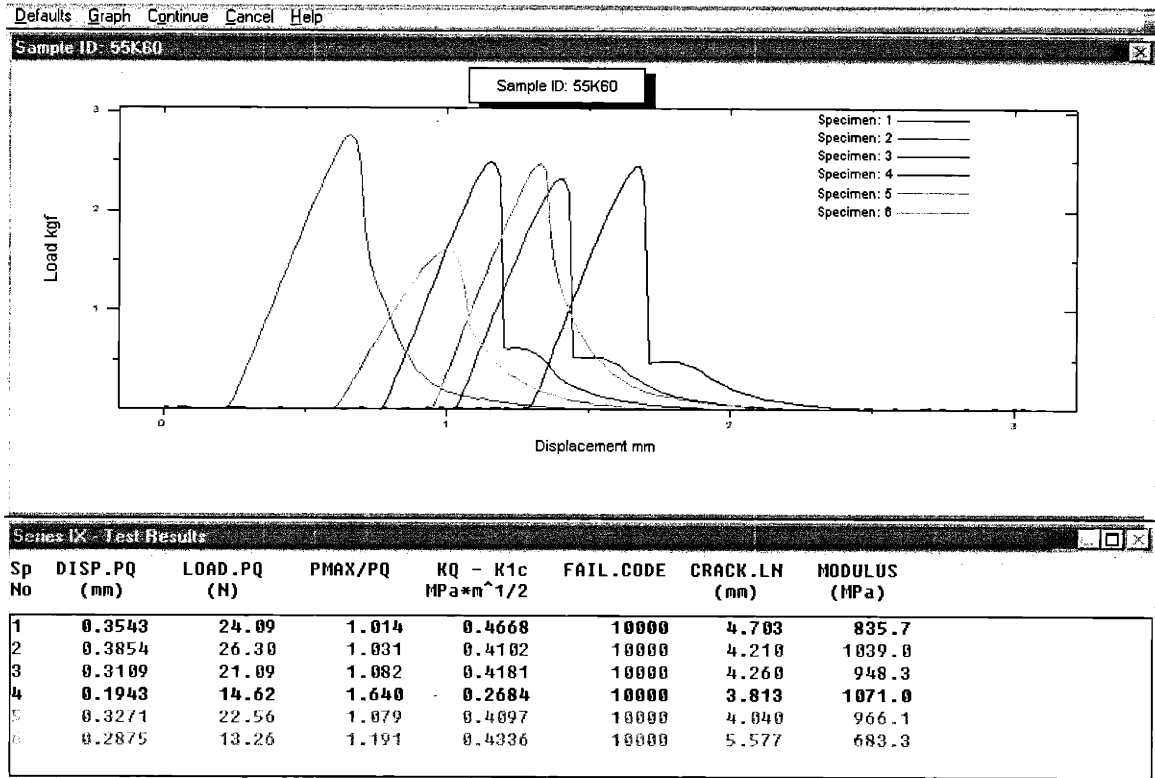


Figure 3-45 DP55— load displacement curves of fracture toughness testing at 60°C.

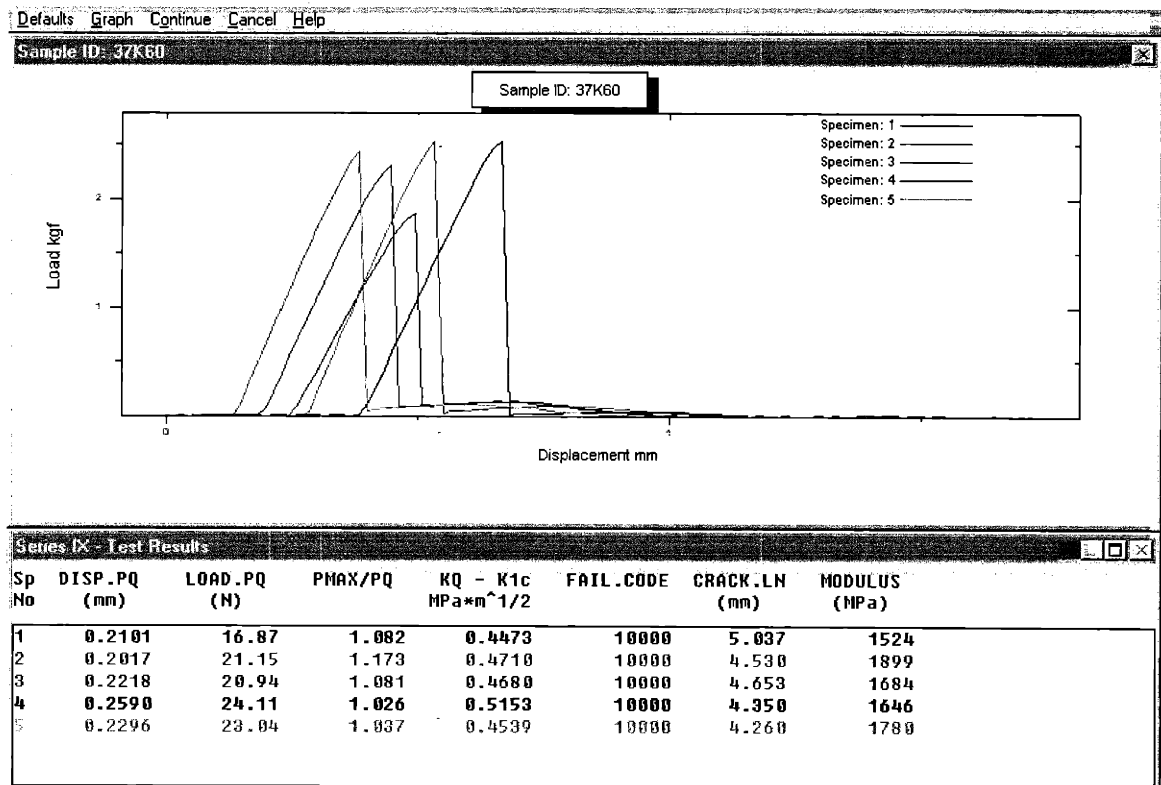


Figure 3-46 DP37— load displacement curves of fracture toughness testing at 60°C.

3.2 Mechanical testing results of Dow Corning 4-3136 condensation cure resin

Both phase I toughened (with 10% KPE) and untoughened 4-3136 resins were also studied for mechanical properties at different temperatures. They were given symbols of 3136T and 3136U, respectively, to simplify later texts. Casting processes and cure cycles can be found in Chapter 2. Testing temperature ranges from -40°C to $+80^{\circ}\text{C}$ for the untoughened 3136 and it is from -40°C to $+60^{\circ}\text{C}$ for the toughened 3136.

The complete data of toughened and untoughened 4-3136 are listed in Table 3-10 and Table 3-11 and plotted in Figure 3-47 through Figure 3-50. Generally, an increase in temperature results in the monotonic drop of modulus and strength of both 3136 resins. The change in strength in both toughened and untoughened resins is very similar and the two curves overlap each other. It is also seen that scattering in the stress data is relatively big. Both 3136 resins are brittle and thus are sensitive to scratch/defect present in the test samples. This results in some premature breakage of test samples during testing. For flexural modulus, we see that the untoughened resin has a consistently higher value than the toughened resin at all temperatures. In both maximum flexural stress and flexural modulus cases, relative changes to RT values at the same temperature are also similar for both resins.

Maximum flexural strains of both resins go up with temperature. In toughened 3136, it increases in a faster fashion and results in a steeper slope of change. This suggests that deformation process in the toughened 3136 is more sensitive to temperature change than the untoughened resin.

In Figure 3-50, the untoughened 3136 has an almost constant fracture toughness value with changing temperature. However, fracture toughness of the toughened 3136 experiences a monotonic increase with decreasing temperature. It also has a constantly higher toughness value than the untoughened resin. Compared to its RT value, toughness of 3136T increases 33% at -40°C and decreases 13% at 60°C . It suggests that toughness

of the toughened resin is more sensitive to temperature change, and this is consistent with what was seen in the modulus and strain behavior.

The calculated plastic zone size of both resins does not change much with temperature. For 3136U, the size increases from about 1 μm to 4 μm from -40°C to 80°C . For 3136T, its size remains about constant in the range of 3-4 μm in the whole temperature range. It also proves that the deformation ability of the toughened resin is bigger at all temperatures. This can be explained by the molecular structure of the resin network. The small PDMS rubber segments incorporated in the toughened network serve as small spring structures between crosslinking points. This increases chain flexibility and facilitates the chain movement.

In general, 3136 condensation cure resin is rigid, brittle and its toughness is not very sensitive to temperature change. With a high content of the $\text{SiO}_{3/2}$ structure, 3136 is highly crosslinked and has a tight network with very little freedom for the chains to become mobile. So the 3136 network is rigid and hard to deform. This is proved by the higher glass transition temperature and broad glass transition behavior of the resin, which can be seen from the DMA plots (Figure 3-51 and Figure 3-52). The untoughened 3136 has very limited network mobility and high rigidity at room temperature and it does not change much with temperature. The toughened 3136, however, has some flexibility offered by the PDMS rubber chains, showing a higher flexural strain value and bigger plastic zone consistently. At low temperature, the deformation ability of 3136T remains and the rigidity goes up, which results in its increasing toughness.

Table 3-10 Mechanical properties of toughened 4-3136 at different temperatures.

Temp.	Maximum flexural stress (MPa)		Maximum flexural strain (%)		Flexural modulus (GPa)		K _{Ic} (MPa m ^{1/2})		P _{max} /P _q	Plastic zone size (μm)
	Ave	Stdev	Ave	Stdev	Ave	Stdev	Ave	Stdev	Ave	Ave
-40°C	60.44	±4.53	3.78	±0.43	2.09	±0.12	0.52	±0.01	1	3.93
-20°C	61.26	±2.82	5.20	±0.70	1.85	±0.07	0.44	±0.01	1	2.74
0°C	52.23	±3.61	4.75	±0.52	1.62	±0.07	0.41	±0.02	1	3.27
RT	50.48	±2.60	5.98	±0.50	1.48	±0.05	0.39	±0.01	1	3.17
40°C	42.41	±2.93	6.14	±0.72	1.19	±0.03	0.39	±0.01	1	4.49
60°C	38.00	±0.71	7.35	±0.23	0.95	±0.02	0.34	±0.02	1	4.25

Table 3-11 Mechanical properties of untoughened 4-3136 at different temperatures.

Temp.	Maximum flexural stress (MPa)		Maximum flexural strain (%)		Flexural modulus (GPa)		K _{Ic} (MPa m ^{1/2})		P _{max} /P _q	Plastic zone size (μm)
	Ave	Stdev	Ave	Stdev	Ave	Stdev	Ave	Stdev	Ave	Ave
-40°C	59.46	±8.88	2.61	±0.54	2.59	±0.07	0.29	±0.01	1	1.26
-20°C	58.29	±7.71	2.79	±0.53	2.44	±0.05	0.27	±0.02	1	1.14
0°C	55.24	±3.88	3.07	±0.45	2.33	±0.10	0.3	±0.03	1	1.56
RT	50.52	±0.36	3.48	±0.11	2.06	±0.04	0.28	±0.03	1	1.63
40°C	45.18	±4.37	3.95	±0.48	1.71	±0.05	0.3	±0.04	1	2.34
60°C	33.88	±3.09	3.64	±0.39	1.33	±0.06	0.28	±0.02	1	3.62
80°C	28.83	±4.33	3.92	±0.35	1.06	±0.14	0.26	±0.01	1	4.31

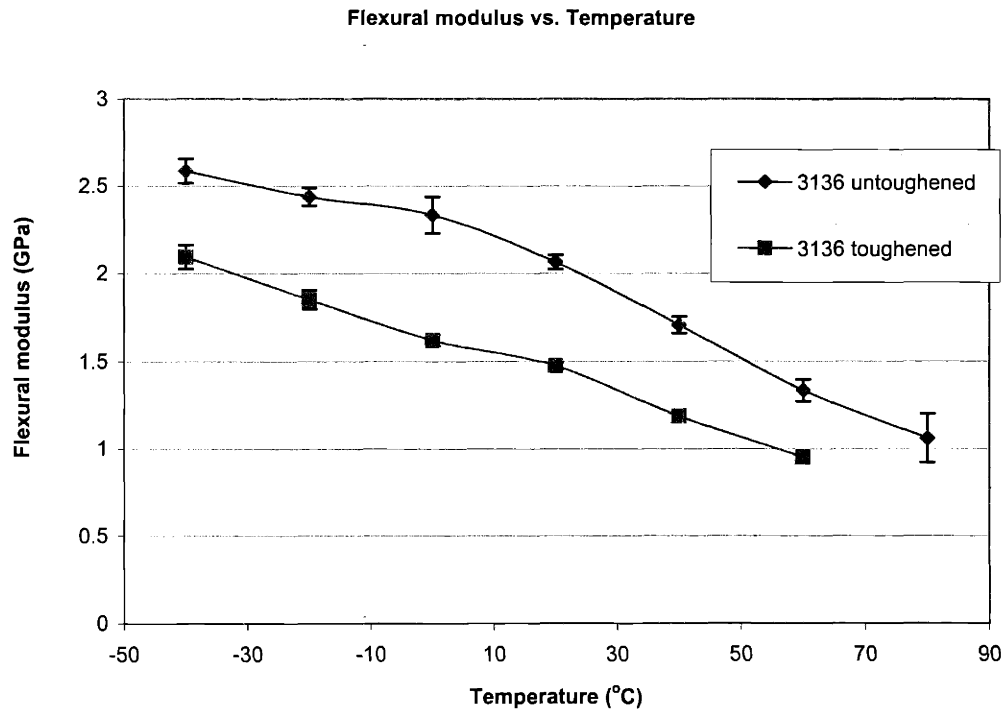


Figure 3-47 Flexural modulus change with temperature for both toughened (with 10% KPE) and untoughened 4-3136 resins.

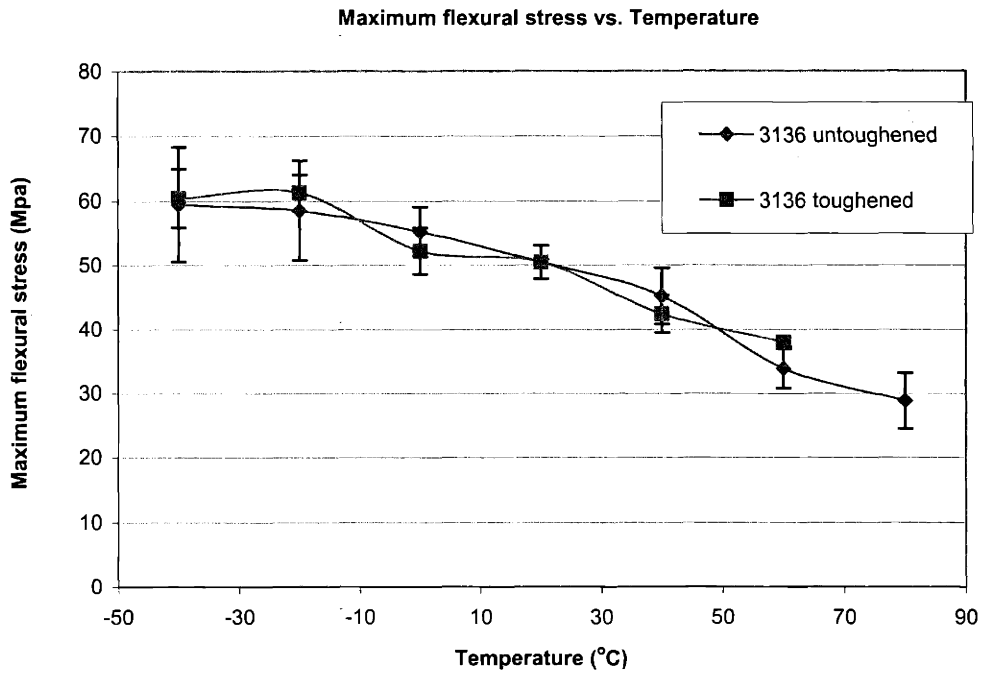


Figure 3-48 Maximum flexural stress change with temperature for both toughened (with 10% KPE) and untoughened 4-3136 resins.

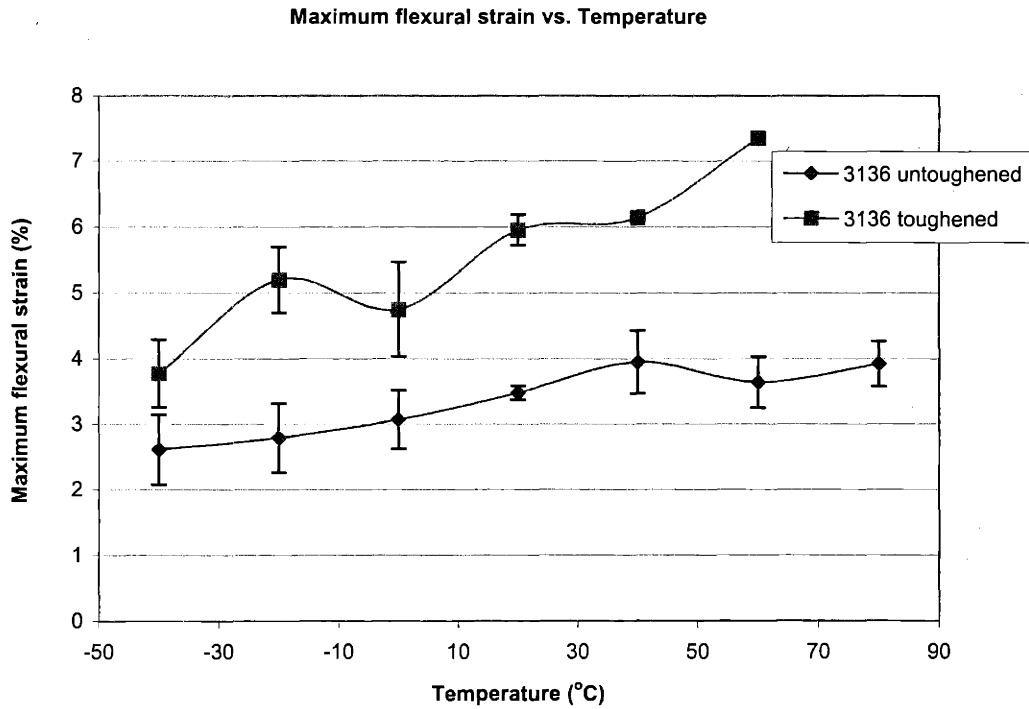


Figure 3-49 Maximum flexural strain change with temperature for both toughened (with 10% KPE) and untoughened 4-3136 resins.

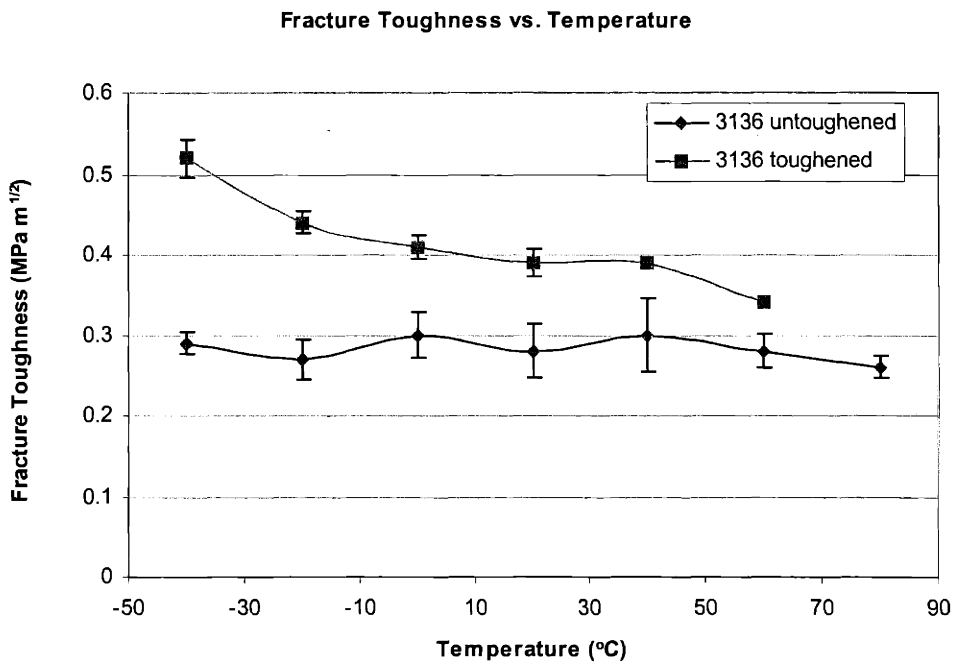


Figure 3-50 Fracture toughness change with temperature for both toughened (with 10% KPE) and untoughened 4-3136 resins.

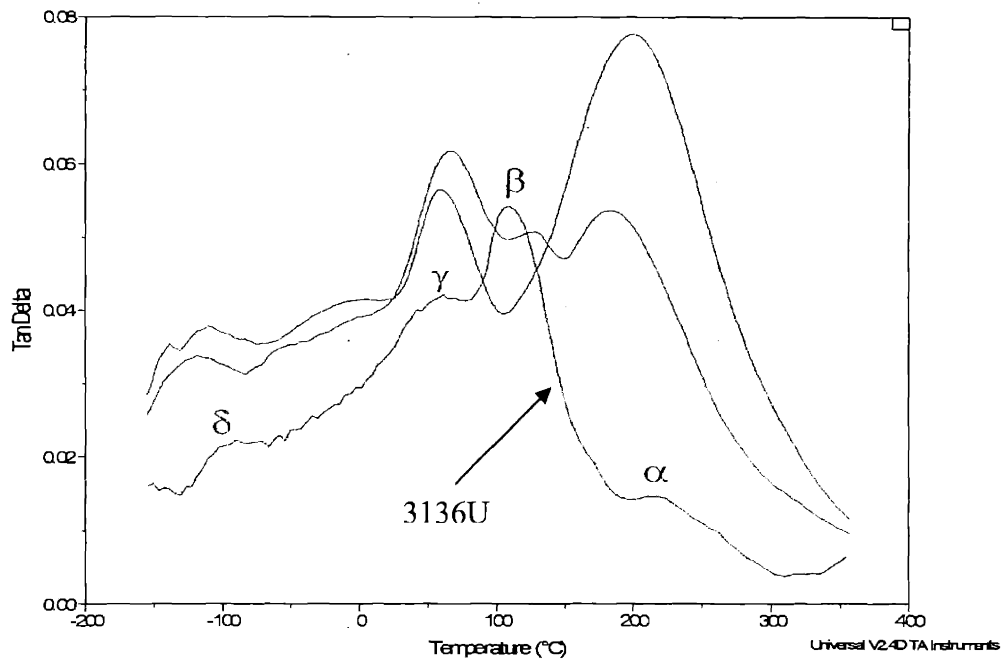


Figure 3-51 Tan Delta plot from DMA of 3136U resin (data provided by Rocky Zhu).

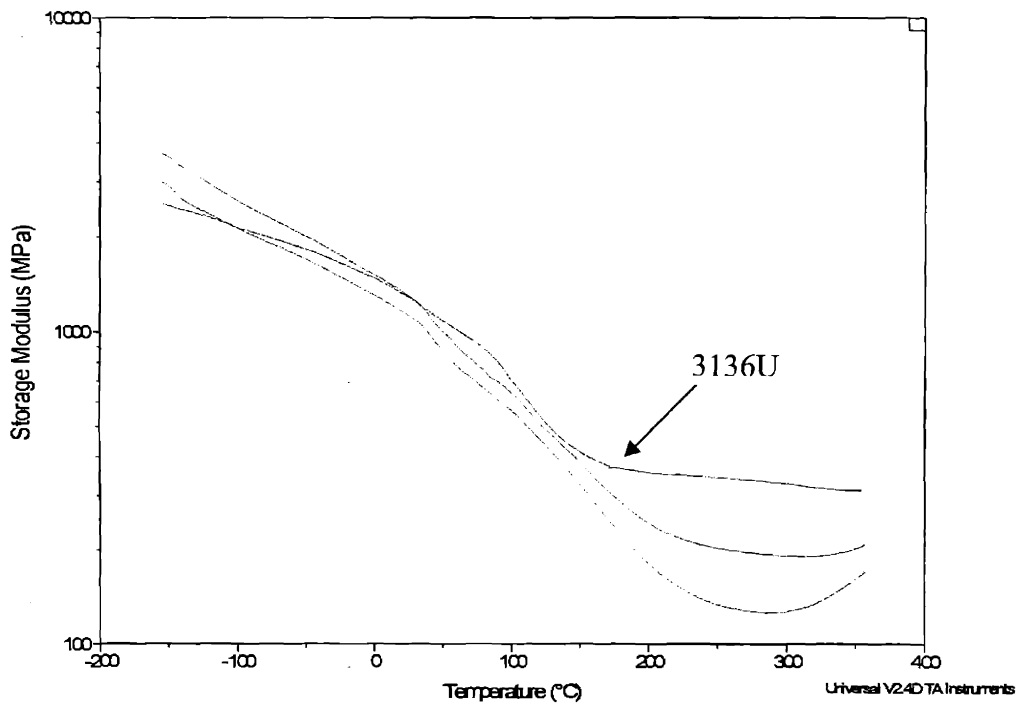


Figure 3-52 Storage modulus plot from DMA of 3136U (data provided by Rocky Zhu).

3.3 SEM analysis of fracture surfaces

SEM observations of fracture surfaces of single edge notched (SEN) samples have been carried out. Samples that were tested at different temperatures were brought to room temperature for SEM analysis. All micrographs in this section are taken with a crack propagation direction from the left to the right.

Because of the complexity of fracture surfaces due to the actual loading rate in the front of the crack tip, the pre-crack front feature/travel, and the resin compositions, only part of the features that are related to fracture mechanisms will be discussed here. When analyzing the results, it is necessary to note the load-displacement curve features of these tests. The detailed testing results including load-displacement plots are presented in Appendix A. A summary of these test curve features is listed in Table 3-12 and Table 3-13 below. In summary, the load-displacement curves show differences near the maximum load point, some having sharp points and others having round tops. This is associated with the amount of deformation occurring during the test. The round maximum points demonstrating non-linearity suggest plastic deformation. The sharp maximum points, on the other hand, are associated with little plastic deformation occurring before breakage. In D/P crosslinked 2672 resins, we see that as P crosslinker content increases, the curves start to show non-linearity at higher temperatures. With B100, we see the non-linearity begin at about 0°C, suggesting network mobility in the resin at this temperature. In the condensation cure resins, non-linearity in load-displacement curves disappears at all temperatures, which is strongly associated with its relative brittleness and lack of chain mobility.

	-60°C	-40°C	-20°C	0°C	20°C	40°C
D100						
K _{Ic}	0.75	0.75	0.69	0.72	0.54	0.28
	-40°C	-20°C	0°C	20°C	40°C	60°C
DP73						
K _{Ic}	0.36	0.65	0.78	0.75	0.54	0.19*
DP55						
K _{Ic}	0.3	0.5	0.64	0.62	0.64	0.43
DP37						
K _{Ic}	0.28	0.44	0.49	0.59	0.57	0.47
P100						
K _{Ic}	0.26	0.26	0.44	0.47	0.44	0.41
B100						
K _{Ic}	0.37	0.46	0.72	1.03	0.96	0.71

Table 3-12 Summary of load-displacement curves in K_{Ic} tests for different crosslinked 2672 resins. (K_{Ic} is in MPa m^{1/2} and data points with * do not meet the test validity criterion of P_{max}/P_q ≤ 1.1.)













	-40°C and -20°C	0°C	20°C	40°C	60°C	80°C
3136U						
K_{Ic}	0.29 & 0.27	0.3	0.28	0.3	0.28	0.26
	-40°C	-20°C	0°C	20°C	40°C	60°C
3136T						
K_{Ic}	0.52	0.44	0.41	0.39	0.39	0.34

Table 3-13 Summary of load-displacement curves in K_{Ic} tests for 3136 resins. (K_{Ic} is in $\text{MPa m}^{1/2}$.)

3.3.1 ADDITION CURE RESIN

3.3.1.1 B100

From B100 samples tested at temperatures above RT (Figure 3-53 through Figure 3-55), we can observe that the fracture surfaces generally possess rough ridge features with multiple steps flowing along the crack propagation direction (from left to right in the figures). One distinct feature is that the lower fracture toughness value is accompanied by coarse features of fewer steps on the fracture surface – suggesting an easiness of crack propagation. This is more obvious when the temperature goes from 40°C (Figure 3-54) to 60°C (Figure 3-55) and causes a drop of about 25% in the toughness value.

However, for samples tested below RT (Figure 3-56 through Figure 3-58), fracture surfaces look quite different. They possess always a small area of steps after the pre-crack front. These areas have much fewer steps than those observed in the fracture surfaces above RT. After this small rough region, there exist mirror like smooth surfaces with very little features, especially at -40°C. The width of the rough band dramatically decreases when the temperature goes from 0°C to -20°C. At -40°C, the average width is only about 20 microns.

Samples of 0°C and 60°C have the same toughness value, and yet their fractographic features look very different. At 60°C, the fracture surface is filled with many elevations. At 0°C, most part of the fracture surface looks mirror smooth, with only a small band of steps right in front of the pre-crack. This might be explained by the difference in sources of toughness at temperatures higher than RT and lower than RT. At temperatures greater than RT, plastic deformation plays an important role in toughness and it causes the rough step features. At temperatures lower than RT, the network has less mobility and thus rigidity contributes more to the overall toughness. Little feature observed on fracture surfaces at these temperatures suggests that not much deformation occurs during fracture.

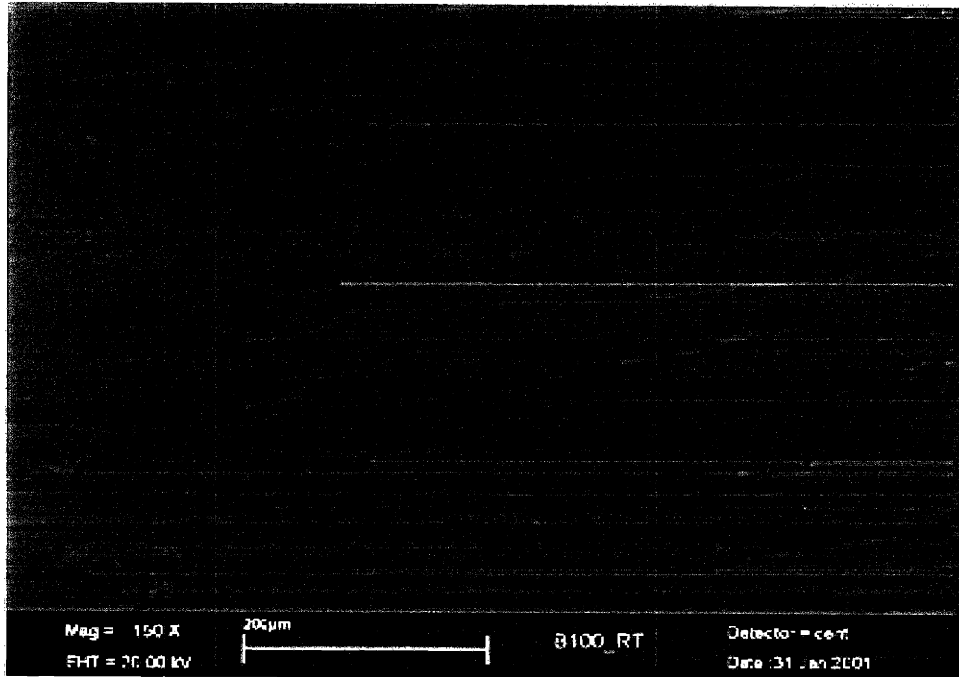


Figure 3-53 SEM micrograph of a B100 SENB sample tested at room temperature (average K_{Ic} value is $1.03 \text{ MPa m}^{1/2}$). (150x) (crack propagating direction \rightarrow)

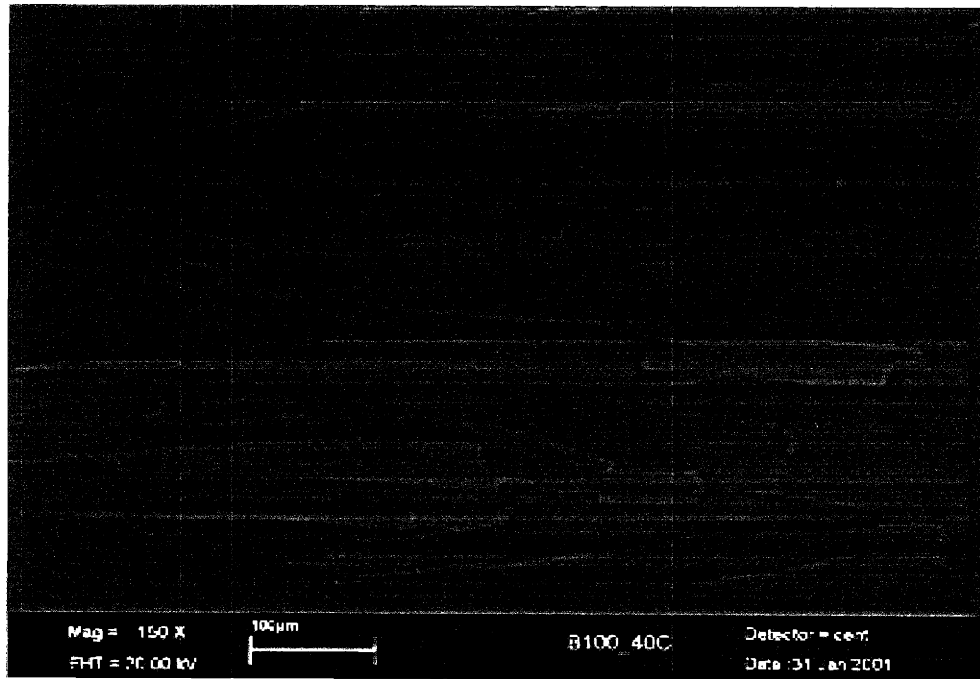


Figure 3-54 SEM micrograph of a B100 SENB sample tested at 40°C (average K_{Ic} value is $0.96 \text{ MPa m}^{1/2}$). (150x) (crack propagating direction \rightarrow)

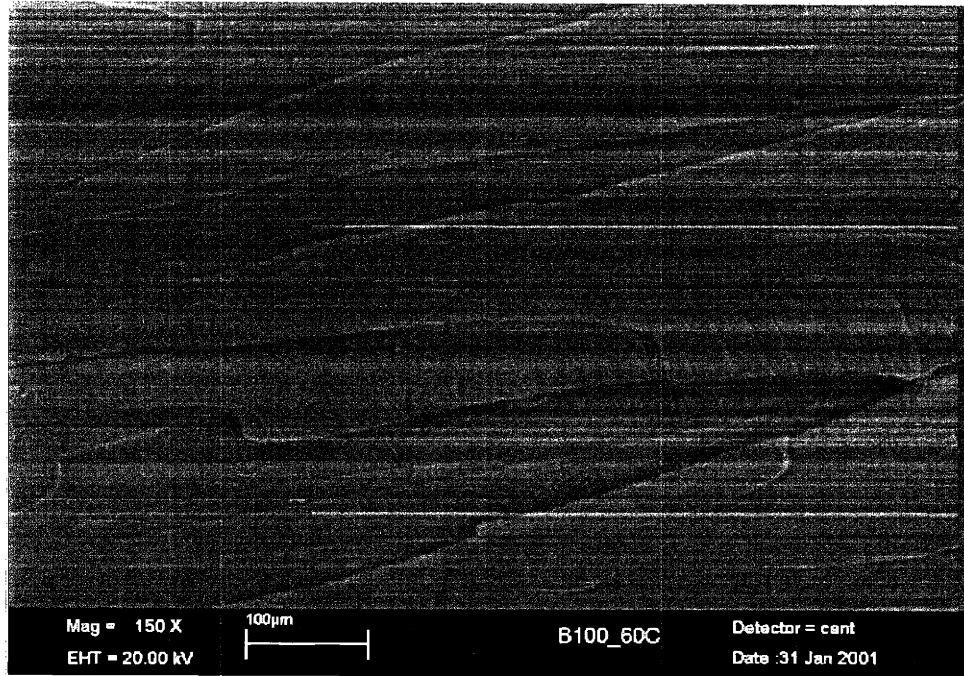


Figure 3-55 SEM micrograph of a B100 SENB sample tested at 60°C (average K_{Ic} value is 0.71 MPa $m^{1/2}$). (150x) (crack propagating direction →)

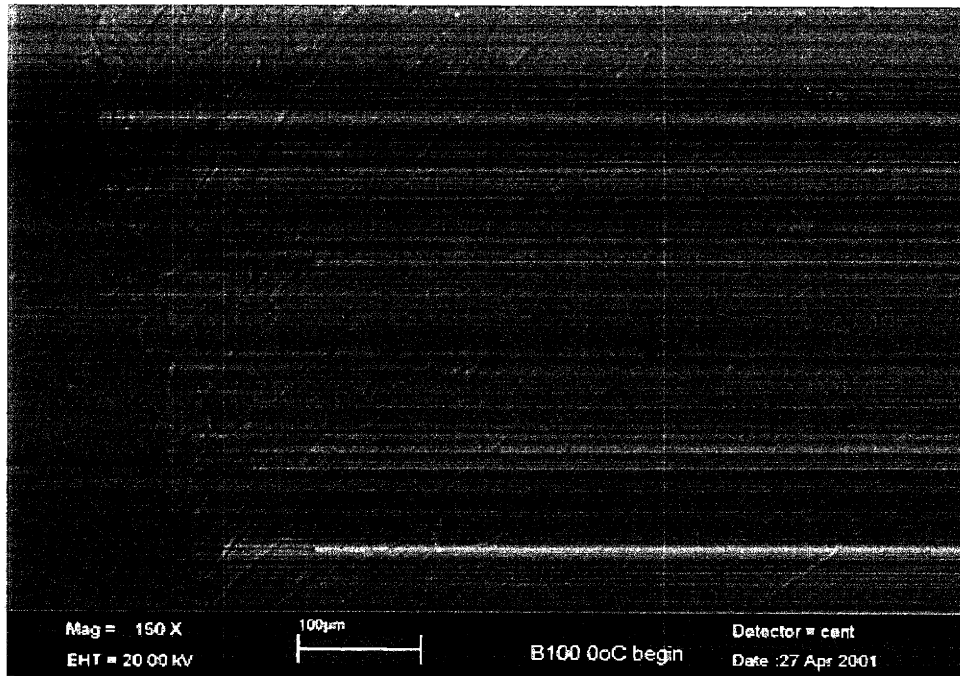


Figure 3-56 SEM micrograph of a B100 SENB sample tested at 0°C (average K_{Ic} value is 0.72 MPa $m^{1/2}$). (150x) (crack propagating direction →)

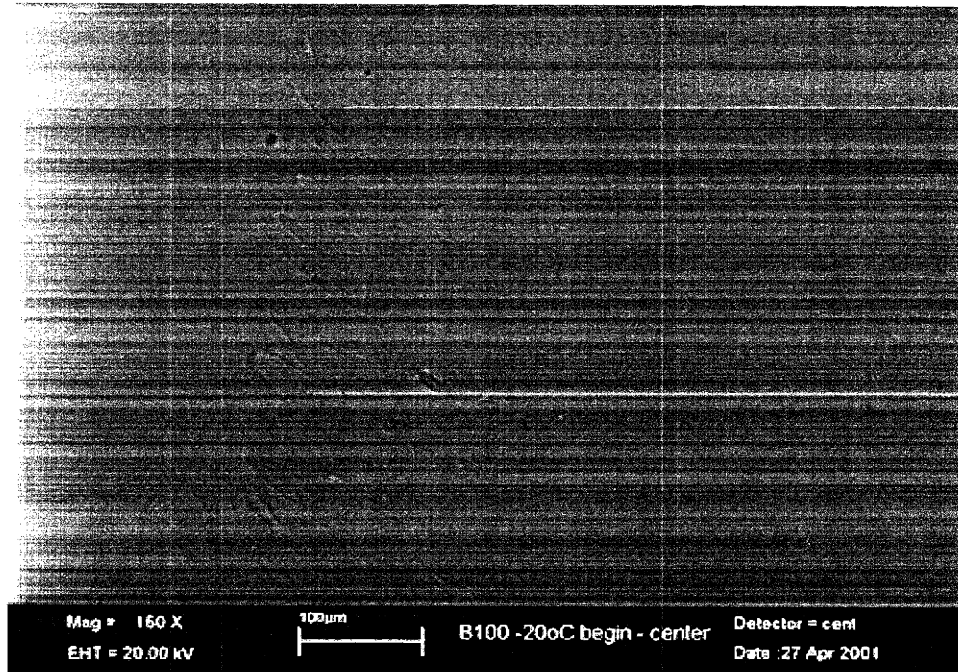


Figure 3-57 SEM micrograph of a B100 SENB sample tested at -20°C (average K_{Ic} value is 0.46 MPa $m^{1/2}$). (150x) (crack propagating direction →)

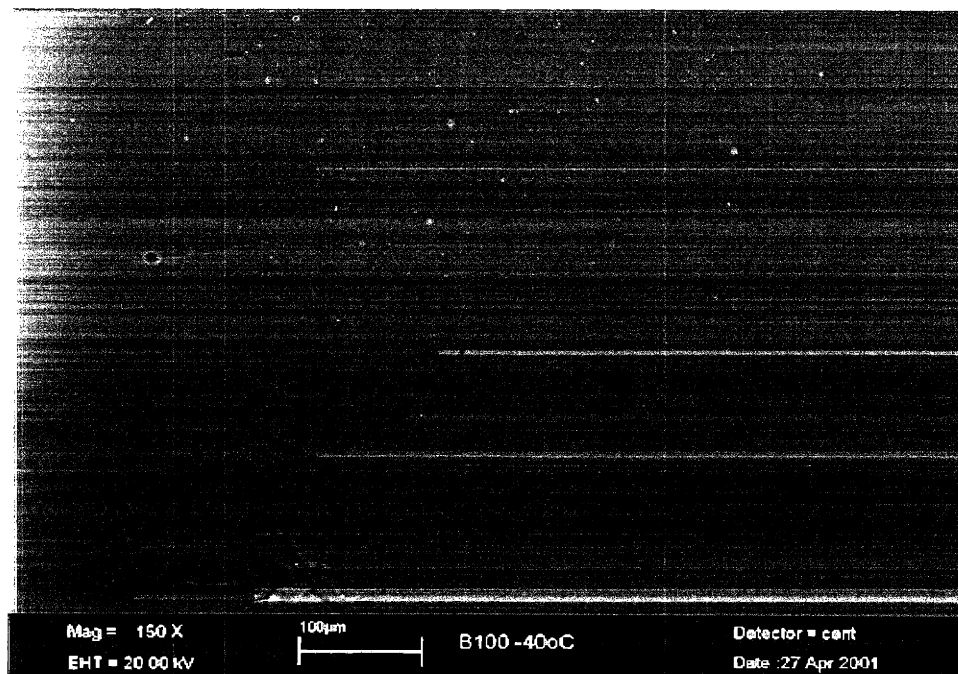


Figure 3-58 SEM micrograph of a B100 SENB sample tested at -40°C (average K_{Ic} value is 0.37 MPa $m^{1/2}$). (150x) (crack propagating direction →)

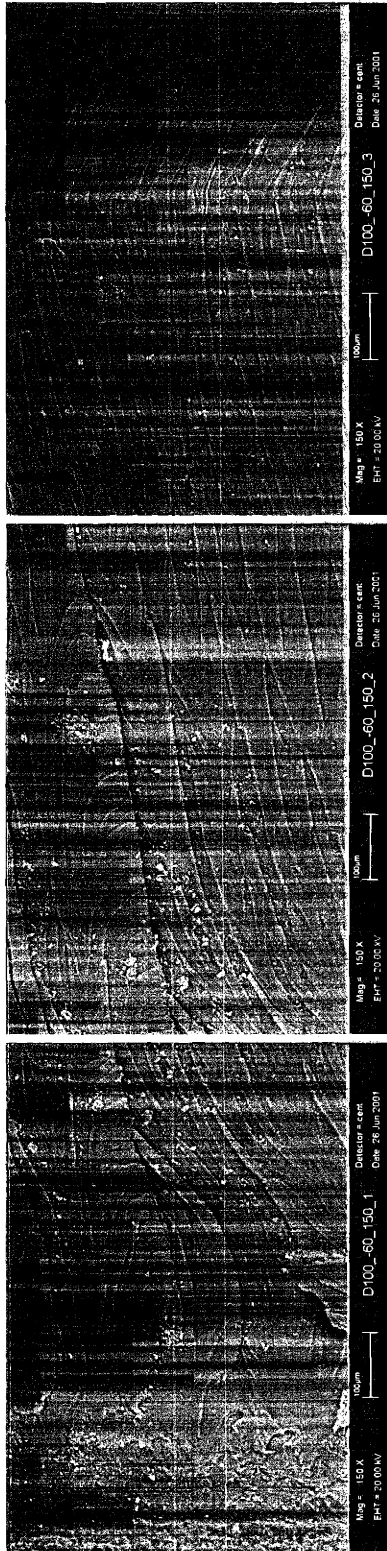
3.3.1.2 D100

For D100, we see exceptional evidence of plastic deformation on the fracture surfaces, particularly at -60°C and -40°C with lots of elevations/steps. At temperatures up to 0°C , The fracture surfaces often reveal a very rough region ((1),(2),(5),(8) and (10) in Figure 3-59) with high elevations after the pre-crack front. This rough region is then followed by a less rough region ((3), (6) and (11) in Figure 3-59) characterized by dense multiple steps with small elevations. Last, they turn into a number of fan-shaped striations and then into a mirror-smooth featureless area ((3) and (6) in Figure 3-59).

At 20°C , the mirror-smooth region disappears and in Figure 3-59 (14) we start to see that the less rough region develops into a second rough region with fewer steps of wider spacing and relatively high elevations. At 40°C , both the fine feature region and the mirror smooth region disappear (Figure 3-59(16) and (17)), the rough region right after the pre-crack extends and develops into a second rough region with fewer steps of wider spacing.

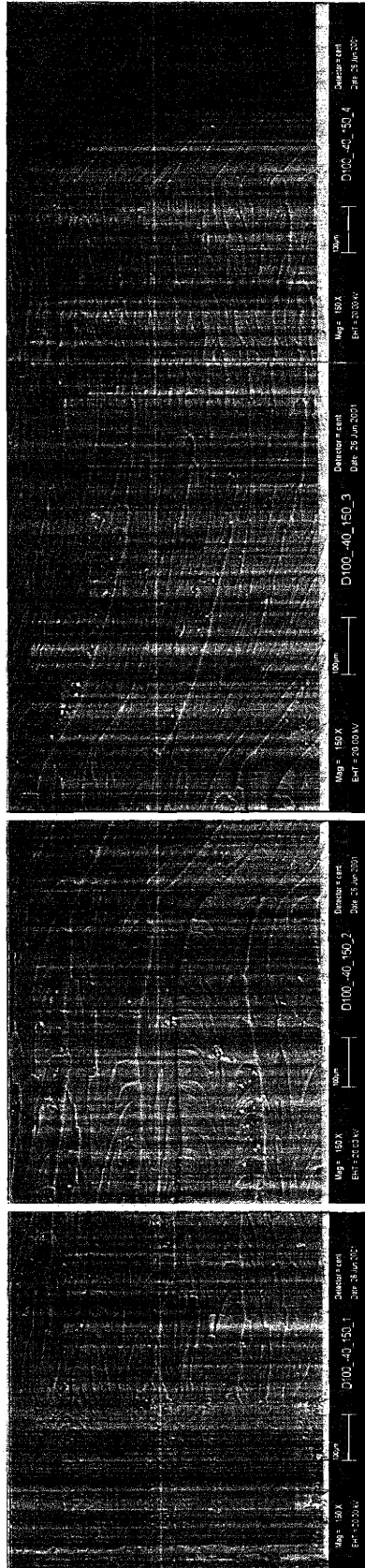
The rough regions are associated with plastic deformation occurring along with the crack propagation, which is mostly in a stable and slow motion. The fine feature regions of dense multiple steps or mirror smooth surface are characterized by the fast crack propagation of the crack, with less resistance and less deformation occurring. This is often accompanied by a drop in the load in the load-displacement curves. The lack of the mirror-smooth surface at RT can be explained by the final constant load in the curve as seen in Figure A-11. At this constant load level, crack propagates in a slow fashion until it reaches failure. At 40°C (Figure A-12), after the load reaches its maximum, the crack propagates continuously in a stable and controllable manner until breakage.

All these fracture surface features prove that D100 is very capable of deforming plastically even at temperatures below 0°C . Deformation accompanies the rupture of surfaces during crack propagation, leaving many steps with high elevations on the fracture surface.



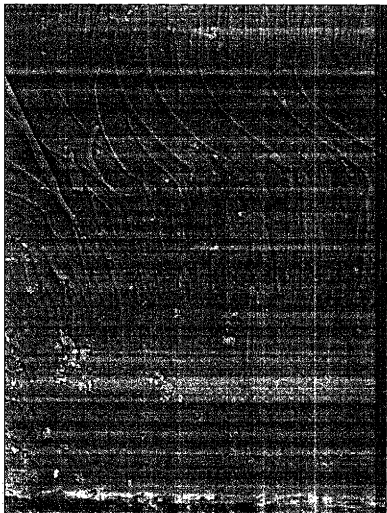
-60°C

(1) pre-crack front + very rough region (2) very rough → less rough region w/ finer features (3) less rough region → fan-shaped area → beginning of mirror smooth region

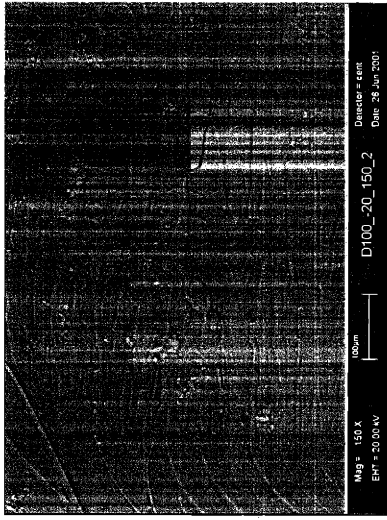


-40°C

(4) pre-crack front + very rough region (5) very rough region (6) very rough → less rough area → fan-shaped area → mirror smooth region

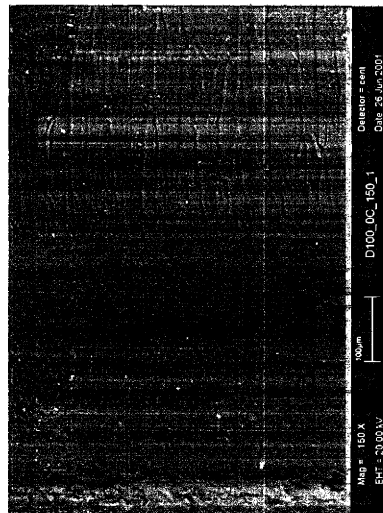


(7) pre-crack front + very rough region

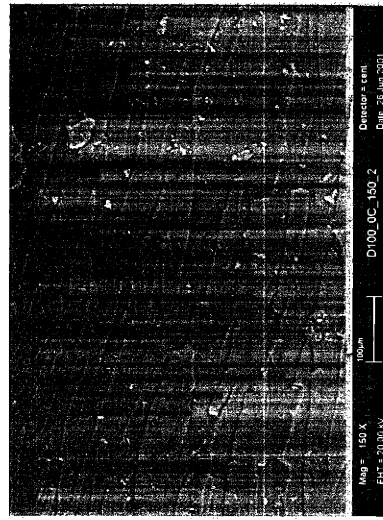


(8) very rough region

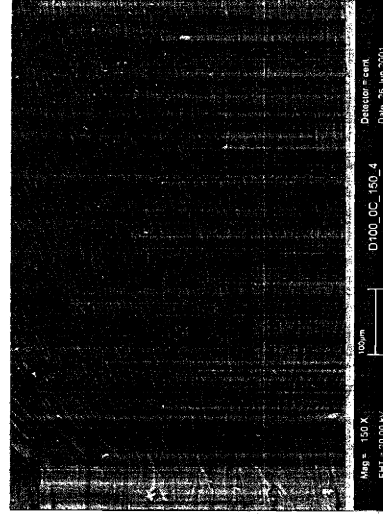
-20°C



(9) pre-crack front + beginning of very rough region

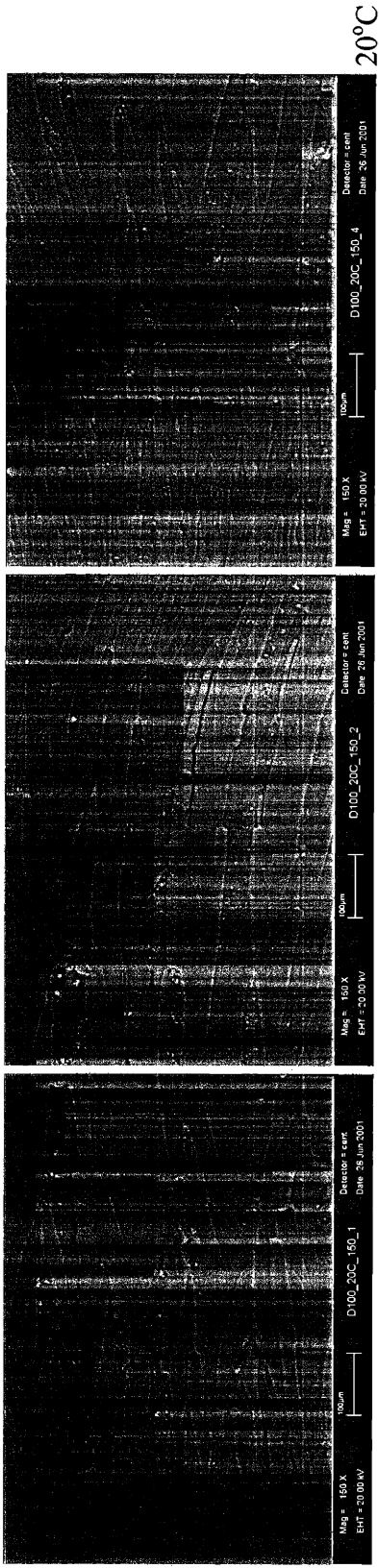


(10) very rough region



(11) very rough → less rough region

0°C

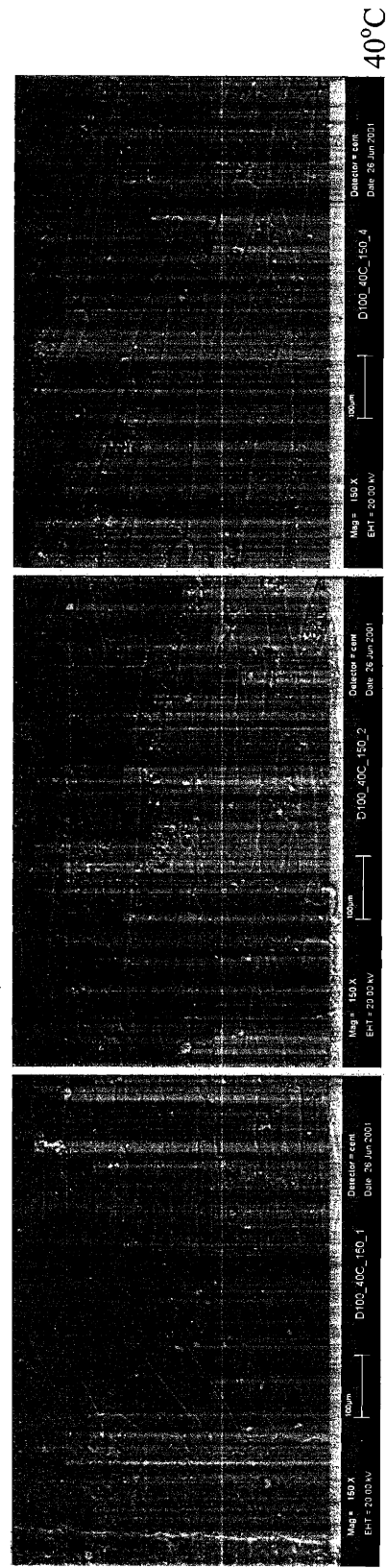


20°C

(12) pre-crack front + very rough region

(13) very rough region → less rough

(14) less rough → 2nd rough region near the end



40°C

(15) pre-crack front + beginning of very rough region

(16) very rough region

(17) very rough region extends to the end

Figure 3-59 Summary of fracture surfaces of D100 K_{Ic} samples tested at different temperatures. (crack propagating direction →)

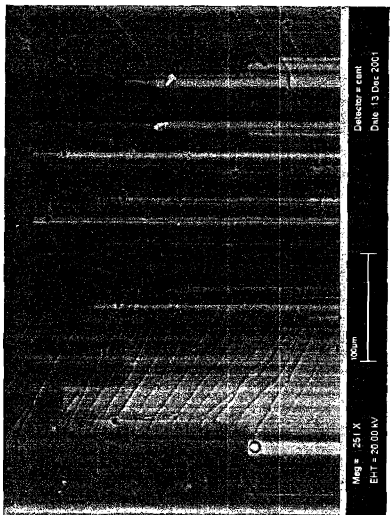
3.3.1.3 DP73

Fracture toughness of DP73 has a peaking pattern similar to that of B100. It has relatively high toughness at RT, which drops both at low temperatures and at high temperatures. Fracture surfaces of DP73 also have features similar to those found in B100.

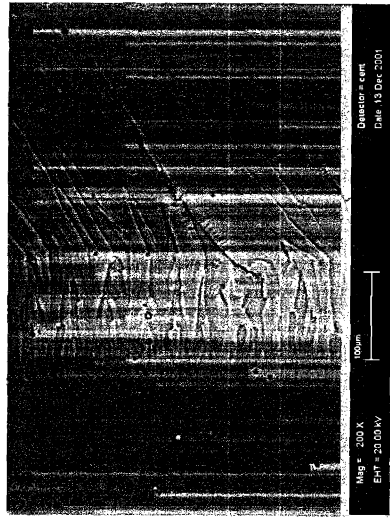
At temperatures below RT, features similar to those of B100 are observed, with small band of few steps right after the pre-crack front. This band becomes wider in width and also has more features as the temperature increases from -40°C to 0°C (Graphs (1) (2) and (3) in Figure 3-60). In graphs (1) (2) and (3), we see some particles on fracture surfaces. These are formed from PDMS rubber contamination in the Pt IV catalyst. Tests were repeated with samples from using an un-contaminated catalyst and the fracture toughness values didn't show much difference.

At 20°C , the rough area immediately next to the pre-crack extends further and develops into a multiple-step fine feature region with denser and narrower steps (Graphs (5) in Figure 3-60). The 40°C surface is similar, except that a second rough area develops in the end (Graphs (9) in Figure 3-60). At 60°C , we don't see the fine feature region, but a well-developed and extended rough region exists throughout the fracture surface. This is associated with the deformation ability at that temperature, which results into a stable and slow crack propagation mode.

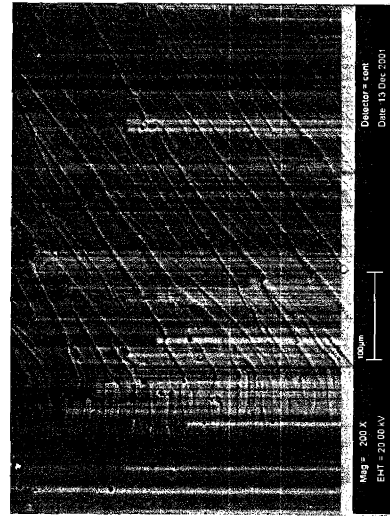
Compare (4), (7), and (10) in Figure 3-60, we observe that the features become coarser as the temperature goes from 20 to 40 and 60°C . This resembles what is seen in the B100 case, suggesting a decrease in resistance to fracture and accompanied by a drop in toughness value.



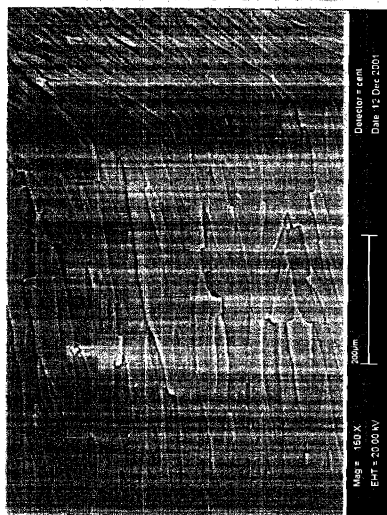
(1) narrow band with few steps



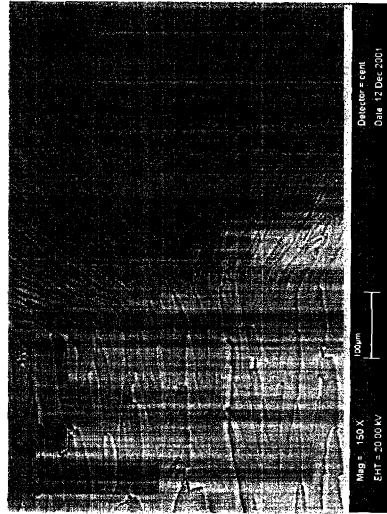
(2) narrow band with more steps



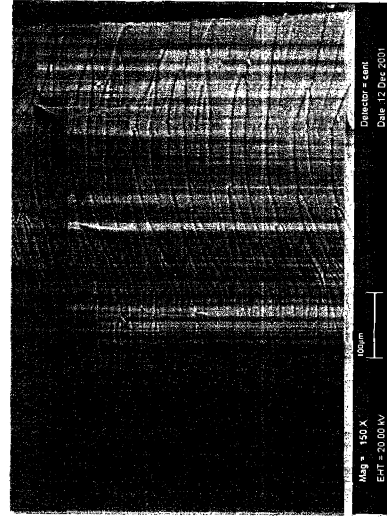
(3) band becomes wider with more steps



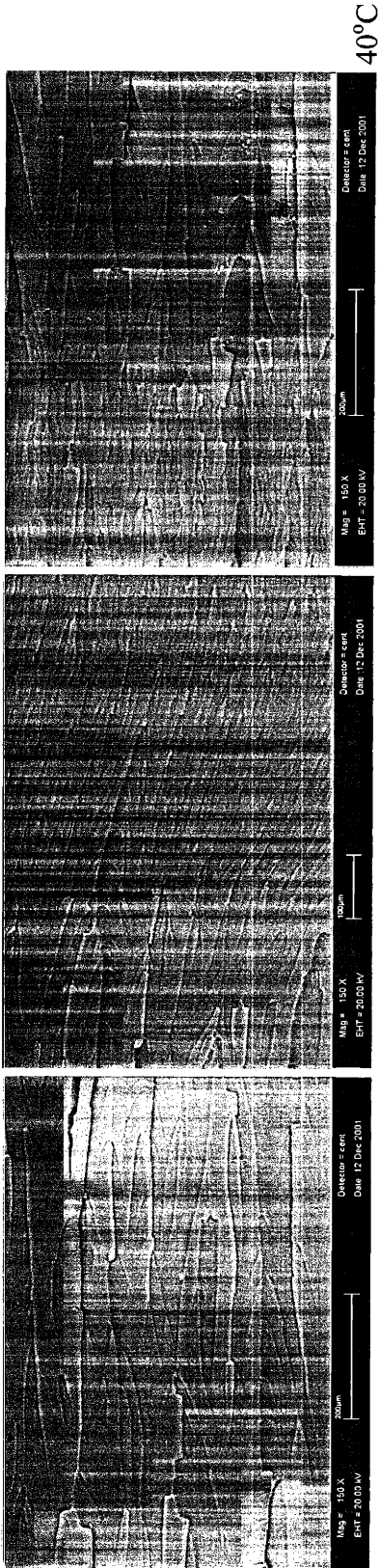
(4) rough area next to the pre-crack front



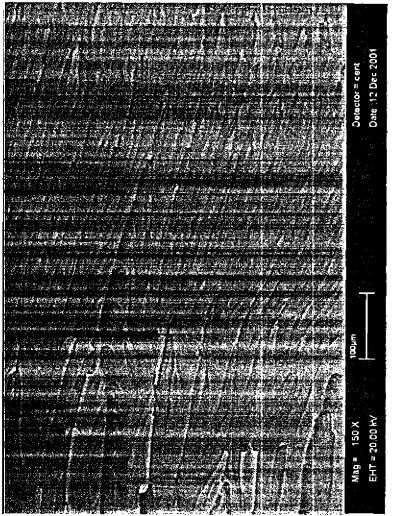
(5) rough area → less rough area of small steps



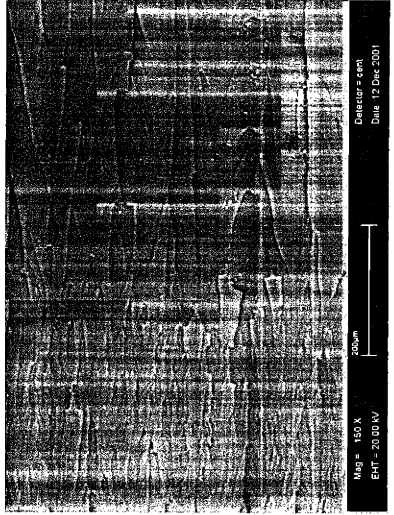
(6) small step → rough area near the end



(7) rough area

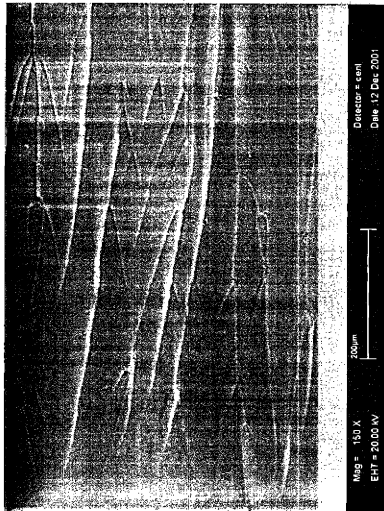


(8) into a less rough area of narrow steps

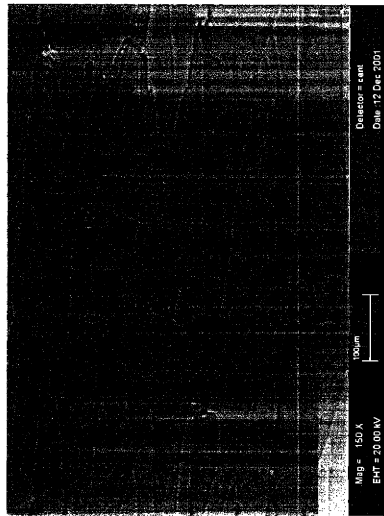


(9) narrow step → second rough area

40°C



(10) rough area



(11) rough area extending further

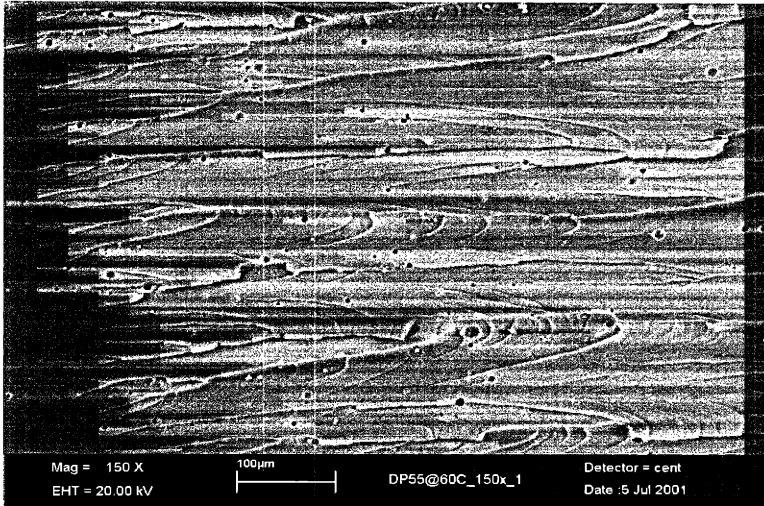
60°C

Figure 3-60 Summary of DP73 fracture surfaces of K_{Ic} tests at different temperatures. (crack propagating direction →)

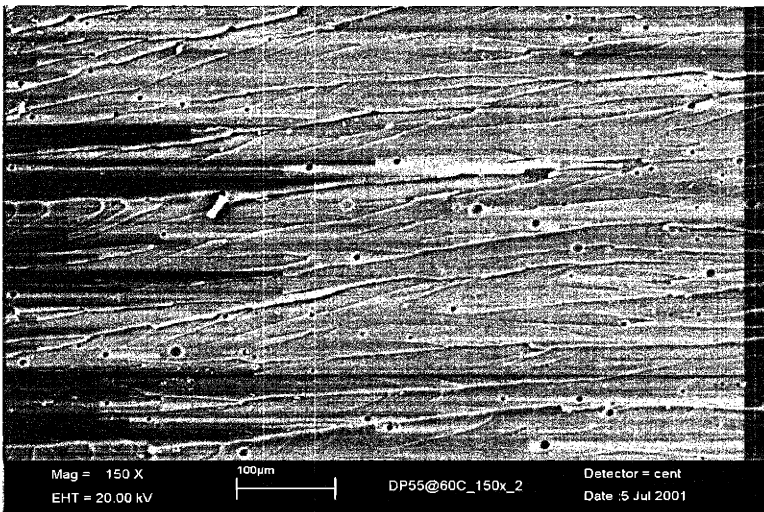
3.3.1.4 DP55

DP55 has similar fracture surface features to DP73. However, compared to those in DP73, fracture surfaces of DP55 generally have coarser steps and smaller rough area because of their lower toughness values. There is one exception at 60°C, at which temperature the toughness of DP55 is twice as high as that of DP73. From Figure 3-61, we see that the sample surface undergoes a first rough → second rough region transition. Compared to Figure 3-60 (10) and (11), we see that fracture surface of DP55 at 60°C obviously experiences more fracture resistance suggested by more step/striation features, which correspond well with its higher toughness.

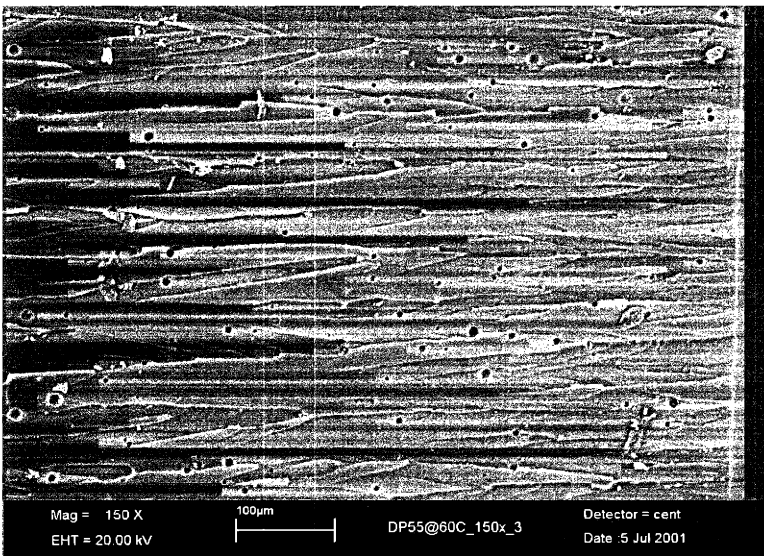
Particles in this sample are also from the same PDMS contamination of the Pt IV catalyst but were found to have little effect on the toughness value.



(1) rough area after pre-crack



(2) rough area → 2nd rough area



(3) 2nd rough region extending to the end

Figure 3-61 Fracture surfaces of a DP55 K_{Ic} sample tested at 60°C. (crack propagating direction →)

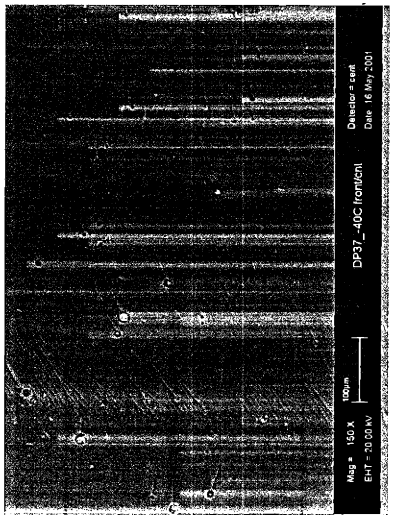
3.3.1.5 DP37

DP37 system is relatively brittle compared to D100 and other DP's discussed before. At -40°C , -20°C and 0°C (Figure 3-62 (1) (2) and (3)), we only see a small rough band following the pre-crack, and then a featureless smooth area appears. The steps in the rough band become slightly denser as temperatures goes up. These features are related to lack of deformation in the polymer network at these temperatures.

At 20°C , the rough band after the pre-crack grows much longer and it fans into a smooth region. In the fan region, we start to see small branching features (Figure 3-62 (4)). At both 40°C and 60°C , the first rough area becomes more extended, which should be related to the increase in deformation ability. Then it fans into a less-rough and fine feature area with multiple small steps (Figure 3-62 (7) & (10)). In the end, a rough region appears, particularly extensive at 60°C (Figure 3-62 (11)). This is associated with the slow crack propagation near the end of breakage, which appears as the shoulder region in the load-displacement curve near the end (Figure A-30).

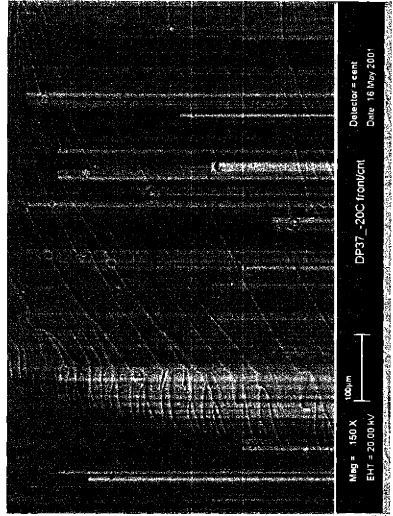
Compared to what is seen in DP73 and DP55 at temperatures above RT, DP37 has smaller deformation ability presented by the smaller rough regions and very fine steps. Compare toughness values of DP73 and DP37 at 60°C , they have similar values but their toughness sources are different. In DP37, rigidity contributes more to its overall fracture resistance than the deformation ability does. While in DP73, chain flexibility and the resultant network mobility is its toughness source. The differences in fracture features between DP73 and DP37 at 60°C prove that different mechanisms lead to the fracture resistance of these two systems.

P100 has similar features to DP37 because their toughness values are close and their mechanisms of fracture resistance are similar.



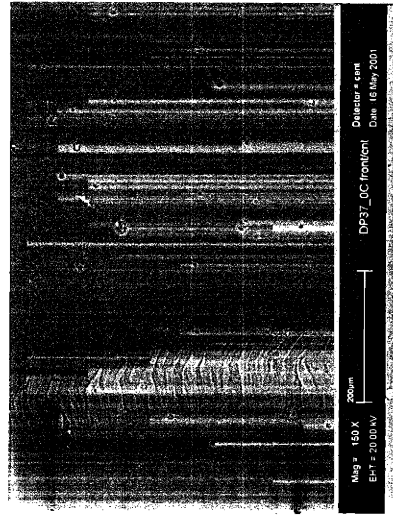
0°C

(1) small band with little features



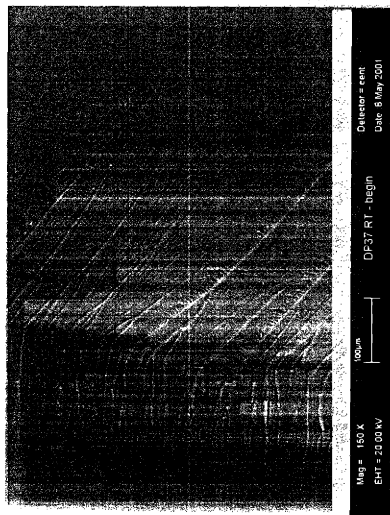
-40°C

(2) small band with few steps

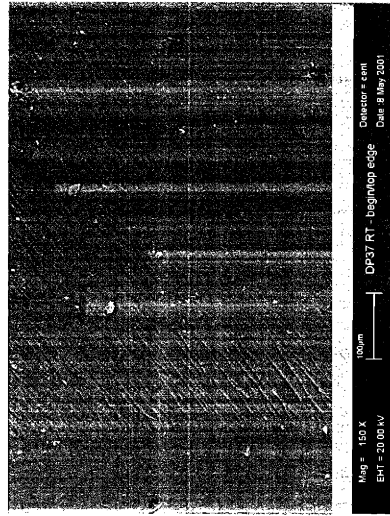


-20°C

(3) small band with few steps



(4) pre-crack rough area + fan region



20°C

(5) multiple narrow step area

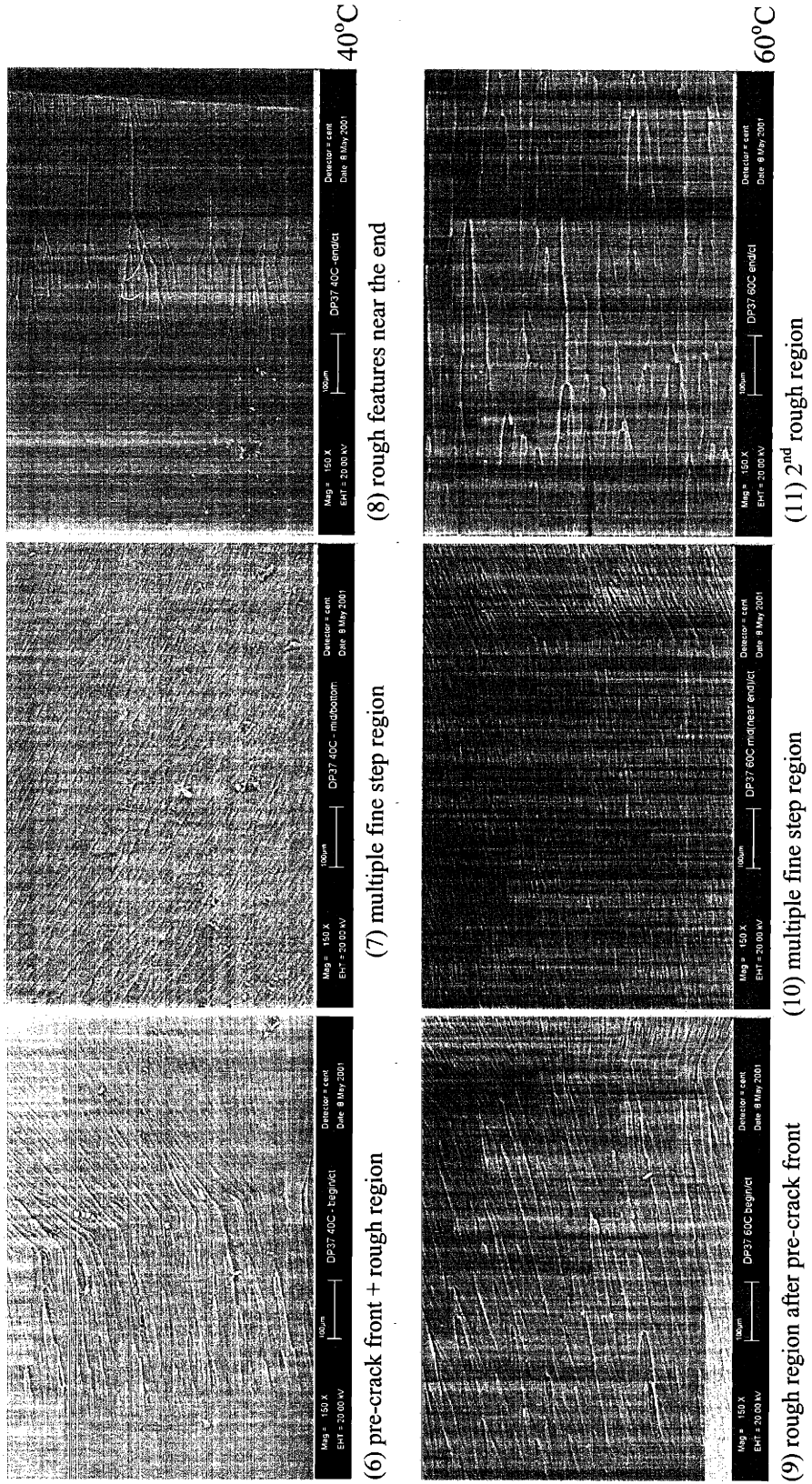
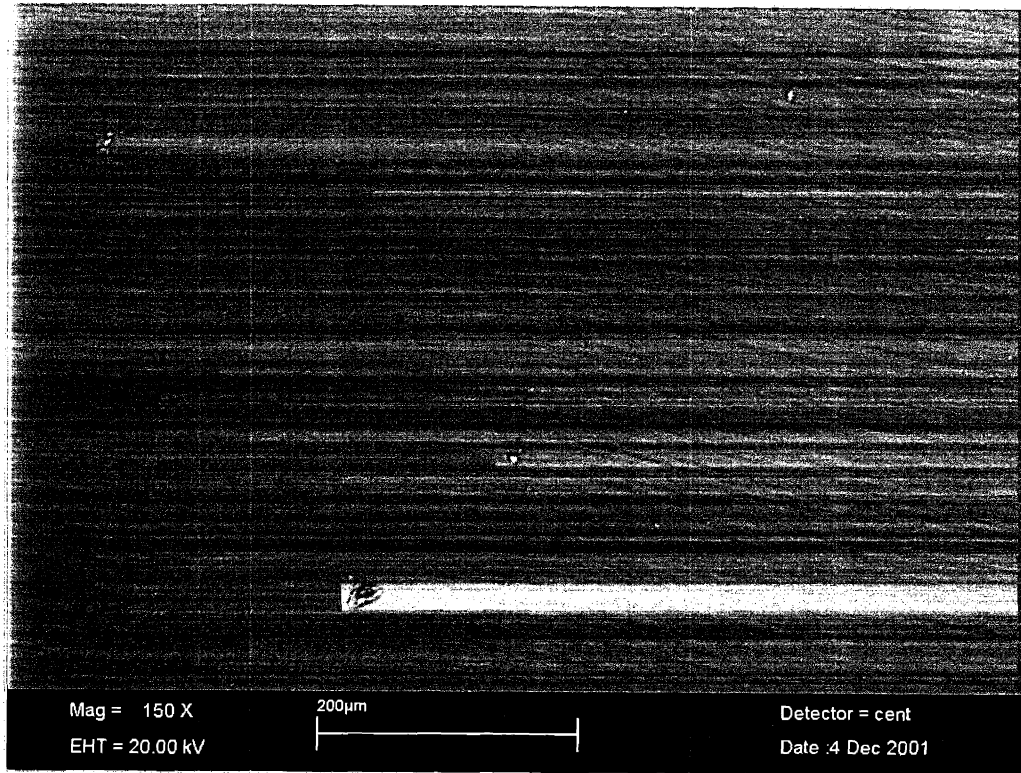


Figure 3-62 Fracture surfaces of DP37 K_{1c} samples tested at different temperatures. (crack propagating direction →)

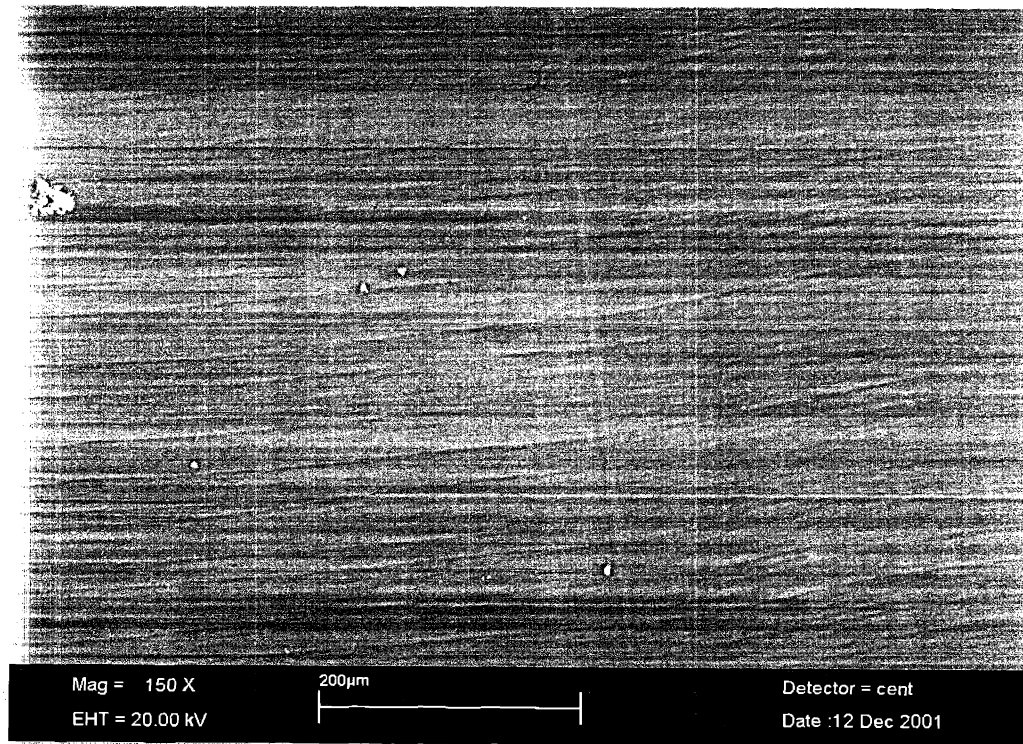
3.3.2 CONDENSATION CURE RESIN

At temperatures above RT, toughened 3136 have fracture surfaces of similar features with extended region of multiple dense and fine steps after the pre-crack region. In Figure 3-63 (a) and Figure 3-63 (b), the fracture surfaces at 20°C and 40°C look very similar. Compare (a) with (b) in Figure 3-64, the steps become slightly coarser as temperature increases from 20°C to 60°C. This results in a slightly lower toughness value at 60°C.

For the un-toughened 3136, fracture surfaces of samples tested below 40°C have interleaving rough and smooth areas. Starting from the pre-crack front, it has a sequence of rough, smooth, rough, smooth, rough, and smooth areas. The only difference lies in the propagating length of these areas. At -40°C, -20°C and 0°C, the rough areas form very thin bands. At 20°C and 40°C, they extend greatly. An example of the look of these rough bands is shown in Figure 3-65. At 60°C and 80°C, the rough region extends to the whole fracture surface, leading to the disappearance of the smooth areas. The rough features resemble much of those at lower temperatures, but seem to have a coarse structure of wider-spaced steps (Figure 3-66 and Figure 3-67).

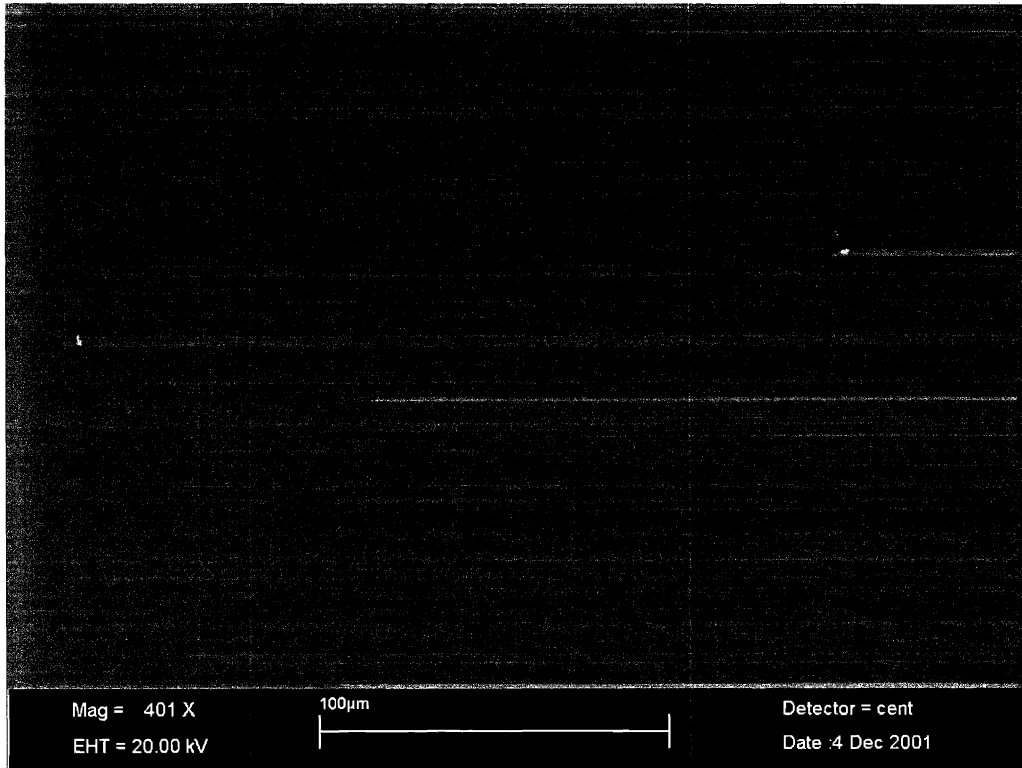


(a) 20°C

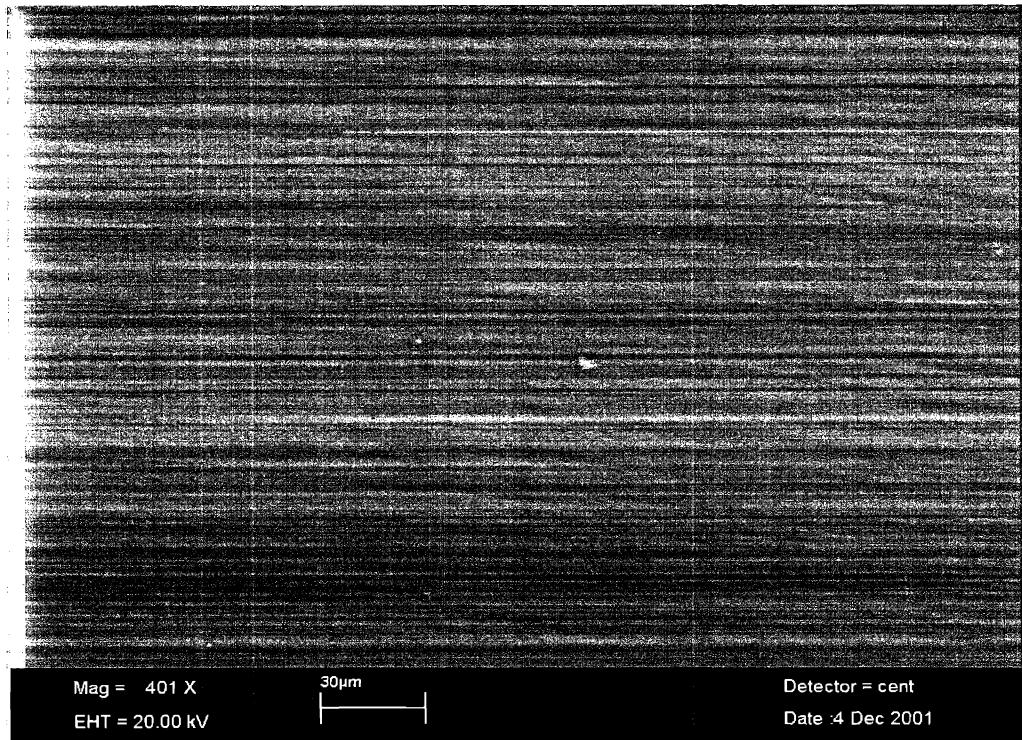


(b) 40°C

Figure 3-63 Fracture surfaces of 3136T K_{Ic} samples: (a) 20°C & (b) 40°C with same toughness $0.39\text{MPa m}^{1/2}$. (crack propagating direction →)



(a) 20°C



(b) 60°C

Figure 3-64 Fracture surfaces of 3136T K_{Ic} samples: (a) 20°C ($0.39 \text{ MPa m}^{1/2}$) & (b) 60°C ($0.34 \text{ MPa m}^{1/2}$). (crack propagating direction →)

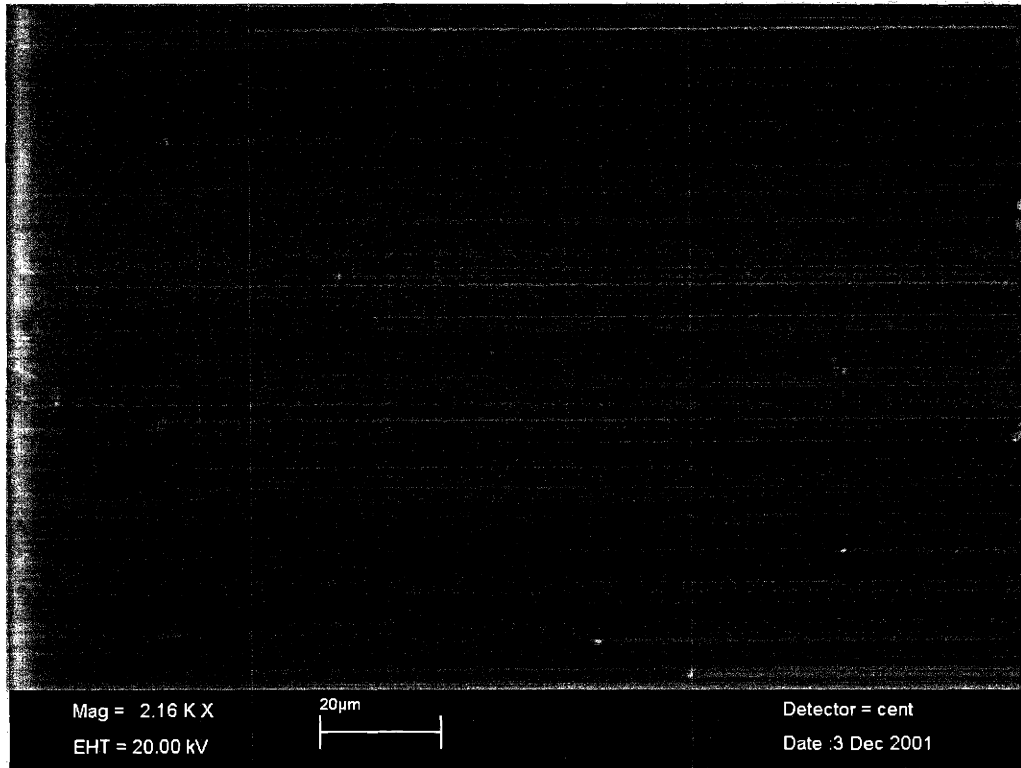


Figure 3-65 Fractograph of the rough band in 3136U K_{Ic} samples tested at 20°C. (crack propagating direction →)

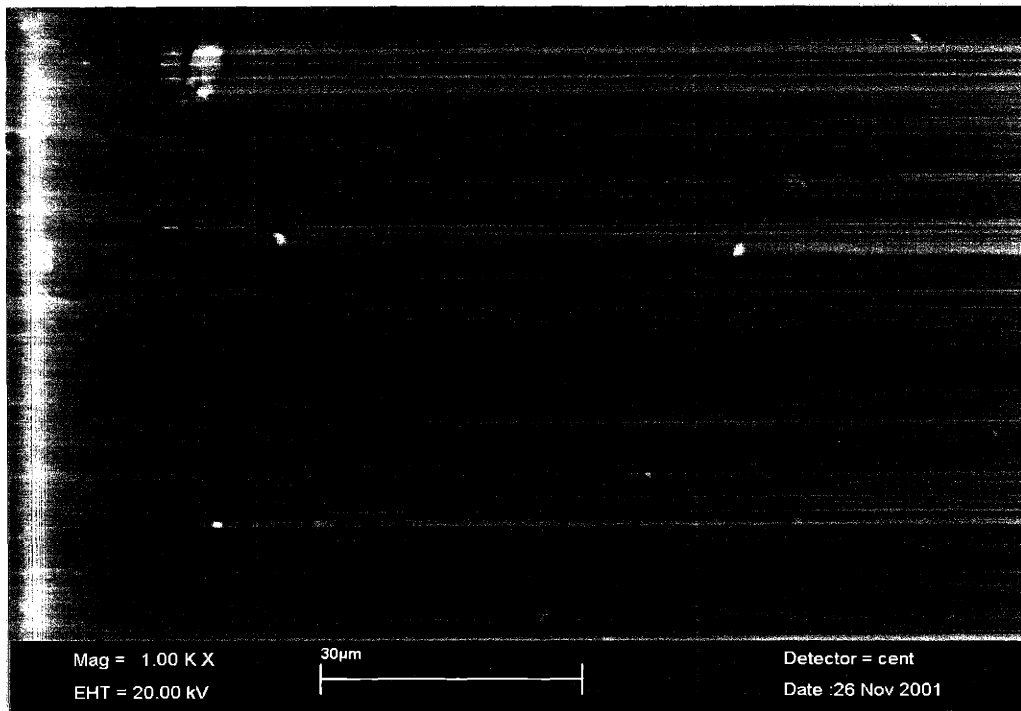


Figure 3-66 Fractograph of 3136U K_{Ic} sample tested at 60°C. (crack propagating direction →)

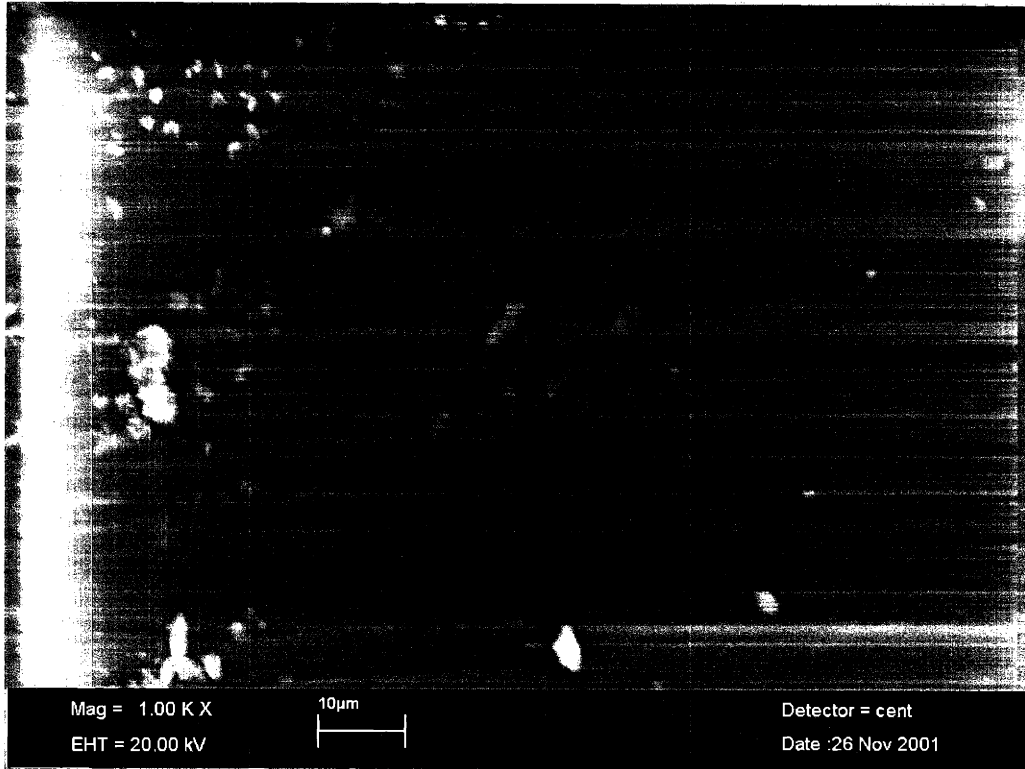


Figure 3-67 Fractograph of 316U K_{Ic} sample tested at 80°C. (crack propagating direction →)

3.3.3 SUMMARY

In summary, fracture surfaces of K_{Ic} samples tested at different temperatures are analyzed. For 2672 resins, fracture features are consistent with their deformation and fracture mechanism. This is especially notable in the DP systems. These are helpful evidences in explaining the differences in fracture behavior and deformation abilities in addition cure resins with different crosslinkers.

In 3136 resins, fracture features with fewer deformation features suggest this is a rigid system with small network mobility. The difference between 3136U and 3136T lies in how extensive the rough features are present. The fracture surface features are also consistent with the fracture toughness results.

3.4 Conclusion and proposed mechanism

From flexural property results, we can conclude that the maximum flexural strength and flexural modulus of the silicone resins decrease with increasing temperature. The extent of the magnitude in change is determined by different resin systems. The flexural properties of the addition cure resin are more sensitive to temperature changes, compared to the condensation cure resins. The addition cure resins also differ among systems with different crosslinkers. The fracture toughness results demonstrate that the addition cure resin experiences a peaking behavior, while the condensation resin has a monotonic change of small magnitude. SEM analyses on fracture surfaces reveal that both silicone resins demonstrate different fracture features under different testing temperatures. Some fracture samples show substantial deformation accompanying fracture, while others show little. The mechanical behavior above is determined by the network structure of the silicone resins, including crosslinking density, molecular structure, and intra- and inter-molecular interactions.

Toughness is a way of measuring the ability of the material to deform and to absorb energy before fracture. Because silicone resins are thermoset resins with crosslinked network, they often have small deformation ability. In addition, these crosslinking points do not change with parameters like temperature. An increase in temperature only provides thermal energy for molecules to overcome energy barriers when subjected to applied stress. Fracture toughness behavior of the silicone resin can be explained by the proposed mechanism below. The competition between rigidity and yielding leads to the change in fracture toughness with temperature. The deformation ability of the network is an important source of toughness. At low temperatures, if the network still has enough inherent mobility, the increase in its rigidity at these temperatures will cause the overall fracture toughness to increase. However, if the network is frozen and loses its mobility under such temperatures, the overall toughness will drop even with the increasing rigidity. At elevated temperatures, silicone resin networks usually lose their rigidity substantially. Molecules become flexible and move relatively easily under the supply of thermal energy. The rigidity loss is dominant

compared to the mobility increase effect at elevated temperatures, so the overall toughness values always decrease. In general, at temperatures below the glass transition temperature, competition and balance between rigidity and mobility of the silicone resin network result in its toughness change with temperature.

References:

1. Kinloch AJ, Young RJ. *Fracture behavior of polymers*: Applied Science Publishers, 1983.
2. Ward IM, Hadley DW. *An introduction to the mechanical properties of solid polymers*. Chichester, England: John Wiley and Sons Ltd, 1993.

PART II SILICONE RESIN COMPOSITES

CHAPTER 4. Background and scope of research

4.1 Composites

Composite materials, which usually involve the bonding of two or more materials, have been studied extensively for many years. Composites is a broad terminology these days, which can refer to a metal matrix composite, a polymer matrix composite, a ceramic matrix composite, or the nano-composite of growing interests recently. The matrix and the reinforcements can be different materials or the same material, for example, carbon-carbon composite.

Composite material is usually used to balance or improve the properties of one phase by adding another. The advantages of composites compared to other simple materials are: higher specific strength and specific modulus, better fatigue properties, environmental resistance for example moisture resistance, and safety when damage occurs. Some advantages are clear to see on a polymer matrix composite. The mechanical properties and thermal and dimensional stability of polymer matrix is greatly improved by incorporating strong reinforcing materials such as glass fiber or carbon fiber. These materials are usually of high temperature application possibilities.

4.1.1 POLYMER COMPOSITES

The components of a polymer matrix composite (or laminate), which is what we study in this research work, consist of a polymer material matrix and a reinforcement. The matrix can be thermoplastic or thermoset resins. Commonly used thermoplastics matrix materials are: polycarbonate (PC), polyamide-imide (PAI), polyether-ether ketone (PEEK), polyacetals, polyphenylene sulfide (PPS). Examples of thermoset matrix materials are: epoxy, polyester, vinyl ester, and phenolic. Compared to the thermoplastic matrix, the advantages of using a thermoset resin matrix include thermal stability, chemical resistance, and creep resistance. Although thermosets have relatively low fracture resistance (i.e. a low fracture toughness and impact resistance) compared to

thermoplastics, they are used widely because of its thermal stability and ease of processing. Silicone resins also belong to the thermoset category, and yet they have not been fully explored as a matrix material due to their brittleness. Details of research work on silicone resin composites made so far will be discussed in a later section.

Fiber reinforcements are in the forms of continuous fibers, short and discontinuous fibers, and woven 2-D or 3-D fiber textiles. Commonly used materials include graphite, carbon, glass, and some polymer materials like Kevlar. Glass fibers are now still probably the most commonly used fibers among all after they became widely available from the 1940s. They are cheap and have high tensile strength and good insulating properties. In addition to these, they are chemical resistant, heat resistant, fire resistant, and moisture resistant. Their disadvantages include low static fatigue properties, relatively high density and low tensile modulus. Among the types of glass fibers, E-glass is of the lowest cost and is the most widely used one, whose main components include SiO_2 , Al_2O_3 and CaO . E-glass has both good strength and water degradation resistance.

Woven fabric in sections thereafter is referred as those 2-D textiles formed from continuous fibers. Although woven fabric laminates lose some tensile modulus and tensile strength compared to the longitudinal properties of uni-directional composites (largely due to inter-fiber friction of woven textile), the former demonstrate better inter-laminar strength and damage tolerance. They also have more balanced properties and good stability in the warp and fill (i.e. 0° and 90°) directions. The lay-up process of the laminates is also faster and easier to control than that of the uni-directional fiber composites. Along with their low cost of the woven fabrics, woven fabric laminates are very common in structural material applications.

Typical examples of primary fabric weaves are plain, basket, and satin weave [1]. Plain weave is the most common and is formed by weaving the warp and fill yarn in an over-one-under-one fashion. It is good for wet lay-up applications because it is easily wet by resins. Basket weave is similar to plain weave but with two or more warp yarns going over or under two or more filling yarns, which make them more pliable. Satin weave is typically available in four harness satin (Crowfoot), five harness satin or eight harness

satin. In these weaving styles, one warp yarn is carried over several filling yarns before going under a filling yarn. The fabric is more pliable and can fit to complex contoured and spherical surfaces. Take eight-harness satin as an example: the yarns are woven with a warp yarn over seven and under one filling yarns. Composites made of this type of textile have comparatively high strength and are common to the aerospace industry. An illustration of the eight-harness satin weave fabric is shown below in Figure 4-1 [2]:

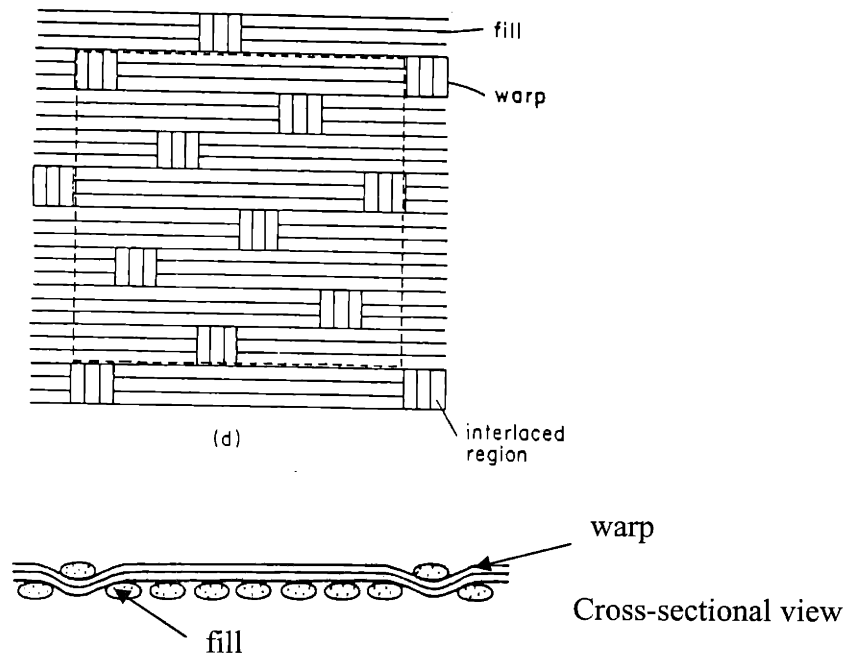


Figure 4-1 Eight harness satin weave pattern of woven fiberglass textile.

Because of different characteristics and properties of fiber reinforcements, proper selection of fiber type, form, amount, orientation, and weaving pattern is crucial in deciding the final properties and applications of the composites.

Polymer matrix composites have been used widely due to their processing convenience, low density, and high specific properties. Their applications vary from sporting goods, automotive industry, aircraft, military, and space applications, where weight reduction and good mechanical properties are important. For sporting goods, applications include rackets, golf shafts, and fishing poles, where strength is needed but

weight is always undesirable [3]. For aircraft applications, glass reinforced polymer composites are used in aircraft cabin interior, wings, and other components [4].

4.1.2 MECHANICS OF COMPOSITES

4.1.2.1 Uni-directional composites

In a composite with uniformly distributed continuous fiber throughout a void free matrix and with perfect bonding between fibers and the matrix, consider the elastic deformation of the composite: the elastic modulus E_c and strength σ_c along the fiber direction are given by the rule of mixture

$$E_c = E_f V_f + E_m (1 - V_f) \quad \text{Equation 4-1}$$

$$\sigma_c = \sigma_f V_f + \sigma_m (1 - V_f) \quad \text{Equation 4-2}$$

where V_f is the volume fraction of fibers, and subscripts m and f stand for matrix and fiber, respectively. The composite properties depend on the characteristics of both matrix and fibers and the fiber content.

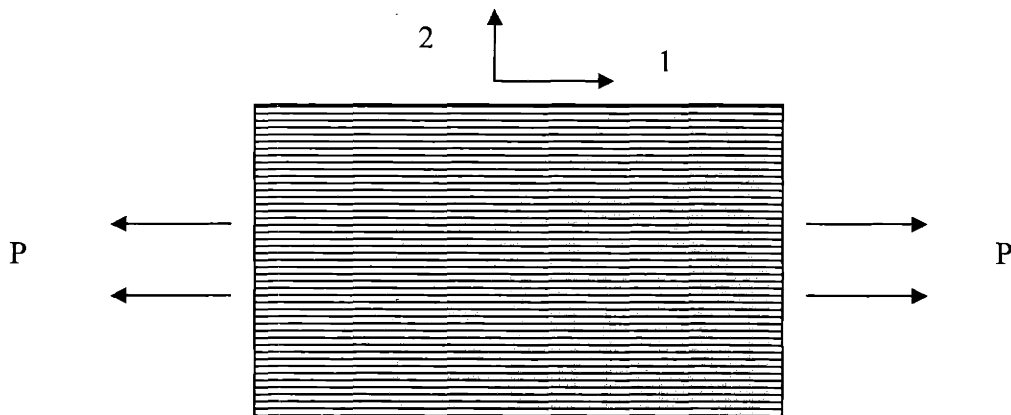


Figure 4-2 Illustration of a uni-directional fiber composite under load.

4.1.2.2 Mechanics of a lamina (single-ply)

A lamina (a ply or a layer) is constructed by fibers and a thin layer of matrix. In addition to the abovementioned assumptions, assume both materials are isotropic, the longitudinal stress σ_c carried by the composite is also given by Equation 4-2.

The elastic modulus along the fiber direction of the composite is given by the rule of mixture: (With standard stress notations - 11 and 22 stand for the normal directions and 12 is the shear direction)

$$E_{11} = E_f V_f + E_m (1 - V_f) \quad \text{Equation 4-3}$$

and the transverse modulus (normal to the fiber direction) is given by:

$$E_{22} = \frac{E_f E_m}{E_m V_f + E_f (1 - V_f)} \quad \text{Equation 4-4}$$

where E_f and E_m are the elastic moduli of the fiber and matrix respectively.

The Poisson ratios of the lamina are:

$$\nu_1 = \nu_f V_f + \nu_m (1 - V_f) \quad \text{Equation 4-5}$$

&

$$\nu_2 = \nu_1 \frac{E_{22}}{E_{11}} \quad \text{Equation 4-6}$$

The above equations present a simple and ideal picture of how the composite strength is dependent upon the properties of both matrix and fibers, and the fiber volume content. Because fibers often possess a much higher modulus than the matrix material, the composite longitudinal modulus is usually between the values of the fibers and the matrix. Fibers also become the main load carrier in the composite along the longitudinal direction and often constitutes of the major fractions of the composite. In real situations, the mechanics become more complicated with the presence of voids inside the matrix,

with imperfect adhesion characteristics between fibers and the matrix, and the internal stress caused by fiber and matrix thermal mismatch.

The stress-strain behavior of the lamina in the normal directions in Figure 4-2 is given by:

$$\varepsilon_{11} = \frac{\sigma_{11}}{E_{11}} - \nu_2 \frac{\sigma_{22}}{E_{22}} \quad \text{Equation 4-7}$$

&

$$\varepsilon_{22} = \frac{\sigma_{22}}{E_{22}} - \nu_1 \frac{\sigma_{11}}{E_{11}} \quad \text{Equation 4-8}$$

From Equations 4-7 and 4-8, we can see that the lamina behaves like an orthotropic material in spite that both matrix and fibers are isotropic. The behavior of the composite is changed due to the presence and distribution of unidirectional fibers.

4.1.2.3 Mechanics of a laminate composite

When a number of laminas are stacked in the thickness direction, a laminate is constructed. The stacking sequence and pattern of laminas can lead to substantially different properties of the final laminate and thus is the one of the key factors in designing a laminate / composite.

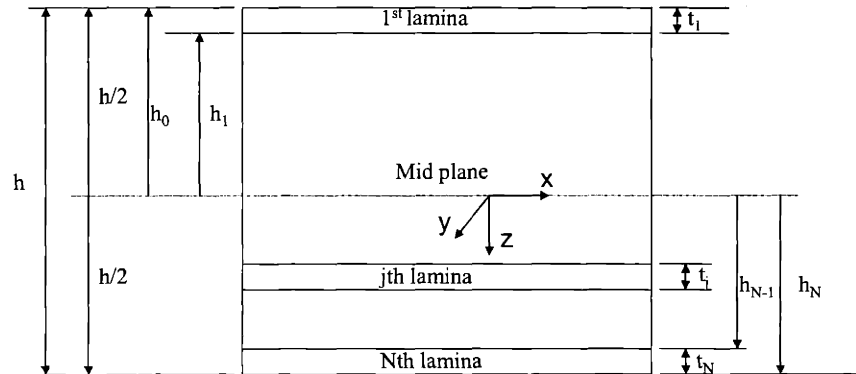


Figure 4-3 Construction of a laminate from laminae [5].

Classical lamination theory is used to characterize the stress and strain state in each lamina of a laminate [5-7]. The forces and moments are expressed through a few useful stiffness matrices: $[A]$ extensional stiffness matrix, $[B]$ coupling stiffness matrix, and $[D]$ bending stiffness matrix. They are presented through the following equations [5, 7]:

$$\begin{bmatrix} F_{xx} \\ F_{yy} \\ F_{xy} \end{bmatrix} = [A] \begin{bmatrix} \varepsilon_{xx}^o \\ \varepsilon_{yy}^o \\ \varepsilon_{xy}^o \end{bmatrix} + [B] \begin{bmatrix} k_{xx} \\ k_{yy} \\ k_{xy} \end{bmatrix} \quad \text{Equation 4-9}$$

$$\begin{bmatrix} M_{xx} \\ M_{yy} \\ M_{xy} \end{bmatrix} = [B] \begin{bmatrix} \varepsilon_{xx}^o \\ \varepsilon_{yy}^o \\ \varepsilon_{xy}^o \end{bmatrix} + [D] \begin{bmatrix} k_{xx} \\ k_{yy} \\ k_{xy} \end{bmatrix} \quad \text{Equation 4-10}$$

$$A_{mn} = \sum_{j=1}^N (\bar{Q}_{mn})_j (h_j - h_{j-1}) \quad \text{Equation 4-11}$$

$$B_{mn} = \frac{1}{2} \sum_{j=1}^N (\bar{Q}_{mn})_j (h_j^2 - h_{j-1}^2) \quad \text{Equation 4-12}$$

$$D_{mn} = \frac{1}{3} \sum_{j=1}^N (\bar{Q}_{mn})_j (h_j^3 - h_{j-1}^3) \quad \text{Equation 4-13}$$

$$\bar{Q}_{mn} = \begin{bmatrix} \bar{Q}_{11} & \bar{Q}_{12} & \bar{Q}_{16} \\ \bar{Q}_{12} & \bar{Q}_{22} & \bar{Q}_{26} \\ \bar{Q}_{16} & \bar{Q}_{26} & \bar{Q}_{66} \end{bmatrix} \quad \text{Equation 4-14}$$

where F_{xx} and F_{yy} are normal force resultants, and F_{xy} is shear force resultant; M_{xx} and M_{yy} are bending moment resultants, and M_{xy} is twisting moment resultant; ϵ_{xx} and ϵ_{yy} are midplane normal strains and γ_{xy} is midplane shear strain in the laminate; k_{xx} , k_{yy} are bending curvatures in the laminate, and k_{xy} is the twisting curvature; N is the number of laminae; $(\bar{Q}_{mn})_j$ represents elements in the stiffness matrix $[\bar{Q}]$ of the j^{th} lamina; h_{j-1} is the distance from midplane to the top of the j^{th} lamina and h_j is to the distance to the bottom of the j^{th} lamina (see Figure 4-3). Matrices of $[A]$, $[B]$, and $[D]$ have 9 nonzero components for general orthotropic condition.

Simplifications can be made when $[B]$ is zero for symmetric laminates and $[A]$ is zero for balanced laminates. Common way of applying the laminate theory is calculating through available software to simplify the math and conversion of matrices. Much analytical and modeling work has been performed on the basis of the classical lamination theory described above. One example is three analytical models, i.e. mosaic model, fiber crimp mode and bridging model, presented by Chou and Ishikawa to characterize thermo-mechanical behavior of two-dimensional woven fabric composites [2].

4.1.2.4 Sandwich beam stress analysis

Mechanics of a sandwich beam is introduced here as an approximation of hybrid matrix composite stress analysis. A sandwich beam is usually made up of a high modulus skin and a low density core like foam. These beams can be made to meet specific performance requirements by choosing appropriate skin and core materials and by designing them in the correct dimensions.

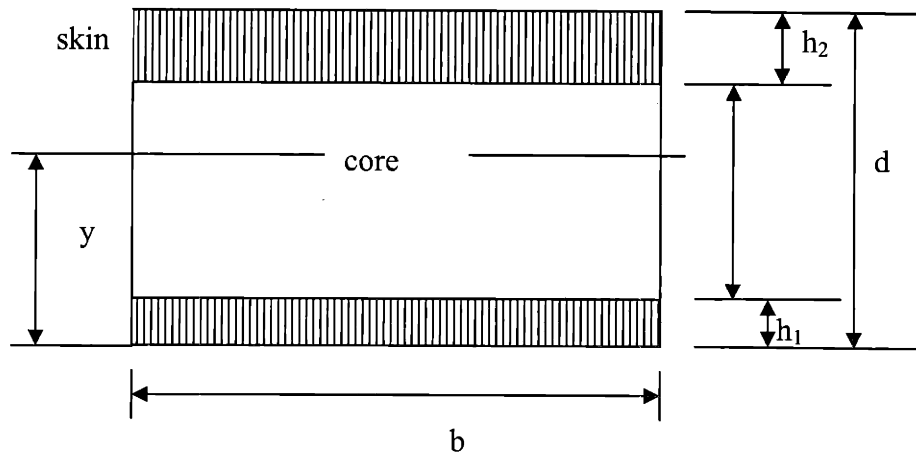


Figure 4-4 Construction of a sandwich beam with skin and core materials.

From homogeneous beam theory, in a sandwich section of width b and depth d shown in Figure 4-4, neutral axis of the beam can be found at position y [8]:

$$y = \frac{1}{2} \left[\frac{E_s d^2 - (E_s - E_c) \{ (d - h_2)^2 - h_1^2 \}}{E_s d - (E_s - E_c)(d - h_1 - h_2)} \right] \quad \text{Equation 4-15}$$

where E_s is the skin modulus, and E_c is the core modulus. When h_1 is equal to h_2 in a symmetric structure, the neutral axis is at the center of the depth, i.e. the position of $d/2$.

Under the condition of $h_1 = h_2 = h$, the stiffness of the beam is obtained through [8]:

$$S = \frac{bd^3}{12} E_s \left[1 - \left(\frac{E_s - E_c}{E_s} \right) \left(1 - \frac{2h}{d} \right)^3 \right] \text{Equation 4-16}$$

by which the elastic behavior of the beam is predicted through the elastic moduli of the skin and core and the beam dimensions.

4.1.2.5 Interlaminar shear stress

Interlaminar stresses are important in load transfer in the laminate and are essential to the mechanical properties of the composite. They exist in a laminate because of interactions between adjacent layers. These interactions result from differences in Poisson ratios and coefficients of mutual influence between laminas.

A laminate with x - y plane parallel to the lamination which is subjected to load in the x direction can develop stresses out of the x - y plane such as σ_{zz} , τ_{yz} and τ_{xz} . These stresses are named interlaminar stresses and are normally determined by finite element analysis [7]. Generally, all three stresses can exist in a laminate. Often, if there is no extension-shear coupling effect, there is only τ_{xz} – and this is the case for balanced laminate (θ - θ). A cross ply laminate ($0^\circ/90^\circ$) would only have a Poisson ratio mismatch between layers and thus τ_{yz} and σ_{zz} are non-zero [5]. Interlaminar shear strength is defined as the shear strength parallel to the plane of lamination, which is τ_{xz} . It is often determined by matrix properties and fiber/matrix interfacial properties. Stronger matrix, better adhesion strength between fiber and matrix and higher matrix resin content can lead to higher interlaminar shear strength of a composite. Experimentally it can be determined by short-beam shear test in accordance with the ASTM standard D 2344-84 [9], in which a three-point bending test is performed on samples with small span-to-thickness ratio to ensure a horizontal shear failure between laminas.

In the short-beam shear test, the homogeneous beam equations are considered as the theoretical basis [5, 9]:

$$\sigma_{normal}^{max} = \frac{3P}{2bh} \left(\frac{L}{h} \right) \text{Equation 4-17}$$

$$\sigma_{shear}^{max} = \frac{3P}{4bh} \text{ Equation 4-18}$$

At a small enough L/h ratio (the recommended L/h ratio is often between 4 and 5), the beam will fail in an interlaminar shear fashion with cracking occurring parallel to the laminate plane and between laminas. At small L/h ratios, the normal stress in the laminate is low and the maximum stress present in the laminate is equal to the maximum interlaminar shear strength at midplane. In this way, testing short beam flexural specimens can obtain the interlaminar shear strength value.

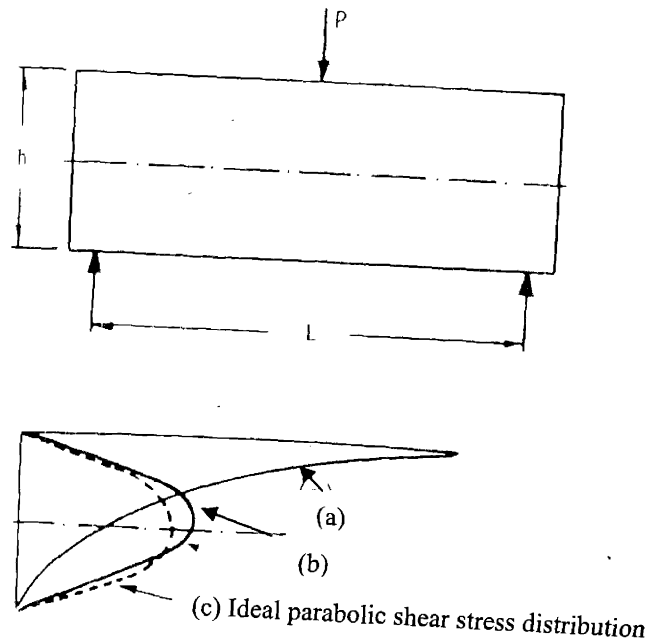


Figure 4-5 Shear stress in a short beam shear test specimen. (a) near the support points; (b) near the midspan; (c) ideal parabolic shear stress [5].

Shear stress distribution in the short beam is illustrated in Figure 4-5. However, it has been noted that failure modes other than mid-plane interlaminar shear can also occur during the short beam tests due to non-ideal stress distributions in the laminates. For example, fiber breakage similar to that occurs during flexural failure when the maximum tensile or compressive stress is reached on the outside fiber; or buckling of the beam due to inelastic deformation [10, 11]. Under these conditions, measurements of interlaminar

shear strength by this method are not accurate. In general, the short beam shear test is a simple way of measuring the interlaminar shear strength and thus has been used widely.

4.1.3 ENVIRONMENTAL EFFECTS

For polymeric composites, the environmental factors, including humidity, heat, fire, UV light, and chemical substances, influence many of their applications. These can cause degradation of the polymer matrix or change the interface properties between matrix and fibers. The result is reduction in mechanical or physical properties of the composites.

4.1.3.1 Moisture absorption

Moisture gets into a composite laminate by surface absorption and diffusion. Moisture in a composite can penetrate the matrix polymer and cause dilation of the matrix and a reduction in T_g of the matrix resin. It also attacks the interface of matrix and fibers and results in interfacial strength loss. Moisture level in a composite often causes reduction in its properties like strength and stiffness, interlaminar shear strength, and fatigue performance [5, 12-15]. Moisture can also induce strains inside the laminate, causing a change in the stress state of the material [6].

Upon exposure, the moisture content of a composite often increases quickly in a linear fashion at the beginning and then reaches the equilibrium content after a certain time. The behavior of moisture content versus time will depend on factors like: matrix and reinforcement material properties, composite void content, experienced stress level, and the exposed environment including temperature and humidity level.

Assuming the composite is a single-phase Fickian material and the diffusion constant D_z is independent of time, its moisture concentration change with time behaves according to Fick's law [16]:

$$\frac{\partial c}{\partial t} = D_z \frac{\partial^2 c}{\partial z^2} \text{ Equation 4-19}$$

where c is the moisture concentration, z is the through thickness distance, t is time, and D_z is the Fickian diffusion constant of the composite through z direction. For a laminate

with fiber direction parallel to the laminate surface and the fiber diffusion constant is much smaller compared to the matrix diffusivity, D_z can be approximated by [5, 17]:

$$D_z = D_m \left(1 - 2\sqrt{\frac{v_f}{\pi}} \right) \text{ Equation 4-20}$$

where D_m is the matrix diffusion coefficient and v_f is the fiber volume content.

Assuming that D_z does not change with z and also it is a 1-D steady state problem, the moisture concentration in the composite at a given ambient relative humidity level can be predicted by [5, 17, 18]:

$$M(T, t) = M_b + G(T, t)(M_m - M_b) \text{ Equation 4-21}$$

where M_b is the initial moisture concentration, M_m is the equilibrium moisture content, and $G(T, t)$ is the moisture absorption function which can be expressed as [17]:

$$G(T, t) = 1 - \frac{8}{\pi^2} \sum_{j=0}^{\infty} \frac{\exp\left[-(2j+1)^2 \pi^2 \left(\frac{D_z(T)t}{h^2}\right)\right]}{(2j+1)^2} \text{ Equation 4-22}$$

with a laminate of thickness h and both sides exposed to moisture.

At the initial linear region of moisture content vs. time^{1/2} curve, G can be approximated by [5]:

$$G \approx 4 \times \left(\frac{D_z(T)t}{\pi^2 h^2} \right)^{1/2} \text{ Equation 4-23}$$

After equilibrium is reached at longer time exposure, G can be simplified to [5]:

$$G(T, t) \approx 1 - \frac{8}{\pi^2} \exp\left[-\left(\frac{\pi^2 D_z(T)t}{h^2}\right)\right] \text{ Equation 4-24}$$

The time needed for a composite laminate to reach its equilibrium moisture content at a temperature T is given by [17]:

$$t_{\max}(T) = \frac{0.67h^2}{D_z(T)} \quad \text{Equation 4-25}$$

from which we can see that the time needed is independent of the ambient humidity level but depends on temperature.

4.1.3.2 Elevated temperature

Polymers and polymer composites under heat may be subject to both physical and chemical changes. Short exposure could drive out moisture, solvents, relieve internal stress, and advance curing of the thermoset resins. These effects sometimes improve the laminate properties or keep them constant. However, upon a longer exposure of heat, degradation of laminates and reduction in properties can happen. For a continuous fiber or woven fabric reinforced polymer laminate, thermal aging at elevated temperature for a long period of time can cause a reduction in mechanical properties. The laminates can also experience weight loss and deterioration due to oxidation or thermal degradation.

Laminates tested at high temperatures often experience loss of strength and stiffness due to the thermal softening effect of polymer at elevated temperatures. This effect is more clearly observed in the matrix dominant properties.

Upon first exposing the graphite/epoxy composites to 500°C for 4 seconds and then immediately for tensile testing, Greszczuk has found that the longitudinal tensile modulus is only a quarter of its room temperature value. The longitudinal strength is also about 50% of its room temperature value [19]. In terms of residual properties of composites after exposure to elevated temperatures, a similar graphite/epoxy composite was heated to 315°C for 40 minutes and was found to lose about 40% of its tensile strength. For flexural strength, the loss was even greater – at 66% [20].

4.1.3.3 Fire performance

Generally, polymer matrix composites have more problems of fire damage compared to metals and their composites. Fire properties of polymer matrix composites are becoming more important as their applications in aircraft interiors, marine applications and other structural applications become common. Fire exposure of these composites can cause disintegrity of the matrix materials, release heat, toxic gas and smoke, and change both their physical and mechanical properties.

An experimental investigation has been performed by exposing a graphite/epoxy composite to a propane flame and studying the damage thus caused. The charring of epoxy begins at approximately 300°C. Measurements of the rate of mass loss suggest that the mass loss is consistent with an Arrhenius rate law. Upon reaching 350°C, the matrix based properties even reduce to zero [21]. Here we see the importance of the fire resistance of the matrix material to the overall composite fire performance.

Many fire standards were set up by the military, government, and scientific institutes. The two used by this research work are cone calorimetry test as specified in ASTM standard E2067-00a [22] and Ohio State University (OSU) fire test in accordance with the Federal Aviation Administration in FAR 25.853(d), Appendix F, Part IV [15].

In the cone calorimetry test specified by ASTM standard E2067, fire response of the tested material is measured in the heat release of specimens as a function of time. The testing environment is full scale and usually involves rigorous setup of testing burn room, which is enclosed in an enclosure room made of fire resistant building materials. This enclosure room contains the burn room, the calorimeter, and the hood and exhaust collection system. The burn room is used to burn tested specimens. The exhaust collection system is used to collect all the combustion products leaving the burnt specimen, and there is a gas analysis system inside the exhaust duct that analyzes the combustion gas for oxygen, carbon monoxide, carbon dioxide, and etc. Usually the testing is expensive due to the details involved in setting up testing rooms, exhaust systems, and instruments for measuring. The heat release is determined by the oxygen

consumption, which is decided from oxygen concentration and exhaust gas flow rate measurements [22].

The oxygen consumption based heat release rate measurement avoids the complexity of directly measuring heat. Instead the oxygen consumption measurement is used, which is simple to implement and also accurate. The theory is based on Thornton's rule, which suggests that it is enough to measure the oxygen consumption in a combustion system to determine the net amount of heat release. Under complete combustion, a constant amount of net heat is released for every unit of oxygen consumption. Approximately, for every 1 kg of oxygen consumed, 13.1 MJ heat are released. This has been obtained from Thornton's observation from studying many organic fuels [23].

The simplest case for rate of heat release measurement exists when only oxygen concentration measurements are used for calculation. This is possible by filtering away water vapor and CO₂ in the combustion gas, leaving only O₂ and N₂. Under this situation, the rate of heat released is calculated by:

$$\dot{q} = 13100 \text{kJ/kg} \times 1.10 \times \dot{m}_e \times \frac{X_{O_2}^A - X_{O_2}^A}{(1.105 - 1.5X_{O_2}^A)} \quad \text{Equation 4-26}$$

where $X_{O_2}^A$ is the original mole fraction of oxygen and $X_{O_2}^A$ is the measured mole fraction of oxygen in exhaust flow; \dot{m}_e is the mass flow rate in exhaust duct (kg/s), and \dot{q} the rate of heat release is in the unit of kW. Other more complicated calculations of heat release rate using concentration measurements of other gases like CO₂ and CO are presented in the ASTM standards and can be found in references [22, 23].

The OSU test standard is used by FAA to determine the heat release rate of cabin materials exposed to radiant heat [24]. Samples are placed vertically and subjected to radiant heat of the desired heat flux density of 3.5 W/cm². A thermopile was used to monitor the temperature differences between air entering the testing environmental

chamber and that leaving. The thermopile output voltage differences are used to calculate the heat release rate:

$$HRR = \frac{(V_m - V_b)K_n}{0.02323} \text{ Equation 4-27}$$

where the V_b is the baseline voltage (mv), V_m is the measured thermopile voltage (mv), K_n is the calibration factor (kW/mv), and 0.02323 has the unit of m².

The two fire standards above are more related to this research work and thus are presented in details, there are still many others available but it is beyond the scope of this thesis to mention them all.

4.2 Silicone resin composites

The most attractive properties of silicone resin composites are highly associated with the thermal stability, moisture resistance, and fire resistance of the matrix resin itself. Because of fire retardant properties, thermal stability, low moisture pick-up and low dielectric constant of silicone resins, applications of using them as matrix materials for composites include composite tooling materials, aircraft interior, space based composite mirrors, and high temperature radomes. Potential space based composite applications provide an important direction of research and development of the resins. Silicone composites also have been used as ceramic precursors [25].

Fire properties of some silicone resin composites have been studied by several researchers. Koo et al. [26] have studied the performance of silicone resin matrix composites with different reinforcements like glass, silica, quartz, Nextel (Al_2O_3), and Nicalon (S₂C). The composites have been developed by Hitco Technologies, Inc. and licensed to Cytec Fiberite, Inc. The silicone polymers SM8000 are polysiloxanes and cured with a catalyst involving the crosslinking of polymer chains into a 3-D network. Resin matrix has been first mixed with silica fillers and catalyst, and then the mixture is used to impregnate the reinforcing fibers to form prepregs. The prepregs are cured by compression or autoclave molding. Thermal tests involve using a simulated solid rocket motor, producing aluminum oxide particle-laden exhaust environment with measured heat fluxes from 2,840 to 13,700 kW/m², a flame temperature ~ 2,200°C, and the velocity of the exhaust ~ 2,000 m/s. Test results of silicone resin composites and phenolic resin based composites have demonstrated that mass loss and peak erosion results of the former all greatly outperformed the latter [27]. A small scale test method - Scaled Ducted Launcher - for testing ablative materials for use in missile launchers has been performed. The silicone resin matrix with silica fabrics and quartz fabrics both outperform the phenolic resin matrix composites with the same reinforcements, with silicone composites having 25% and 50% average erosion, respectively. With the Quarter-Scale Launcher test to simulate the fluid flow patterns which has the same interior geometry, gas flow paths,

and mass flow rate as the full-scale launcher, quartz fiber reinforced silicone composites are found to be more erosion resistant and chemically diffusive during the uptake entrance region, forming a tough char layer [26-33] [34-36].

Textron Systems Corporation has developed a family of DI[®] silicone resins with high temperature properties and low dielectric constants [37]. Laminates of the DI resin matrix and 2-D quartz fabrics are found to be thermally stable to 538°C. Mechanical property data at 538°C suggest that such composite maintains its room temperature values of the tensile modulus, and those of both compressive and flexural modulus and strength. The only exception is that it loses about half of its ultimate tensile strength compared to the room temperature value. These composites also have low dielectric constants (~3 at temperatures between 24°C and 1000°C), low thermal conductivity (0.43 W/mK at room temperature), excellent thermal shock resistance, and good ablation performance. They have been aimed in space applications like re-entry vehicle antenna windows and radomes.

Dow Corning silicone resin laminates have been studied for use in the aircraft cabin interiors [38, 39]. Both methyl and phenyl silicone resin composites with either Nicalon S_iC or E-glass fabrics have been processed and studied for their fire performance and thermal stability. The methyl silicone resin composites have peak heat release rates below 10 kW/m² and are found to be essentially non-burning. This is very low compared to the peak heat release rate of 60 kW/m² in phenolic resin composites. Silicone resin composites also produce very little smoke and the CO yield is less than 0.01%. The addition cure phenyl silicone resin, on the other hand, demonstrate low flammability but not non-burning characteristic because of higher carbon content present in the resin. Both composites didn't ignite when subject to continuous sparking. As a conclusion, both silicone resin composites exhibit good fire resistant properties.

Dow Corning has also developed several composites of addition cure resin X1-2672 with graphite, quartz and glass fibers or fabrics for both composite tooling and space based applications [40, 41]. Moisture strain of the 2672 resin is about 3000 ppm after approximately 1200 hours exposure to a 100% relative humidity environment at

room temperature. As a comparison, cyanate ester resin has a moisture strain ~6500 ppm. The weight change in 2672 resin is ~0.4 wt% after 1200 hours when reaching the equilibrium and this value is comparable to that of cyanate ester resin. The 2672 resin has a dielectric constant about 2.8. The 2672 silicone resin with quartz fabric has a dielectric constant of ~3.1 and a loss tangent from 0.003 -0.015, comparable to the commercial cyanate ester/quartz fabric laminate. With an addition of 50 vol% hollow glass particles, the dielectric constant was lowered to 1.84 and a loss tangent was 0.003-0.005 [41]. The 2672 resin/quartz (with no sizing) composite showed no color change after exposure at 850°F (454°C) for 15 minutes, accompanied by a weight loss of 1.60%. The composite showed slightly darkened color after exposure at 1000°F (538°C) for 10 minutes [40].

Justis has studied condensation cure silicone resin (Dow Corning 4-3136) composite as her undergraduate thesis research project [42]. She made composite laminate in a press with the Phase I and Phase II toughened 3136 and Hexcel 7781 8-harness satin weave fiberglass cloth. A spray method was used to impregnate the fabric with 3136 resin and a final composite has a resin content ~40%, with a 14 plies of fabrics, and ~ 0.25” thickness. A vacuum bag technique was observed not successful in producing sound and void free sample. So a spring loaded mold in an evacuated press was used instead and was found to produce sound composite samples. Silicone resin 3136 laminates were charred at 1200°C and 1400°C for 20 minutes in air. At 1200°C, amorphous SiCO phase and heating to 1400°C resulted in the conversion of SiCO into SiC crystallites suggested by x-ray diffraction analysis results.

In summary, studies of different silicone composites have found that they have good thermal properties, low dielectric constants, and fire resistance.

4.3 Scope of composite research

The scope of the composite research work in this thesis is to investigate both Dow Corning condensation and addition cure silicone resin composites for their mechanical (including both at room temperature and at elevated temperatures), thermal, and environmental properties. From mechanical property characterizations of silicone resins in Part I of this thesis, it is concluded that the strength and modulus of silicone resins are

relatively low and are also very sensitive to temperature change. The mechanical property retention of silicone resins at elevated temperatures is also not satisfactory – normally resulting in a 50% loss in strength and modulus at 60°C. These characteristics of silicone resins are expected to affect the mechanical properties of their glass composites. On the other hand, both the addition cure and condensation cure silicone composites are expected to demonstrate thermal stability, oxidation resistance, moisture resistance, and fire performance based on their matrix properties.

Based on studies of silicone resins and their composites, the idea of engineering a hybrid composite that combines silicone resin and another organic resin will be explored. The purpose is to utilize the advantages of the silicone resin (i.e. its environmental properties and thermal properties) and those of the organic resin (mainly its mechanical properties) to produce a good composite of structural applications. The concept is to use silicone resin as a matrix material for the skin and the organic resin for the core to process a hybrid resin composite with different skin and core components. The silicone skin would protect the organic core from heat, fire, and moisture, while the organic core would offer good strength and modulus and also good property retention at elevated temperatures. Both fabrication and characterization of the silicone and hybrid composites will be carried out.

References:

1. Hexcel Schwebel Product Information
<http://www.hexcelschwebel.com/FAQ/Product.htm>.
2. Chou T, Ishikawa T. *Analysis and modeling of two-dimensional fabric composites*, in *Textile structural composites*, T Chou, Ko FK, Editors. 1989, Elsevier Science Publishers: Amsterdam, The Netherlands.
3. Spencer BE. *Composites in sporting goods industry*, in *Handbook of composites*, ST Peters, Editor. 1998, Chapman and Hall: London, UK.
4. Hadcock RN. *Aircraft applications*, in *Handbook of composites*, ST Peters, Editor. 1998, Chapman and Hall: London, UK.
5. Mallick PK. *Fiber-reinforced composites: materials, manufacturing and design*. New York, NY: Marcel Dekker, Inc., 1993.
6. Jones FR. *Handbook of polymer-fibre composites*. Polymer science and technology series, ed. DM Brewis, Briggs D. England: Longman scientific and technical, 1994.
7. Jones RM. *Mechanics of composite materials*. Philadelphia, PA: Taylor & Francis, Inc., 1999.
8. Williams JG. *Stress analysis of polymers*. London: Longman Group Limited, 1973.
9. *Standard test method for short-beam strength of polymer matrix composite materials and their laminates, ASTM standard D2344/D2344M-00*. Annual Book of ASTM Standards, 2000. **Vol. 15.03**.
10. Berg CA, Tirosh J, Israeli M. *Analysis of short beam bending of fiber reinforced composites*, in *Composite materials: testing and design (2nd conference)*, ASTM STP 497. 1972, ASTM. p. 206-218.
11. Whitney JM, Browning CE. *On Short-beam shear tests for composite materials*. *Experimental mechanics*, 1985. **25**: 294-300.
12. Shen CH, Springer GS. *Environmental effects on the elastic moduli of composite materials*. *Journal of composite materials*, 1977. **11**: 250.
13. Jones CJ, Dickson RF, Adam T, Reiter H, Harris B. *Environmental fatigue of reinforced plastics*. *Composites*, 1983. **14**: 288.
14. Curtis PT, Moore BB. *The effects of environmental exposure on the fatigue behavior of CFRP laminates*. *Composites*, 1983. **14**: 294.
15. Shen CH, Springer GS. *Effects of moisture and temperature on the tensile strength of composite materials*. *Journal of composite materials*, 1977. **11**: 2.
16. Allen SM, Balluffi RW, Carter WC. *Kinetics processes in materials (3.21 textbook)*. MIT, 1998.
17. Shen CH, Springer GS. *Moisture absorption and desorption of composite materials*, in *Environmental effects on composite materials*, GS Springer, Editor. 1981, Technomic Publishing Co., Inc.: Westport, CT.
18. *Standard test method for moisture absorption properties and equilibrium conditioning of polymer matrix composite materials, ASTM standard D5229/D5229M - 92(Reapproved 1998)*. Annual Book of ASTM Standards, 1998. **Vol. 15.03**.

19. Greszczuk LB. *Behavior of graphite epoxy composites under rapid heating, rapid loading*, in *Final Report, NRL Contract NO. N00014-83-C-2330*. 1984, Naval Research Laboratory, Washington, DC.
20. Grimsley FM, Michaels CE. *Structural repair of a burned composite skin*. AIAA Report 94-1432-CP, 1994: 1024-1030.
21. Kucner LK. *Experimental investigation of fire damage to composite materials*, in *Department of Aeronautics and Astronautics*. 1995, Massachusetts Institute of Technology: Cambridge.
22. *Standard practice for full-scale oxygen consumption calorimetry fire tests, ASTM standard E2067-00a*. Annual Book of ASTM Standards, 2000. Vol. 04.07.
23. Huggett C. *Estimation of rate of heat release by means of oxygen consumption measurements*. Fire and materials, 1980. 4: 61-65.
24. *Test method to determine the heat release rate from cabin materials exposed to radiant heat, FAR 25.853 (d), Amendment 25-83, Appendix F, Part IV*.
25. Baney R, Chandra G. *Pre-ceramic polymers*, in *Concise Encyclopedia of Polymer Science and Engineering*. 1990, Wiley: N.Y.
26. Koo JH, Venumbaka S, Miller MJ, Wilson D, Beckley DA, Calamito D. *Effects of major constituents on the performance of silicone polymer composite*. in *30th International SAMPE Technical Conference*. 1998.
27. Koo JH, Venumbaka S, Weispfenning J, Blackmon C. *Silicone matrix composites for thermal protection*. in *31st International SAMPE Technical Conference*. 1999.
28. Boyer C, Talmy I, Powers J, Duffy J, Haught D, Koo JH. *Development and evaluation of erosion-resistant polymer matrix composite ablators*. in *31st Aerospace Meeting*. 1993. Reno, NV.
29. Miller MJ, Koo JH, Wilson D, Beckley DA. *Effect of reinforcements in a silicone resin composite*. in *32nd Aerospace Sciences Meeting*. 1994. Reno, NV.
30. Koo JH, Miller MJ, Wilson D, Beckley DA. *Performance envelope of a silicone polymer composite*. in *Science of Advanced Materials and Process Engineering Series*. 1994. Covina, CA.
31. VanMeter ML, Koo JH, Wilson D, Beckley DA. *Mechanical properties and material behavior of a glass silicone polymer composite*. in *Science of Advanced Materials and Process Engineering Series*. 1995. Covina, CA.
32. Koo JH, Venumbaka S, Cassidy PE, Fitch JW, Clemens P, Muskopf B. *Evaluation of fire safe polymers/composites for marine applications*. in *Science of Advanced Materials and Process Engineering Series*. 1998. Covina, CA.
33. Koo JH, Venumbaka S, Miller MJ, Wilson D, Beckley DA, Calamito D, Blackmon C. *Thermal performance of a class of silicone matrix composites*. in *Science of Advanced Materials and Process Engineering Series*. 1999. Covina, CA.
34. Beckley DA, Sites J. *Processable silicone composite materials having high temperature resistance*. 1996: U. S. Patent.
35. Beckley DA, Weispfenning J. *Missile launcher thermal protection materials*. 1996, Fiberite, Inc.: Winona, WN.
36. Beckley DA, Sites J. *Processable silicone composite material having high temperature resistance*. 1997: U.S. Patent.

37. Marshall DW. *Radomes based on novel inorganic polymer composites*. SAMPE Journal, 2001. **37**(5): 53-58.
38. Chao TC, Burns GT, Katsoulis DE, Page WC. *Development of silicone resins for use in fabricating low flammability composite materials*. in *42nd SAMPE International Meeting*. 1997.
39. Chao TC, Sarmah SK, Boisvert RP, Burns GT, Katsoulis DE, Page WC. *Non-burning silicone resin composite materials*. in *Proceedings of the 1998 43rd International SAMPE Symposium and Exhibition*. 1998. Part 1 (of 2). Anaheim, CA.
40. Zhu B, Keryk JR, Katsoulis DE, Reese HJ, Buether FJ, King R, Okuyama T, Kemp D, McQuiston E, Mizusawa A, Absafieh AA, Marks J, Wu Y, McGarry FJ. *Fiber reinforced composites of tough rigid siloxane resins*. International SAMPE Symposium and Exhibition, 2002. **47**: 1198-1208.
41. Zhu B, Katsoulis D. *A technical feasibility study on using toughened silicone resins for specialty composite applications*. Dow Corning Technical Report, 2002. **2002-I0000-51834**.
42. Justis N. *Toughened silicone resin composites for high temperature applications*, in *Department of Materials Science and Engineering*. 2000 June, Massachusetts Institute of Technology: Cambridge, MA.

CHAPTER 5. Silicone and hybrid composites - experimental

5.1 Materials and properties

5.1.1 MATRIX MATERIALS

5.1.1.1 Addition cure silicone resin 2672B

Dow Corning addition curable x1-2672 resin is crosslinked with the silylphenylene crosslinker B at a S_iH/S_iV_i ratio of 1.1:1. A rotary evaporator was set up to get rid of the toluene in the original resin mixture and to combine the crosslinker into the resin. This procedure produced the so-called solventless resin, in which the solvent toluene was replaced by the crosslinker B. The residual volatile content was controlled at 0.2 to 0.6 wt%. The resin is cured with 1ppm Pt IV catalyst when used as a composite matrix. Some typical properties of the neat resin are listed in Table 5-1.

Table 5-1 Typical properties of addition cure silicone resin 2672B.

Properties	2672B silicone resin
Viscosity, cP	1700 (at 25°C)
Specific Gravity (g/cm^3)	1.1
T_g , °C	88
Tensile Strength, psi (MPa)	N/A
Tensile Modulus, msi (GPa)	N/A
Elongation, %	N/A
Flexural strength, psi (MPa)	6,696 (46)
Flexural modulus, msi (GPa)	0.24 (1.65)
Flexural strain at yield, %	7.23

Viscosity profile of the 2672 B solventless resin with catalyst is shown in Figure 5-1, which was measured by a viscometer and the data were provided by Dow Corning Corporation. As the temperature goes up, the viscosity of the solventless resin goes down slowly. It has a very rapid increase near the curing temperature range $\sim 150^\circ F$ ($65^\circ C$), which is due to the solidification process of the resin during cure.

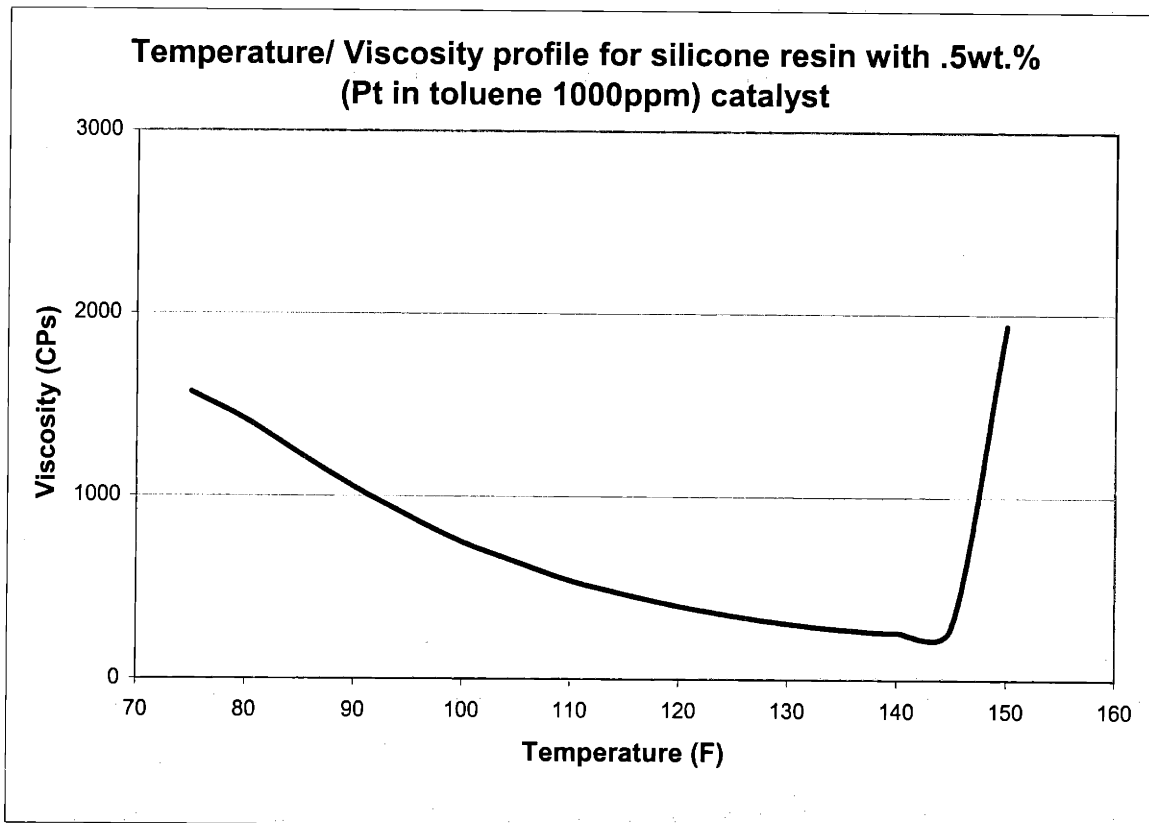


Figure 5-1 Viscosity profile of 2672B solventless resin with heating rate of 3.1°F/min.

5.1.1.2 Condensation cure silicone resin 3136T

Dow Corning 3136T condensation resin is also used as a matrix material to make the composite. 3136T is the phase I toughened 4-3136 resin with short PDMS segment with the degree of polymerization of 55 – 10% KPE. Its curing byproduct is H₂O. Compared to the addition cure resin 2672B, their mechanical properties are similar. 3136T is more brittle, with its room temperature toughness value about 0.40 MPa m^{1/2}. Typical properties of 3136T resin are listed in Table 5-2. As a composite matrix material, the condensation resin was cured with 0.2 wt% Y177 catalyst.

Table 5-2 Typical properties of condensation cure resin 3136T.

Property	Value
Viscosity, cP	solid (at 25°C)
Specific Gravity (g/cm ³)	1.1
Tensile Strength, psi (MPa)	N/A
Tensile Modulus, msi (GPa)	N/A
Elongation, %	N/A
Flexural strength, psi (MPa)	7,322 (50)
Flexural modulus, msi (GPa)	0.21 (1.45)
Flexural strain at yield, %	6

5.1.1.3 Vinyl ester resin

Dow Chemical Derakane Momentum 470-300 vinyl ester resin is an epoxy novolac-based vinyl ester resin designed to provide exceptional mechanical properties at elevated temperatures. It also offers high resistance to solvents and chemicals, good retention of strength and toughness at elevated temperatures, and excellent resistance to acidic oxidizing environment. The resin is carried in about 30 wt% styrene. Its heat distortion temperature is around 150°C. Resin used for composite laminates is cured with 0.5 wt% benzoyl peroxide (BPO) and 0.06 wt% diethylaniline (DEA). Some physical properties and mechanical properties of the neat resin are presented in Table 5-3, from which we see its room temperature flexural properties are significantly higher than those of silicone resins.

Table 5-3 Typical properties of Derakane Momentum 470-300 vinyl ester resin.

Properties	Derakane Momentum 470-300 vinyl ester resin (from Dow Chemical resin information sheet)
Viscosity, cP	300 at 25°C
Specific Gravity (g/cm ³)	1.08
Heat distortion temperature, °C	~150
Tensile Strength, psi (MPa)	12,400 (85)
Tensile Modulus, msi (GPa)	0.52 (3.6)
Elongation, %	3.0-4.0
Flexural strength, psi (MPa)	19,000 (131)
Flexural modulus, msi (GPa)	0.55 (3.8)
Flexural strain at yield, %	-

5.1.1.4 Summary of matrix material abbreviations

The composite study involves using the abovementioned thermoset resins (both organic and silicone) as matrix materials for making fiberglass reinforced composites to achieve thermal stability, moisture resistance, and improved mechanical properties. In order to keep things consistent and easy to follow, each resin is assigned a code to simplify later texts. Abbreviations of these matrix resins are used in referring to the composites made with respective resins.

B - 2672B, Dow Corning addition cure resin X1- 2672 mixed with silylphenylene crosslinker, solventless, cured with Platinum IV catalyst of concentration 1ppm.

T - 3136T, Dow Corning condensation resin 4-3136 toughened with 10% KPE, cured with 0.2 wt% Y177 catalyst

V - Dow Chemical Derakane Momentum 470-300 vinyl ester resin cured with 0.5 wt% benzoyl peroxide (BPO) and 0.06 wt% diethylaniline (DEA)

VB - Hybrid matrix resin of V as the core and B as the skin

V/B 8/4 - Hybrid composite of 8 plies of V core and 2 plies of B skin on each side

V/B 6/6 - Hybrid composite of 6 plies of V core and 3 plies of B skin on each side.

5.1.2 REINFORCEMENT MATERIALS - WOVEN FIBERGLASS FABRIC

Hexcel Schwebel 7781 woven fiberglass (E-glass) fabrics have been used as the reinforcements in this study. Specifications of the fabric can be found in Table 5-4 below [1]. Both heat cleaned and volan finish types have been used: 7781-50-F16 (volan finish) and 7781-38-F12 (heat cleaned with no surface finish). Coupling agents are normally

applied on fiberglass to improve the interfacial strength between fiber and matrix and to protect the glass surface from moisture and other reactive agents. Volan finish is a proprietary surface finishing developed by Hexcel Schwebel to achieve better compatibility between fiberglass fabric and polyester, epoxy or phenolic matrix. The heat cleaned fiberglass fabrics are finished by the heat cleaning process to remove any organic coating on the surface, which usually takes place in an air-circulating oven at 340°C for 15-20 hours. In the continuous heat cleaning process, fiber glass fabric is processed through a carmelizer or coronizer, both of which are high temperature processes that oxidize most of the organic binders and sizing. The fabric is then sent to the next stage of batch oven cleaning, where the fabric is exposed to high temperatures until all organic binders are removed and a pure clean glass fabric is produced [2].

Table 5-4 Specifications of fiberglass fabric used in laminate fabrication.

Density	2.62 g/cm ³
Type of yarns	Warp yarn ECDE 75-1/0 Fill yarn ECDE 75-1/0
Fabric Weight	303 g/m ² (8.95 oz/yd ²)
Weave Style	8H Satin
Nominal Construction yarns/inch	Warp Count 57 Fill Count 54
Fabric Thickness	0.23 mm (9.0 mils)
Breaking Strength	350 lbf/in

5.2 Laminate fabrication procedures

Fiberglass fabrics were cut carefully with a sharp razor blade. An aluminum plate of desired dimension was laid on top of the fabric, and careful cuts were made into the fabric along edges of the plate. Typical laminate dimensions were 6"x7" or 7.5"x7.5". Every laminate consisted of 12 plies of fabric. Extreme care was taken to ensure minimum distortion of the weaving pattern caused by cutting and moving the fabric.

All glass laminates were made by a hand lay-up and expendable vacuum bagging process. Hand lay-up process requires minimum equipment investment and tooling cost, and also offers design flexibility and the possibility of large item production. Two of its main disadvantages are labor intensive and poor quality control. The vacuum bagging process usually involves using bleed-out system to maintain reduced pressures within the bag [3]. Wet lay-up in this thesis was done inside a hood on a piece of non-porous Teflon film. Resins were carefully spread on fabrics by a wooden tongue depressor or a glass slide. This process was done on all 12 plies one after another. The wet lay-ups of the laminates were usually cured in between porous Teflon films, bleeder cloths and non-porous Teflon films inside vacuum bags. (As sketched in Figure 5-2.) Porous Teflon films were used to let through extra resin and volatile byproduct during the curing process. Bleeder papers were used to absorb extra resin and also to provide an air path for volatile byproduct during the cure. The use of bleeder papers was sometimes eliminated if resin content of the composite was already low before cure. The vacuum bag construction involved taping the vacuum bagging films with vacuum sealants, with a vacuum port connecting the bag to a vacuum pump. Composites were then cured in a PHI hot press with pressure applied in the direction perpendicular to the laminate plane.

Materials used for composite lay-up are: Release ease 234 TFNP non-porous Teflon paper (Airtech), Release ease 234TFP-1 – porous Teflon paper (Airtech), bleeder cloth (Airtech), Dahlar[®] release bag film – vacuum bagging film (Airtech), and GS213 vacuum tapes (General Sealant).

5.2.1 FABRICATION PROCEDURE OF 2672B/FIBERGLASS LAMINATES

2672B resin was first mixed with 1ppm Pt IV catalyst. Twelve plies of the woven glass fabrics were impregnated by the mixture layer after layer and formed into a stack. The stacking sequence was 0°. The stacked up fabric with resin was sandwiched between Teflon coated paper and bleeder cloth and then sealed in a vacuum bag.

For sample #1 made of volan finish fiberglass fabric (1106B), 80g resin and 65ul Pt catalyst mixture was used for the wet lay-up. 7781 volan finish glass fabrics were cut into 12 plies of 6"x7". The curing procedure was: 40°C/ 655 KPa/ 1 hour, 85°C/ 655 KPa/ 1 hour, then 175°C/ 827 KPa/ 45 minutes, and 175°C/ 827 KPa/ 5 minutes. A vacuum of ~70-80 KPa was engaged during the curing process. The laminate was then removed from the press and post cured in an air-circulating oven at 200°C for 1 hour without any pressure.

An example laminate of using the heat cleaned fiberglass was made as follows: 75.5g resin and 62ul Pt catalyst mixture was used for the wet lay-up. Heat cleaned 7781 glass fabric was cut into 6"x7" for 12 plies. The curing procedure was: 40°C/83 KPa/10 minutes, 40°C/165 KPa/15 minutes, 40°C/483 KPa/15 minutes, 40°C/655 KPa/20 minutes, 85°C/655 KPa/35 minutes, 85°C/827 KPa/25 minutes and 175°C/655 KPa/1 hour. A vacuum of ~70-80 KPa was engaged during the curing process above. The laminate was then removed from the press and post cured in an air circulating oven at 200°C for 1 hour without any pressure.

The abovementioned cure actually followed the curing schedule of 85°C x 1 hour, 175°C x 1 hour and 200°C x 1 hour. However, the 40°C step was added to ensure enough flow of the resin and thus to get it uniformly distributed in the final laminate. This can not be done at 85°C because the viscosity of 2672B goes up very fast once heated to above 70°C.

Different finishing fabrics resulted in different processing features. Volan finish has led to better wetting of the matrix resin with the glass reinforcements, so it took less time to do the wet lay-up. The heat cleaned fabrics required longer time for the resin to penetrate and thus using it was not as efficient in terms of processing time. However, the heat cleaned fabric was preferred because of its thermal stability. Composites discussed later in this section all use heat cleaned fabrics as the reinforcement materials. The purpose is to improve the high temperature performances and thermal stability of the composites.

5.2.2 FABRICATION PROCEDURE OF 3136T/FIBERGLASS LAMINATES

3136T resin in toluene solution (~60% resin content) was used for wet lay-up. 12 pieces of fiberglass fabrics with desired dimensions were laid out individually on a piece of non-porous Teflon film inside a hood. Resin mixture with Y177 catalyst was spread onto the fabric and then dried overnight to evaporate toluene. Resin coated fiberglass fabrics were dry after one night. It was easy to peel them off the Teflon film and also easy to handle them for stacking up.

An example of the composite made used 83.6g liquid resin (~52.5g solid resin) mixed with 0.2 wt% Y177 catalyst. The curing cycle was 175°C x 1 hour and 200°C x 1 hour. The difficulty of curing 3136T composite lies in its low viscosity at 175°C, which sometimes results in little resin in the fabrics and thus poor mechanical properties of the composite. So for the first few minutes at 175°C, no pressure should be applied to allow time for the resin to gel. One successful example was cured as: 175°C, with no pressure, ~ 5 minutes; 175°C, with ~ 483 KPa pressure and vacuum, 35 minutes; 175°C, with ~ 690 KPa pressure and vacuum, 25 minutes; and finally in the oven at 200°C, 1 hour.

5.2.3 FABRICATION PROCEDURE OF VINYL ESTER/FIBERGLASS LAMINATES

Derakane Momentum 470-300 vinyl ester resin was mixed with curing agent 0.5 wt% benzoyl peroxide (BPO) and 0.06-0.09 wt% diethylaniline (DEA). BPO requires

enough agitation to be dissolved into the resin solution. Resin and curing agent mixture was spread onto 12 plies of 7781 fabrics.

A successful sample was made as follows: 134g vinyl ester resin with 0.67g BPO and 0.12g DEA was used for the wet lay-up. Heat cleaned 7781 glass fabric was cut into 7.5"x7.5" pieces, a total of 12. The curing procedure was: 43°C/62 KPa/30 minutes, 43°C/193 KPa/30 minutes, 85°C/176 KPa/40 minutes, and 85°C/634 KPa/20 minutes. A vacuum of ~70-80 KPa was engaged during the curing process above. The laminate was then removed from the press and post cured in an air-circulating oven at 80°C for 1 hour without any pressure.

5.2.4 FABRICATION PROCEDURE OF (VINYL ESTER+2672B)/FIBERGLASS HYBRID LAMINATES

Hybrid laminates in our research are defined as using two different resins as matrix resins and yet the same kind of fiberglass fabric as the reinforcements. In this study, vinyl ester resin constructs the core and the addition cure silicone resin consists of the skin as sketched in Figure 5-3. Hybrid laminates of vinyl ester and silicone 2672B were fabricated by two methods: sequential cure and co-cure.

5.2.4.1 Sequential cure

Sequential cure means that it involves two steps: first, curing the vinyl ester core laminate completely; second, wet lay-up of silicone resin 2672B on both sides of the cured core and then cure according to the 2672B composite schedule to make the skin. Two examples are shown as below: sample #A and #B.

For sample #A: 74g vinyl ester resin with 0.37g BPO and 0.067g DEA was used for the core lay-up, and 42g silicone 2672B resin with 34 ul Pt IV catalyst was used for the skin lay-up. Heat cleaned 7781 glass fabric was cut into 12 pieces 7"x7.5", 8 for the core and 4 for the skin. The curing procedure of the vinyl ester core was: 43°C/69 KPa/10 minutes, 43°C/262 KPa/10 minutes, 43°C/393 KPa/10 minutes, 85°C/524 KPa/10 minutes, and 85°C/655 KPa/2 hours. A vacuum of ~70-80 KPa was engaged during the curing process above. The laminate was then cooled to room temperature in the press.

Silicone resin skin was fabricated onto both sides of the core laminate, by the same wet lay-up method for 2672B laminate. The curing procedure of the skin was: 43°C/103 KPa/15 minutes, 43°C/331 KPa/10 minutes, 85°C/655 KPa/60 minutes, and 175°C/655 KPa/60 minutes. A vacuum of 70-80 KPa was also engaged during the cure. The final laminate was post cured in an oven at 200°C for 1 hour.

For sample #B: 56g vinyl ester resin with 0.28g BPO and 0.05g DEA was used for the core lay-up. 65g silicone 2672B resin with 53ul Pt IV catalyst was used for the skin lay-up. Heat cleaned 7781 glass fabric was cut into 12 pieces 7"x7.5", 6 for the core and 6 for the skin with 3 on each side. Same curing procedure as mentioned above was applied.

5.2.4.2 Co-cure

Co-cure means that wet lay-up is done on the core and the skin together and they are cured at the same time according to one schedule. Two successful examples are given below: #C - V/B 8/4 (8 plies of core + 4 plies of skin), and #D -V/B 6/6 (6 plies of core + 6 plies of skin).

For sample #C: 90g vinyl ester resin with 0.45g BPO and 0.081g DEA was used for the core lay-up. 50g silicone 2672B resin with 41ul Pt IV catalyst was used for the skin lay-up. Heat cleaned 7781 glass fabric was cut into 12 pieces of 7"x7.5", 8 for the core and 4 for the skin. The curing procedure of hybrid laminate was: 45°C/no pressure/10 minutes, 45°C/103 KPa/5 minutes, 45°C/331 KPa/15 minutes, 85°C/331 KPa/20 minutes, 85°C/496 KPa/40 minutes, and 175°C/655 KPa/1 hour. A vacuum of ~70-80 KPa was engaged during the curing process above. The laminate was post cured in an oven at 200°C for 1 hour.

For sample #D: 100g vinyl ester resin with 0.5g BPO and 0.09g DEA was used for the core lay-up. 65g silicone 2672B resin with 53ul Pt IV catalyst was used for the skin lay-up. Heat cleaned 7781 glass fabrics were cut into 12 pieces of 7"x7.5", 6 for the core and 6 for the skin. The curing procedure of the hybrid laminate was: 45°C/55 KPa/30 minutes, 45°C/262 KPa/15 minutes, 85°C/331 KPa/20 minutes, 85°C/496 KPa/50

minutes, and 175°C/655 KPa/1 hour. A vacuum of ~70-80 KPa was engaged during the curing process above. The laminate was post cured in an oven at 200°C for 1 hour.

5.2.5 SUMMARY

In conclusion, fabrication processes described above have been demonstrated successfully to produce good quality glass laminates with the vinyl ester resin matrix, silicone resin matrices, and hybrid matrix of vinyl ester and 2672B. The hybrid laminate processing methods also prove to be successful, both the sequential cure and the co-cure methods. The co-cured laminates are more efficient in their way of processing because only one-step cure is required. The sequential cured ones, however, involve two-step cure. The key to curing the composite laminate in a hot press involves getting the right temperature and pressure combination to ensure the appropriate amount of resin flow. This is important to achieving a uniform distribution of the resin and also the satisfactory final resin content. Properties of these laminates will be discussed in the next chapter.

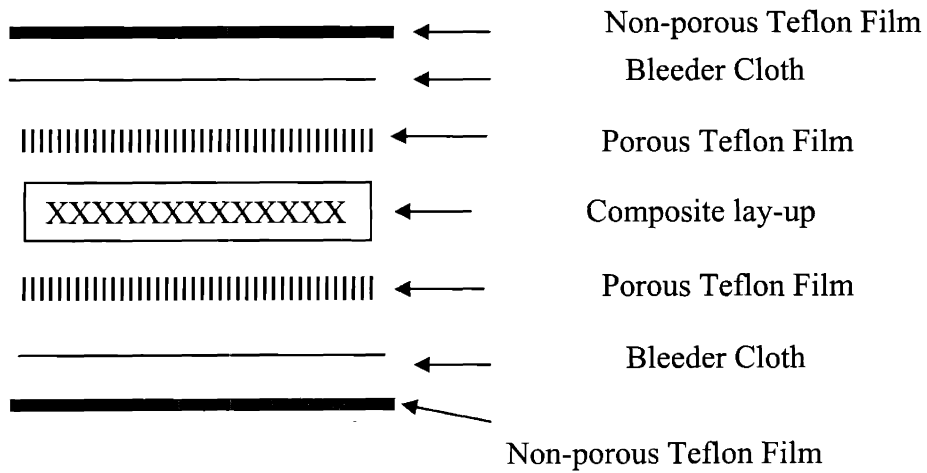


Figure 5-2 Typical set-up for curing composites in the hot press.

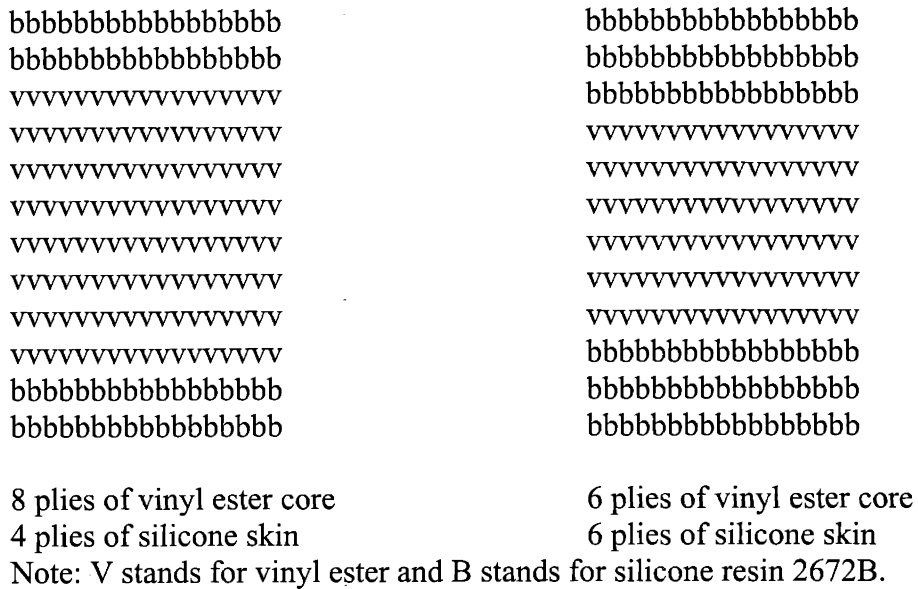


Figure 5-3 Illustration of hybrid laminates of two resin matrices: vinyl ester and silicone 2627B.

5.3 Characterization methods

5.3.1 RESIN WEIGHT CONTENT MEASUREMENT

Resin weight content is measured both by weight and by ignition loss method according to ASTM standard D2854 [4]. The weighing method involved measuring the total weight of a rectangular piece of laminate (usually after trimming off the edges of the cured laminate) and calculating the glass weight by its actual dimensions and fiber density. The difference was the resin weight and then resin content could be calculated.

For ignition method, small pieces cut from the laminate were contained in a ceramic crucible and heated in a Thermolyne 1400 furnace to $\sim 570^{\circ}\text{C}$ - 600°C for a few hours. The heating process in the oven burned away the matrix resin in the laminate. Weight of the sample before and after the removal of the matrix was recorded. Glass fiber weight content was calculated from the ratio of weight-after-heat to weight-before-heat. The balance was the resin weight content.

Results of both methods on a few samples are listed in Table 5-5. In most cases it is comparable. However, in the case of silicone resin laminates, the ignition method does not provide an accurate measurement. It was found that even after ~ 10 hours heating at 600°C , silicone resins still remained on the glass fibers. Silicone resins can't be burned away by heat due to the presence of the Si-O bonds. In other words, ignition is not a good method to remove silicone resin matrix from its glass composite. Another reason causing variation in the ignition test results is that laminates obtained from the hot press are not always homogeneous across the thickness. Small pieces which were randomly cut from the laminate for measurements would cause scattering in the data.

Since in general resin content measured by simply weighing is not a bad approximation, weight method is used primarily. This method is particularly useful for composites containing silicone resins. The SEM micrographs shown in later sections also prove that porosity/void content in the laminate is low, which makes the approximation valid.

The resin content of most laminates in this study is controlled at 30±3 wt%. About 85% of the test specimens in this work have resin content of ~ 28 to 30%. Generally speaking it is not very easy to obtain consistent resin content in every sample, but efforts have been made to make sure that the number is not too far off when comparing properties. The difficulty lies in that the flow characteristics of resins vary much depending on stirring, the original batch property, and the curing procedure using a manual controlled press.

A calculation of the resin volume content using resin density and resin weight content of the composite is presented in Table 5-6. 30 wt% resin content of the composites will give about 50% resin volume content for all composites with different matrices.

Table 5-5 A comparison between resin content obtained by ignition loss method and by weight.

	<-----ignition record----->						resin content	
	before / cruc.	before / total	before/sample	after/cruc.	after total	after/sample	by ignition	by weighing
	g	g	g	g	g	g	%	%
V	59.272	66.2461	6.9741			5.05	0.276	0.27
B	30.7631	33.9602	3.1971	30.8015	33.3651	2.5636	0.198	0.34
T	28.7756	29.8162	1.0406	28.7786	29.6716	0.893	0.142	0.31
V/B 8/4 co-cured	32.1046	35.536	3.4314	32.112	34.5988	2.4868	0.275	0.28

Table 5-6 Calculated volume content of composites with different matrix materials.

Density of 3136T resin (g/cm ³)	1.17
Density of 2672B resin (g/cm ³)	1.10
Density of vinyl ester resin (g/cm ³)	1.08
Density of fiberglass (g/cm ³)	2.62
Resin weight content of composites (%)	30
Fiber weight content of composites (%)	70
2672B volume content of its composites (%)	50
3136T volume content of its composites (%)	49
vinyl ester volume content of its composites (%)	51

5.3.2 DYNAMIC MECHANICAL ANALYSIS

Dynamic mechanical analysis (DMA) has been performed on a T.A. Instrument Model 2980 at the thermal analysis lab at Dow Corning. Tested specimens had rectangular cross-section dimension of 1mm x 3~4 mm, and the clamping distance was ~20mm. The data were collected at frequencies of 0.5, 1, 5, 10, 25 and 50 Hz, and testing temperature range was -150°C ~350°C with a heating rate of 2°C/min. The samples were loaded in tension mode in air.

5.3.3 FLEXURAL PROPERTY TEST

Mechanical properties of composites are usually measured by tensile, compressive, and flexural tests. Tensile and compressive tests are favored for their well-defined stress states and accuracy of measurements. However, flexural tests (both three-point and four-point) are widely used for their simplicity and relative low cost of the fixture. The maximum flexural strength of the composite is the maximum fiber failure stress on the tensile side (bottom side) of the specimen. From the homogeneous beam theory, it is calculated by:

$$\sigma_{\max, \text{flexural}} = 1.5 \times \frac{P_m L}{bh^2} \quad \text{Equation 5-1}$$

where P_m is the maximum load and L , b and h is the span, width and thickness of the composite, respectively. This gives an apparent maximum strength where lamination theory is not used for precise stress analysis. The maximum flexural strength is often observed to be higher than the ultimate tensile strength of the same composite laminate, sometimes even significantly higher [5-7].

The flexural modulus is given by:

$$E_{\text{flexural}} = \text{slope} \times \frac{L}{4bh^3} \quad \text{Equation 5-2}$$

where 'slope' means the slope of the initial linear part of the flexural stress-strain curve. The flexural modulus is also an apparent value combining the effect of both compressive and tensile moduli of the laminate. It also highly depends upon the stacking sequence of the laminate [8].

Three-point bending tests were performed on samples of 3" x 1" (with 2" loading span) according to ASTM standard D790 [9]. Thickness of the sample was about 0.1", which gives a span/thickness ratio of ~ 20. A big ratio is good to reduce shear deflection at the mid loading point. The rate of crosshead moving rate was determined by sample thickness and is calculated by:

$$R = \frac{0.01 \times L^2}{6 \times h} \text{ Equation 5-3}$$

where L is the span and h is the sample thickness. Samples were conditioned at room temperature for two days before being tested on an Instron 4505 machine. The flexural properties measured at elevated temperatures were performed similarly to those in the silicone resins in Chapter 2, where an Instron 3111 chamber was used. Typically high temperature testing was performed by heating samples to the test temperature and then soaking for 30 minutes before applying the force.

5.3.4 SHORT BEAM SHEAR TEST

Short beam strength is a measurement of the interlaminar shear strength of the composite. Short beam strength tests were performed according to ASTM standard D2344 [10]. Samples were cut into precise dimensions by a low speed precision diamond saw. A three-point bending testing jig was modified to have the right loading pin size for the test. Hardened steel pins were glued to the jig with an upper loading roller of 6 mm in diameter and two bottom ones of 3 mm in diameter. Flat samples were used, meeting the criteria of *sample length* = 6 x *thickness*, and *width* = 2 x *thickness*. Span was set at four times of the sample thickness. Typical sample was about 2.5-3 mm in thickness. The crosshead moving rate was at 1 mm/min.

The short beam shear strength is calculated by:

$$F_{sbs} = 0.75 \times \frac{P_m}{b \times h} \quad \text{Equation 5-4}$$

where P_m is the maximum load observed during the test, b is the specimen width, and h is the specimen thickness.

5.3.5 THERMAL AGING PROPERTY TEST

Thermal aging properties were measured by heat aging the composites (vinyl ester, 2672B and VB hybrid) at 100, 135, 170 and 205°C for 10, 100 and 1000 hours. The practice of the tests was determined in reference to the ASTM standard D3045–92, which outlines the standard practice for heat aging of plastics without load [11].

Properties measured were weight and flexural properties. Laminates were cut into ½” x 3” specimens with a water-cooling diamond table saw. Approximately 20 specimens could be cut from each laminate. Five were used to get the baseline flexural properties and the rest were used for heat aging. Three-point bending flexural tests were performed at room temperature after thermal aging was completed. The property loss/retention was obtained by comparing the data after aging with the baseline. Specimens for heat aging were weighed both before and after the aging, and weight loss percentages were calculated.

5.3.6 THERMOGRAMETRIC ANALYSIS

Thermogravimetric analysis was done on a Texas Instrument TGA7. Sample weight was about 10-20mg. The testing temperature range was 20 to 800°C, and the heating rate was 10°C/min. Gas flow rate was at 20 ml/min. Tests were performed in air and data were collected in a computer controlled program.

5.3.7 MOISTURE ABSORPTION TEST

The moisture absorption properties were measured according to procedures B and C in ASTM standard D5229-92 [12]. Samples were cut with a diamond saw into size of ~ 2"x2" or 2.5" x 2.5" squares. In the case of samples were with sealed edges, silicone sealant was used.

Tests were performed at room temperature (22°C) and two humidity level conditions were created. One was at 100% relative humidity and the other was at 50% relative humidity. These were obtained by putting either distilled water (for 100% R.H.) or saturated calcium nitrate solution (for 50% R.H.) at the bottom of closed desiccators. Tested specimens were contained inside the desiccator without direct contact with the solution by the support of a ceramic disc. A dial hygrometer was used to monitor the humidity level inside the desiccators.

Cut samples were first dried at 65°C for about 24 hours. Dried samples were weighed before they were put inside the enclosed environments. This was the initial specimen mass W_o . They were also weighed at certain time intervals after they were subject to the humid environment. This was taken as the current specimen mass W_i . The average moisture content was calculated by:

$$M\% = \frac{W_i - W_o}{W_o} \times 100 \quad \text{Equation 5-5}$$

The weighing time intervals varied from 24 hours at the beginning of the test to 5-7 days near the end.

5.3.8 FIRE PROPERTY TEST

Fire performance was measured by both OSU test and cone calorimetry test. The samples were prepared at MIT and sent to outside testing labs: Delsen Testing Laboratories Inc. for OSU test and Omega Point Laboratories for the cone calorimetry flammability test.

OSU test was performed in reference to the Federal Aviation Regulation test method FAR 25.853 (d) to determine the heat release rate from cabin materials exposed to radiant heat [13, 14]. Samples of 6"x6" were cut and pre-conditioned at $21\pm 3^{\circ}\text{C}$ and $50\pm 5\%$ relative humidity for at least 24 hours. Specimens were tested vertically with ignition source coming from the sides. Cone calorimetry flammability test required a sample dimension of 4"x4" [15]. The specimens were subjected to heat sources in a horizontal position.

5.3.9 SCANNING ELECTRON MICROSCOPE ANALYSIS

Scanning electron microscope (SEM) analysis was performed on a Leo-438VP machine (Leo Electron Microscopy Ltd.) at MIT. The acceleration voltage was set at 20KV. A Variable Pressure Mode, which involves the back-scattered detector, was used for observing the composite, and this required no gold coating on plastic sample surfaces.

Composite samples were first cut with a diamond saw and then polished cross-sectionally to obtain a smooth surface. Micrographs were taken on the polished surfaces to observe defects (including porosity and inclusions), fiber distribution, and fiber orientation inside the matrix.

References:

1. Hexcel Schewebel Product Information
<http://www.hexcelschwebel.com/FAQ/Product.htm>.
2. Hexcel Schewebel website
<http://www.hexcelschwebel.com/faq/process/cleaning.htm>.
3. Sidwell DR. *Hand lay-up and bag molding*, in *Handbook of composites*, ST Peters, Editor. 1998, Chapman & Hall: London.
4. *Standard test method for ignition loss of cured reinforced resins, ASTM standard D2584-02*. Annual Book of ASTM Standards, 2002. **Vol. 08.02**.
5. Bullock RE. *Strength ratios of composite materials in flexure and in tension*. Journal of Composite Materials, 1974. **8**: 200.
6. Whitney JM, Knight M. *The relationship between tensile strength and flexure strength in fiber-reinforced composites*. Experimental Mechanics, 1980. **20**: 211.
7. Whitney JM, Daniel IM, Pipes RB. *Experimental mechanics of fiber reinforced composite materials*. Brookfield Center, CT.: Society for Experimental Mechanics, 1984.
8. Chiao CC, Moore RL, Chiao TT. *Measurement of shear properties of fiber composites. Part 1: Evaluation of test methods*. Composites, 1977. **8**: 161.
9. *Standard test methods for flexural properties of unreinforced and reinforced plastics and electrical insulating materials, ASTM standard D790-92*. Annual Book of ASTM Standards, 1992. **Vol. 08.01**.
10. *Standard test method for short-beam strength of polymer matrix composite materials and their laminates, ASTM standard D2344/D2344M-00*. Annual Book of ASTM Standards, 2000. **Vol. 15.03**.
11. *Standard practice for heat aging of plastic without load, ASTM Standard D3045-92 (Reapproved 1997)*. Annual Book of ASTM Standards, 1997. **Vol. 08.02**.
12. *Standard test method for moisture absorption properties and equilibrium conditioning of polymer matrix composite materials, ASTM standard D5229/D5229M - 92(Reapproved 1998)*. Annual Book of ASTM Standards, 1998. **Vol. 15.03**.
13. *Test method to determine the heat release rate from cabin materials exposed to radiant heat, FAR 25.853 (d), Ammendment 25-83, Appendix F, Part IV*.
14. DOT/FAA/AR-00/12, *Aircraft Materials Fire Test Handbook*, April 2000.
15. *Standard practice for full-scale oxygen consumption calorimetry fire tests, ASTM standard E2067-00a*. Annual Book of ASTM Standards, 2000. **Vol. 04.07**.

CHAPTER 6. Silicone and hybrid composites – results and discussion

Results of experimental work as shown in the previous section will be presented and discussed in this chapter. Abbreviations of the sample information identification will be the same as those in the previous chapter.

6.1 Mechanical properties

In this section, results of flexural properties of the composites, both at room temperature and elevated temperatures, and their short beam shear strength are presented and discussed. All samples have twelve plies of 7781 glass fabric cloth. The fiberglass cloth used has a heat cleaned finish unless otherwise noted.

6.1.1 FLEXURAL PROPERTIES AT ROOM TEMPERATURE

Flexural samples have been tested under three point bending. Sample orientation is kept at warp, unless otherwise noted. The maximum flexural strain data are listed here for the completeness of testing results but are not included in detailed discussion. Discussions will focus on the stress and modulus data.

6.1.1.1 3136T composite

From Table 6-1, it is seen that 3136T composite has moderate strength and modulus at room temperature. Delamination has been observed during the failure of flexural samples. It has also been observed that 3136T composites with higher resin content, say 29-30 wt%, appeared to be stronger and more rigid than those with 20-25 wt% resin. The latter delaminate easily and thus the laminates lose their strength.

Table 6-1 Mechanical properties of 3136T laminate at room temperature.

ID	Fabric	Thickness	Resin content	Loading rate	Max. Flex. strain	Max. Flex. stress	Flex. Modulus
	7781	mm	wt. %	mm/min	%	MPa	GPa
T	clean	2.65	29	1.62	1.5 ±0.28	295.17 ±22.27	23.79 ±5.86

6.1.1.2 2672B composite

Flexural properties of 2672B composites are listed in Table 6-2. As a comparison, glass fabric with clean surface finish results in higher strength and modulus of the composite. The volan finish is effective in improving the wettability between fiberglass and silicone resin matrix, and thus shortens the wet lay-up time. However, testing results suggest that the coating has a negative effect on the strength and rigidity of the composites. Based on this, work in other composites will focus on clean fiberglass fabric. Heat cleaned glass should also offer advantages to the thermal stability of the composites.

Table 6-2 Mechanical properties of 2672B laminates at room temperature.

ID	Fabric	Thickness	Resin content	Loading rate	Max. Flex. strain	Max. Flex. stress	Modulus
	7781	mm	wt. %	mm/min	%	MPa	GPa
B#1	volan	2.59	31	1.69	1.42 ±0.11	247.12 ±12.20	18.06 ±0.97
B#2	clean	2.70	33	1.59	1.69 ±0.05	329.65 ±9.58	22.96 ±0.76

6.1.1.3 Vinyl ester composite

The mechanical properties of the vinyl ester laminate are presented in Table 6-3. The strength of the vinyl ester composite is almost 1.5 times that of the 2672B composite. The flexural modulus of the vinyl ester composite is also about 30% higher than the B

composite. This can be explained by the fact that the vinyl ester resin is a stronger matrix. The results also suggest that the flexural modulus and strength of composites are very dependent upon the matrix properties.

Here we can see one possible reason of combining vinyl ester resin and 2672B silicone resin to make the hybrid composite – to improve the mechanical properties. Of course, this is under the assumption that the two resins are compatible and there is no detrimental effect caused by the interface between the two.

Table 6-3 Mechanical properties of vinyl ester laminate at room temperature.

ID	Fabric	Thickness	Resin content	Loading rate	Max. Flex. strain	Max. Flex. stress	Modulus
	7781	mm	wt. %	mm/min	%	MPa	GPa
V	clean	2.37	27	1.82	1.68 ± 0.08	477.69 ± 19.65	30.34 ± 2.34

6.1.1.4 VB hybrid composite

As described in detail in Chapter 5, vinyl ester and 2672B hybrid composites have been made in different structures with different curing schedules. Two curing techniques have been used: sequential cure and co-cure. Two laminate constructions were experimented: 8 plies of the vinyl ester core plus 4 plies of 2672B skin (V/B 8/4); and 6 plies of the vinyl ester core plus 6 plies of 2672B skin (V/B 6/6).

Room temperature flexural properties of these hybrid laminates are presented in Table 6-4. Comparing the co-cured and sequential cured laminates, we can see that the co-cured procedure produces a composite with better strength and modulus. For the sequential cured and co-cured laminates, their composition and curing cycles are essentially the same. The main difference lies in the process of forming the interface between the vinyl ester and 2672B resins. The curing reaction during co-cure cycle seems to have created a stronger interface between the two resins. Observations during the

bending tests find that sequential cured samples often fail by interfacial delamination between the two resins. Such failure pattern is not typical of the co-cured samples, which appear to have good interfacial bonding. Their failure pattern resembles those laminates with single resin matrix – mostly by matrix cracking induced delamination and final fiber breakage of the outer fiber layer on the tensile side of the specimen.

If comparing laminates made by the same curing method but with different core/skin structures, the effect of 8/4 and 6/6 core/skin structure on their mechanical properties is not as substantial. We see that the 8/4 construction has a slight advantage in its strength and stiffness over the 6/6 co-cured samples, which can be explained by a higher resin content of strong vinyl ester in the V/B 8/4 structure.

Table 6-4 Mechanical properties of VB hybrid laminates at room temperature.

ID	Fabric	Description	Thickness	Resin content	Loading rate	Max. Flex. Strain	Max. Flex. stress	Modulus
	7781		mm	wt.%	mm/min	%	MPa	GPa
VB #C	clean	V/B 8/4, Seq cure	2.81	33	1.53	2.34 ±0.08	382.67 ±19.31	20.82 ±1.59
VB #D	clean	V/B 6/6, Seq cure	2.67	34	1.61	1.91 ±0.12	358.40 ±8.62	21.17 ±0.55
VB #A	clean	V/B 8/4, co-cure	2.47	27	1.74	1.95 ±0.07	516.71 ±50.82	29.03 ±3.52
VB #B	clean	V/B 6/6, co-cure	2.53	28	1.7	2.19 ±0.12	479.48 ±13.65	24.27 ±1.03

6.1.1.5 Summary

As a summary, room temperature flexural properties of 3136T, B, V, and VB composites are described in Figure 6-1 and Figure 6-2. 2672B and 3136T composites have comparable strength and modulus because their matrix materials have similar mechanical properties as characterized in the resin work in Chapter 3 (summarized below in Table 6-5). Both toughened silicone resins are suitable for being used as matrix

materials for composites. The 2672B composite mechanical properties are less sensitive to the matrix resin content. A laminate of reasonable strength and stiffness can be obtained at a resin content around 23 wt%. On the other hand, the 3136T composite with the same resin content would easily lead to matrix cracking and delamination. This might be due to the toughness difference in the matrix resins. The organic vinyl ester resin composite has both higher stress and higher modulus compared to the silicone resin composites, largely due to its strong and stiff matrix.

For the VB hybrid composites, the V/B 8/4 co-cured hybrid composite has both high stress and modulus, comparable to the vinyl ester composite. Sequential cured laminates generally have lower strength and modulus compared to the co-cured ones. The main difference is in the interfacial characteristics between the two matrix resins V and B due to different curing processes. Mechanical property results suggest that the co-cured laminates possess a better interface structure than the sequential cured ones.

From the results we see the proof of the advantage of engineering vinyl ester resin with silicone resin 2672B to make a hybrid composite to achieve better mechanical properties. The flexural test results suggest that the two resins are compatible and they form a strong interface with the co-cure procedure. This is proved by the strength and stiffness of the co-cured hybrid composites, particularly the V/B 8/4 hybrid composite.

According to the sandwich beam stress analysis in Chapter 4, we can model the hybrid composite as a sandwich beam with a skin of 2672B laminate and a core of vinyl ester laminate. If we plug numbers of the skin and core stiffness into Equation 4-16 in Chapter 4, assuming there is perfect bonding between the skin and core, the co-cured V/B 8/4 modulus can be expressed in terms of modulus of individual core and skin laminates as: $(19E_B + 8E_V)/27$, which is smaller than E_V . Since E_B is about 3/4 of E_V , the overall modulus of the V/B 8/4 hybrid composite should be around 82% of E_V . The experimental value, however, proves that the hybrid composite is about 95% (Figure 6-1) as rigid as the vinyl ester composite. On the other hand, the strength of the co-cured V/B 8/4 hybrid composite is also comparable to that of the vinyl ester composite (Figure 6-2). These

suggest that the hybrid effect causes more than a simple addition of the skin and core composite properties, but it results in greater mechanical performances.

Table 6-5 Summary of silicone resin properties, both used as the matrix materials for composites.

	Maximum flexural stress (MPa)		Maximum flexural strain (%)		Flexural Modulus (GPa)		K _{Ic} (MPa m ^{1/2})	
	Ave	Stdev	Ave	Stdev	Ave	Stdev	Ave	Stdev
2672B	46.17	±1.27	7.23	±0.28	1.63	±0.06	1.03	±0.06
3136T	50.48	±2.60	5.98	±0.50	1.48	±0.05	0.39	±0.01

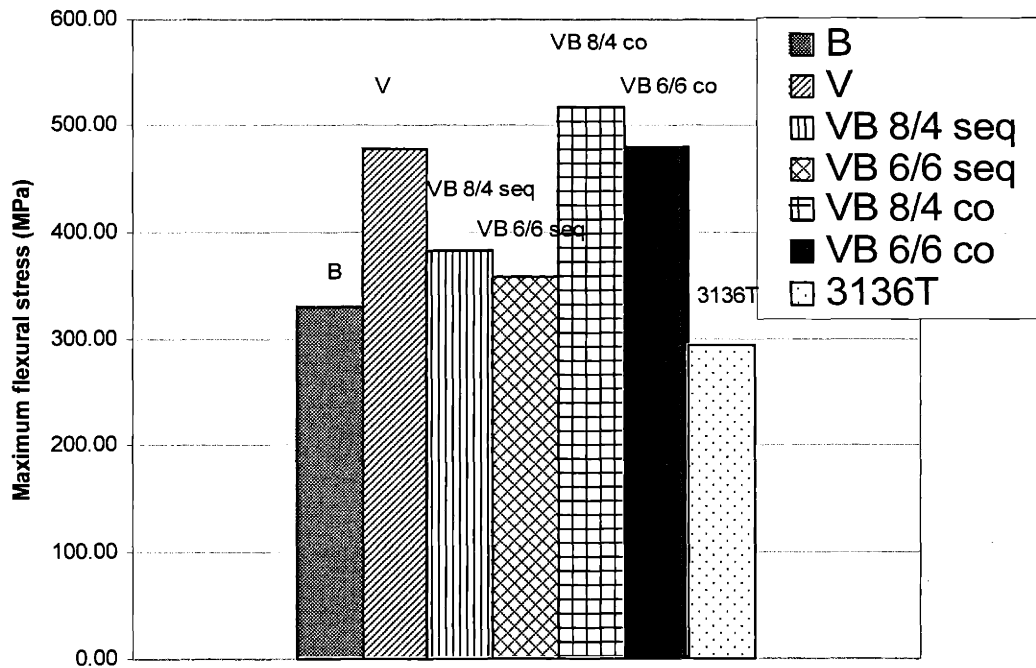


Figure 6-1 Summary of room temperature maximum flexural stress of T, B, V and VB composites.

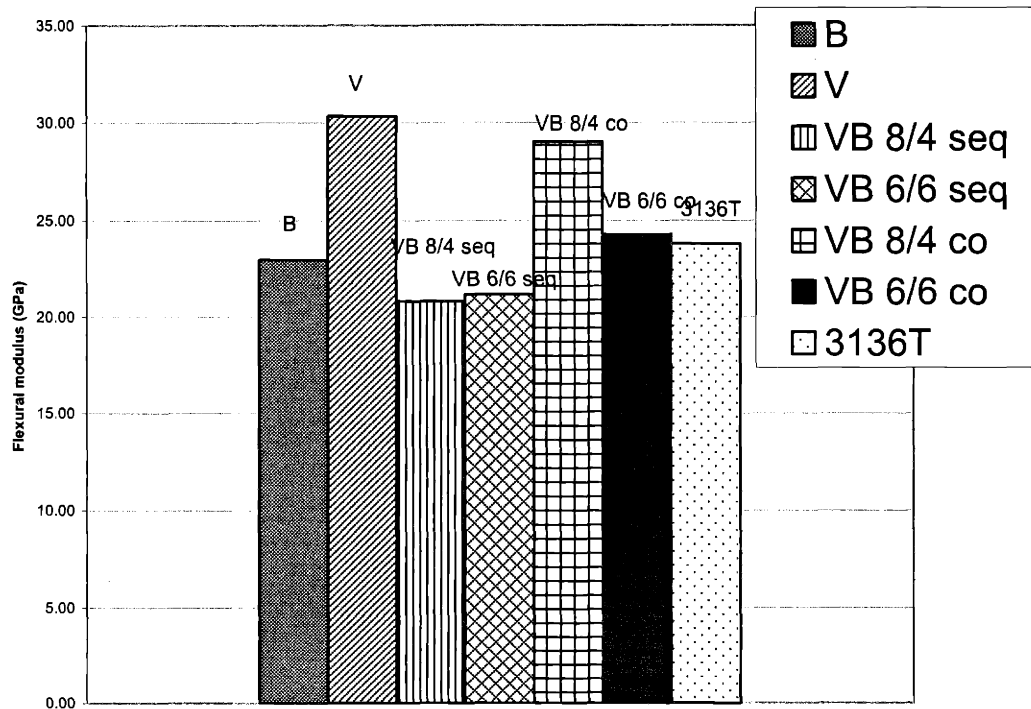


Figure 6-2 Summary of room temperature flexural modulus of T, B, V and VB composites.

6.1.2 FLEXURAL PROPERTIES AT ELEVATED TEMPERATURES

6.1.2.1 3136T composite

Change in flexural properties of 3136T composite with temperature is described in Figure 6-3 and Table 6-6. Both maximum flexural stress and flexural modulus decrease with temperature. At 80°C, the stress is about 60% of its room temperature value and the modulus drops to about 80%. At 150°C, both the stress and the modulus remain at about 20-30% of their room temperature values. This substantial decrease should come from the thermal softening effect of the silicone resin matrix. 150°C is in the range of its glass transition temperature, which results in the strength loss in the resin and thus a substantial decrease in its composite strength and modulus. Again, this suggests that the matrix properties are very important to the final composite properties. Any changes affecting the matrix properties will lead to changes in the composite properties as well.

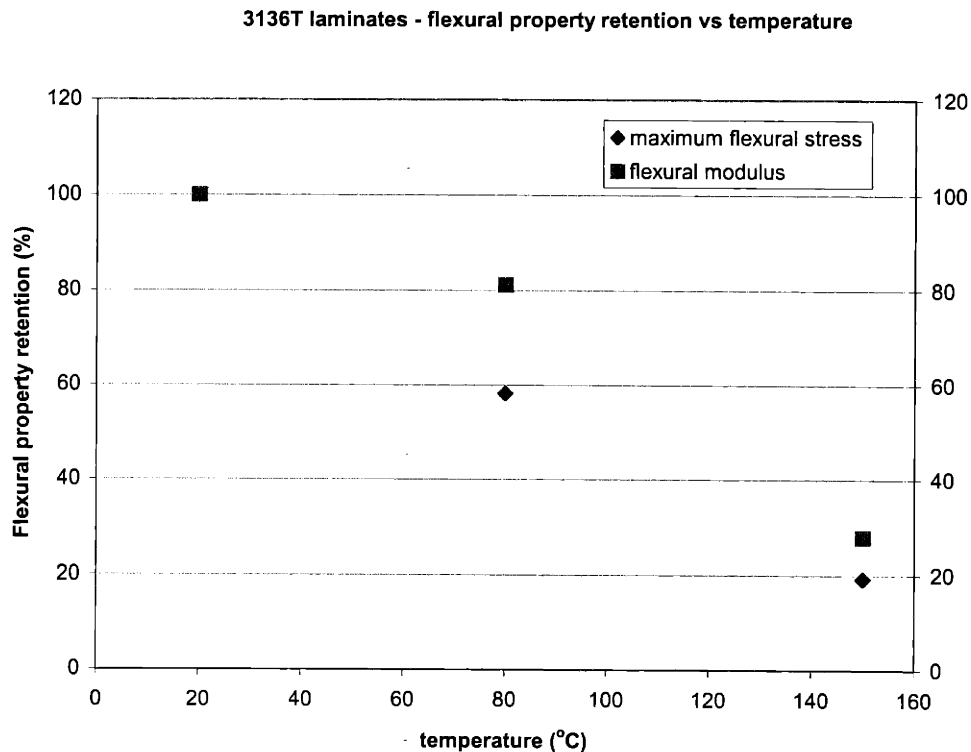


Figure 6-3 Flexural property retention versus temperature for 3136T composite.

Table 6-6 Flexural properties at different temperatures for 3136T composite.

ID	Fabric	Thickness	Resin content	Loading rate	Max. Flex. strain	Max. Flex. stress	Flex. Modulus
	7781	mm	wt.%	mm/min	%	MPa	GPa
T 20C	clean	2.65	29	1.62	1.5 ±0.28	295.17 ±22.27	23.79 ±5.86
T 80C	Clean	2.65	29	1.62	1.15 ±0.12	171.69 ±22.75	19.31 ±4.55
T 150C	Clean	2.65	29	1.62	1.46 ±0.09	56.68 ±0.55	6.62 ±0.62

6.1.2.2 2672B composite

Flexural property retention versus temperature for 2672B composite is shown in Figure 6-4 with data listed in Table 6-7. The decrease in both stress and modulus is very substantial at 80°C, which leaves both variables at only about 30% of their room temperature values. At 150°C, the stress goes down slightly further with the modulus remaining about the same. Big loss in strength and stiffness of 2672B composite at 80°C can be explained by the fact that 2672B matrix has a glass transition temperature at 88°C. Thus, thermal softening effect of the 2672B resin is great at temperatures like 80°C and 150°C. This is consistent with the results of the flexural property change with temperature in 2672B resin presented in Chapter 3. At 60°C, the modulus and flexural decrease in 2672B resin is about 40-50%.

2672B laminates - flexural property retention vs temperature

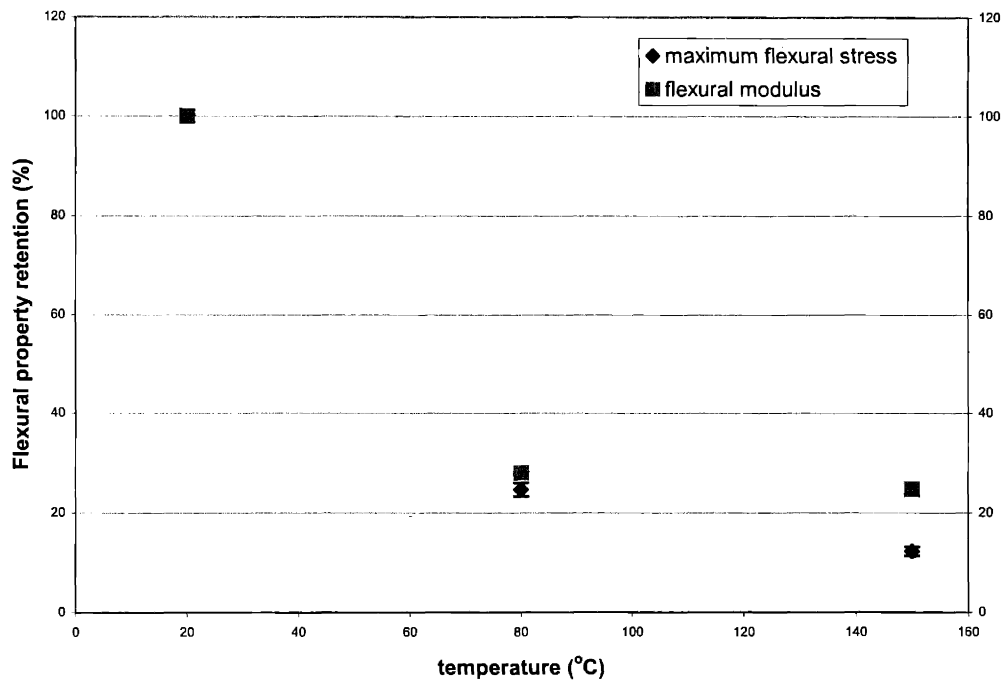


Figure 6-4 Flexural property retention versus temperature for 2672B composite.

Table 6-7 Flexural properties of 2672B composite at different temperatures.

ID	Fabric	Thickness	Resin content	Loading rate	Max. Flex. strain	Max. Flex. stress	Flex. modulus
	7781	mm	wt. %	mm/min	%	MPa	GPa
B 20C	clean	2.4	22.5	1.79	1.52 ±0.15	365.30 ±23.10	29.58 ±2.41
B 80C	clean	2.4	22.5	1.79	1.7 ±0.19	90.12 ±4.83	8.27 ±0.90
B 150C	clean	2.4	22.5	1.79	0.87 ±0.12	45.02 ±4.83	7.31 ±1.72

6.1.2.3 Vinyl ester composite

Flexural property versus temperature plot is presented in Figure 6-3 for vinyl ester composite. The retention of its strength is obviously good, giving ~70% at 80°C and 60% at 150°C. The modulus is slightly inferior and but at 150°C still remains at ~50% of its room temperature value. The reason is closely related to the high heat distortion temperature (~150°C) of the vinyl ester resin. Again, the composite properties are much dependent upon the characteristics of the matrix.

Here we see another possible reason of engineering the hybrid matrix composite, vinyl ester resin would offer better property retention at higher temperatures due to its higher T_g .

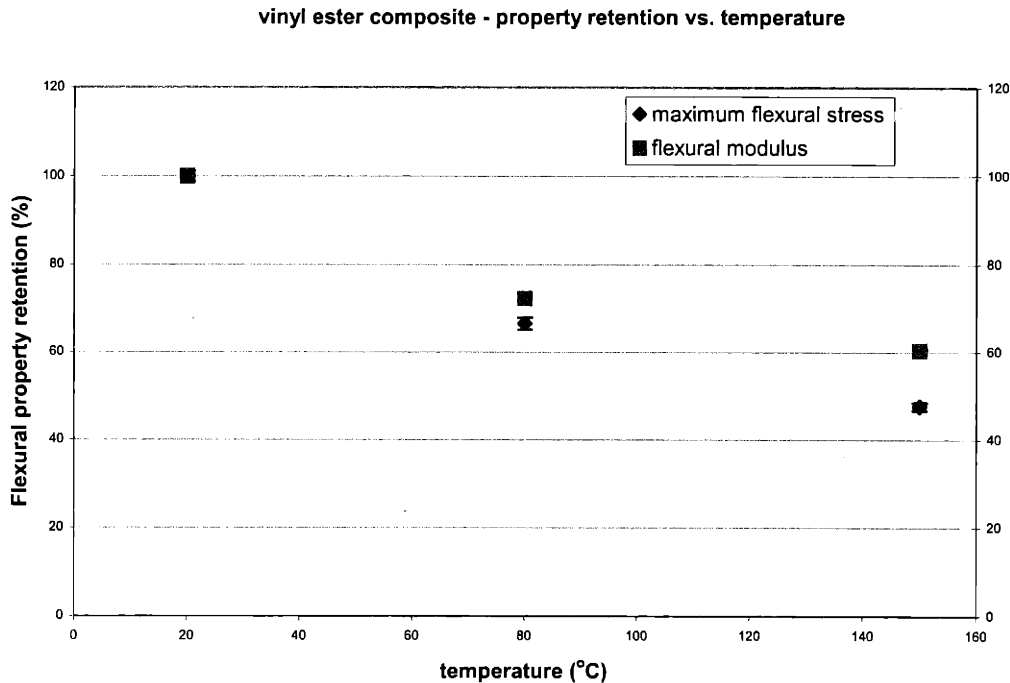


Figure 6-5 Flexural property retention versus temperature for vinyl ester composite.

Table 6-8 Flexural properties of vinyl ester composite at different temperatures.

ID	Fabric 7781	Thickness mm	Resin cont wt.%	Loading rate mm/min	Max. Flex. strain %	Max. Flex. stress MPa	Flex. modulus GPa
V 20C	clean	2.37	27	1.82	1.68 ±0.08	477.69 ±19.65	30.34 ±2.34
V 80C	clean	2.37	27	1.82	1.67 ±0.03	317.51 ±15.44	21.93 ±0.97
V 150C	clean	2.37	27	1.82	1.49 ±0.11	227.47 ±5.45	18.34 ±0.69

6.1.2.4 VB hybrid composite

Although the thermal softening effect of 3136T composite is not as big as that of the 2672B composite, it has not been chosen as the skin material in constructing the hybrid composites. The attempts to use it in processing hybrid composites have been mainly unsuccessful, because 3136T is a condensation cure resin and produces volatile byproduct during cure. The existence of the water by-product results in void/porosity problem at the hybrid resin interface due to the difficulty of driving it out during cure. Thus, 2672B has been used in the hybrid composites and changes in VB hybrid composite mechanical properties with temperature are presented below.

For the hybrid laminates of V/B 6/6, the property retention vs. temperature is shown in Figure 6-6 and Figure 6-7. For the sequential cured laminates, modulus retention is about 75% and 40% at 80°C and 150°C, respectively. The stress has lower values of 40% and 25% at 80°C and 150°C, respectively. For the co-cured laminates, flexural properties are better at both temperatures, resulting in relative modulus of 90% and relative stress of 80% at 80°C, and relative modulus of 60% and relative stress of 40% at 150°C.

For the V/B 8/4 hybrid composites, a similar trend is observed that the co-cured composite has better property retention at elevated temperatures compared to the sequential cured composite. For the sequential cured V/B 8/4, modulus retention is 50-

55% at both temperatures, stress retention is 75% and 40% at 80°C and 150°C, respectively. For the co-cured V/B 8/4, modulus retention is 95% and 75% at 80°C and 150°C, respectively; and the corresponding stress retention is 85% and 60% (Figure 6-8, Figure 6-9, and Table 6-10). It is also observed that overall property retention of V/B 8/4 structure is better than that of V/B 6/6 structure. This could be partly explained by the presence of higher vinyl ester resin content. The increase in this higher T_g matrix content results in stronger and stiffer composites and also attributes to better property retention at elevated temperatures.

During flexural tests at high temperatures, the sequential cured laminates often delaminate first at the interface of the two resins. This further proves that the sequential cured laminates have a weak interface. In comparison, the co-cured composites do not delaminate easily, both at room temperature and at higher temperatures.

It is also noted that the temperature retention and absolute values of stress and modulus of the co-cured V/B 8/4 are even better than those of the vinyl ester composite (Figure 6-10 and Figure 6-11). One reason could be due to the stronger interface formed between two resins as discussed before. Another possibility is that the vinyl ester core is shielded against the heat by the silicone skin and thus has better performance at elevated temperatures.

All results above suggest that the hybrid composites, particularly the co-cured composite, prove to have good property retention at elevated temperatures.

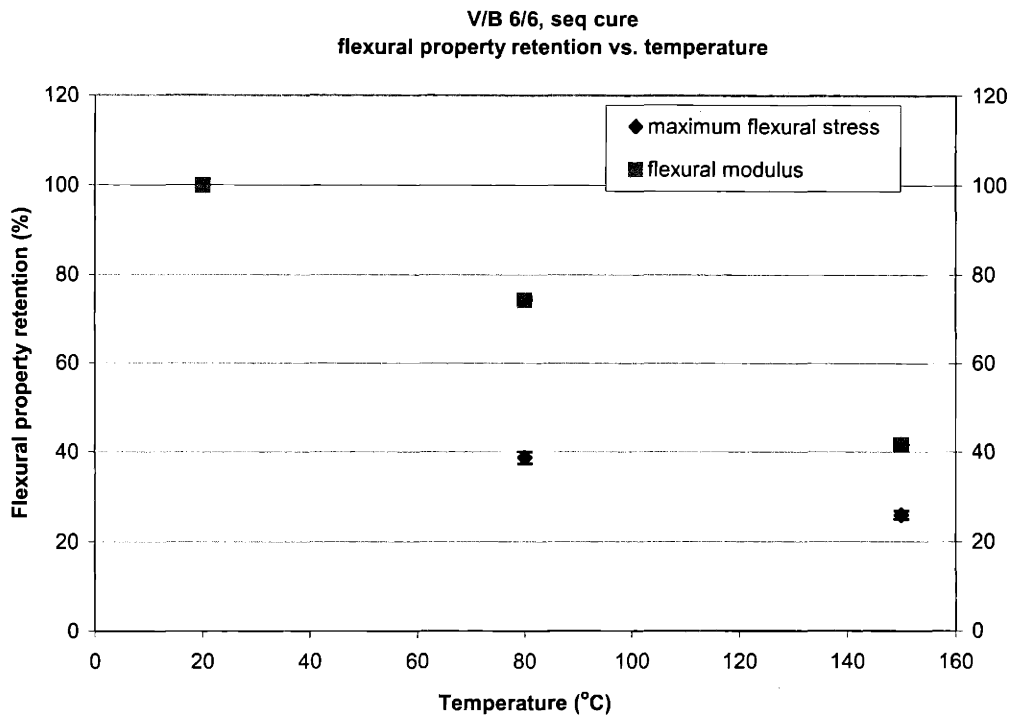


Figure 6-6 Flexural property retention versus temperature for sequential cured V/B 6/6 hybrid composite.

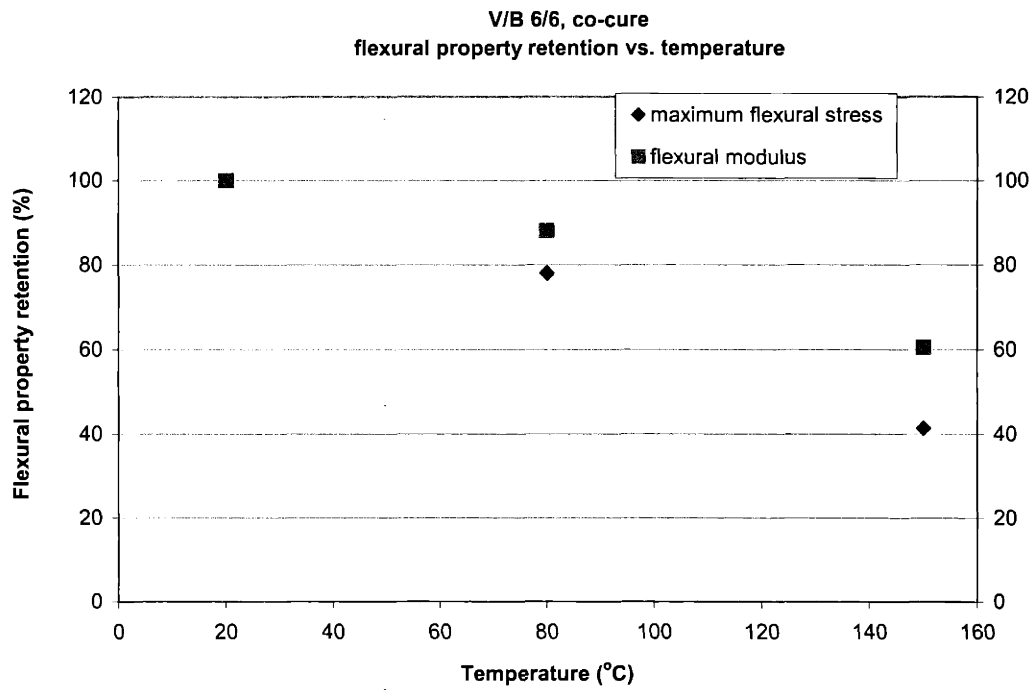


Figure 6-7 Flexural property retention versus temperature for co-cured V/B 6/6 hybrid composite.

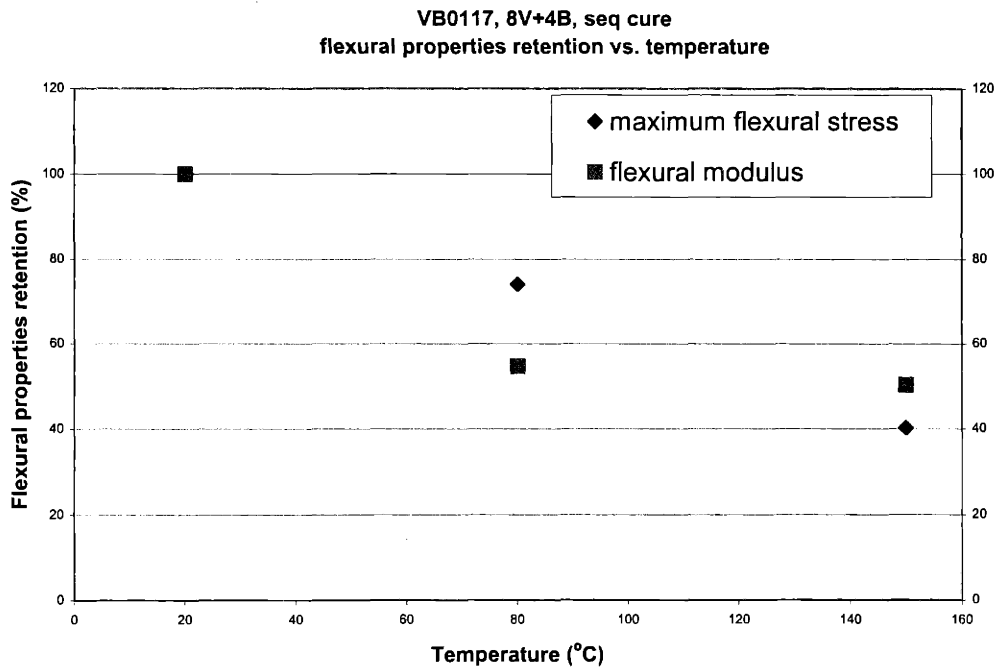


Figure 6-8 Flexural property retention versus temperature for sequential cured V/B 8/4 hybrid composite.

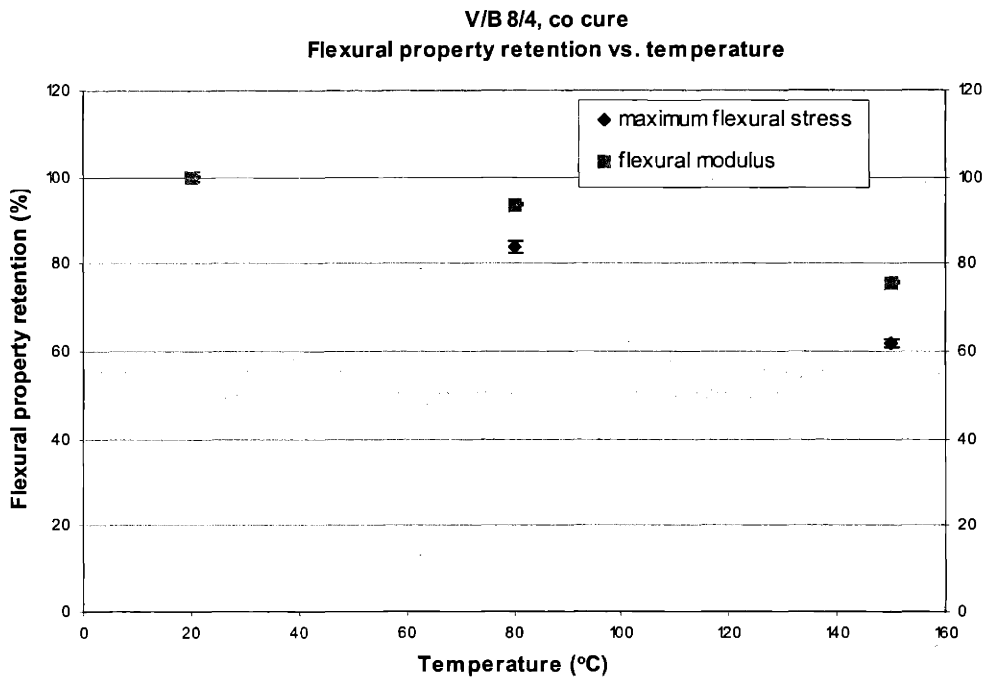


Figure 6-9 Flexural property retention versus temperature for co-cured V/B 8/4 hybrid composite.

Table 6-9 Properties of V/B 6/6 composites, sequential cured and co-cured, at different temperatures.

ID	Description	Thickness mm	Resin content wt.%	Loading rate mm/min	Max. Flex. strain %	Max. Flex. stress MPa	Flex. modulus GPa
V/B 6/6	V/B 6/6, seq cure	2.67	34	1.61	1.91 ±0.12	358.40 ±8.62	21.17 ±0.55
V/B 6/6 80C	V/B 6/6, seq cure	2.67	34	1.61	1.38 ±0.06	138.73 ±9.31	15.72 ±1.38
V/B 6/6 150C	V/B 6/6, seq cure	2.67	34	1.61	3.75 ±0.10	93.01 ±6.34	8.83 ±1.03
V/B 6/6	V/B 6/6, co-cure	2.53	28	1.70	2.19 ±0.12	479.48 ±13.65	24.27 ±1.03
V/B 6/6 80C	V/B 6/6, co-cure	2.53	28	1.70	2.17 ±0.06	373.92 ±11.24	21.37 ±1.24
V/B 6/6 150C	V/B 6/6, co-cure	2.53	28	1.70	2.10 ±0.25	198.30 ±26.96	14.69 ±1.72

Table 6-10 Properties of V/B 8/4 composites, sequential cured and co-cured, at different temperatures.

ID	Description	Thickness mm	Resin content wt.%	Loading rate mm/min	Max. Flex. strain %	Max. Flex. stress MPa	Flex. modulus GPa
V/B 8/4	V/B 8/4, seq cure	2.81	33	1.53	2.34 ±0.08	382.67 ±19.31	20.82 ±1.59
V/B 8/4 80C	V/B 8/4, seq cure	2.81	33	1.53	3.38 ±0.07	283.25 ±16.13	11.38 ±0.62
V/B 8/4 150C	V/B 8/4, seq cure	2.81	33	1.53	3.21 ±0.06	154.03 ±13.58	10.48 ±1.10
V/B 8/4	V/B 8/4, co-cure	2.47	26	1.74	1.95 ±0.07	516.71 ±50.82	29.03 ±3.52
V/B 8/4 80C	V/B 8/4, co-cure	2.47	26	1.74	1.78 ±0.08	432.39 ±16.34	27.17 ±2.48
V/B 8/4 150C	V/B 8/4, co-cure	2.47	26	1.74	1.53 ±0.11	320.13 ±28.41	22.00 ±0.41

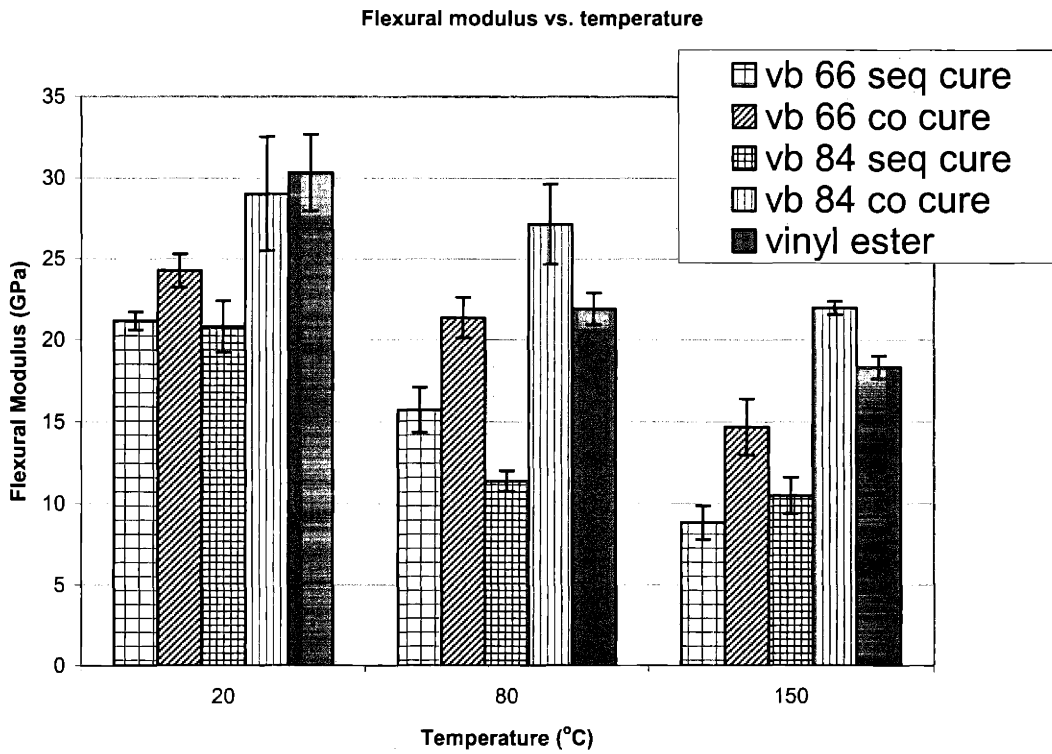


Figure 6-10 Summary flexural modulus versus temperature for VB hybrid composites.

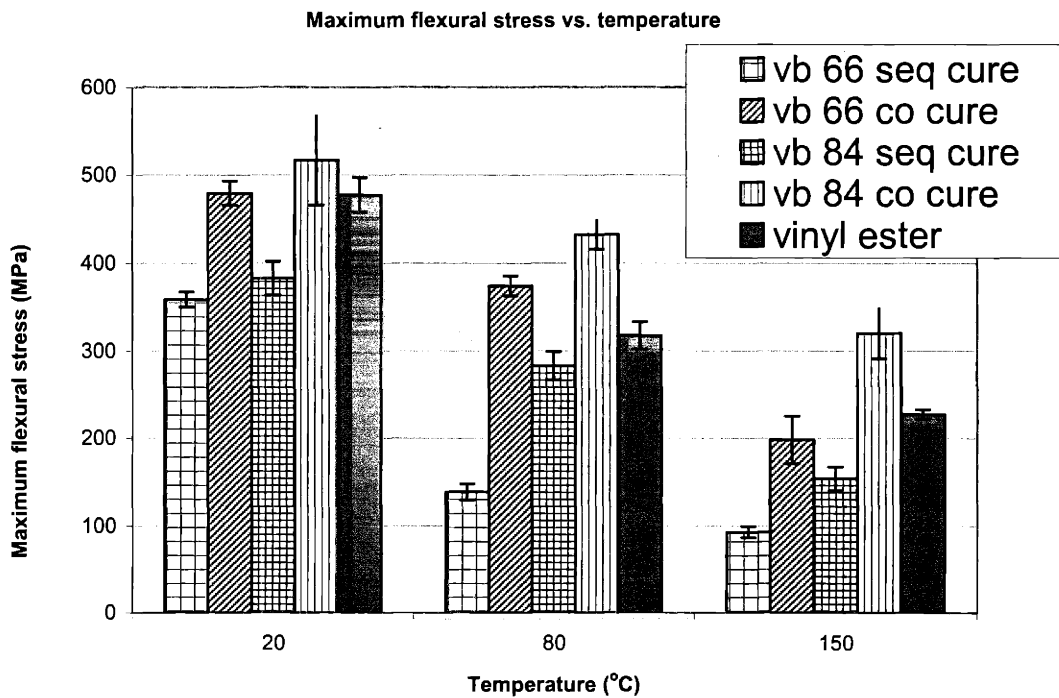


Figure 6-11 Summary of maximum flexural stress versus temperature for VB hybrid composites.

6.1.2.5 Summary

In summary, for the pure resin composites, vinyl ester resin composite has the highest property retention at elevated temperatures. Silicone resin composites are very sensitive to temperature changes in the aspect of their mechanical properties, with both silicone resin composites losing as much as 80% of their flexural properties at 150°C. 3136T condensation silicone resin composite has better property retention at 80°C compared to the 2672B matrix composite.

The results suggest that the composite flexural property change with temperature is closely related to their matrix property change with temperature, which is mainly attributed to the mechanical behavior and glass transition behavior of the polymer matrices.

For the V/B hybrid composites, we see better property retention in the co-cured laminates, possibly due to a stronger interface formed during co-cure. Between the co-cured laminates, the V/B 8/4 hybrid performs better than the V/B 6/6 hybrid, possibly due to higher vinyl ester resin content in the V/B 8/4. Flexural property retention of V/B 8/4 co-cured hybrid composite is exceptional good, better than the pure vinyl ester resin composite (Figure 6-12 and Figure 6-13) This can be explained by the possibilities of stronger interface formed between V and B and of the shielding effect against heat offered by the 2672B skin.

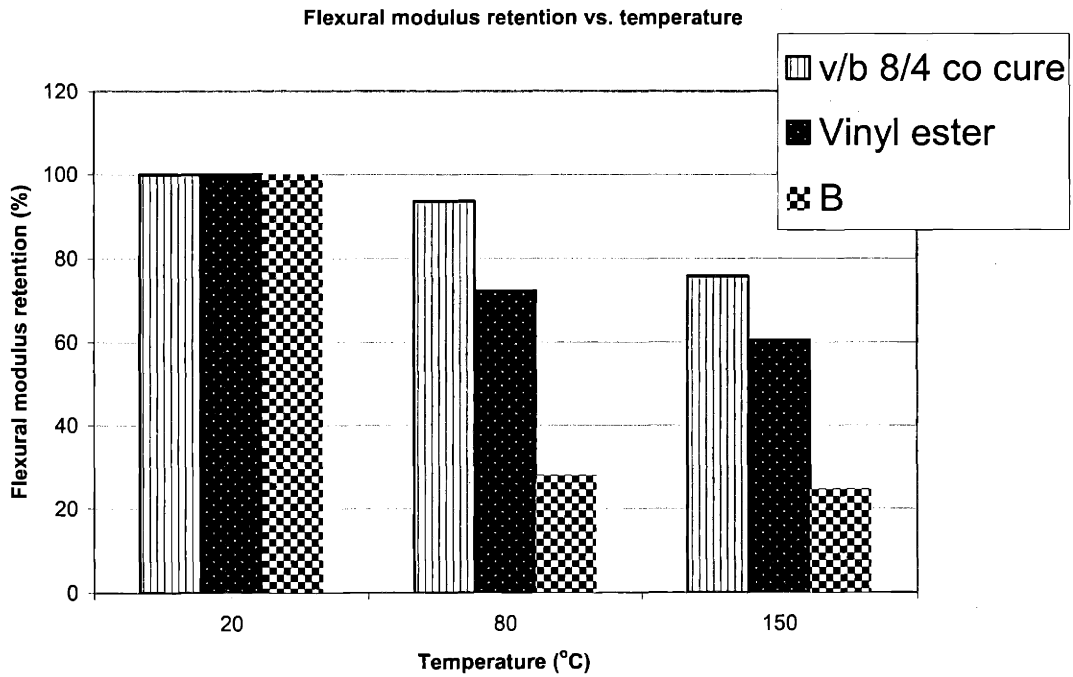


Figure 6-12 Summary of flexural modulus retention vs. temperature for V, B and V/B 8/4 co-cured composites.

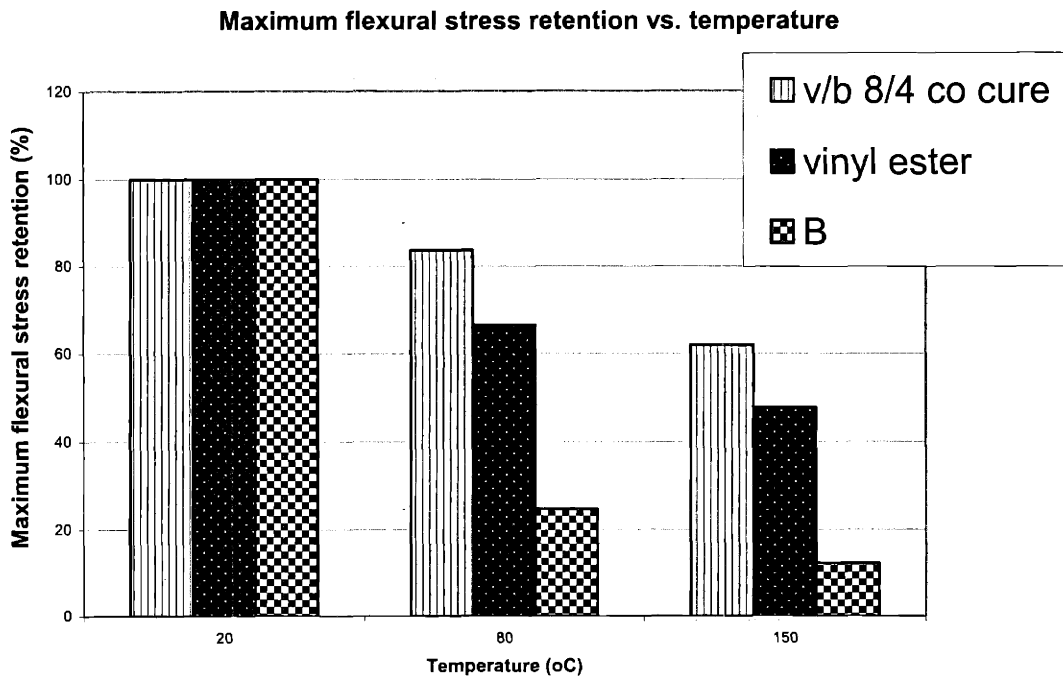


Figure 6-13 Summary of maximum flexural stress retention vs. temperature for V, B and V/B 8/4 co-cured composites.

6.1.3 SEM ANALYSIS OF FLEXURAL SAMPLES

SEM analysis has been performed on room temperature flexural samples of B, V and VB hybrid (co-cured V/B 8/4) composites. The micrographs are shown in Figure 6-14 to Figure 6-17. We see all samples are sound castings and have few pores/voids. At the tensile side of the specimens, fiber breakage on the outside layer occurs in all samples. Moving into the center layers, matrix cracking is also very obvious. The conclusion is that samples start to fail by matrix cracking first and sometimes delamination between fiber and matrix can happen. The final failure of the samples is always accompanied by fiber breakage on the tensile side of the specimens.



Figure 6-14 SEM micrograph of vinyl ester composite after flexural test.

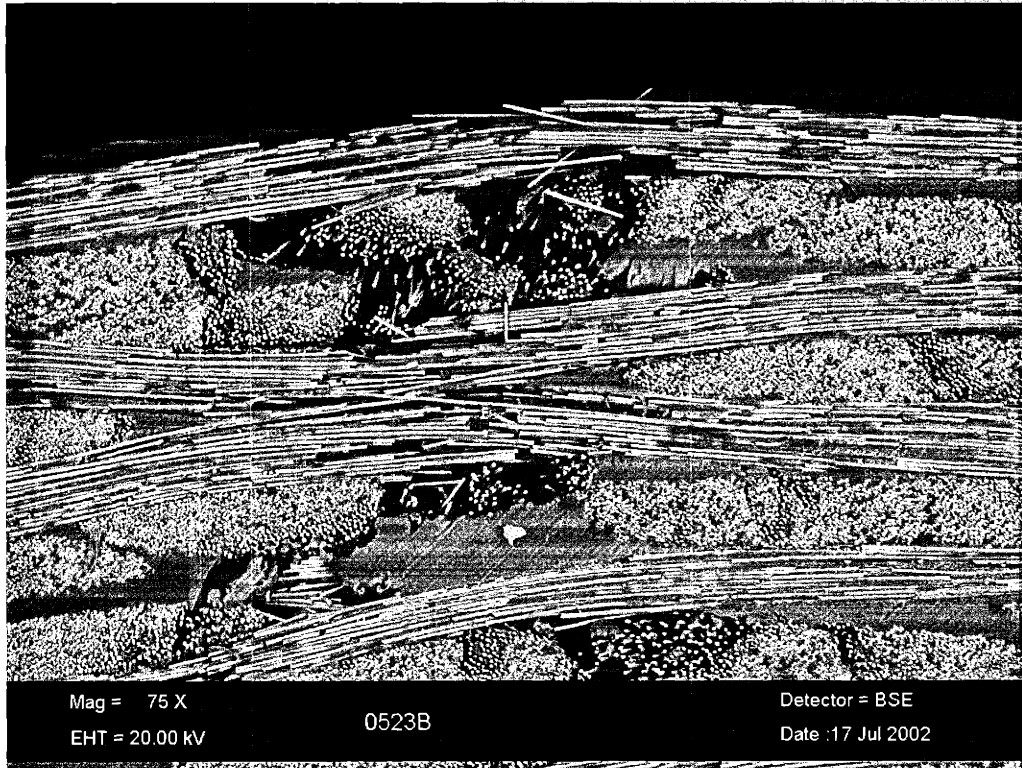


Figure 6-15 SEM micrograph of 2672B composite after flexural test.



Figure 6-16 SEM micrograph of V/B 8/4 co-cured hybrid composite – near the tensile side of the specimen.



Figure 6-17 SEM micrograph of V/B 8/4 co-cured hybrid composite after flexural test – near the center of the specimen.

6.1.4 INTERLAMINAR SHEAR STRENGTH

3136T, vinyl ester, 2672B, and co-cured V/B 8/4 hybrid composites have been tested for their short beam shear strength. The results are listed in Table 6-11. The short beam stresses of both silicone resin composites are close in values. This demonstrates that both resin composites have similar interlaminar shear strength, which suggests that the two composites have similar matrix properties and matrix/fiber interfacial shear strength.

It is clear that the co-cured V/B 8/4 hybrid composite has higher shear strength than both 2672B and vinyl ester composites. The higher strength indicates that the hybrid composite has a stronger matrix/fiber interface or better matrix properties. This is consistent with the flexural property results presented in previous sections of this chapter.

Co-cured hybrid matrix of vinyl ester and silicone 2672B lead to exceptional mechanical properties of the composite. This suggests from another point that the co-cured hybrid resin matrix has different chemical/physical characteristics from the two pure resins, and these changes in the matrix properties improve the mechanical behavior of the hybrid composite.

Table 6-11 Short beam strength of vinyl ester, silicone and hybrid composites.

sample	resin content %	span mm	crosshead rate mm/min	short beam strength MPa	stdev MPa
T	31.0	11.2	1	20.84	±0.86
B #1	32.3	11.8	1	21.23	±0.17
B #2	29.4	10.4	1	21.52	±0.24
V #1	29.9	11.0	1	37.69	±2.35
V#2	29.4	10.8	1	40.50	±0.29
V/B #1	31.1	11.1	1	46.72	±2.00
V/B #2	30.7	11.4	1	46.19	±0.80

Note: V/B – hybrid composite of co-cured V/B 8/4.

#1 and #2 suggest samples are from different laminates.

6.2 Environmental effects

Environmental effects on the composites are discussed in this section. Results including moisture absorption, thermal properties, and fire performance are presented. Silicone resin, vinyl ester and VB hybrid composite have been studied. In this result and discussion section, the VB hybrid specifically refers to the V/B 8/4 co-cured composite unless otherwise noted.

6.2.1 MOISTURE ABSORPTION

The results of non-sealed samples are summarized in Figure 6-18 and Figure 6-19 ($M\%$ vs. $\text{Time}^{1/2}$). Comparing the V, B, and VB (co-cured V/B 8/4) curves in the 49.7%R.H. figure (Figure 6-18), it is clear that throughout the time scale B has the lowest water absorption capacity, much lower than both V and VB. Compare V and VB, initially VB has the lower moisture content than V. After about 150 hours, the hybrid composite does not prove to be more water resistant than the vinyl ester laminate. Later the weight gain in VB hybrid even increases faster than that in V. Both vinyl ester and VB hybrid composites do not reach equilibrium at the end of moisture exposure for 1369 hours. The final moisture content of VB composite is about 0.04 wt% higher than that of V composite.

At 100% R.H. (Figure 6-19), the 2672B laminate still consistently has the lowest moisture absorption capacity. Now, the vinyl ester composite has the highest moisture content and reaches its equilibrium content of 0.64 wt% after about 900 hours. The weight change in VB increases linearly with time without reaching its equilibrium. Its curve sits about half way between the V curve and the B curve – which suggests that at 100% humidity level the hybrid composite is more resistant to water than the vinyl ester composite. The effect of the hybrid matrix on the composite moisture resistance is more obvious in this case. This effect can be explained by the protection effect from the 2672B silicone skin due to its excellent moisture resistance.

For the sealed samples, results are presented in Figure 6-20 and Figure 6-21. Both silicone resin composites (T and B) show similar moisture content at equilibrium at both humidity levels and their curves are the lowest among all. The moisture contents of the VB hybrid composites are between the V and B values at both humidity levels. At 49.7% R.H., VB curve appears closer to the V curve. Also, moisture contents in VB composites do not reach equilibrium under both humidity levels and they increase in a linear fashion.

A summary of the moisture absorption test results of the composites at all experimental conditions is listed in Table 6-12. In general, the sealed samples and non-sealed samples are not much different in terms of both the final equilibrium moisture content and the initial rate of increase in moisture content. This suggests that the edge effects in moisture absorption of these composite laminates are not big. In other words, compared to absorption occurring through both sides of the specimens, the amount of water going through the edges is small and can be ignored. Similar rate of increase in the linear region also suggests that the moisture absorption functions of these composites are close and so are the diffusion coefficients of water in the composites. Two sets of unusual data points (as shown in bold fonts in the table) show the sealed samples have a greater rate of increase than the non-sealed samples. These might be caused by variations in the testing samples rather than by other mechanisms.

Table 6-12 also demonstrates that the equilibrium moisture contents in the composites depend on the matrix resin properties. Silicone resin matrices are moisture resistant and their composites have consistently lowest equilibrium moisture contents. On the other hand, vinyl ester composites often have the highest equilibrium moisture contents.

Moisture absorption results of matrix resins of vinyl ester and silicone (B and T) are shown in Figure 6-22. Vinyl ester is far less moisture resistant than both silicone resins. Another graph plotting the moisture induced strain in 2672B also indicates that it is very small compared to that in cyanate ester resin (Figure 6-23). In conclusion, silicone resins have superior moisture resistance compared to some of the commercial organic resins, like vinyl ester and cyanate ester. In fact, the vinyl ester resin and cyanate ester

resin are low moisture pick-up resins compared to some other common organic resin like epoxy.

The water resistance of the silicone resins can be explained by their low surface energies and low surface tension. In polysilsesquioxane, the intermolecular interaction is low between side groups on the main chain, and the Si-O main chain is flexible in terms of torsion and rotation. This results in the possibility of arrangements of the methyl or phenyl side groups along the surface and the interface, which possesses a low energy configuration and creates shielding effect to the siloxane chain.

Matrix characteristics greatly influence the moisture resistance of their composites, resulting in low moisture absorption in silicone resin composites and yet relatively high moisture pick-up in vinyl ester composites. For the VB hybrid composite, the 2672B silicone skin protects the vinyl ester core to some extent, both in terms of equilibrium moisture content and the rate of moisture content increase at the beginning of the process. This effect is more distinguished at the 100% R.H. level. However, the silicone skin protection effect is not as obvious at 49.7% R.H.

Table 6-12 Summary of moisture absorption test results of all composites.

relative humidity	equilibrium weight change (%)				slope of initial linear part			
	49.7% R.H.		100% R.H.		49.7% R.H.		100% R.H.	
	sealed	un-sealed	sealed	un-sealed	sealed	un-sealed	sealed	un-sealed
B	0.04	<0.01	0.20	0.15	0.006	0.001	0.008	0.008
V	0.17*	0.09*	0.68	0.64	0.006	0.003	0.035	0.024
V/B 8/4 co-cured	0.16*	0.12*	0.48*	0.43*	0.004	0.003	0.013	0.012
T	0.03	-	0.20	-	0.006	-	0.027	-

Data with * are moisture contents corresponding to the longest exposure time (1369 hours) of the experiment during which equilibrium states have not been observed.

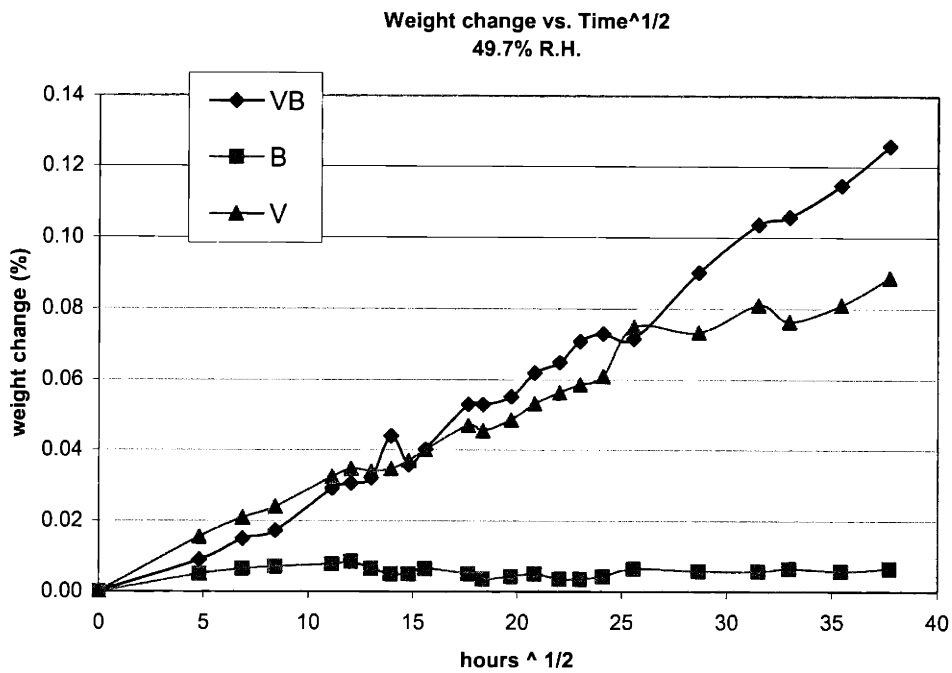


Figure 6-18 Moisture content vs. time^{1/2} in V, B, and VB hybrid laminates (with non-sealed edges) at 49.7% R.H.

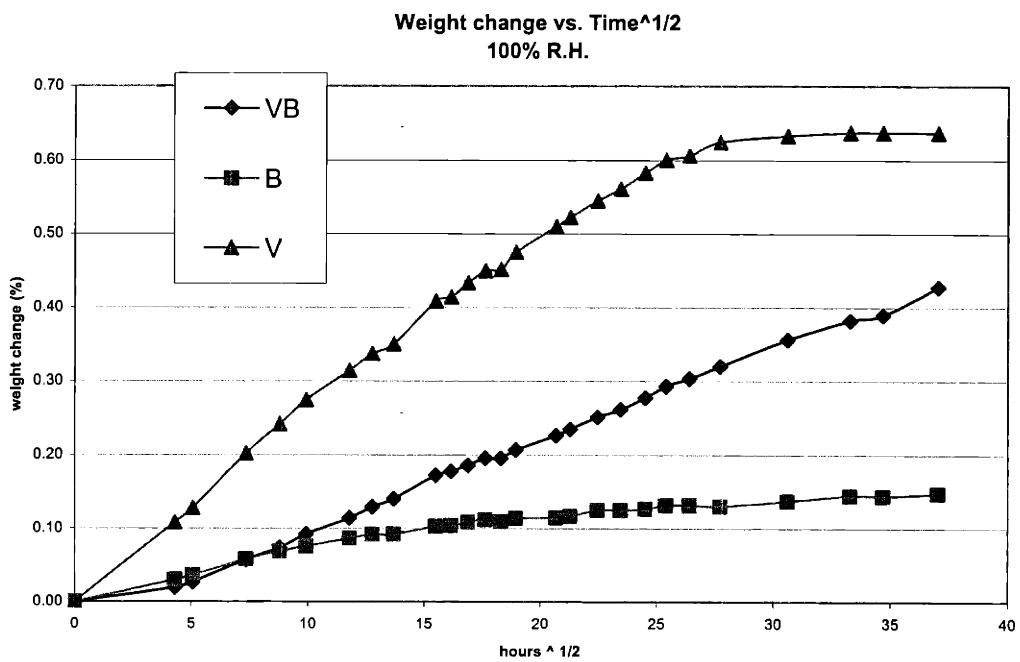


Figure 6-19 Moisture content vs. time^{1/2} in V, B, and VB hybrid laminates (with non-sealed edges) at 100% R.H.

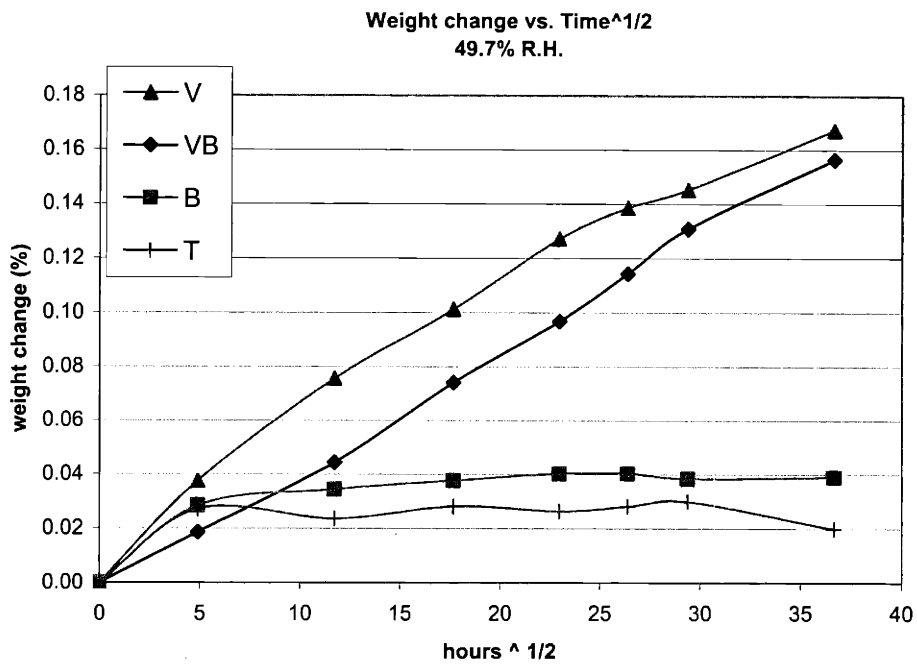


Figure 6-20 Moisture content vs. time^{1/2} in V, B, and VB hybrid laminates of sealed edges at 49.7% R.H.

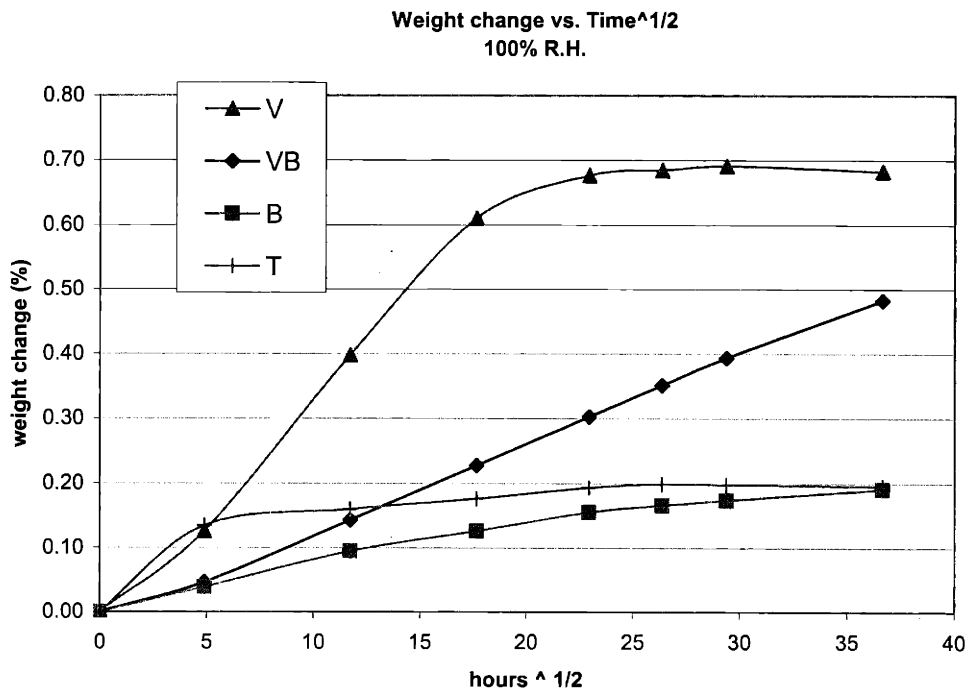


Figure 6-21 Moisture content vs. time^{1/2} in V, B, and VB hybrid laminates of sealed edges at 100% R.H.

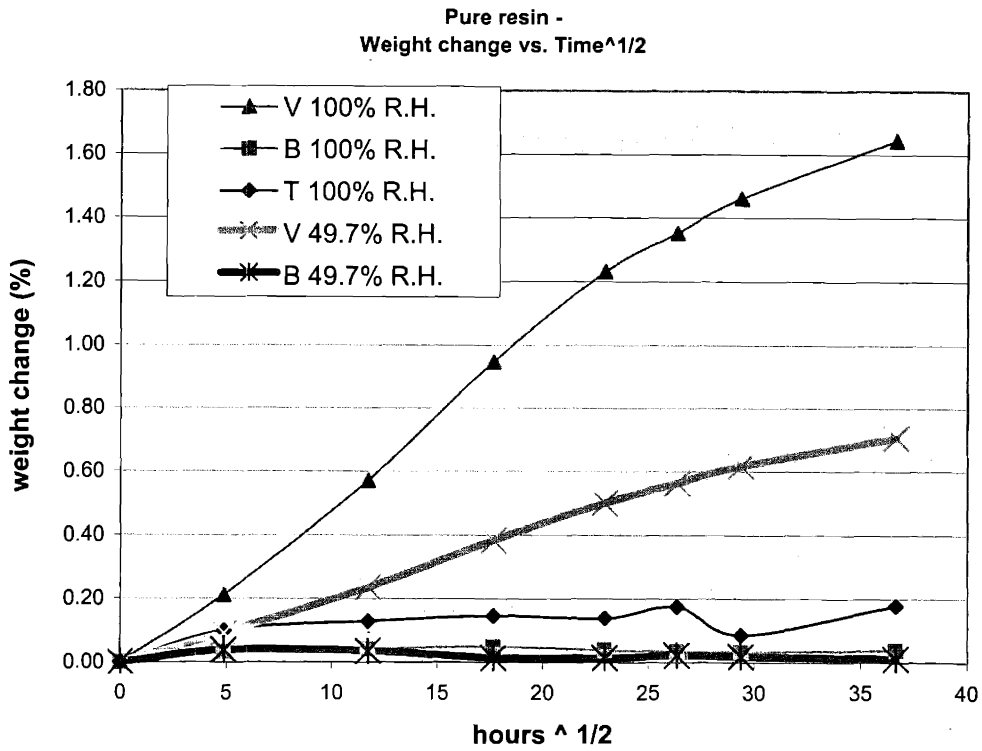


Figure 6-22 Moisture content vs. time^{1/2} in vinyl ester, 2672B and 3136T resins at both 100% and 49.7% R.H.

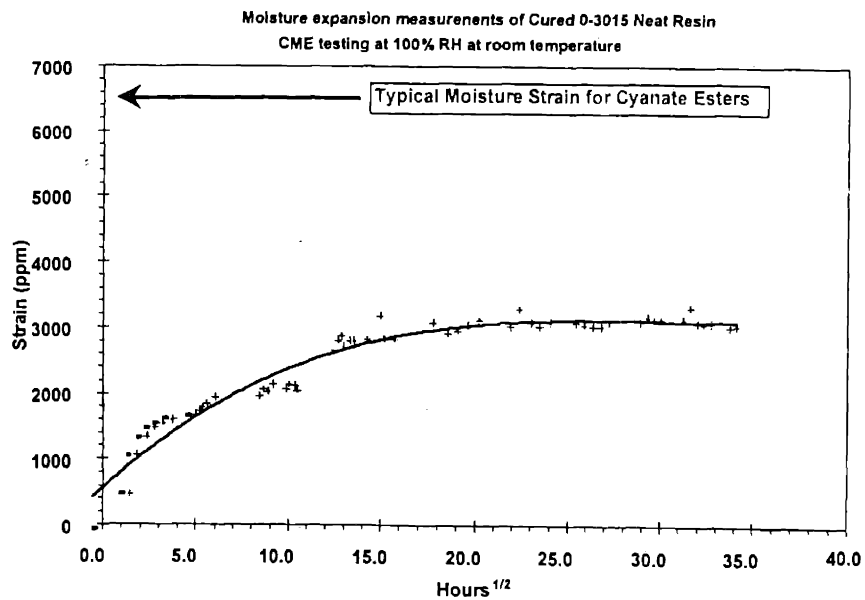


Figure 6-23 Moisture absorption induced strain of 2672B resin. (Data from Dow Corning Corp.)

6.2.2 THERMAL AGING PROPERTIES

6.2.2.1 Weight loss

It is expected that heat aging at an elevated temperature would cause weight losses in composites due to degradation effect by heat and oxygen. Weight loss results of B, V and VB hybrid (co-cured V/B 8/4) composites are plotted in Figure 6-24 through Figure 6-26. Data obtained after various aging hours are consistent: vinyl ester composite always has the biggest weight loss and 2672B has the smallest weight loss, with the VB hybrid curve in between but positioned closer to the B curve. At 10 hours, vinyl ester composite has a big weight loss compared to VB hybrid and B at all temperatures. The difference between VB and B is only identifiable at 170°C, showing VB having a bigger weight loss. At 100 hours, the trend is similar, with a strange data point at 170°C for vinyl ester composite, which might be due to experimental variations. At 1000 hours, the same trend still establishes, with a much greater difference among V, B and VB at 205°C. At this temperature, the weight loss of vinyl ester composite is close to 8%, that of VB hybrid is 3%, and that of B is 1%.

It is clear that as temperature goes up, oxidation and other degradation process occur in all composites. The degree to which this occurs is very dependent upon the matrix resin type. The thermal effect is greatest in vinyl ester composite. Since vinyl ester is an organic resin, the C-C bonds and C-H bonds are more susceptible to thermal and oxidative attack. Compared to this, silicone resin has a much greater performance at elevated temperatures because oxidation of the Si-O bonds and Si-Si bonds occurs at a much smaller rate and magnitude. The oxygen in siloxane is in a high oxidation state and the bond has a partial ionic nature. This keeps the siloxane bonds from reduction reaction until higher temperatures. The experimental data demonstrate a small increase in the weight loss of silicone composite with temperature, which is consistent with the general concept of better thermal and oxidative stability of silicone resins compared to organic resins like vinyl ester. It is also clear that the 2672B silicone resin skin in the VB hybrid composite is effective in protecting the vinyl ester core from thermal degradation. The V/B 8/4 co-cured laminate has weight loss values close to those in the silicone composite,

which is much smaller compared to that in vinyl ester composite in most cases. From this we can see another advantage of using silicone resin as a skin matrix in the hybrid composite to improve its thermal and oxidative stability.

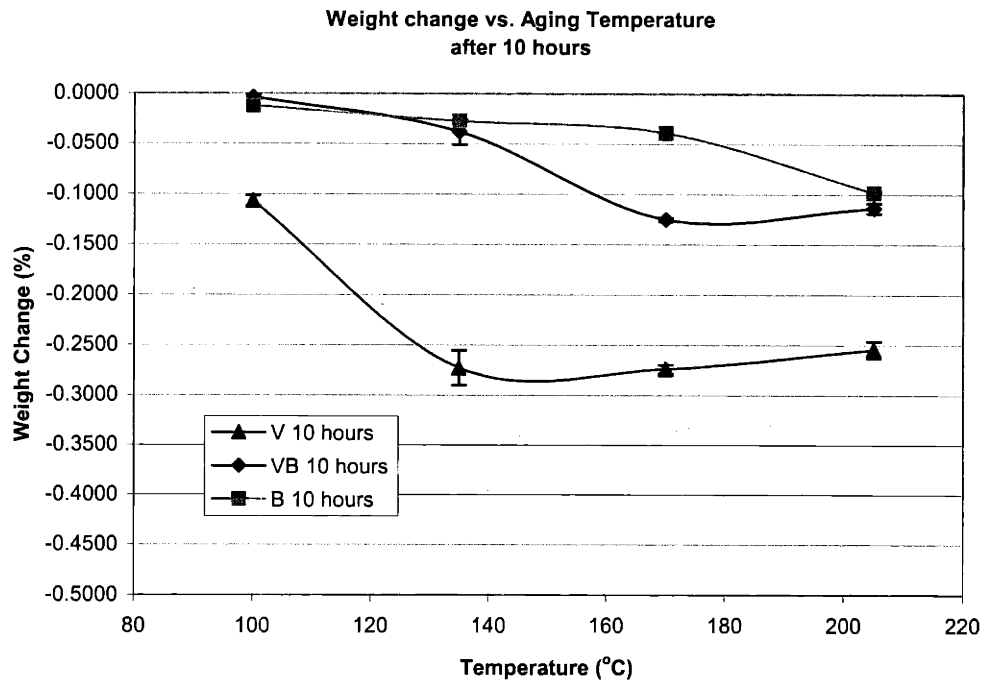


Figure 6-24 Weight loss vs. aging temperature for V, B, and V/B 8/4 co-cured composites after aging for 10 hours.

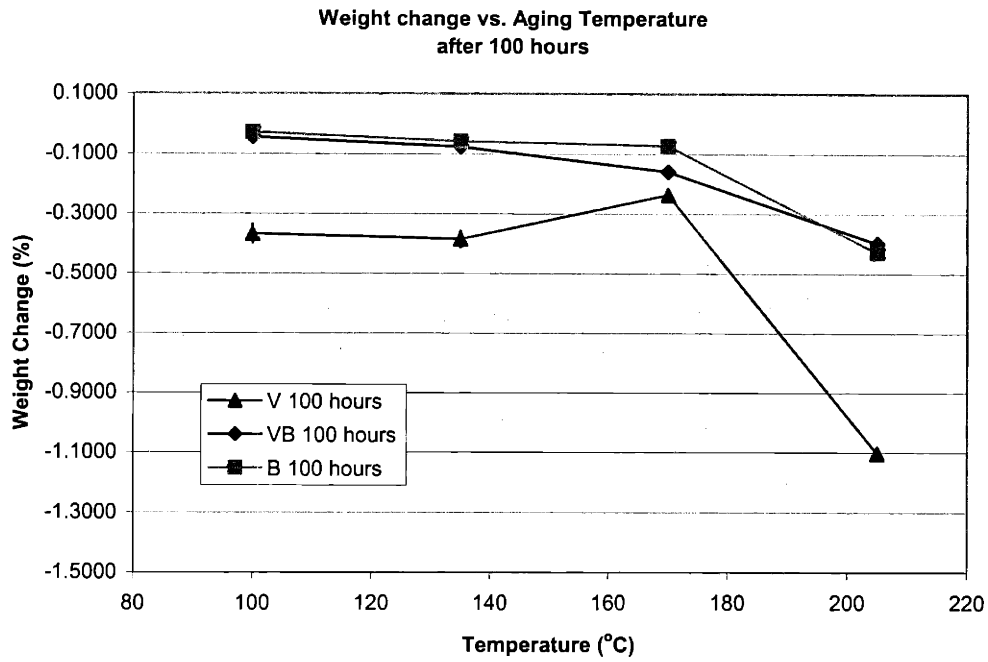


Figure 6-25 Weight loss vs. aging temperature for V, B, and V/B 8/4 co-cured composites after aging for 100 hours.

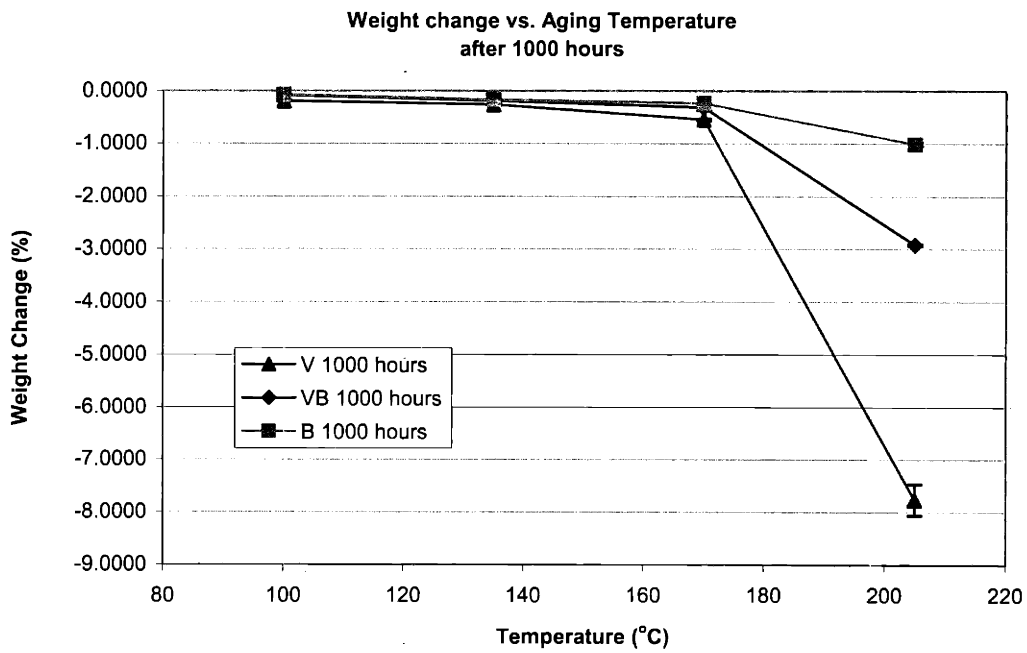


Figure 6-26 Weight loss vs. aging temperature for V, B, and V/B 8/4 co-cured composites after aging for 1000 hours.

Table 6-13 Summary of weight loss of composites subject to thermal aging. VB stands for V/B 8/4 co-cured hybrid composite.

Sample	resin content %	Aging temp. °C	Aging hours hours	Average wt. Change %	stdev
VB	30.3	100	10	-0.004	0.0025
VB	30.3	135	10	-0.038	0.0128
VB	30.5	170	10	-0.125	0.0019
VB	30.3	205	10	-0.114	0.0052
VB	30.5	100	100	-0.045	0.0025
VB	30.5	135	100	-0.076	0.0033
VB	30.5	170	100	-0.159	0.0103
VB	30.5	205	100	-0.399	0.0237
VB	30.5	100	1000	-0.085	0.0069
VB	28.6	135	1000	-0.188	0.0097
VB	28.6	170	1000	-0.316	0.0526
VB	28.6	205	1000	-2.920	0.0175
B	33.8	100	10	-0.012	N/A
B	33.8	135	10	-0.027	N/A
B	29.4	170	10	-0.039	0.0057
B	33.8	205	10	-0.098	N/A
B	33.8	100	100	-0.029	N/A
B	33.8	135	100	-0.059	N/A
B	29.4	170	100	-0.073	0.0136
B	33.8	205	100	-0.429	N/A
B	29.4	100	1000	-0.074	0.0065
B	29.65	135	1000	-0.173	0.0135
B	29.65	170	1000	-0.237	0.0085
B	29.65	205	1000	-1.011	0.0416
V	29.05	100	10	-0.107	0.0052
V	29.05	135	10	-0.273	0.0172
V	29.4	170	10	-0.274	0.0044
V	29.05	205	10	-0.255	0.0194
V	29.11	100	100	-0.367	0.0315
V	29.11	135	100	-0.385	0.0270
V	29.4	170	100	-0.236	0.0122
V	29.11	205	100	-1.104	0.0893
V	29.4	100	1000	-0.193	0.0086
V	29	135	1000	-0.263	0.0201
V	29	170	1000	-0.548	0.0217
V	29	205	1000	-7.761	0.2957

6.2.2.2 Flexural property retention

It is now time to see the effect of aging on flexural properties of the V, B, and VB composites. Aged samples have been tested with three-point bending and the results were compared to the baseline data obtained from room temperature testing of samples without aging. The relative changes in flexural properties are presented in Figure 6-27 through Figure 6-32.

It is observed that the flexural modulus and maximum stress changes are far more complicated than the weight losses after thermal aging. The effect of heat aging sometimes increases the stress and modulus levels and sometimes decreases them. Generally, weight loss is a measurement of physical property change during the aging process. However, flexural property change will depend on both the physical and chemical changes occurring in the composites and thus is more complicated.

After 10 hours of aging in Figure 6-27, the flexural modulus of vinyl ester and VB hybrid increases or stays constant at all temperatures, with a very big increase occurring at 170°C. Flexural modulus of B composites shows a slight decrease throughout the temperature range. The maximum stress curves in Figure 6-30 shows ups and downs with temperatures, but mostly with a positive change due to an increase in the composite strength.

After 100 hours, the VB 8/4 hybrid composite undergoes about 3-4% increase in modulus except an increase of ~10% at 170°C. The vinyl ester composite, however, increases ~8% in modulus except for ~5% at 205°C. Fluctuations occur in the modulus of B composites, with the magnitude between -1% and +1% (Figure 6-28). The maximum flexural stress in Figure 6-31 presents a sharp decrease in V composites from 16% to -1% and a moderate increase in the B composite stress from 2% to 10%. The VB hybrid has a constant increase of 6% in stress from 100°C to 170°C and then the value goes to 2% at 205°C.

After 1000 hours (Figure 6-29 & Figure 6-32), flexural modulus for vinyl ester composite starts to decrease above 135°C and reaches the extreme of -17% at 205°C. The

2672B composite experiences a consistent decrease, with the values going from -2% to -12%. The VB hybrid has about 2-3% increase in modulus at 100°C, 135°C and 170°C. Then it drops to -10% at 205°C. Overall, it seems that the 2672B resin protects the vinyl ester core from heat degradation, resulting in a steady positive change in modulus of a few percent at temperatures below 170°C. At the extreme temperature of 205°C, it also causes the modulus to drop less dramatic. The flexural stress of the hybrid composite, however, undergoes a decrease of 24% at 205°C.

Aging results in terms of mechanical properties suggest that both chemical and physical changes can occur during the aging process. It is reasonable that at relatively low temperatures with short aging periods, the heat could result in a more complete cure in the thermoset resins and thus increase their composite performance. On the other hand, at higher temperatures and longer aging hours, the oxidation process has detrimental effects on properties of the matrix resins and their composites. The effect of thermal/oxidation resistance of the silicone skin in protecting the vinyl ester core can only be observed in some data points. It is not as obvious as what is seen from the weight loss data. Partly the reason is the complexity of flexural property change after thermal exposure.

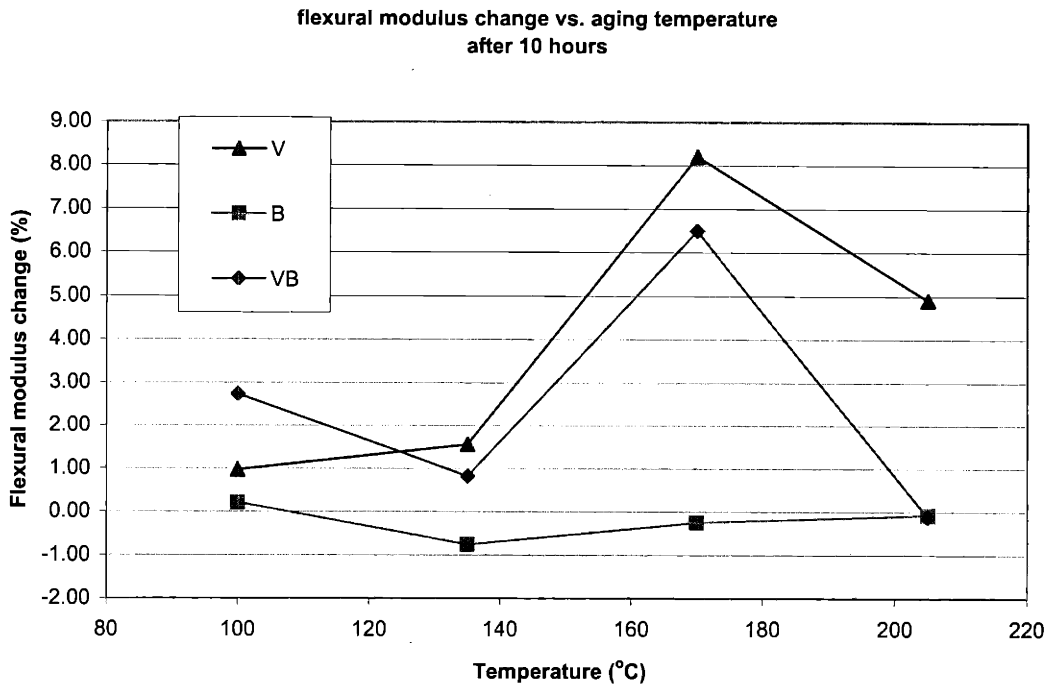


Figure 6-27 Flexural modulus change vs. aging temperature for V, B, and VB composites after aging for 10 hours.

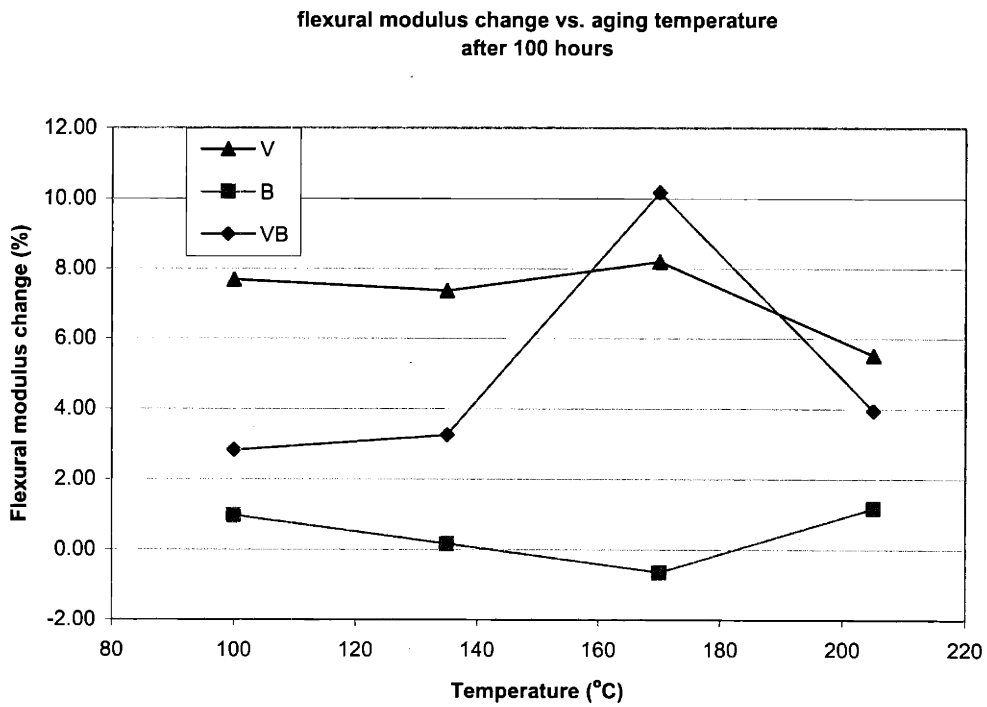


Figure 6-28 Flexural modulus change vs. aging temperature for V, B, and VB composites after aging for 100 hours.

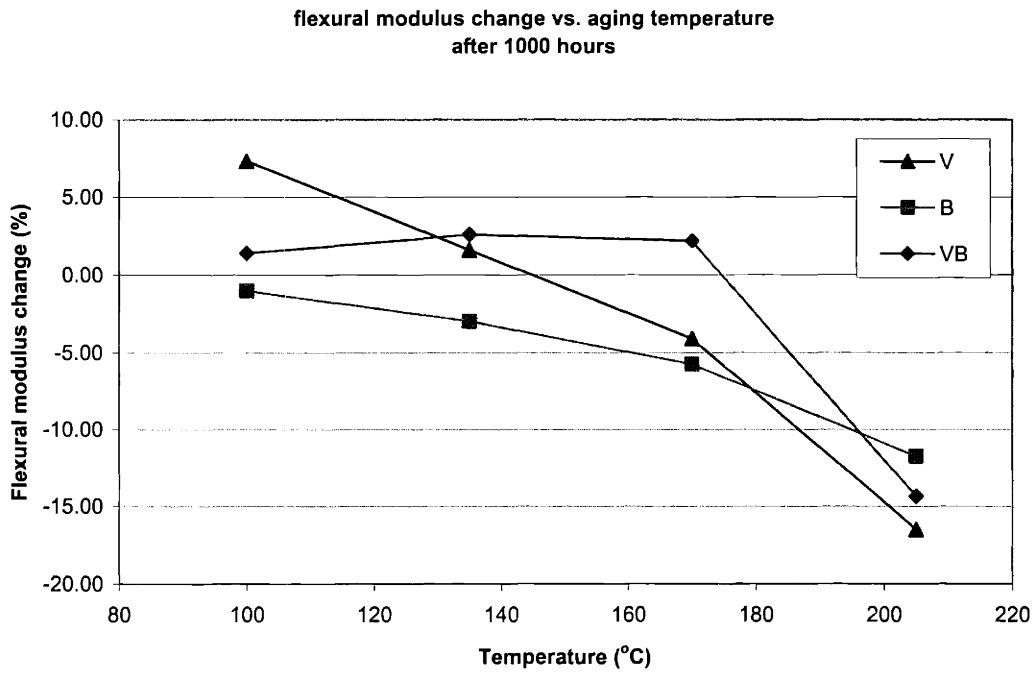


Figure 6-29 Flexural modulus change vs. aging temperature for V, B, and VB composites after aging for 1000 hours.

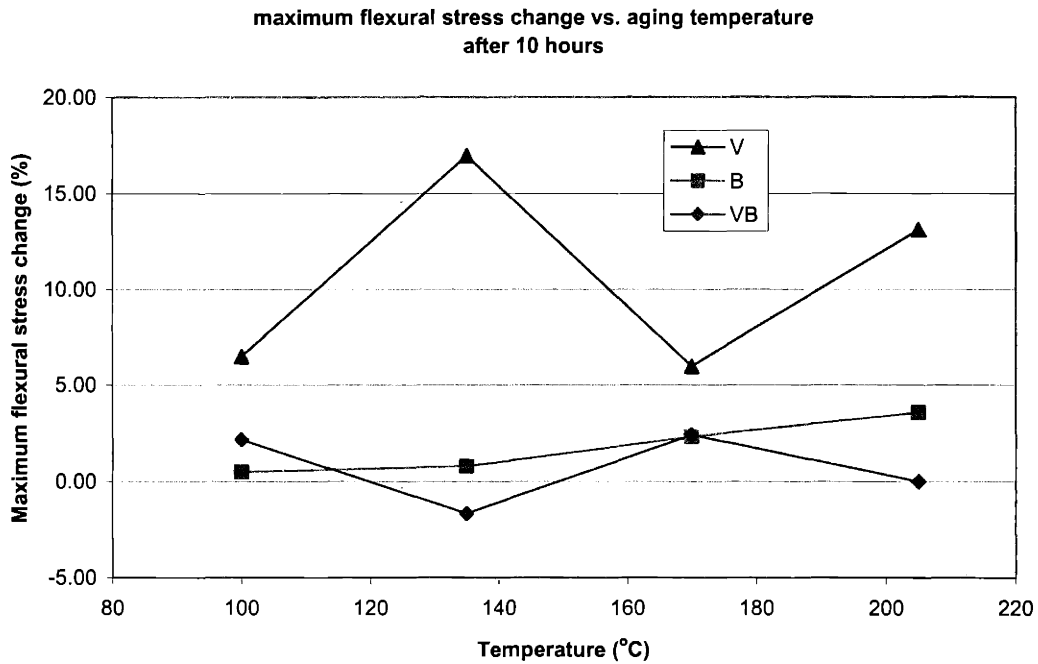


Figure 6-30 Maximum flexural stress change vs. aging temperature for V, B and VB composites after aging for 10 hours.

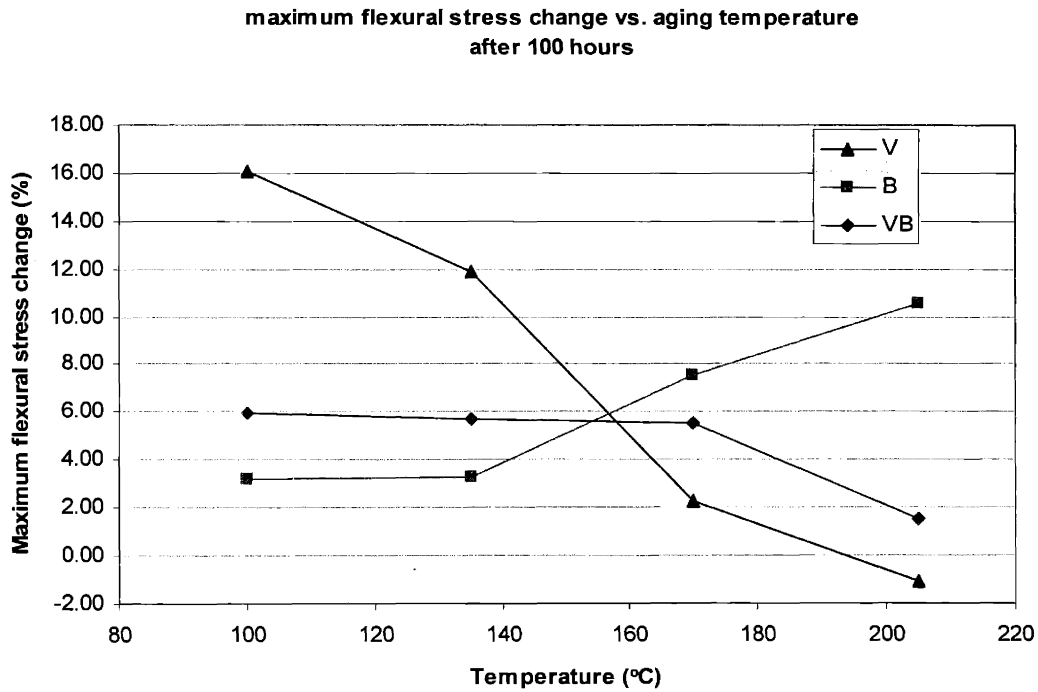


Figure 6-31 Maximum flexural stress change vs. aging temperature for V, B, and VB composites after aging for 100 hours.

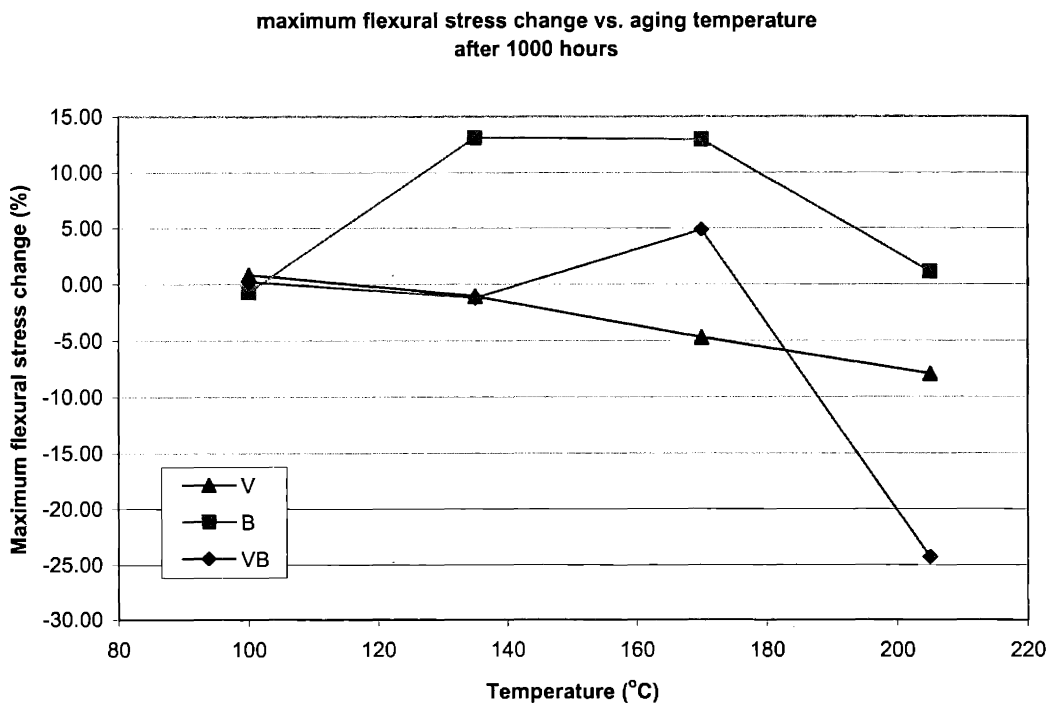


Figure 6-32 Maximum flexural stress change vs. aging temperature for V, B, and VB composites after aging for 1000 hours.

6.2.2.3 Thermogravimetric analysis

The thermal stability of composites made of silicone and vinyl ester resins has also been studied by the thermogravimetric analysis. TGA results of both composites and neat resins are presented in Figure 6-33 and Figure 6-34. Let's take 5% weight loss temperature of the material for comparison. For pure resins: it is 397°C for vinyl ester, 533°C for silicone 2672B, and 563°C for 3136T. Silicone resins also experience the same amount of weight loss at higher temperatures. For example, vinyl ester resin experiences 20% weight loss around 450°C but silicone resins experience the same loss only after 700°C. This suggests that both silicone resins have higher thermal stability than the vinyl ester resin. The data also suggest that addition cure 2627B resin is less thermal resistant than the condensation cure 3136T resin due to higher carbon content in the 2672B network.

The 5% weight loss temperatures of V and VB hybrid composites are 404°C and 422°C, respectively. The weight loss in VB at higher temperatures is a slower process compared to the V composite. V composite has 25% weight loss at 508°C. While for the VB hybrid, this does not happen until around 593°C. This also proves the capability of the silicone resin skin layer in providing thermal protection to the hybrid composite. The 5% weight loss temperatures of B and T composites are at 583°C and 610°C, respectively. This proves that the silicone resin composites have far superior thermal stability compared to the vinyl ester composites.

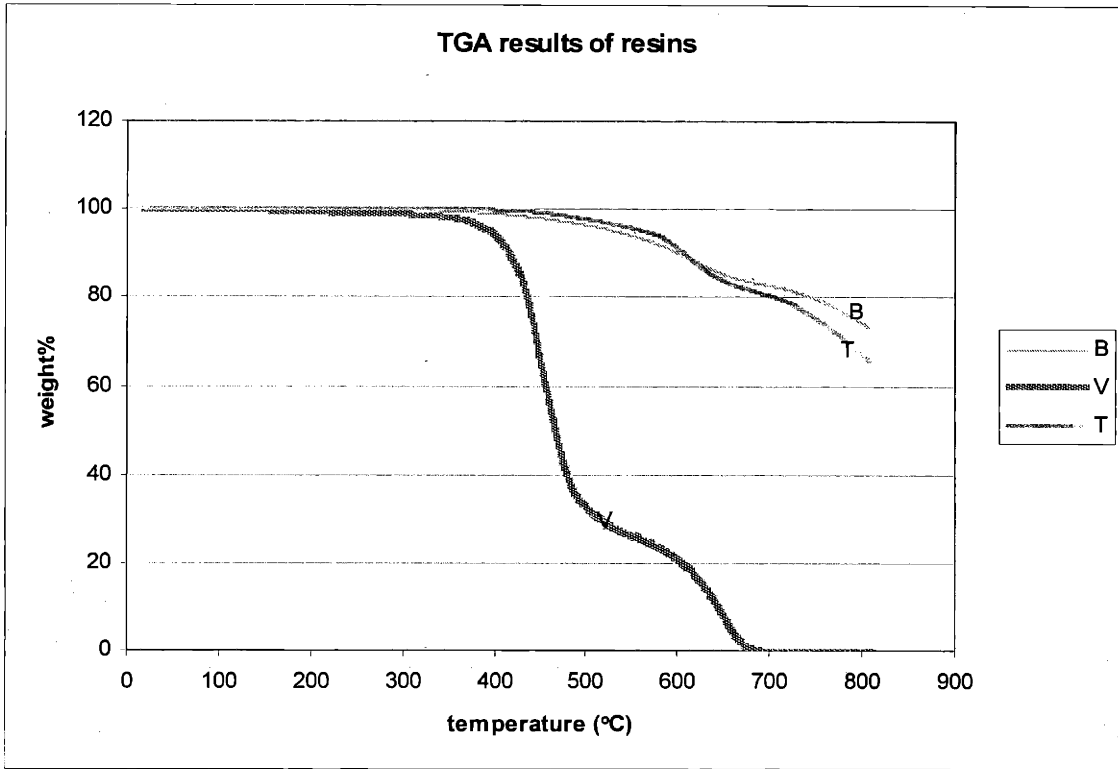


Figure 6-33 TGA of vinyl ester, 2627B and 3136T resins.

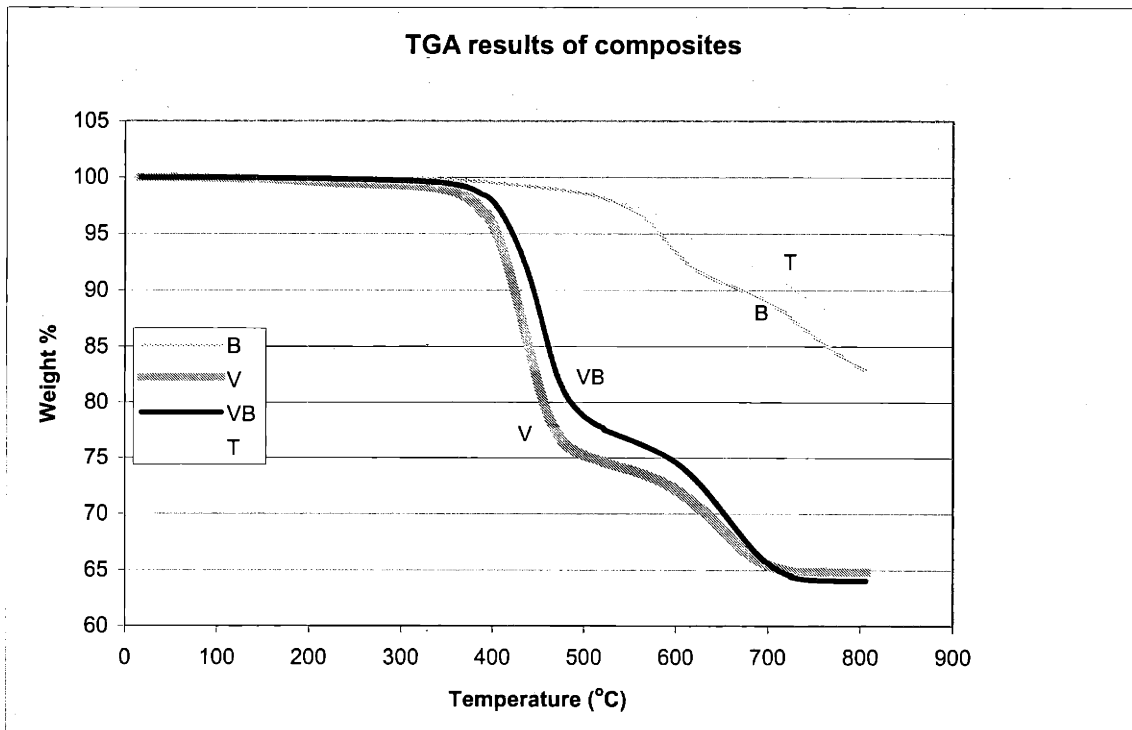


Figure 6-34 TGA of vinyl ester composite, 2672B composite and V/B hybrid composite.

6.2.3 FIRE PERFORMANCE

Fire test results including OSU test and cone calorimetry test are summarized in Table 6-14 and

Table 6-15. From the OSU test results, we see that silicone resin composite B has the lowest peak heat release rate and total heat release rate. The VB hybrid has a mid value between the vinyl ester composite and the 2672B composite. However, the result of 3136T composite does not make much sense as it has higher peak release rate than the 2672B. Theoretically, the lower carbon content of the 3136T resin should give rise to better fire resistance than 2672B.

Table 6-14 OSU test results of vinyl ester, silicone and hybrid resin composites.

Resin	weight (g)	thickness (inch)	Resin content (%)	Time to peak heat (s)	Peak HRR (kW/m ²)	Total HRR at 2 minutes (kW/m ²)
2672 B	112	0.09	25	212	31.1	10.8
Vinyl ester	111	0.097	24	238	40.5	14.2
V/B 8/4 co cure	120	0.11	30	292	35.7	10.7
3136 T	115	0.1	27	161	37.1	18.7

* HRR – heat release rate

The cone calorimetry test results of the composites are shown in

Table 6-15. The peak heat release rate data of the silicone resin composites are the lowest among all, with 3136T having a lower value. The peak heat release rate of the hybrid composite still has the value between those of V and B, which suggests that the silicone resin skin makes the hybrid composites more fire resistant. The average heat release rate also shows the same trend. Compare data of the sequential cured and the co-cured V/B 8/4 hybrid composites, we see the co-cured laminate has a slightly lower peak heat release rate.

Table 6-15 Cone calorimetry test results of vinyl ester and silicone resin composites.

Resin	Resin cont (%)	t _{lg} (s)	Pk HRR (KW/m ²)	Ave HRR (KW/m ²)		
				60 s	180 s	300 s
vinyl ester	21	44	349	284.8	141.4	94.8
2672 B	35	127	143.9	97.8	106.4	77.3
V/B 8/4, co cure	23	32	213.7	133.2	120	76.2
V/B 8/4, sequential cure	26	47	228.1	190.8	93.4	59.4
3136T	31	59	89	30.5	56.4	44.2

t_{lg} time to sustained ignition

Pk HRR peak heat release rate

Ave HRR average heat release rate, after ignition

In conclusion, fire test results prove that the silicone resin composites are more fire resistant than the vinyl ester composites. The hybrid composites also benefit from the silicone resin skin and have a lower heat release rate compared to the vinyl ester composites. We see the advantage of utilizing the silicone skin to protect the vinyl ester core from fire attack.

6.3 DMA and proposed explanation

DMA graphs of B, V and VB hybrid (V/B 8/4 co-cured) composites are shown in Figure 6-35, Figure 6-36 and Figure 6-37, respectively. From the analysis, we see an interesting phenomenon in the change of T_g in these composites. B composite has a $\text{Tan } \delta$ peak at around 85°C . Vinyl ester composite has the α peak around 150°C . On the graph of the hybrid composite, we see two major peaks in the $\text{Tan } \delta$ curve: one at $\sim 75^\circ\text{C}$ and the other at $\sim 190^\circ\text{C}$. These two peaks should be corresponding to T_g 's of the silicone resin and vinyl ester resin in the hybrid composite, respectively. In other words, the T_g 's of the hybrid composite do not show simple addition effect but they move away from each other: T_g of 2672B moves to a slightly lower temperature and T_g of vinyl ester moves to a higher temperature.

It is possible that the styrene contained in the vinyl ester resin diffuses to the silicone resin. At the same time the crosslinker inside silicone resin can diffuse to the vinyl ester side. Styrene reacts with both vinyl groups of the silicone resin and the Si-H groups in its crosslinker. This affects the crosslinking reaction of the silicone resin by changing its stoichiometry, and lowers the T_g of silicone in the hybrid laminate. At the same time, decrease in the styrene content in vinyl ester results in a smaller extent of polymerization of styrene, which has a lower glass transition temperature. This leads to the higher T_g of vinyl ester resin and explains for the good property retention at elevated temperature for the hybrid composite.

To estimate the T_g of the vinyl ester resin containing styrene, we can use the empirical relation of glass transition temperature for random copolymer to approximate [1]:

$$\frac{1}{T_g} = \frac{w_1}{T_{g1}} + \frac{w_2}{T_{g2}} \quad \text{Equation 6-1}$$

where w_1 and w_2 are the weight fractions of the monomer in the copolymer, and T_{g1} and T_{g2} are their T_g 's respectively. It is straightforward to see that a decrease in the weight fraction of the low T_g constituent will increase the T_g for polymer.

In order to verify the effect of styrene content on the glass transition temperature of the resin, two experiments have been performed on both the vinyl ester resin and the hybrid composite. One resin sample (VL) was stirred with a stirring rod constantly under the hood for 24 hours to remove styrene before it was cured. The weight loss after this step was about 10%. Another resin sample (VS) was cured without this step. For the hybrid composite, two samples VB1 and VB2 of co-cured V/B 8/4 were made. Wet lay-up of the vinyl ester core of VB1 was placed inside the hood for about 1 day before it was co-cured with the addition cure silicone skin. VB2 was cured after the wet lay-up of the vinyl ester core has been placed inside the hood for three days. DMA results of these samples are plotted in Figure 6-40 and Figure 6-41. The resin samples are shown in VL and VS curves. VL (resin with less styrene) has a higher glass transition just as expected. As the styrene content decreases, the T_g of the vinyl ester resin moves to a higher temperature. Hybrid composite VB1 is made of vinyl ester resin that has about the same styrene content as VL and also has a similar vinyl ester glass transition temperature. The vinyl ester peak in VB2 is slightly higher than that in VB1, with VB2 containing smaller amount of styrene than VB1. These results provide information on how styrene diffusion affects the chemical reaction inside the hybrid composites. Diffusion and reaction of styrene seems to play a key role.

Figure 6-39 illustrates the reactive groups inside the hybrid composite matrices and near the interface between vinyl ester resin and addition cure silicone resin. The vinyl ester resin has vinyl groups from the styrene and vinyl ester. The silicone side has the vinyl groups from silicone and Si-H from its crosslinker. In addition to changes inside both resins from diffusion, changes also happen at the two resin interface. At the interface, reaction could happen between the vinyl groups present in the vinyl ester and the vinyl or the SiH groups present in the addition cure silicone resin. The effect of the inter-resin vinyl-vinyl reaction or vinyl-SiH might form a stronger network and interface between the resins. The reaction also reduces the number of reaction sites inside the

silicone network and results in lower crosslinking density from the Si-H /vinyl reaction inside silicone resin. The vinyl group depletion in the vinyl ester could result in a slightly lower crosslinking density. However, it seems the beneficial effect of a stronger interface is dominant. The co-cured hybrid has strong mechanical properties at room temperature as well.

The above proposed mechanism provides reasonable explanation of strong mechanical properties and good property retention of the co-cured V/B hybrid composite. DMA results provide indirect information for this; however, direct evidence of chemical reaction and compositional change at the interface is hard to obtain.

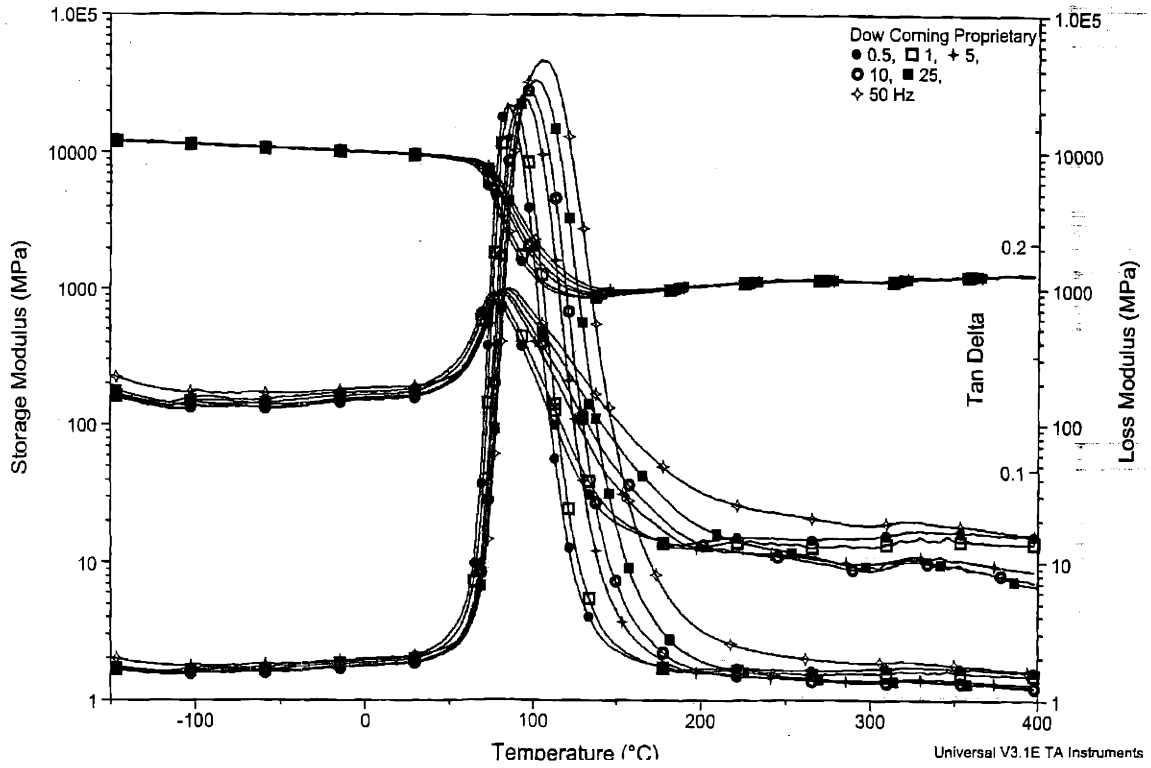


Figure 6-35 DMA of 2672B composite.

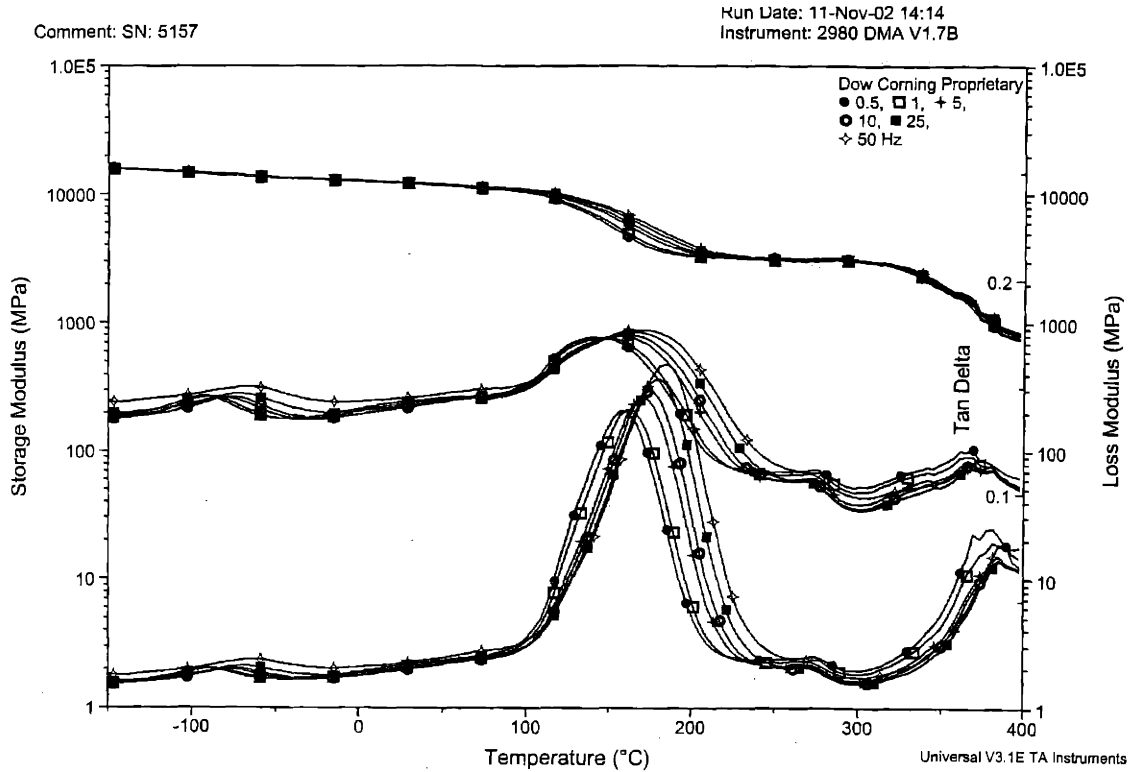


Figure 6-36 DMA of vinyl ester composite.

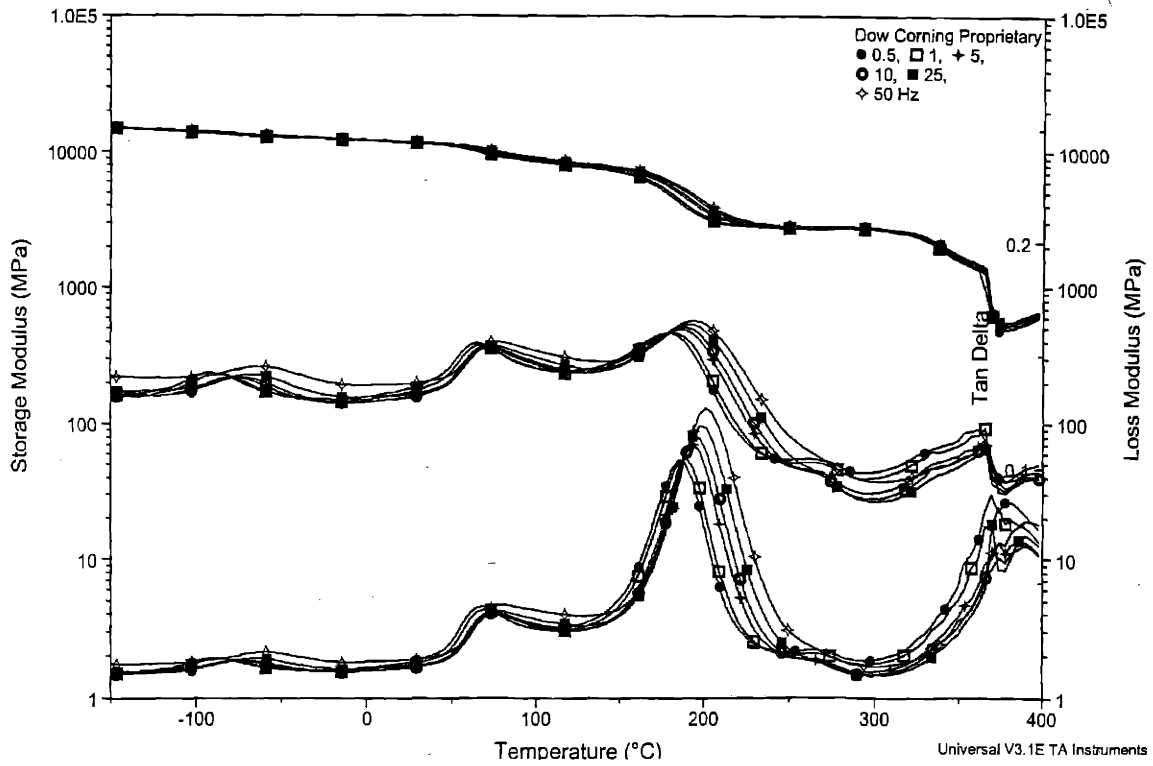


Figure 6-37 DMA of co-cured V/B 8/4 composite.

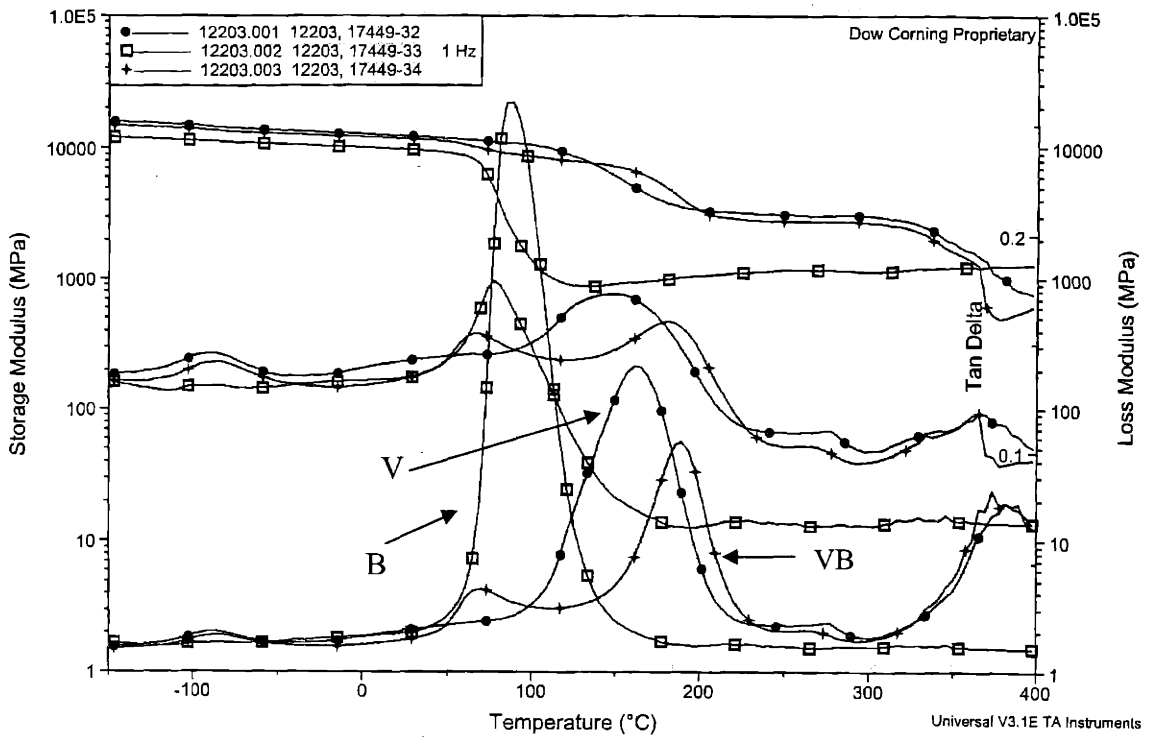


Figure 6-38 DMA graph overlay of V, B and VB composites.

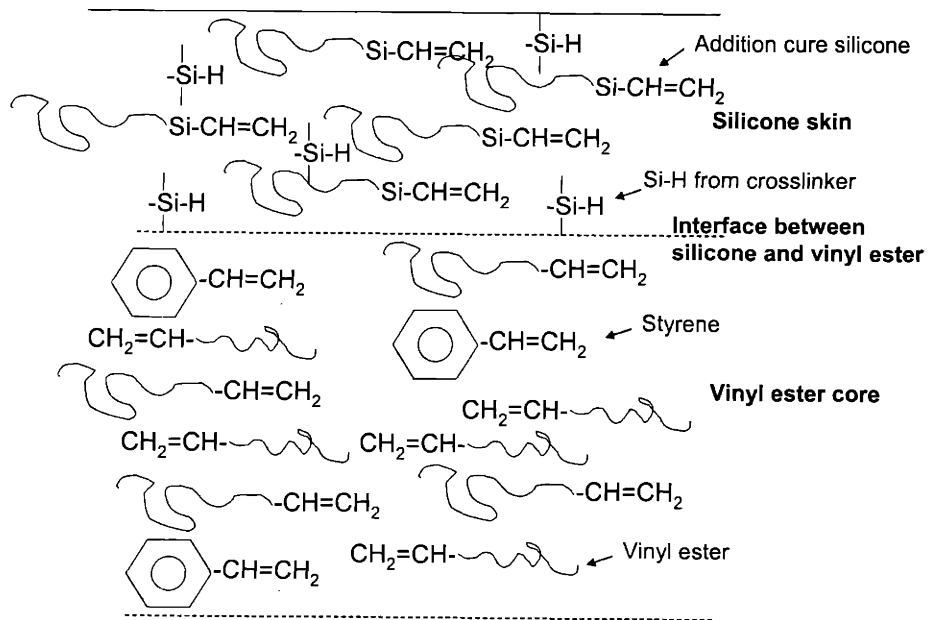


Figure 6-39 Illustration of reactive groups at the interface of vinyl ester resin and addition cure silicone resin inside the hybrid composites.

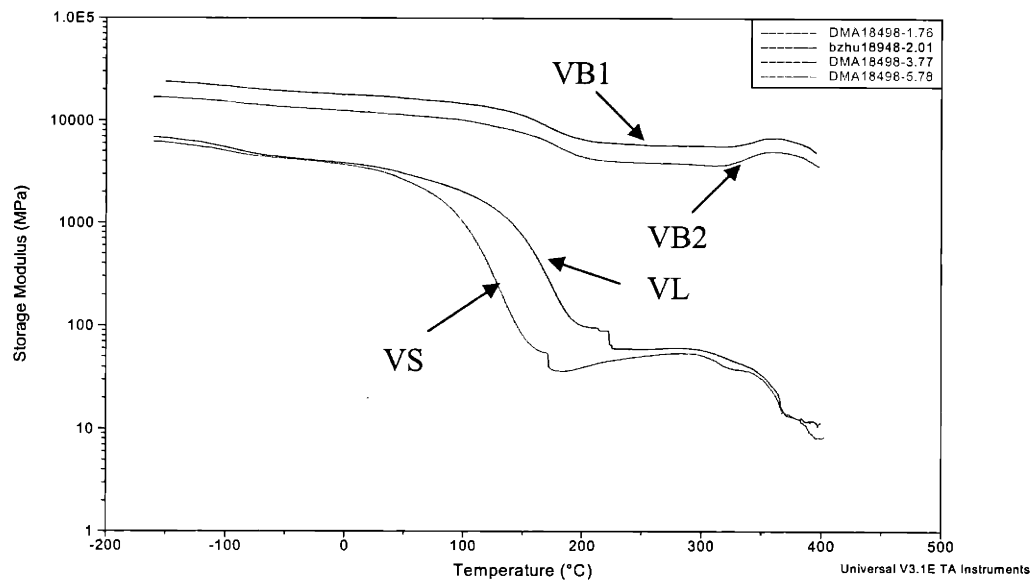


Figure 6-40 Storage modulus of vinyl ester resins VS and VL and hybrid composites VB1 and VB2.

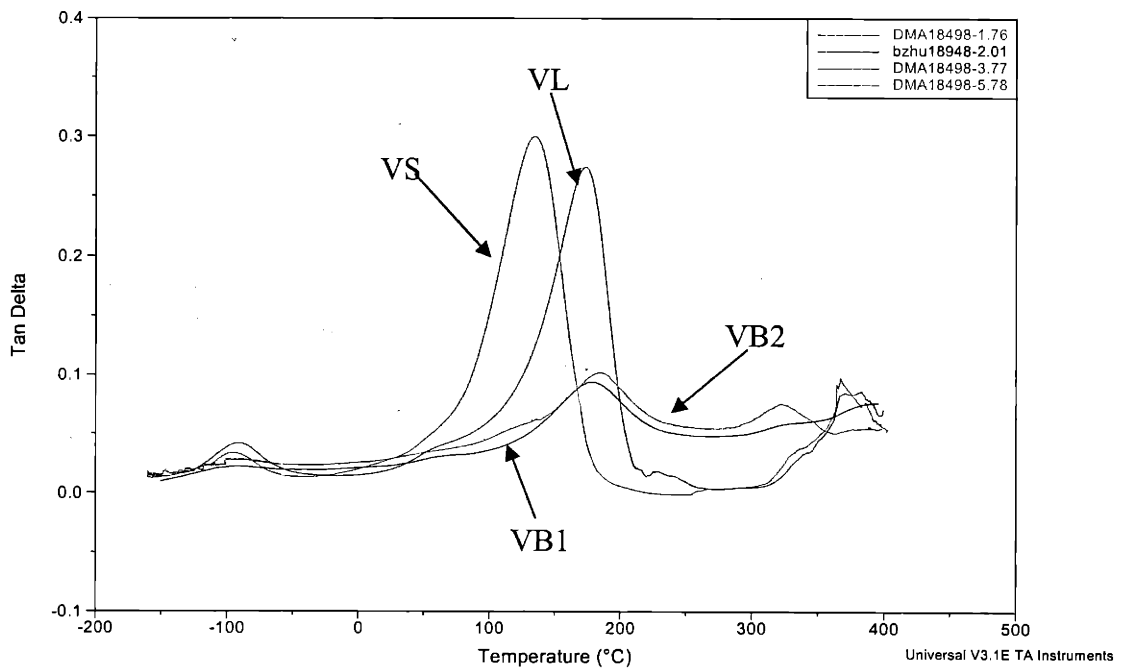


Figure 6-41 Tan δ of vinyl ester resins VS and VL and hybrid composites VB1 and VB2.

6.4 Summary

Fiberglass silicone composites of both addition cure (2672B) and condensation cure (3136T) resins have comparatively weak mechanical properties, which are attributed to the resin matrix mechanical properties. Their mechanical property retentions at elevated temperatures are weak, due to their relatively low glass transition temperatures. These results of the composites are consistent with the resin property results in Part I. On the other hand, the composites are thermally stable, having small weight loss suggested by both the thermal aging data and TGA analysis. The composites also have good moisture resistance, with the 3136T composite being slightly inferior to the 2672B one. Fire performance data from both the OSU test and the cone calorimetry test are not conclusive on the 3136T composite, but showing consistency of a low heat release rate in the 2672B composite.

Silicone resin hybrid composites are hybrid matrix composites made of addition cure resin 2672B skin and vinyl ester resin core by two curing procedures – sequential cure and co-cure. The co-cure process proves to be better in terms of mechanical properties. The hybrid composites generally have higher strength and modulus than the silicone resin 2672B composite due to the properties of the vinyl ester resin. At elevated temperatures, the hybrid composites have better property retention than the 2672B composite, partly due to the strong vinyl ester core and partly due to the protection offered by the 2672B skin.

The co-cured V/B 8/4 composite has the best strength and modulus among all composites, even higher than the vinyl ester composite, which is un-common according to the sandwich beam stress analysis. The V/B 8/4 co-cured composite also demonstrates unusual property retention compared to the vinyl ester composite. The short beam shear test results indicate that the shear strength of this hybrid composite is particularly higher. All these suggest the two resin matrices are compatible and the co-cure procedure is effective in forming a strong interface. DMA data of the composites suggest that in the co-cured hybrid composite, two peaks identifying the vinyl ester and the silicone move away from each other. This is explained by the hypothesis that styrene diffusion from the

vinyl ester resin results in its reaction with the vinyl group or Si-H group in the silicone. This reduces the crosslinking density of the silicone resin and thus lowers its T_g . Loss of styrene content as a lower T_g component in the vinyl ester resin also elevates its T_g . This explains for the property retention at elevated temperature of the hybrid composite. Inter-resin vinyl-vinyl and vinyl-Si-H reaction also explains for a strong interface between the vinyl ester and silicone.

In most cases, the moisture absorption measurements of hybrid composites is less than that in the vinyl ester composite at both 49.7% and 100% relative humidity levels suggest that the silicone resin skin in the hybrid composite (V/B 8/4 co-cure) serves as a barrier to moisture diffusion to some extent. At 49.7% relative humidity, the effect is not as obvious as observed at 100% R.H. level. At 100% R.H. level, the hybrid composite shows a linear increase in the moisture content with time^{1/2}. The difference between samples of sealed and non-sealed edges is not great.

Thermal aging has been performed at 100, 135, 170 and 205°C for 10, 100 and 1000 hours. In terms of weight loss, the V/B 8/4 co-cured hybrid composite experiences lower weight loss compared to vinyl ester composite under all circumstances. At 205°C, weight loss of all composites increases dramatically. However, data of the hybrid composite are closer to those of the B composite, suggesting an effectiveness of silicone skin in improving the thermal resistance of the hybrid. The TGA data also prove this: with 5% weight loss temperatures of vinyl ester composite and hybrid composite being 400°C and 425°C, respectively. The flexural properties after thermal aging are more difficult to interpret than the weight loss data, suggesting both physical and chemical changes can occur during the aging process. At shorter time periods, the aging process affects the properties of the vinyl ester composite more than those of the 2672B.

Fire performance results of both OSU and cone calorimetry tests prove that silicone resins are fire resistant than the organic vinyl ester resin. The data also demonstrate that the heat release rate of the hybrid composite is in between that of the silicone composite and that of the vinyl ester composite. The improved fire performance

in hybrid composite suggests that the silicone resin skin serves as a good heat barrier to fire damage on the vinyl ester core.

References:

1. Rosen SL. *Fundamental principles of polymeric materials*. New York, NY: John Wiley and Sons, Inc., 1993.

CHAPTER 7. Conclusions

The mechanical properties of two Dow Corning silicone resins are studied, in particular the effect of temperature. The addition cure resins crosslinked with different crosslinkers all show a big decrease in strength and modulus with temperature. The extent of these changes depends on the crosslinking system, with hexamethyltrisiloxane showing the greatest increase at low temperatures. The fracture toughness data all demonstrate peaks with temperature changes. The peaking temperatures are often at $62\pm 4^\circ\text{C}$ below the T_g . This can be explained by the competing effects between contributions from yielding deformation and rigidity to toughness. At certain temperature below T_g , movements of molecules are limited in some way but the temperature is not down to the range of creating a frozen network. This offers the maximum benefit from both rigidity and the network mobility. At very low temperatures, the effect of molecular mobility is completely lost and this leads to a low toughness. On the other hand, at high temperatures, the mobility of the network is not a problem, but the rigidity of the resin is greatly reduced, thus also a low toughness value is observed. For the hexamethyltrisiloxane crosslinked resin (D100), the peaking temperature occurs at around 100°C below T_g . This can be explained by the flexibility of the network caused by the D crosslinker, thus a lower temperature is needed to reach the optimal rigidity and yielding balance. The rate effect on B100 system is not very conclusive. However, in general, the effect of temperature on fracture toughness is more obvious than that of the testing rate.

Temperature effect on the condensation cure resin 3136 is different, showing a much less dramatic change in strength, modulus and toughness with temperature. The effect of temperature on toughened 3136T is more distinguished than that on the untoughened 3136 due to the toughening effect of short PDMS rubber chains, which provides mobility to the network.

On the basis of understanding the temperature effect on mechanical behavior of silicone resins, the tough systems of B100 (2672B) and 3136T are studied for their fiberglass composite applications.

Properties of silicone resin composites are observed to be much dependent upon the resin matrix characteristics. Both silicone resin composites (2672B and 3136T) generally have good thermal stability, moisture resistance and fire performances but comparatively weak mechanical properties. Their property retention at elevated temperatures is low, which is mainly explained by the low glass transition temperatures for silicone resins. This corresponds well with the results of the flexural property change with temperature for the matrix resins.

An organic resin – vinyl ester resin – is used to explore the idea of engineering hybrid composites with 2672B silicone skin and vinyl ester core. The purpose of the silicone skin is to ensure thermal stability, fire performance, and moisture resistance of the composites. The purpose of the core is to provide strength, rigidity, and property retention at high temperatures. The process of fabricating the hybrid composites proves to be successful, with the co-cured procedure demonstrating better mechanical results. The hybrid composites generally turn out to have strong mechanical properties and good property retention at elevated temperatures, with improved thermal stability, moisture resistance, and fire performance. The co-cured V/B 8/4 composites demonstrate exceptionally good mechanical properties and property retention at elevated temperatures, which can be explained by the interface compatibility and chemical reactions between the two resins. Silicone resins are successfully used as composite matrix materials to achieve better environmental properties, which are the major advantages of silicone resins.

CHAPTER 8. Future work

Future work of the silicone resin composites can continue with the proposed work below.

- (1) Continue the vinyl ester/silicone hybrid work by altering the core/skin structure, the interface chemistry, and the curing schedule to obtain the best hybrid composites in terms of properties and processing efficiency.
- (2) Continue studying silicone resins composites by using different fiber reinforcements, or other forms of reinforcements. Both graphite and quartz can be used for high temperature applications and may be selected as the reinforcements for the silicone resin composites.
- (3) Study the hybrid composites using the same addition cure silicone resin as the skin but changing the core matrix resin. The chosen matrix resin has to have the right chemistry to be compatible with the silicone resin. Epoxy resin has been tried in this research work but its overall properties, both mechanical and environmental, are not as attractive as the vinyl ester /silicone hybrid composite.
- (4) Try to use the condensation cure resin 3136T as the skin material to make hybrid composites. Some work has been done in this area with the selected core matrix resins as epoxy and phenolic. Major difficulty lies in the poor interface structure between the two resins, mostly due to delamination and void formation at the interface from the water byproduct during cure.

Future work of the silicone resin can explore its thin film properties, which have not been studied extensively. Research work can focus on producing good thin film from

silicone resins and characterize their properties. One potential area is to find how the mechanical behavior of thin silicone resin film differs from bulk material, in terms of both toughness and stress-strain behavior. If a silicone thin film becomes ductile and resistant to cracking, the laminate structure of these films might result in good cracking resistance.

The abovementioned possible research directions should always aim at commercializing the silicone resin applications in real-life situations, which is the ultimate goal of all the research work.

Appendix A. Load-displacement curves and results of fracture toughness tests of silicone resins

Figure A - 1 to Figure A - 6	Addition cure silicone resin B100
Figure A - 7 to Figure A - 12	Addition cure silicone resin D100
Figure A - 13 to Figure A - 18	Addition cure silicone resin DP73
Figure A - 19 to Figure A - 24	Addition cure silicone resin DP55
Figure A - 25 to Figure A - 30	Addition cure silicone resin DP37
Figure A - 31 to Figure A - 36	Addition cure silicone resin P100
Figure A - 37 to Figure A - 42	Condensation cure silicone resin 3136T
Figure A - 43 to Figure A - 49	Condensation cure silicone resin 3136U

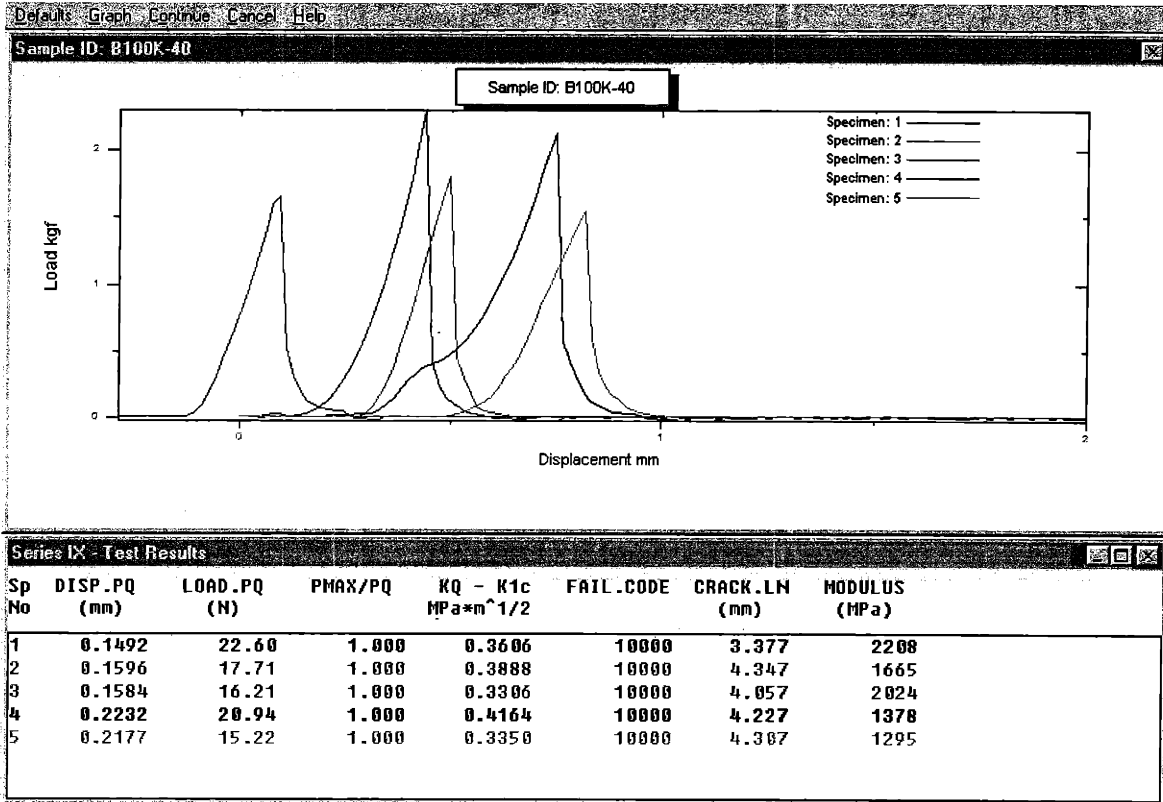


Figure A - 1 Fracture toughness test results of B100 at -40°C.

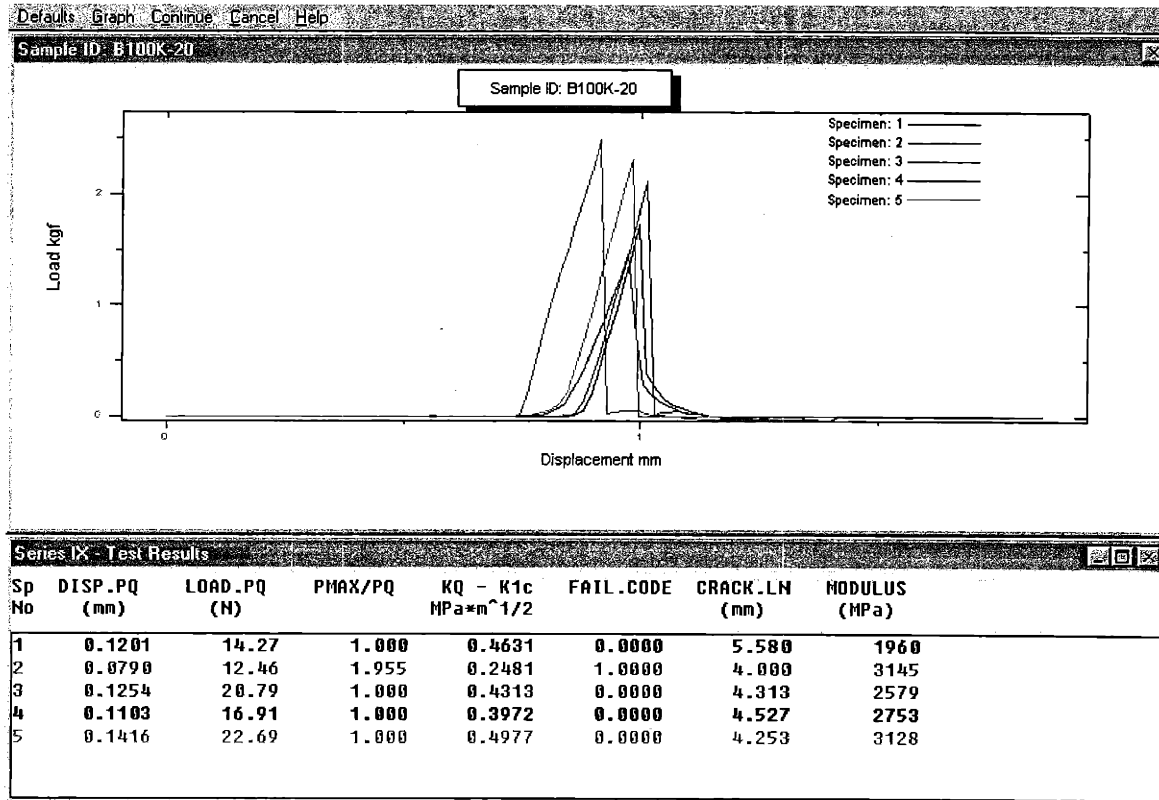


Figure A - 2 Fracture toughness test results of B100 at -20°C.

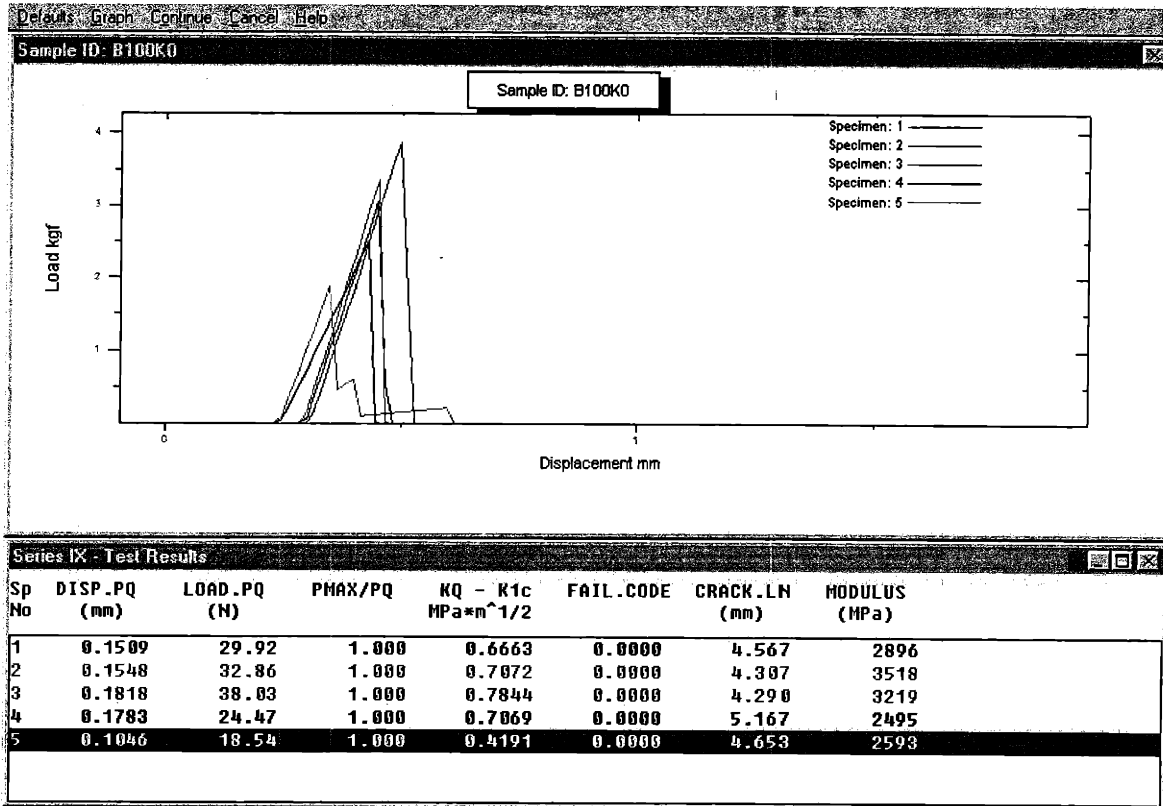


Figure A - 3 Fracture toughness test results of B100 at 0°C.

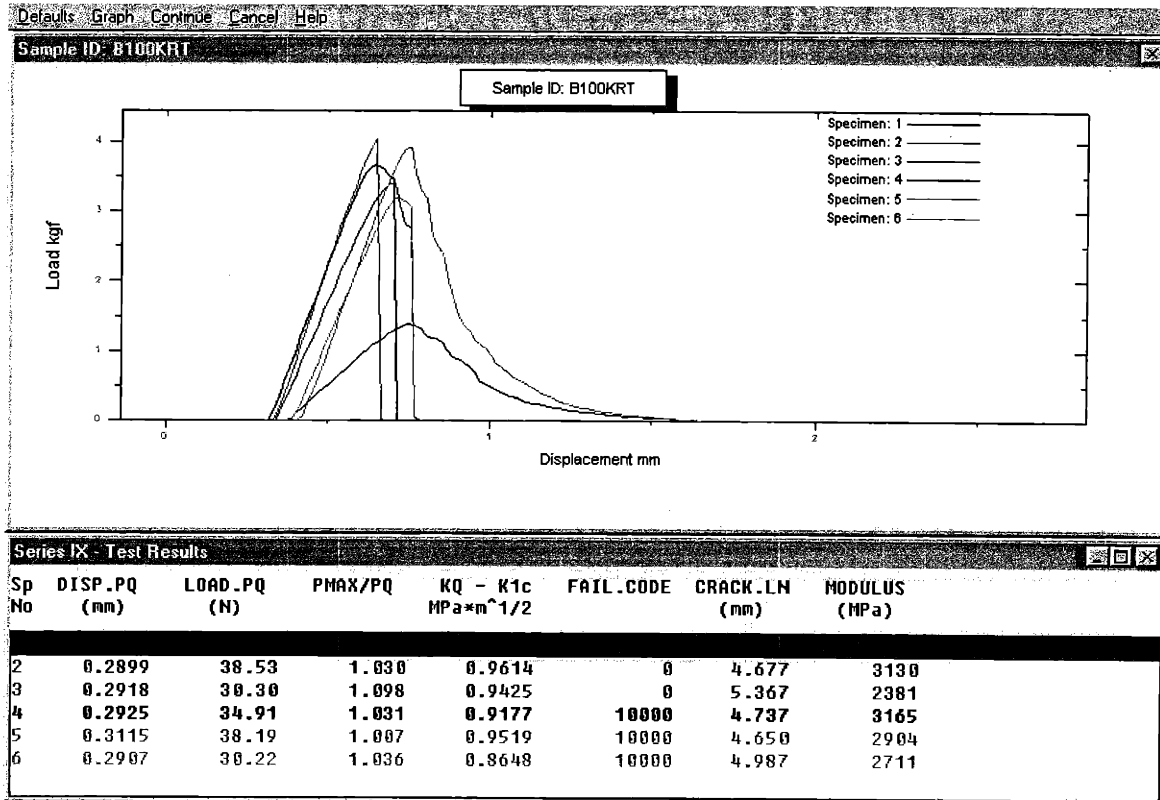


Figure A - 4 Fracture toughness test results of B100 at 20°C.

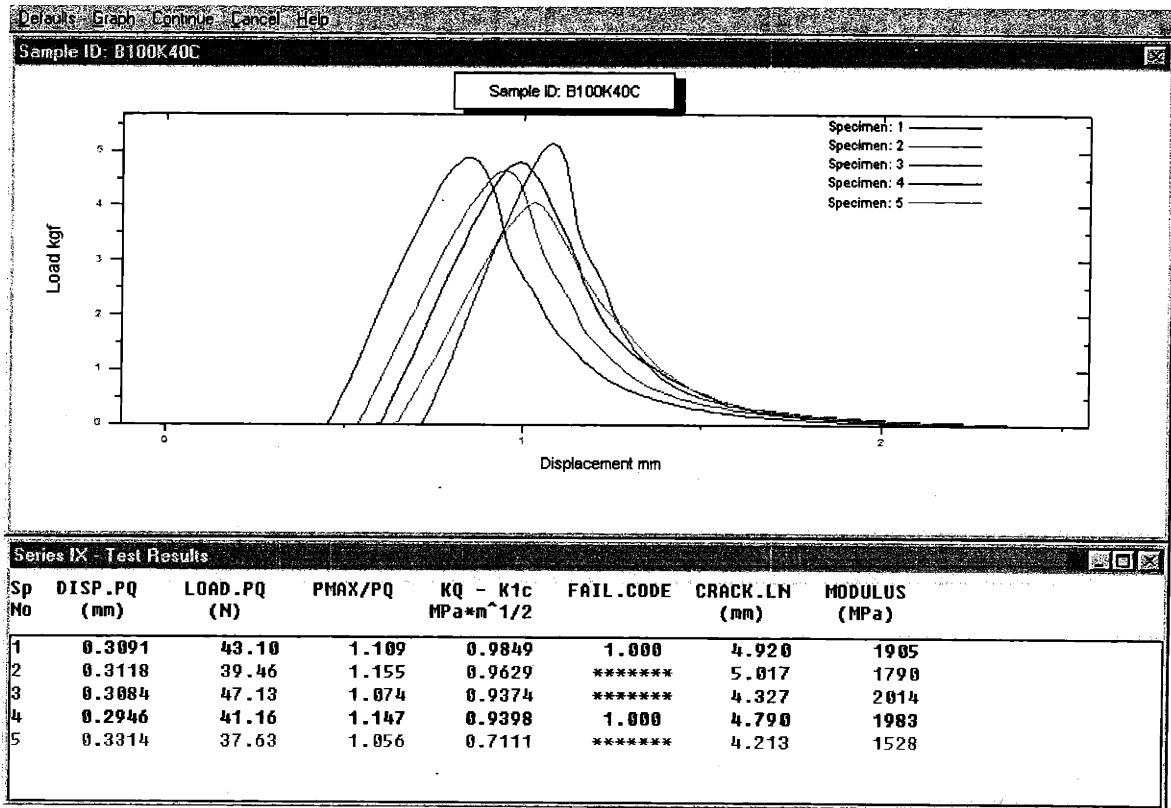


Figure A - 5 Fracture toughness test results of B100 at 40°C.

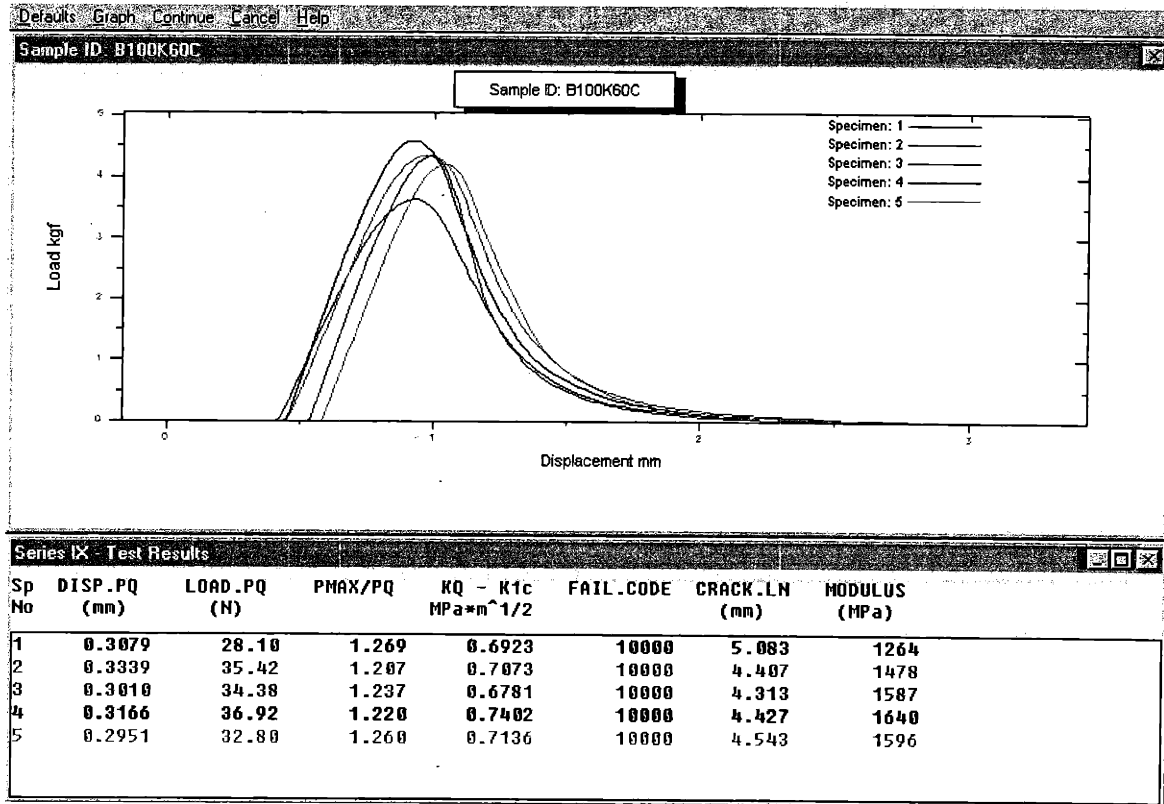


Figure A - 6 Fracture toughness test results of B100 at 60°C.

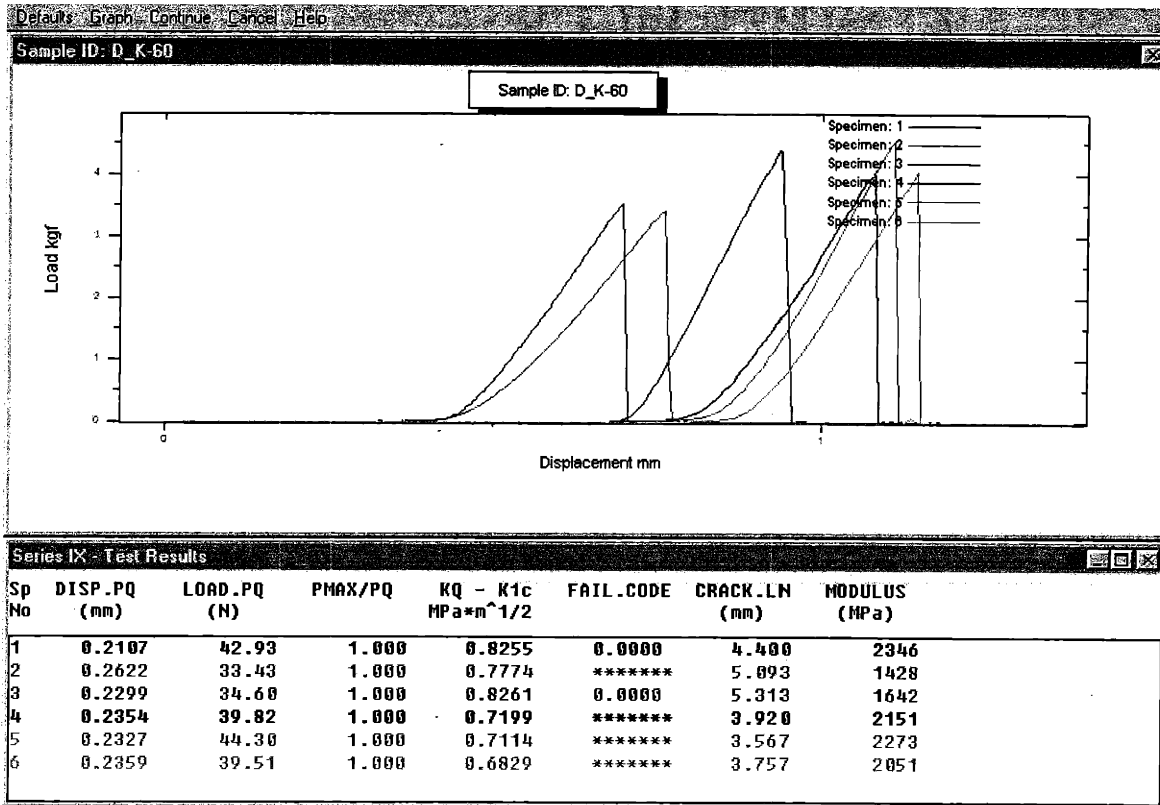


Figure A - 7 Fracture toughness test results of D100 at -60°C.

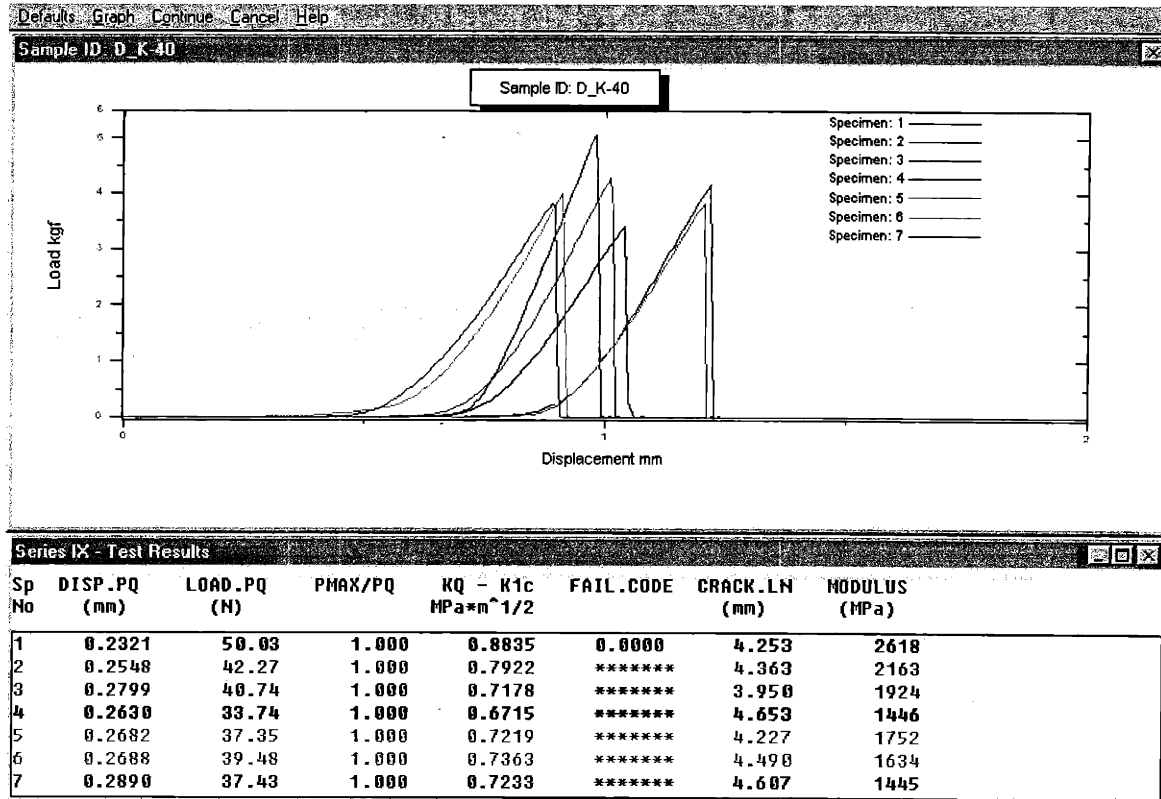


Figure A - 8 Fracture toughness test results of D100 at -40°C.

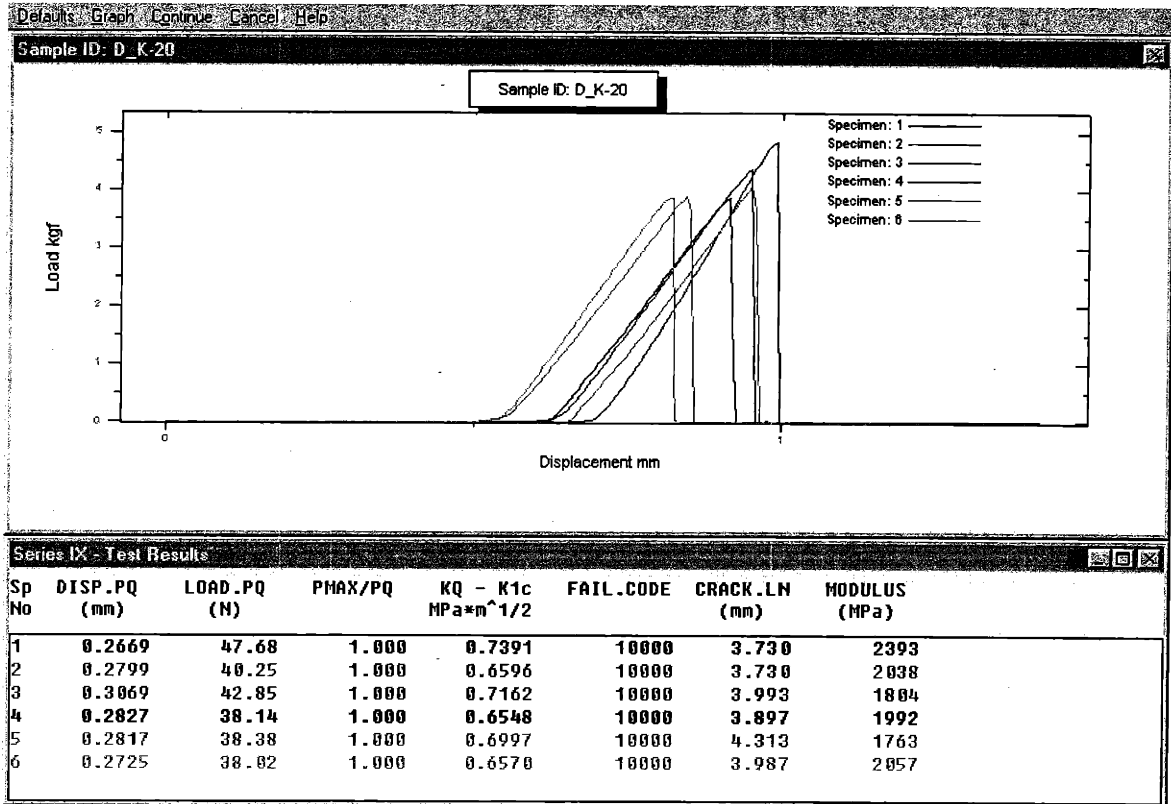


Figure A - 9 Fracture toughness test results of D100 at -20°C.

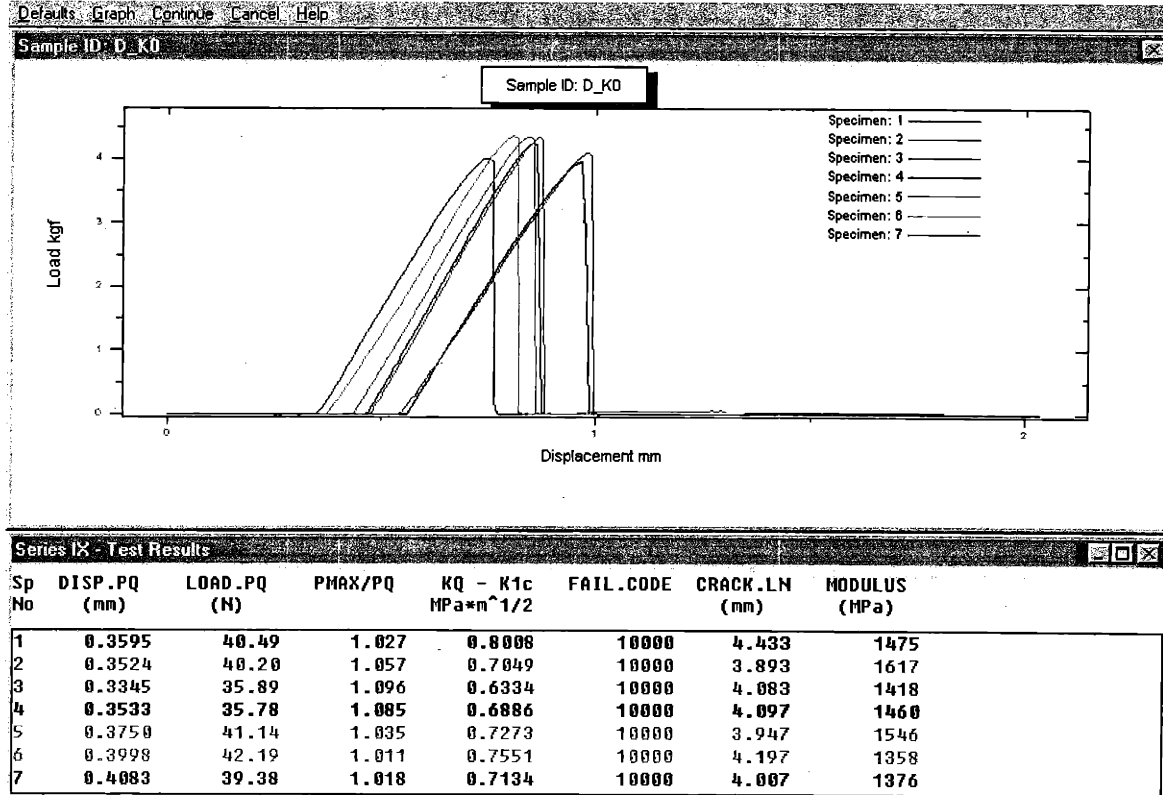


Figure A - 10 Fracture toughness test results of D100 at 0°C.

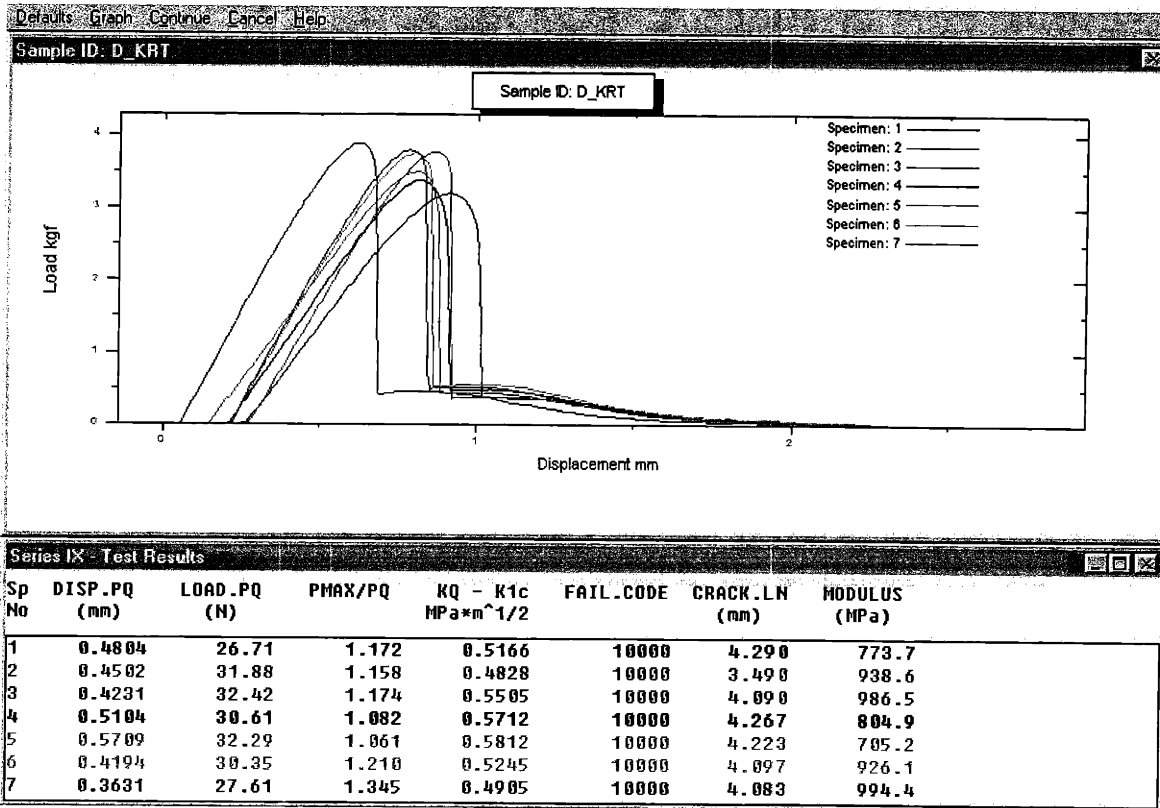


Figure A - 11 Fracture toughness test results of D100 at 20°C.

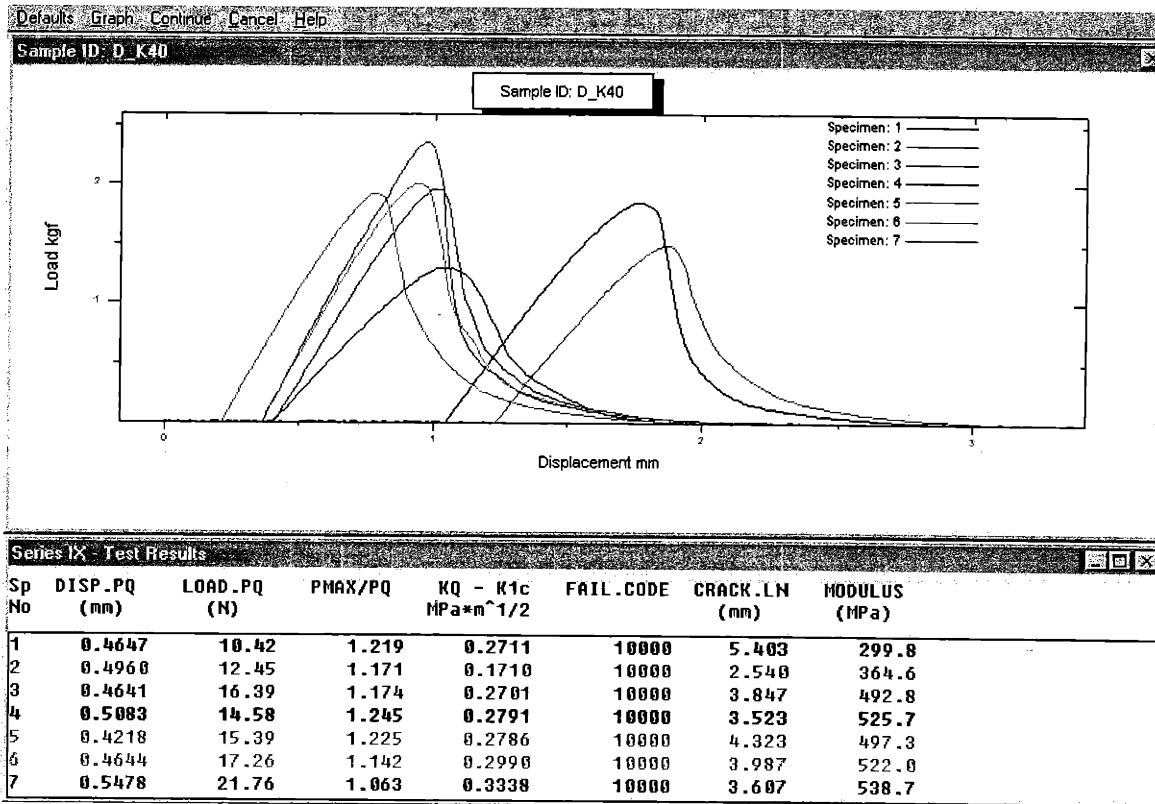


Figure A - 12 Fracture toughness test results of D100 at 40°C.

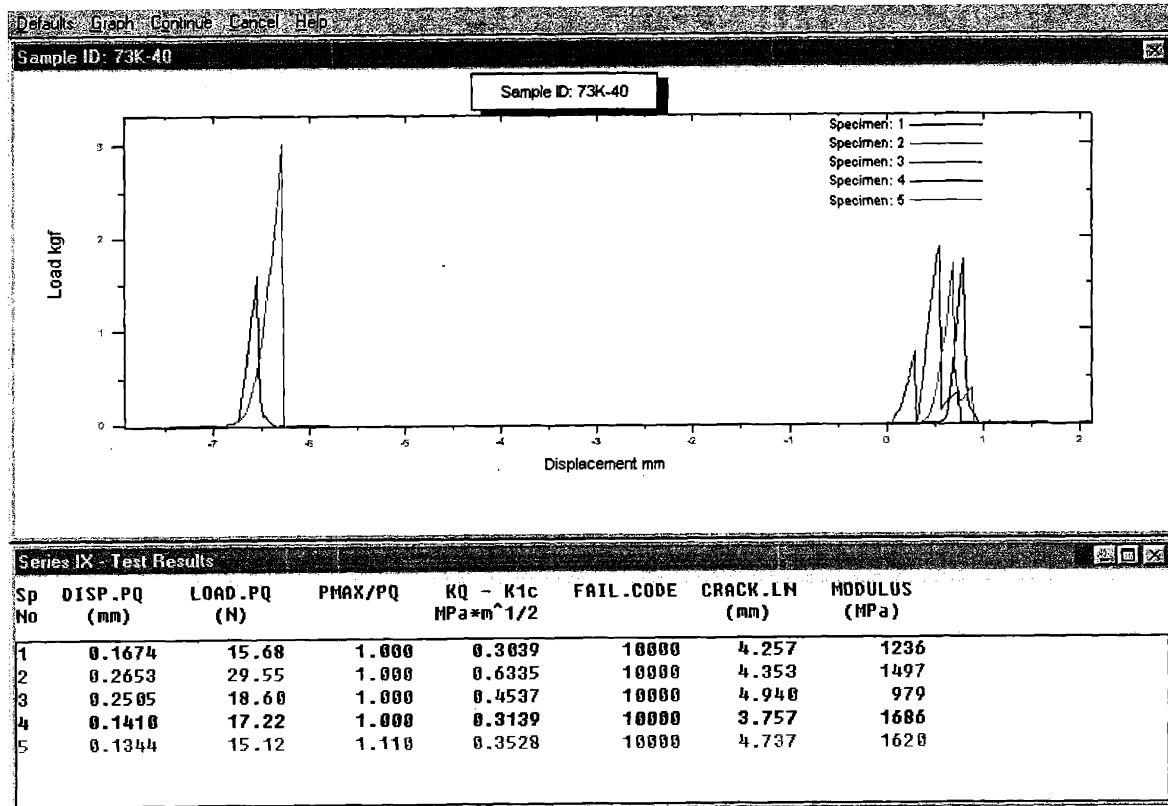


Figure A - 13 Fracture toughness test results of DP73 at -40°C.

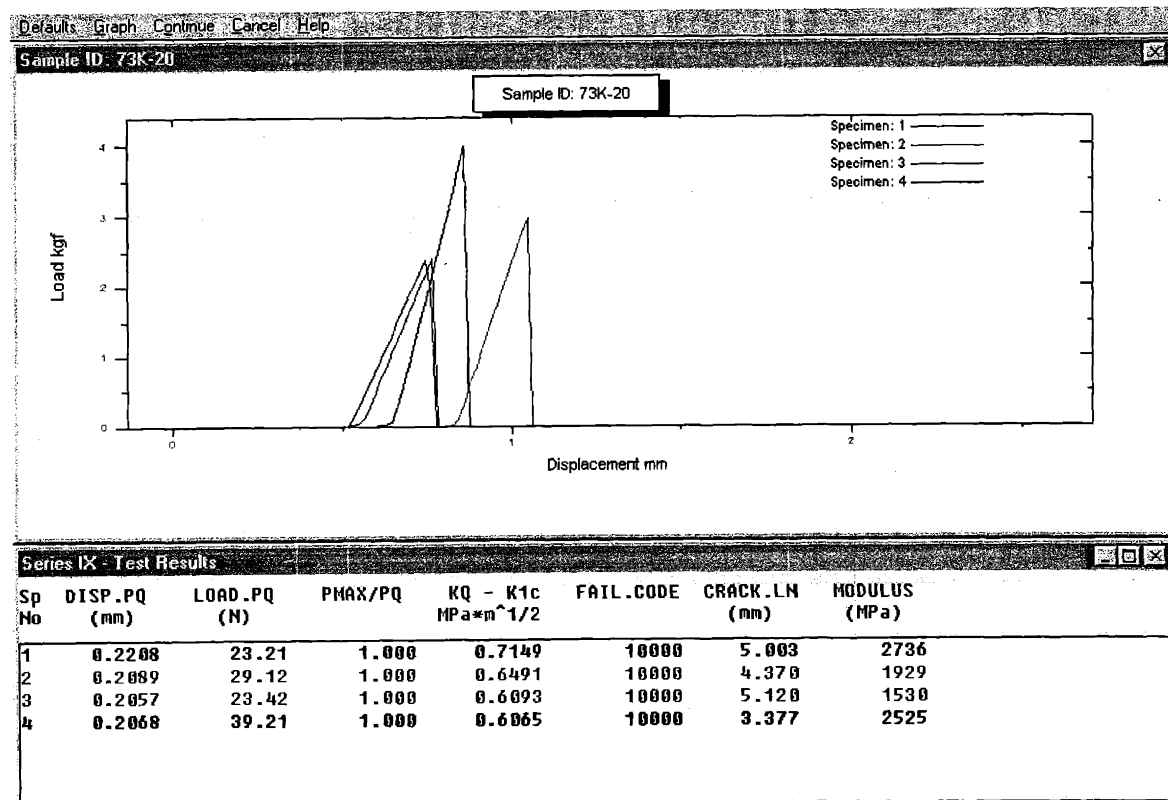


Figure A - 14 Fracture toughness test results of DP73 at -20°C.

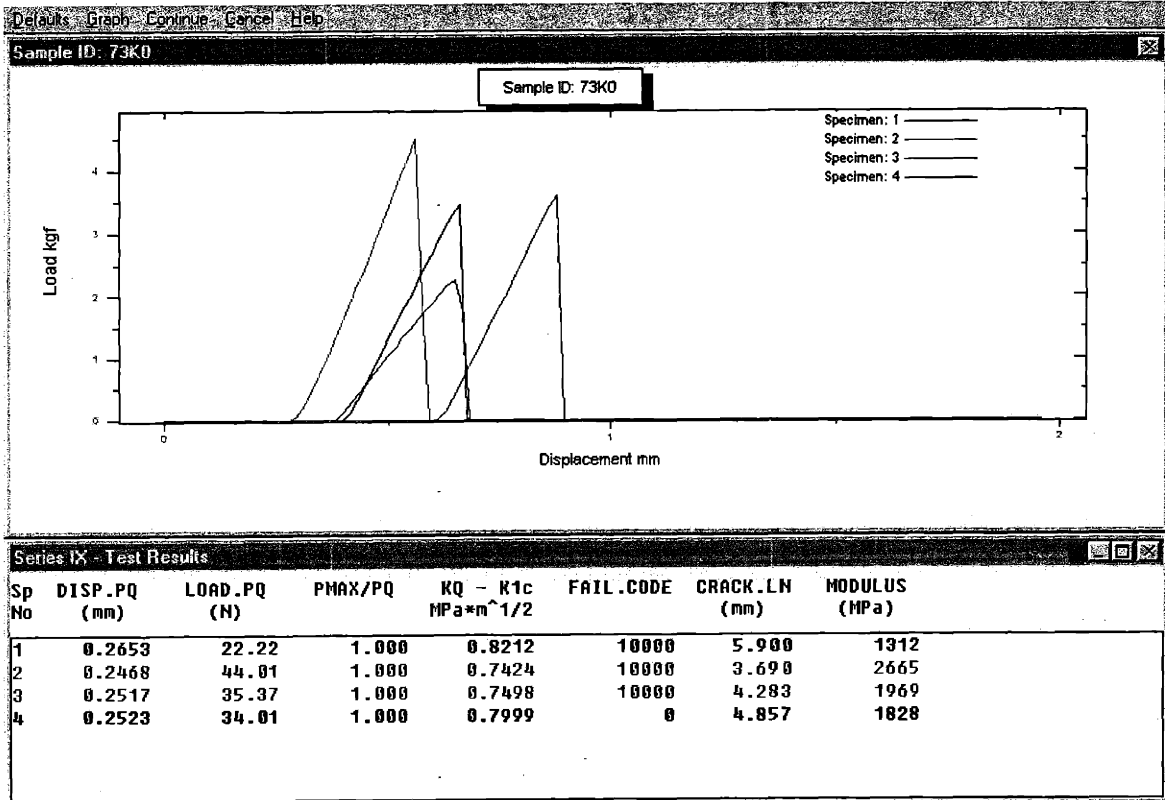


Figure A - 15 Fracture toughness test results of DP73 at 0°C.

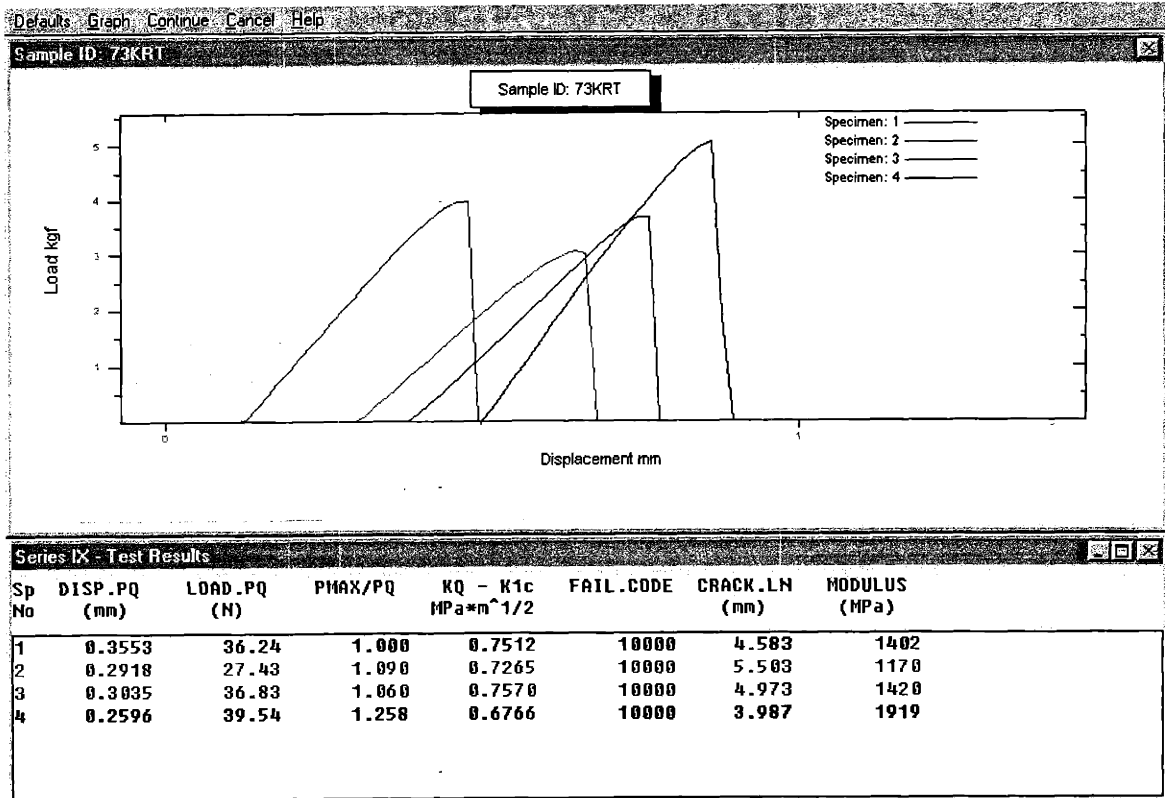


Figure A - 16 Fracture toughness test results of DP73 at 20°C.

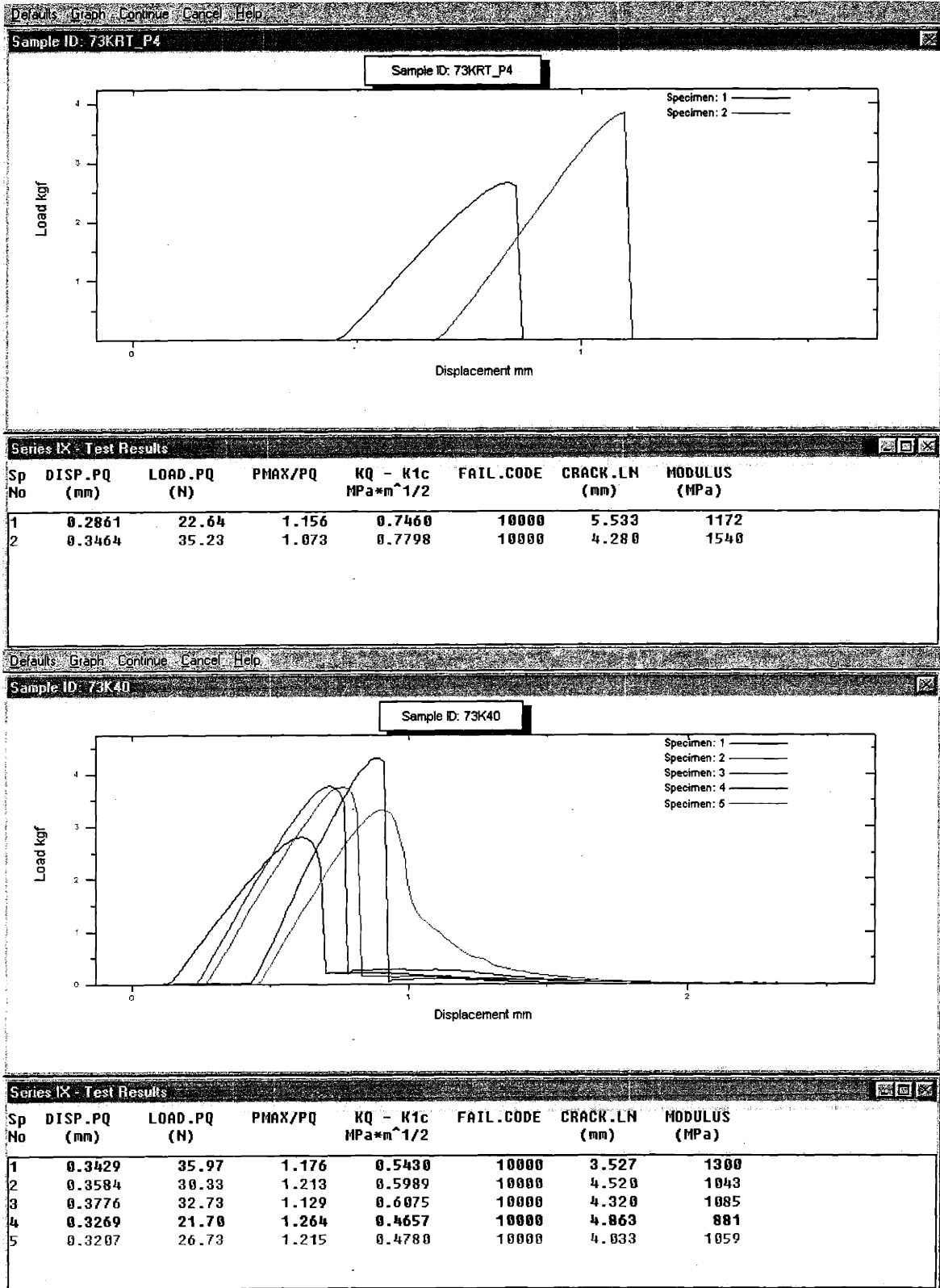


Figure A - 17 Fracture toughness test results of DP73 at 40°C.

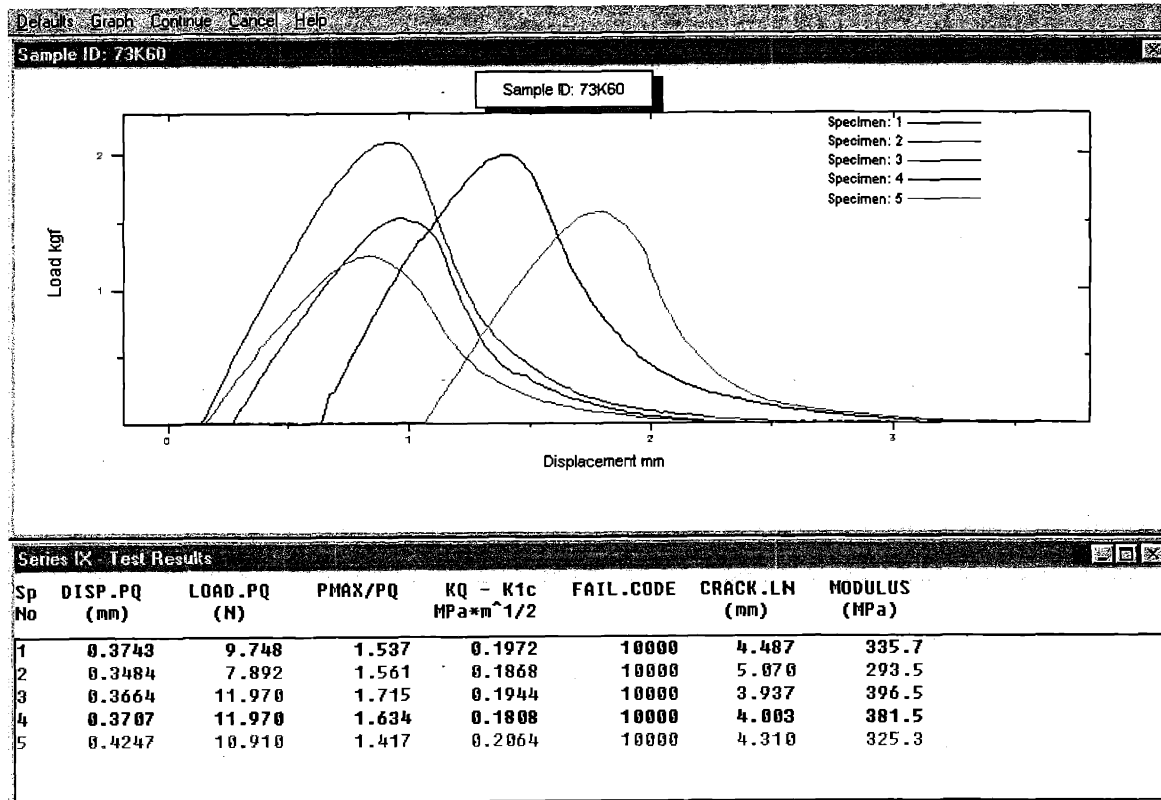


Figure A - 18 Fracture toughness test results of DP73 at 60°C.

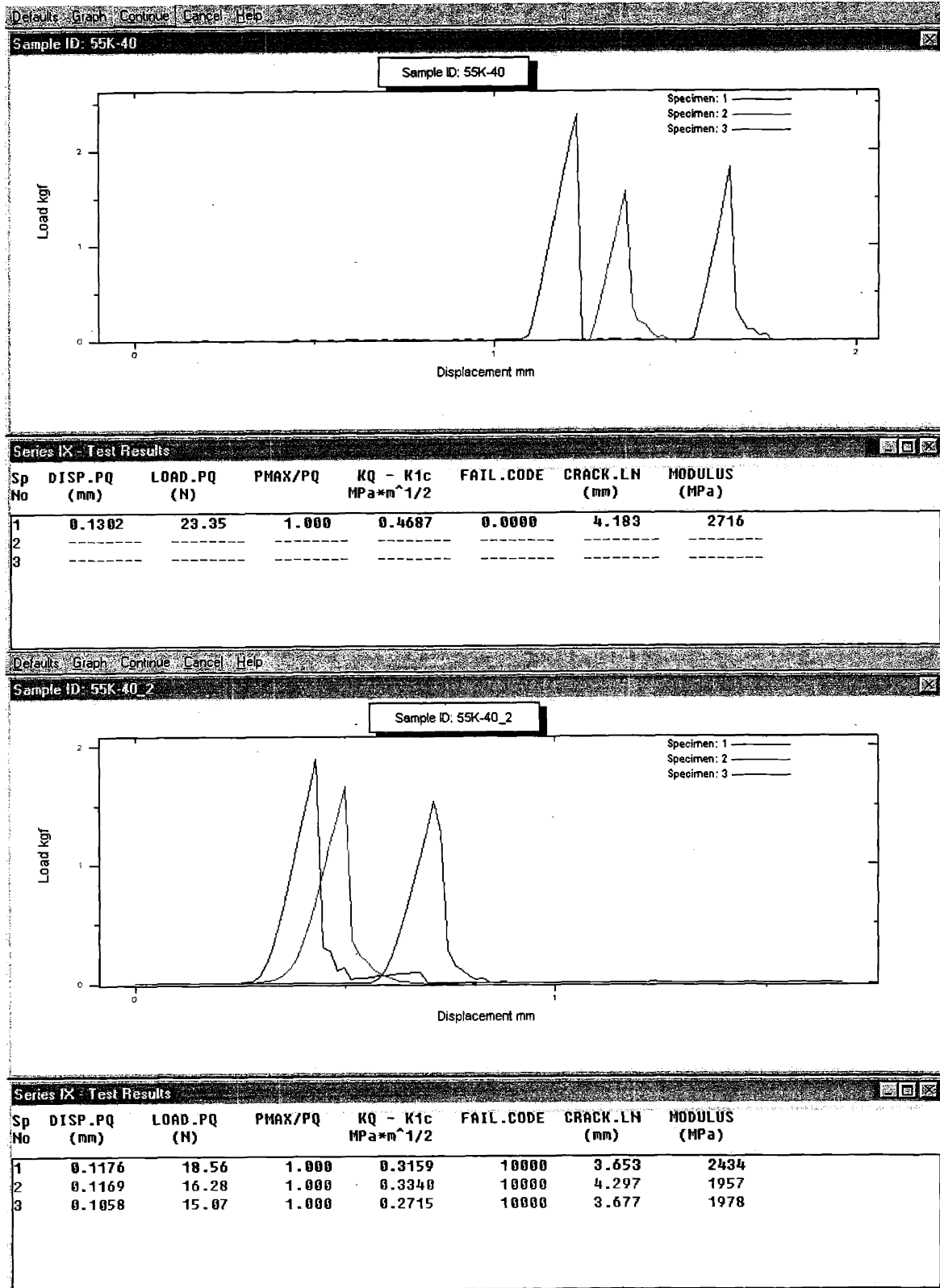


Figure A - 19 Fracture toughness test results of DP55 at -40°C.

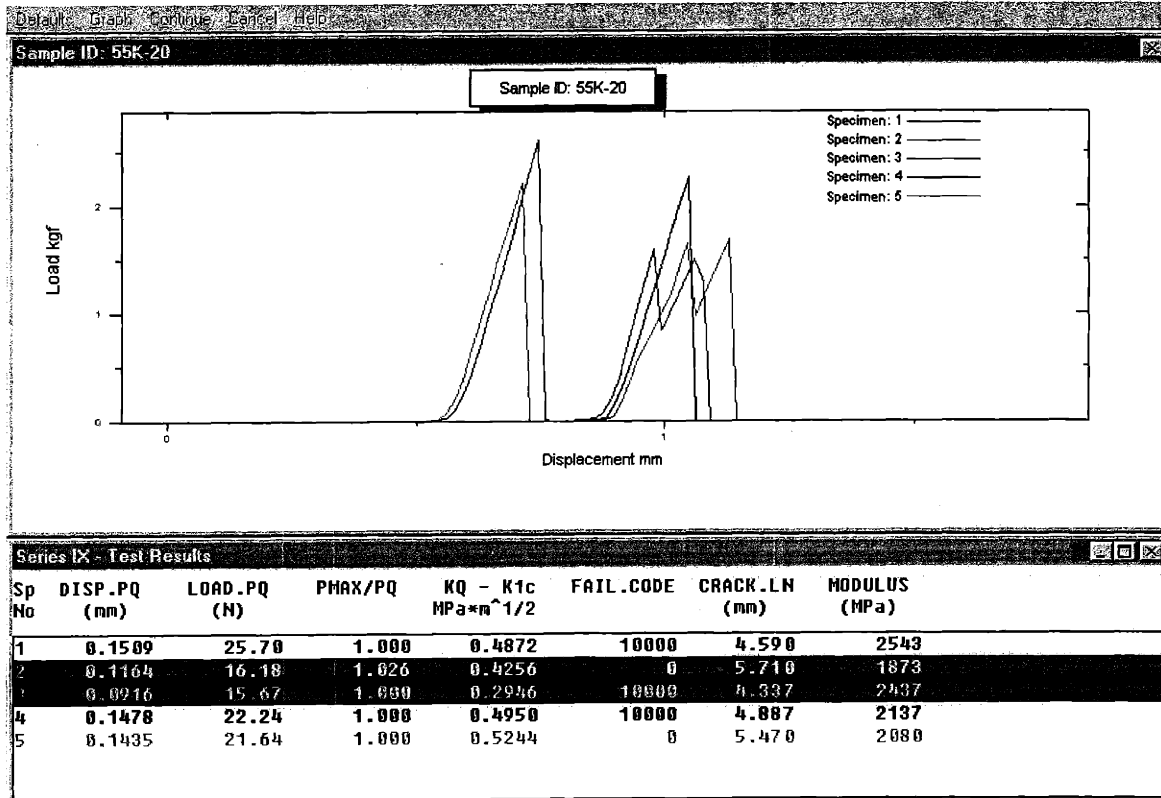


Figure A - 20 Fracture toughness test results of DP55 at -20°C.

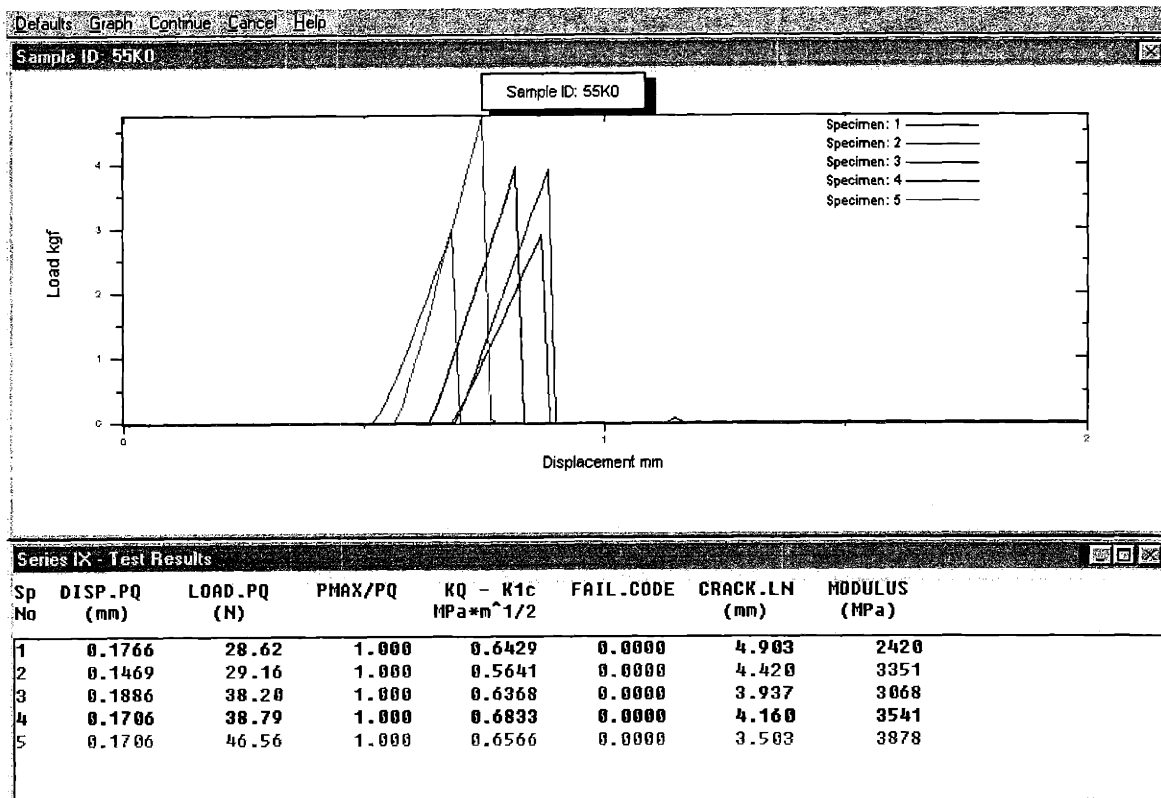


Figure A - 21 Fracture toughness test results of DP55 at 0°C.

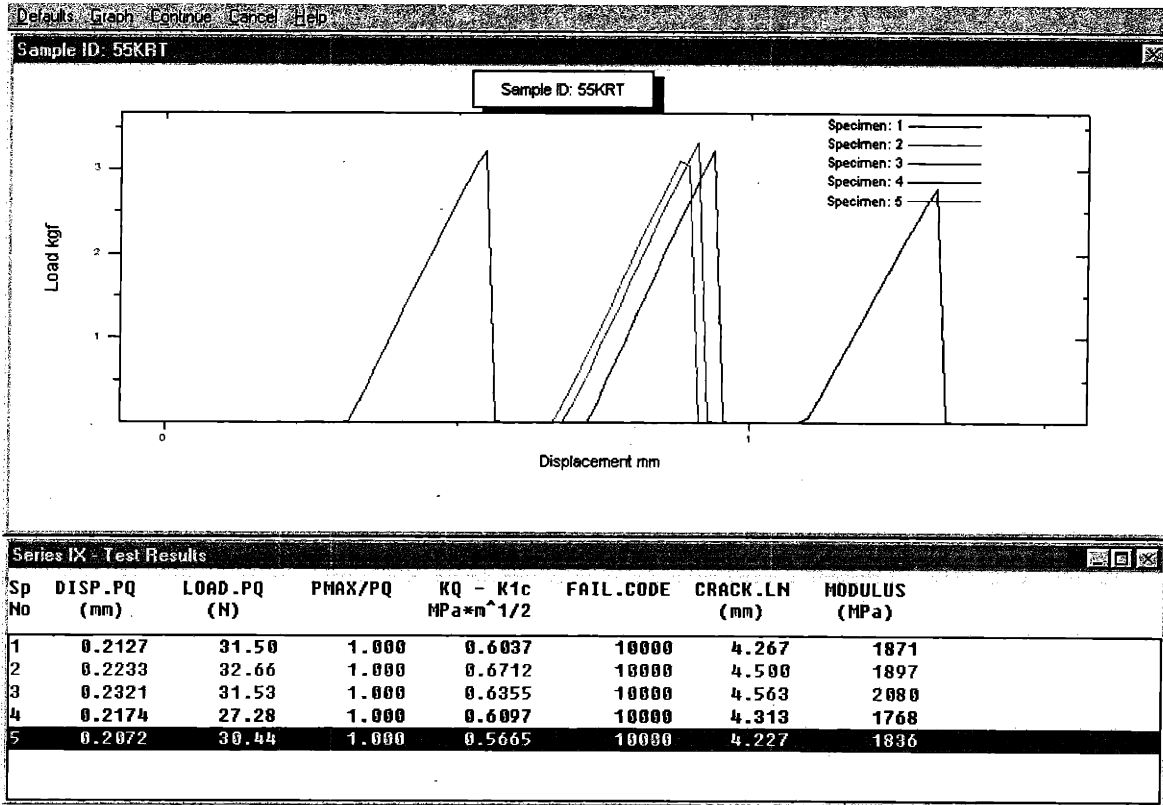
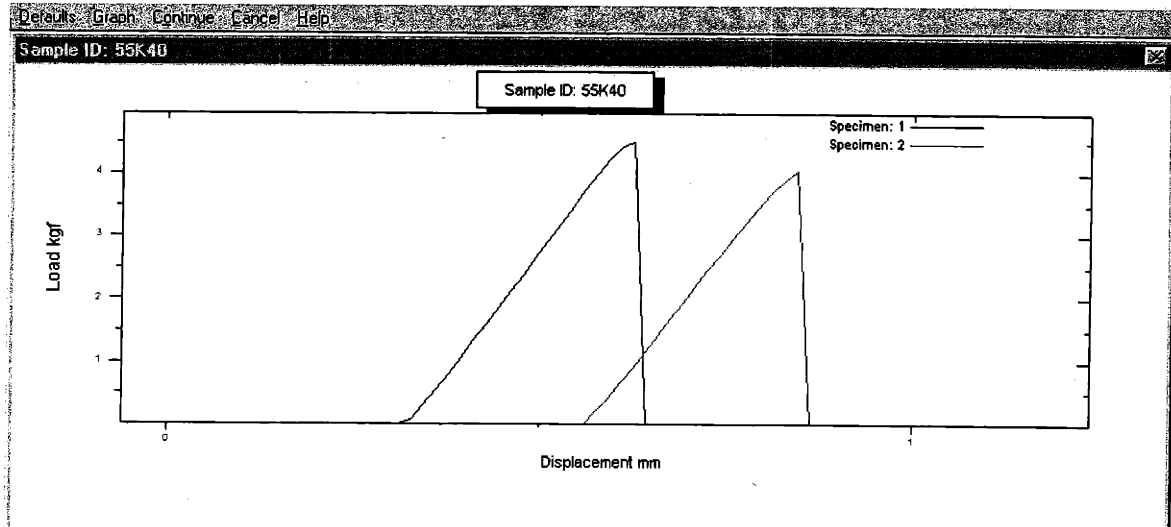
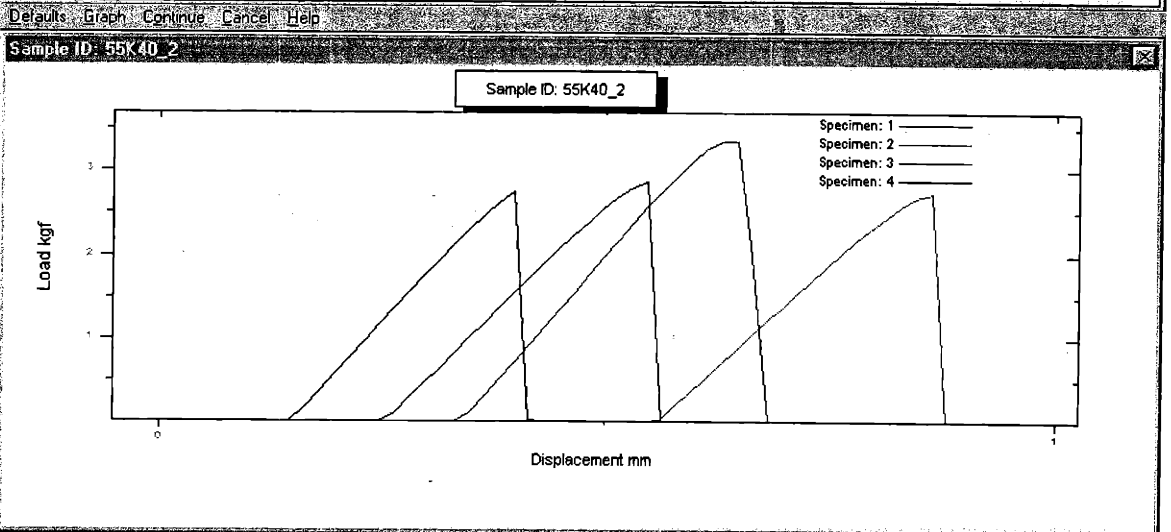


Figure A - 22 Fracture toughness test results of DP55 at 20°C.



Series IX - Test Results

Sp No	DISP.PQ (mm)	LOAD.PQ (N)	P _{MAX} /P _Q	K _Q - K _{1c} (MPa*m ^{1/2})	FAIL.CODE	CRACK.LN (mm)	MODULUS (MPa)
1	0.2953	44.27	1.000	0.6853	10000	3.823	2254
2	0.2729	39.65	1.000	0.6840	10000	3.797	2577



Series IX - Test Results

Sp No	DISP.PQ (mm)	LOAD.PQ (N)	P _{MAX} /P _Q	K _Q - K _{1c} (MPa*m ^{1/2})	FAIL.CODE	CRACK.LN (mm)	MODULUS (MPa)
1	0.2758	27.40	1.025	0.6996	10000	5.523	1505
2	0.2670	25.17	1.064	0.6088	10000	5.097	1404
3	0.2710	31.92	1.030	0.6514	10000	4.720	1846
4	0.2143	24.24	1.111	0.5018	10000	4.917	1822

Figure A - 23 Fracture toughness test results of DP55 at 40°C.

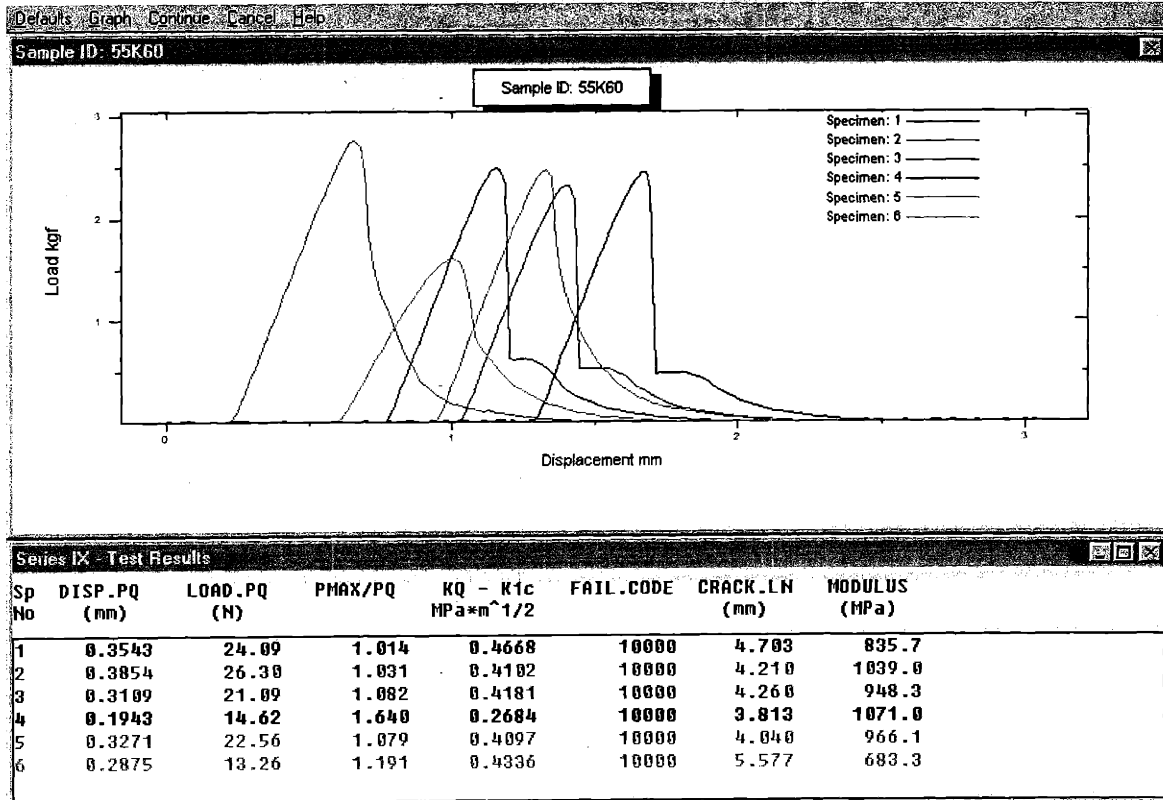
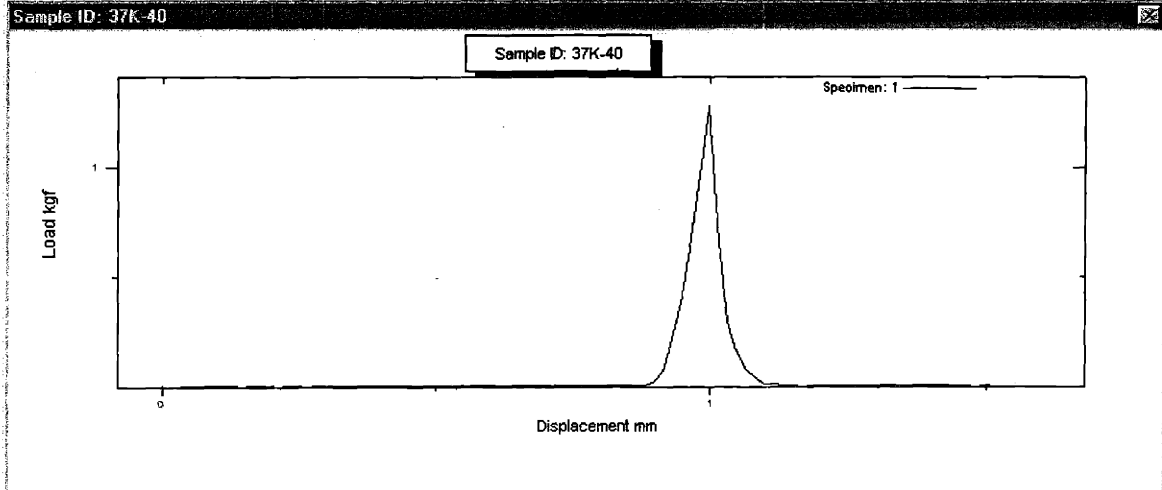


Figure A - 24 Fracture toughness test results of DP55 at 60°C.

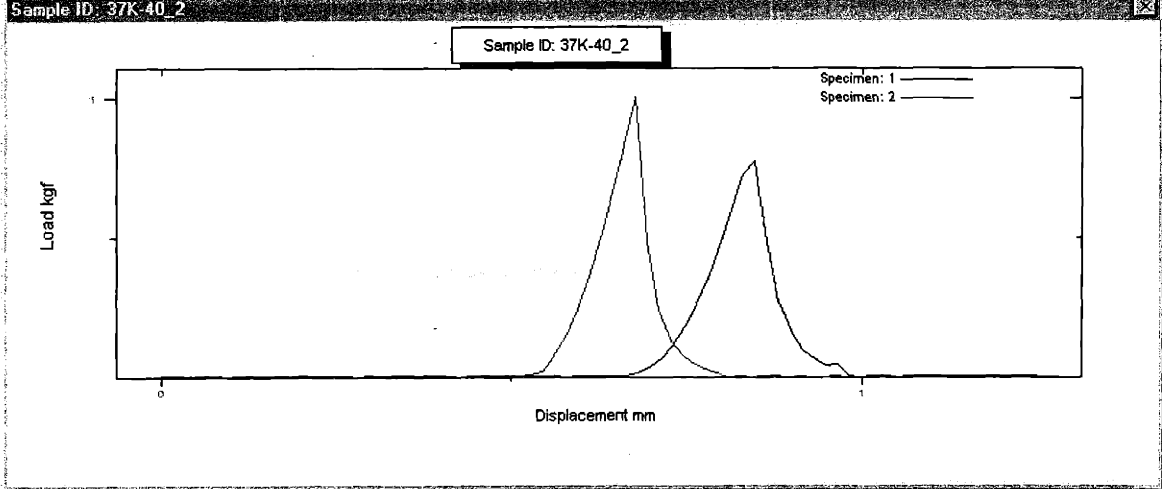
Defaults Graph Continue Cancel Help



Series IX - Test Results

Sp No	DISP.PQ (mm)	LOAD.PQ (N)	P _{MAX} /P _Q	K _Q - K _{1c} (MPa*m ^{1/2})	FAIL.CODE	CRACK.LN (mm)	MODULUS (MPa)
1	-----	-----	-----	-----	-----	-----	-----

Defaults Graph Continue Cancel Help



Series IX - Test Results

Sp No	DISP.PQ (mm)	LOAD.PQ (N)	P _{MAX} /P _Q	K _Q - K _{1c} (MPa*m ^{1/2})	FAIL.CODE	CRACK.LN (mm)	MODULUS (MPa)
1	0.1092	7.617	1.000	0.1451	10000	4.083	1037
2	-----	-----	-----	-----	-----	-----	-----

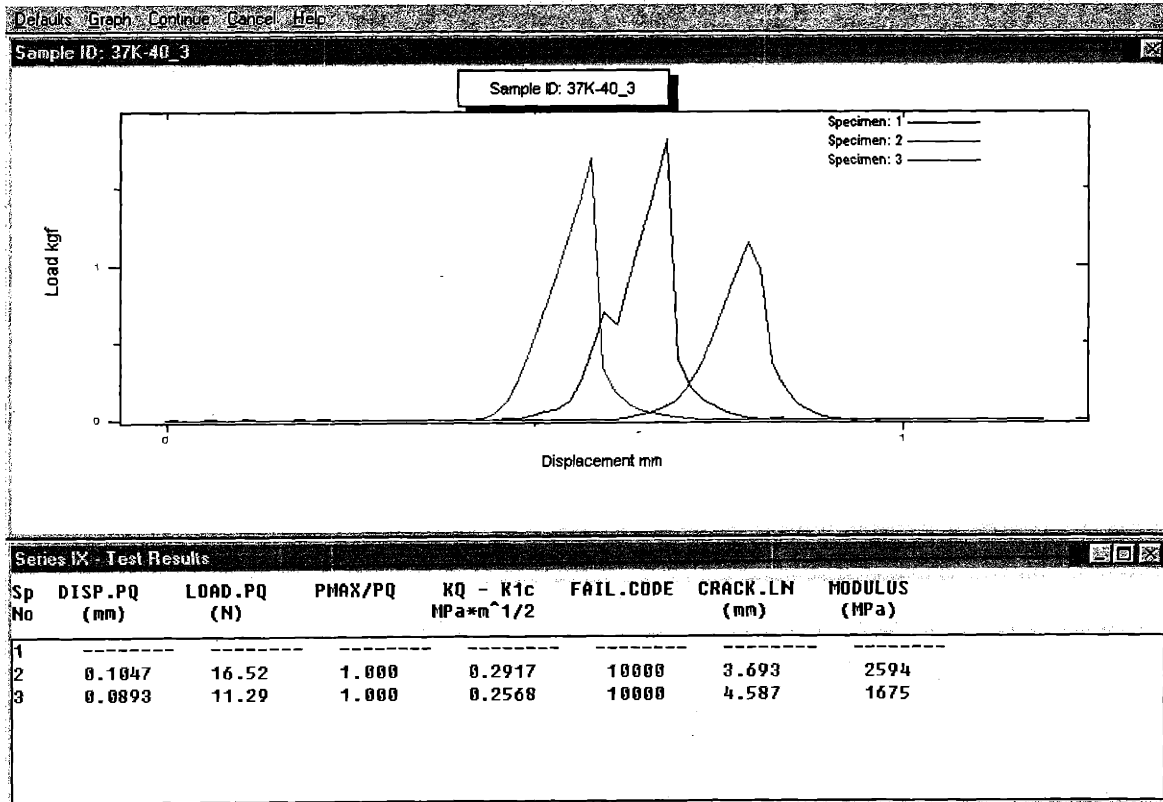


Figure A - 25 Fracture toughness test results of DP37 at -40°C.

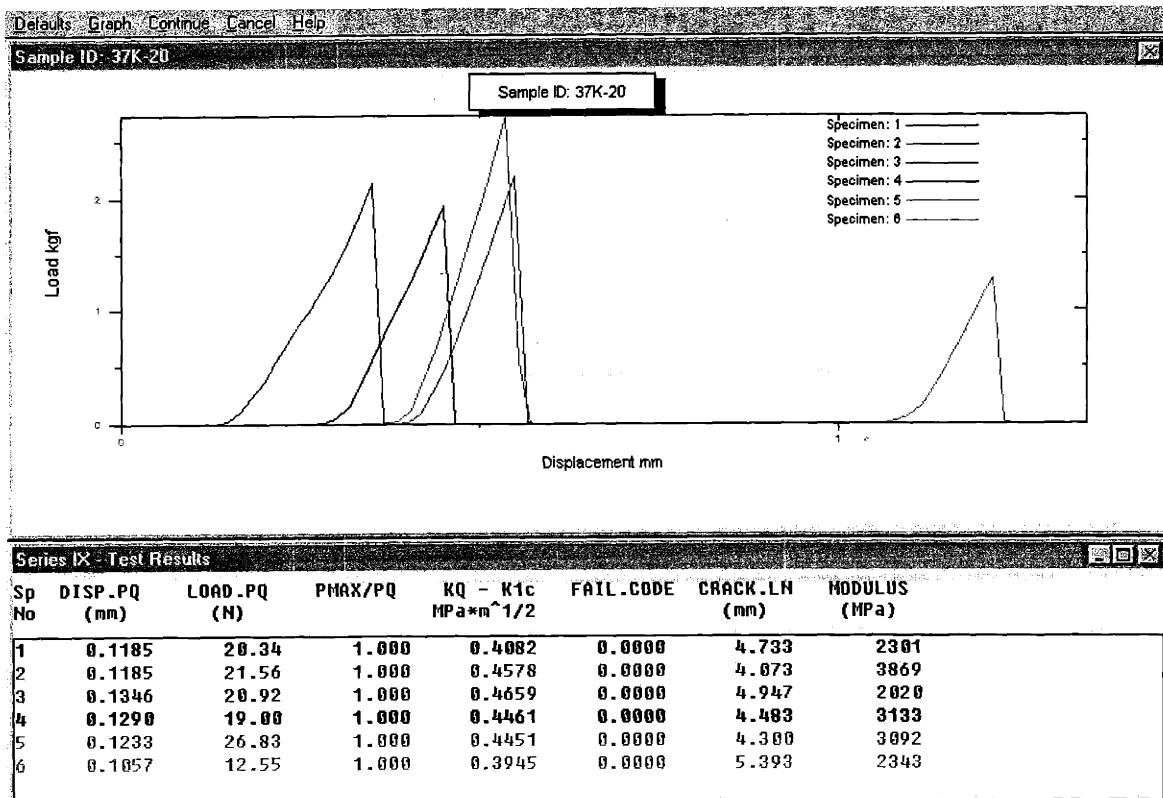


Figure A - 26 Fracture toughness test results of DP37 at -20°C.

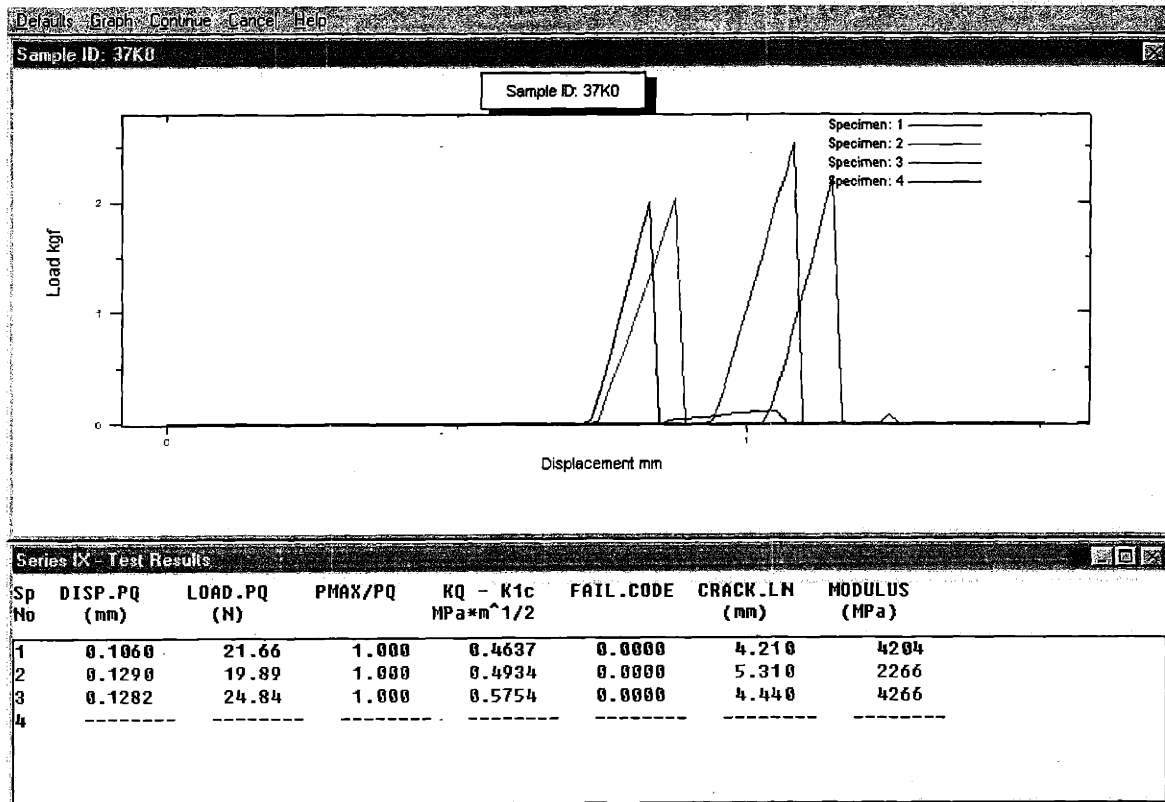


Figure A - 27 Fracture toughness test results of DP37 at 0°C.

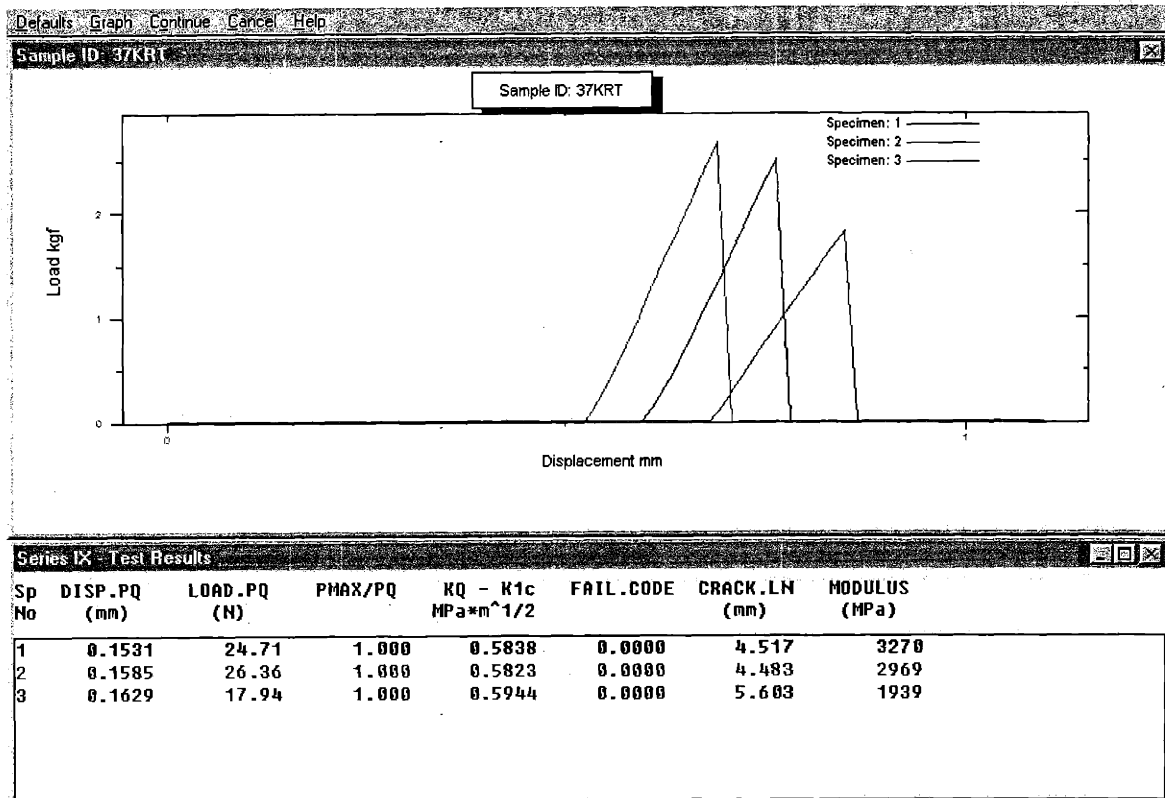


Figure A - 28 Fracture toughness test results of DP37 at 20°C.

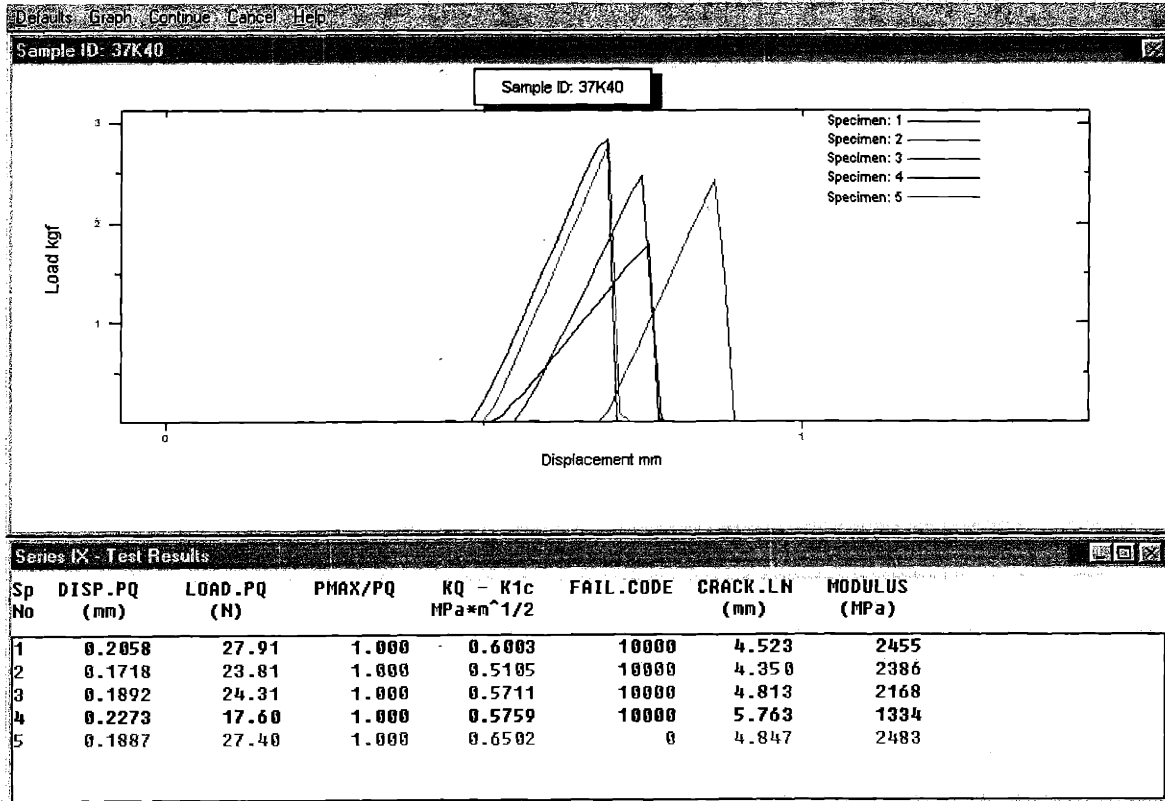


Figure A - 29 Fracture toughness test results of DP37 at 40°C.

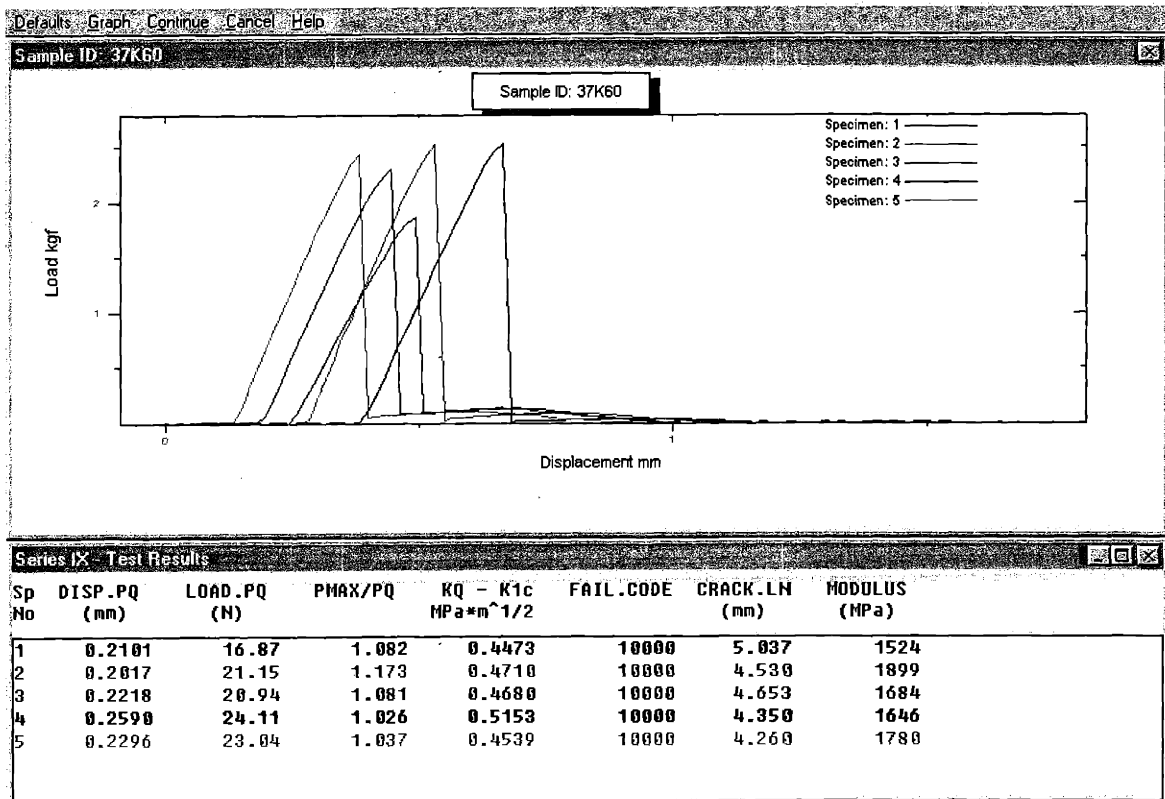


Figure A - 30 Fracture toughness test results of DP37 at 60°C.

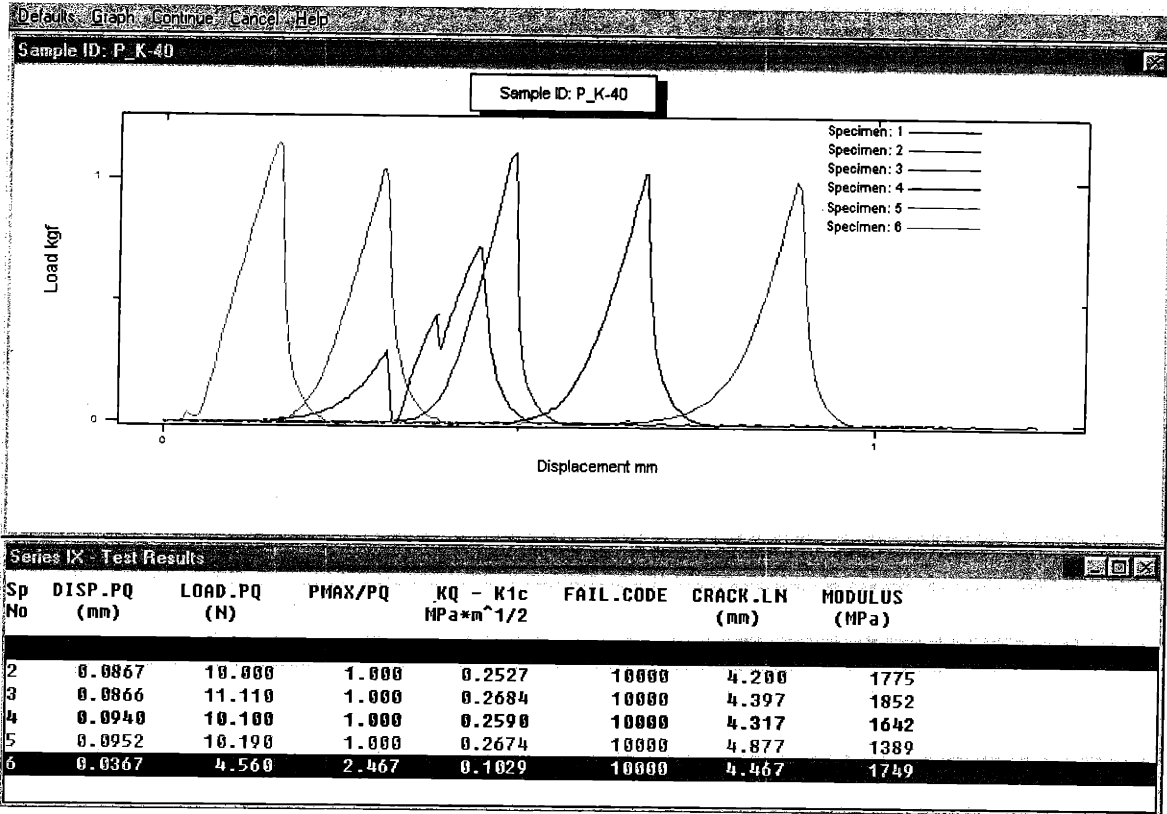


Figure A - 31 Fracture toughness test results of P100 at -40°C.

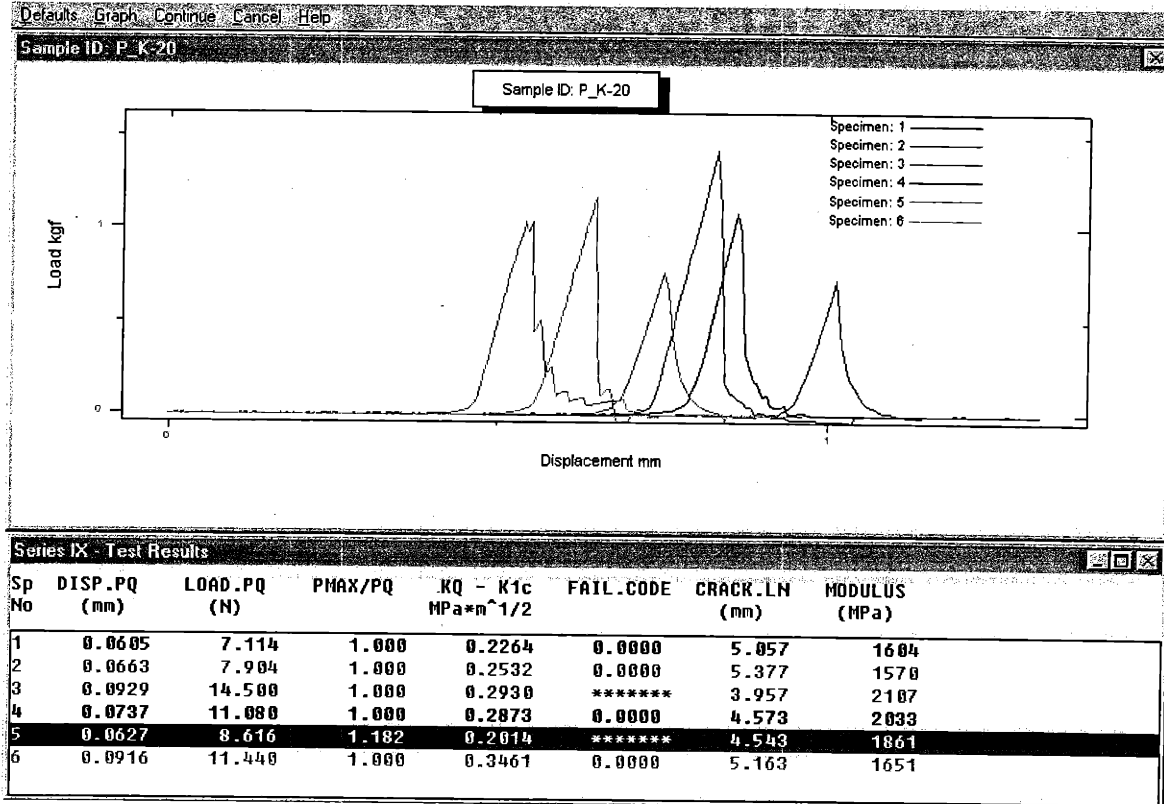


Figure A - 32 Fracture toughness test results of P100 at -20°C.

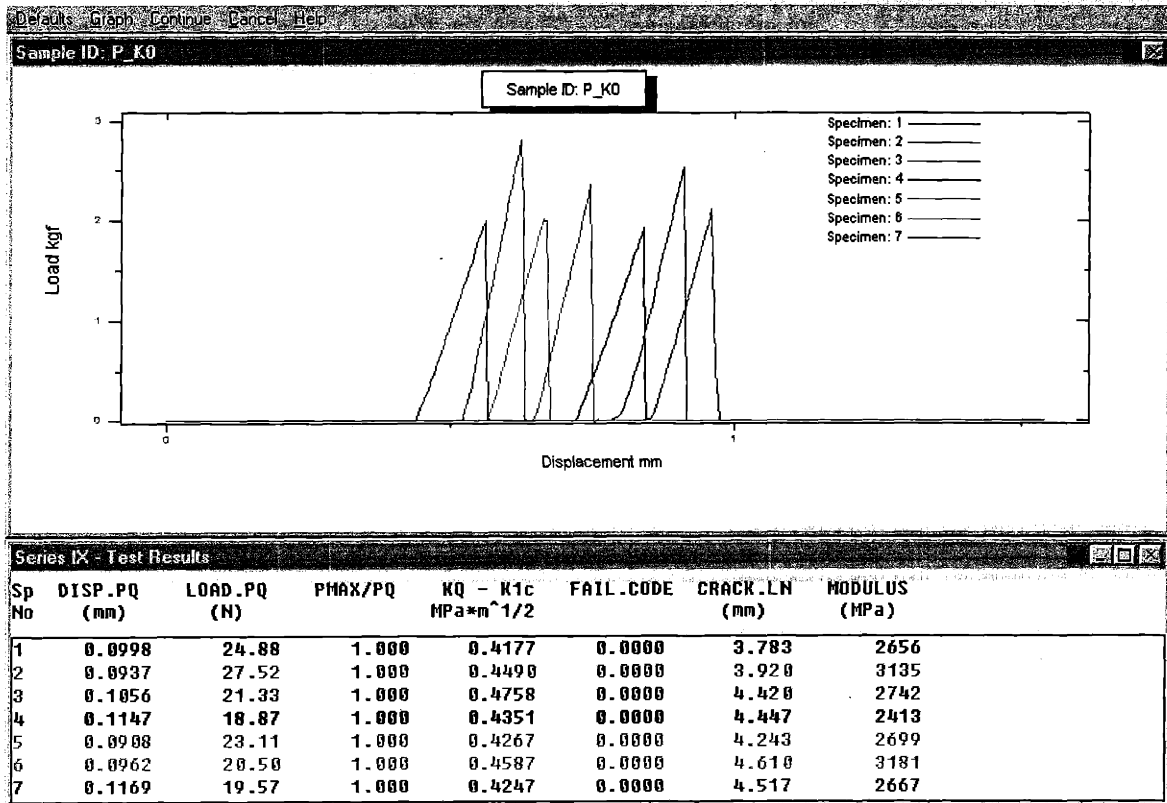


Figure A - 33 Fracture toughness test results of P100 at 0°C.

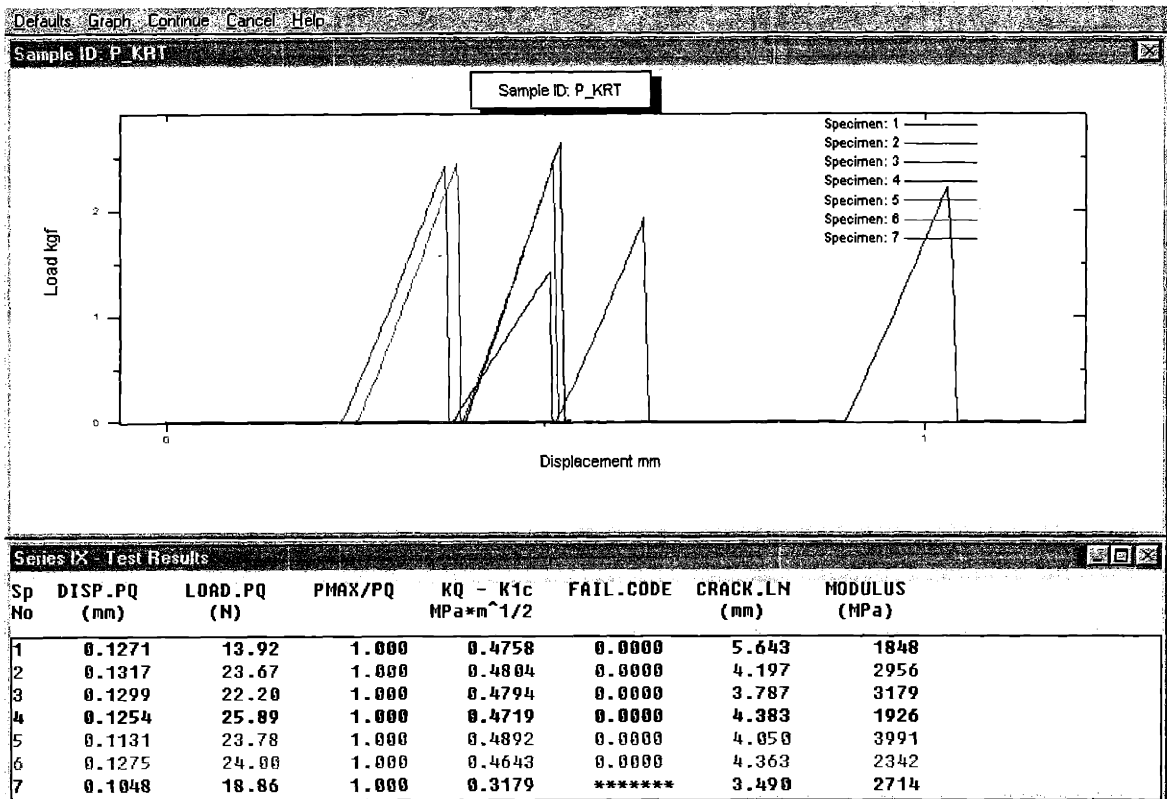


Figure A - 34 Fracture toughness test results of P100 at 20°C.

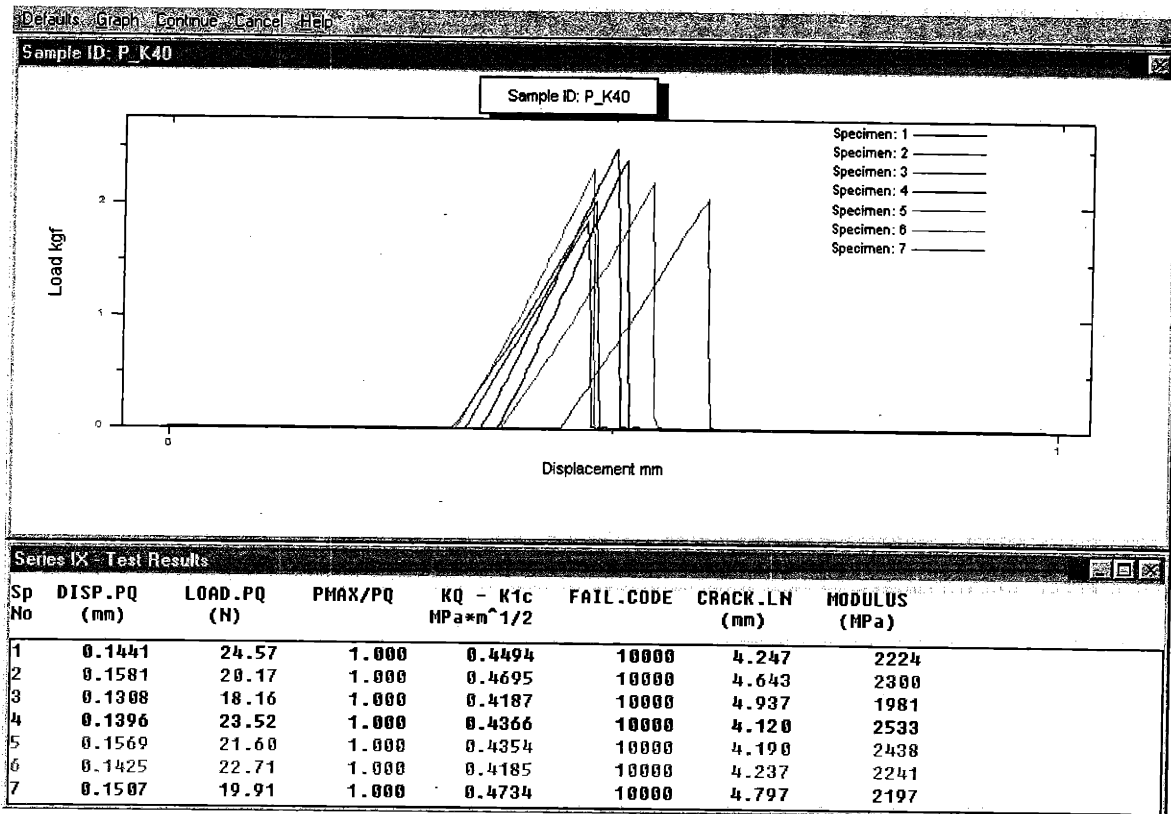


Figure A - 35 Fracture toughness test results of P100 at 40°C.

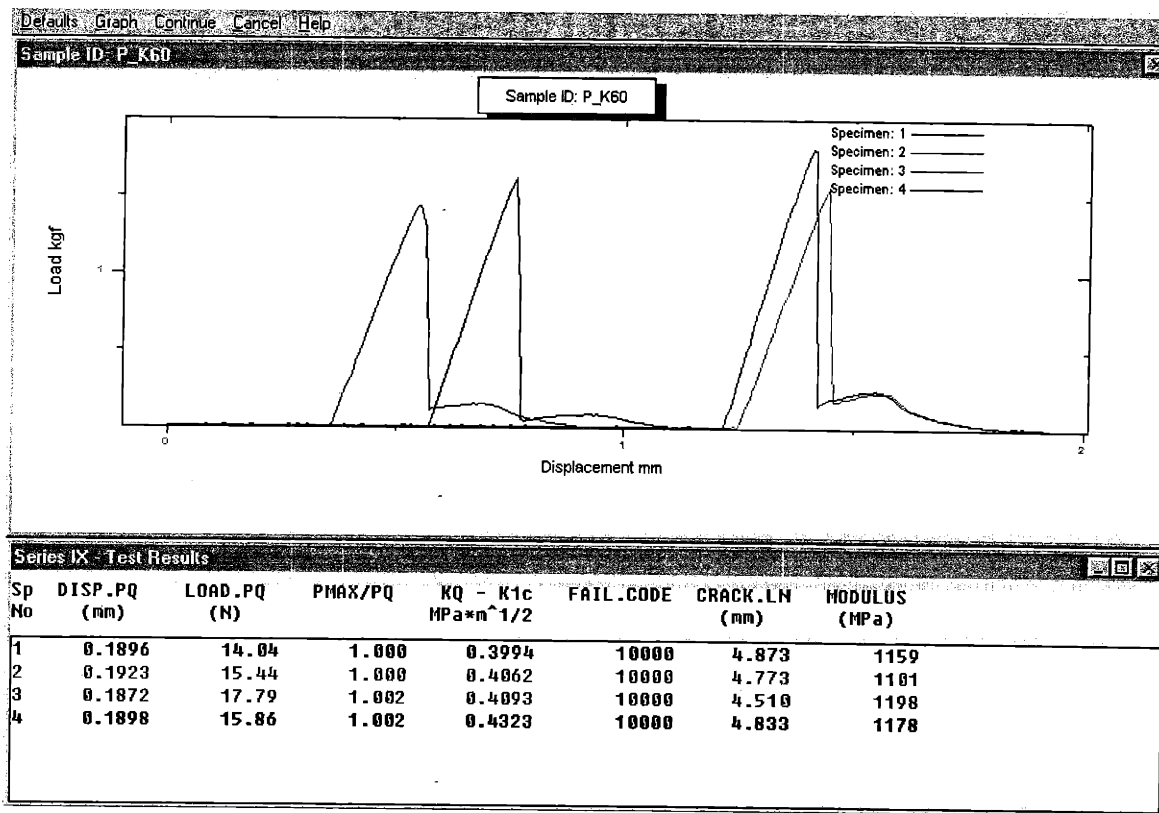


Figure A - 36 Fracture toughness test results of P100 at 60°C.

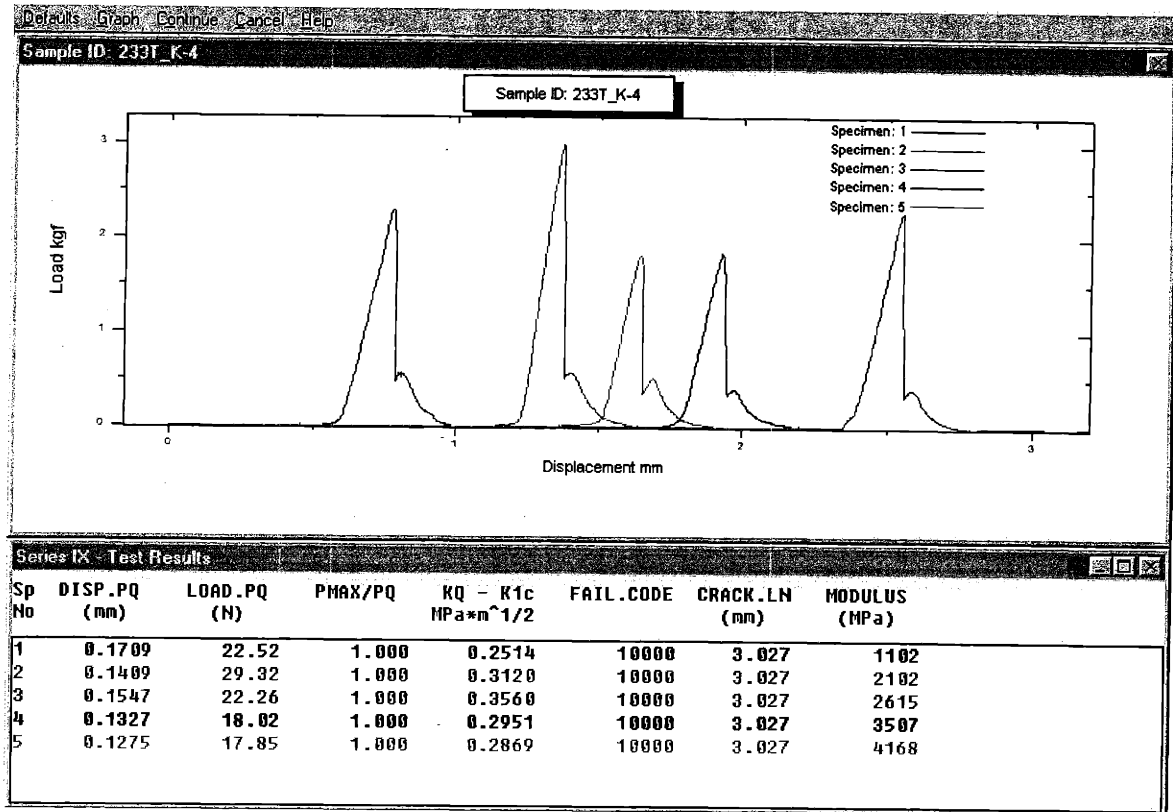


Figure A - 37 Fracture toughness test results of toughened 3136 (3136T) at -40°C.

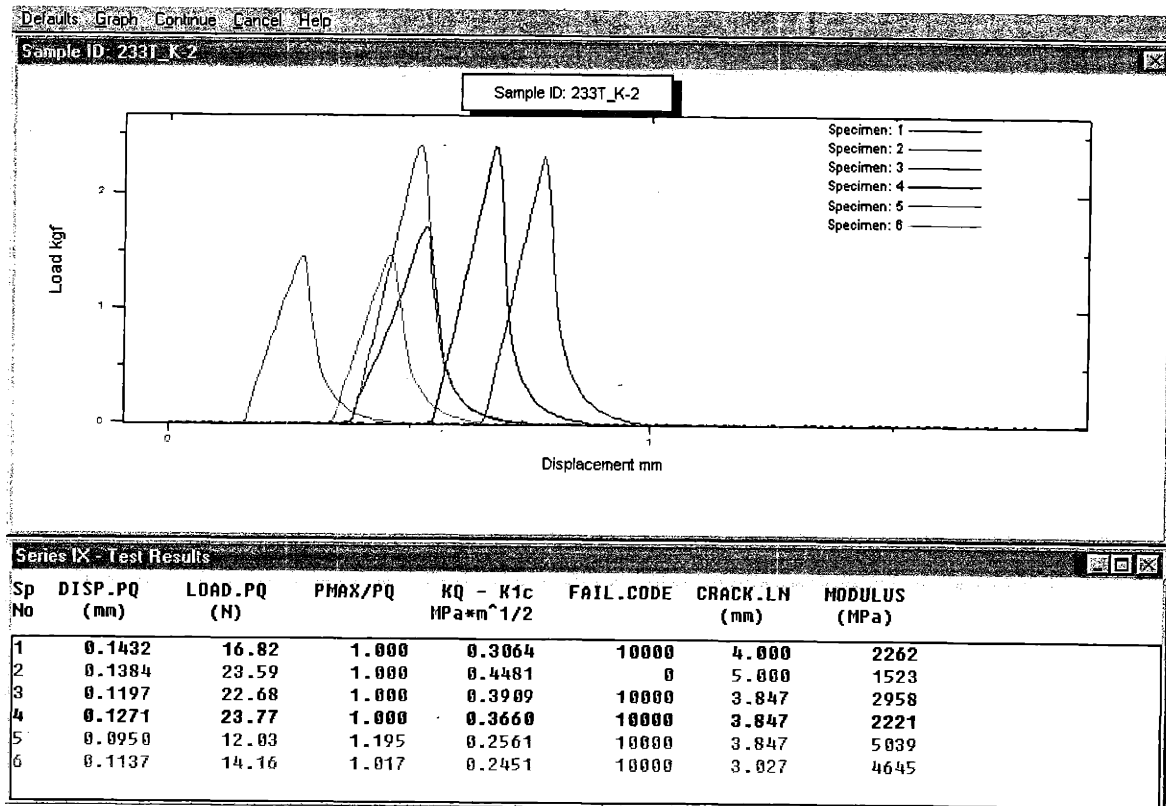


Figure A - 38 Fracture toughness test results of toughened 3136 (3136T) at -20°C.

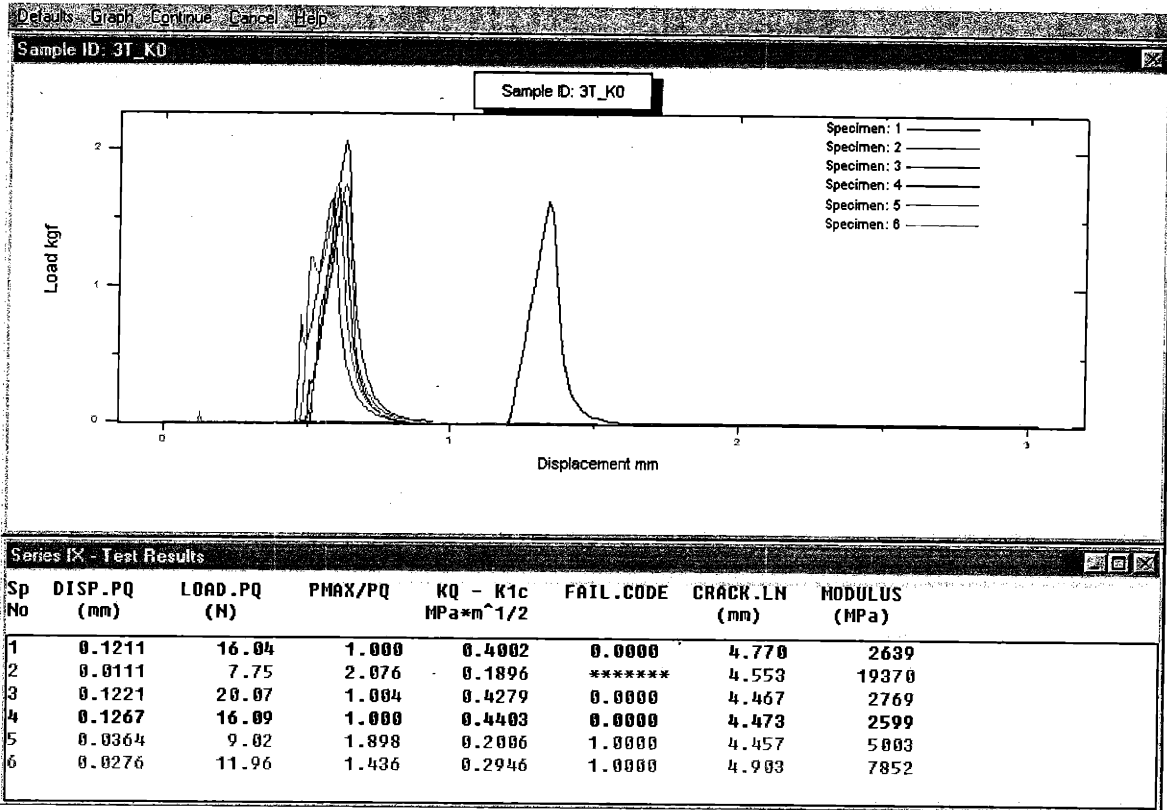


Figure A - 39 Fracture toughness test results of toughened 3136 (3136T) at 0°C.

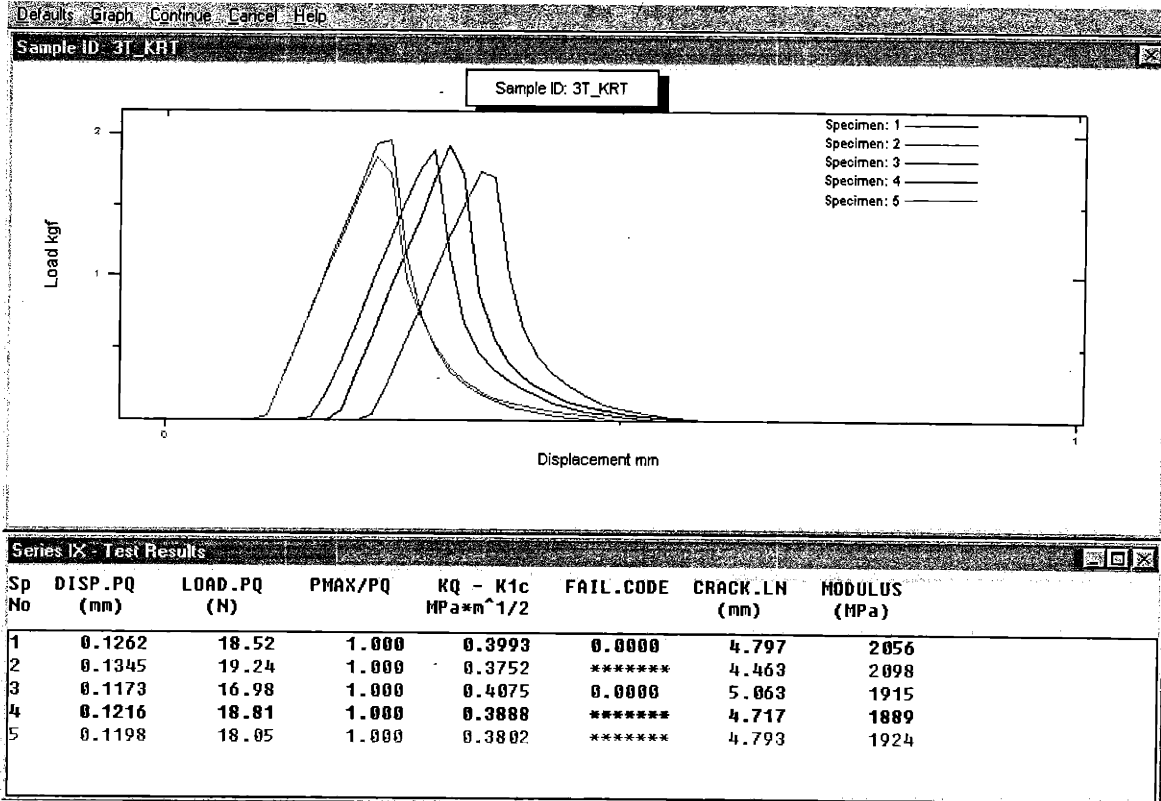


Figure A - 40 Fracture toughness test results of toughened 3136 (3136T) at 20°C.

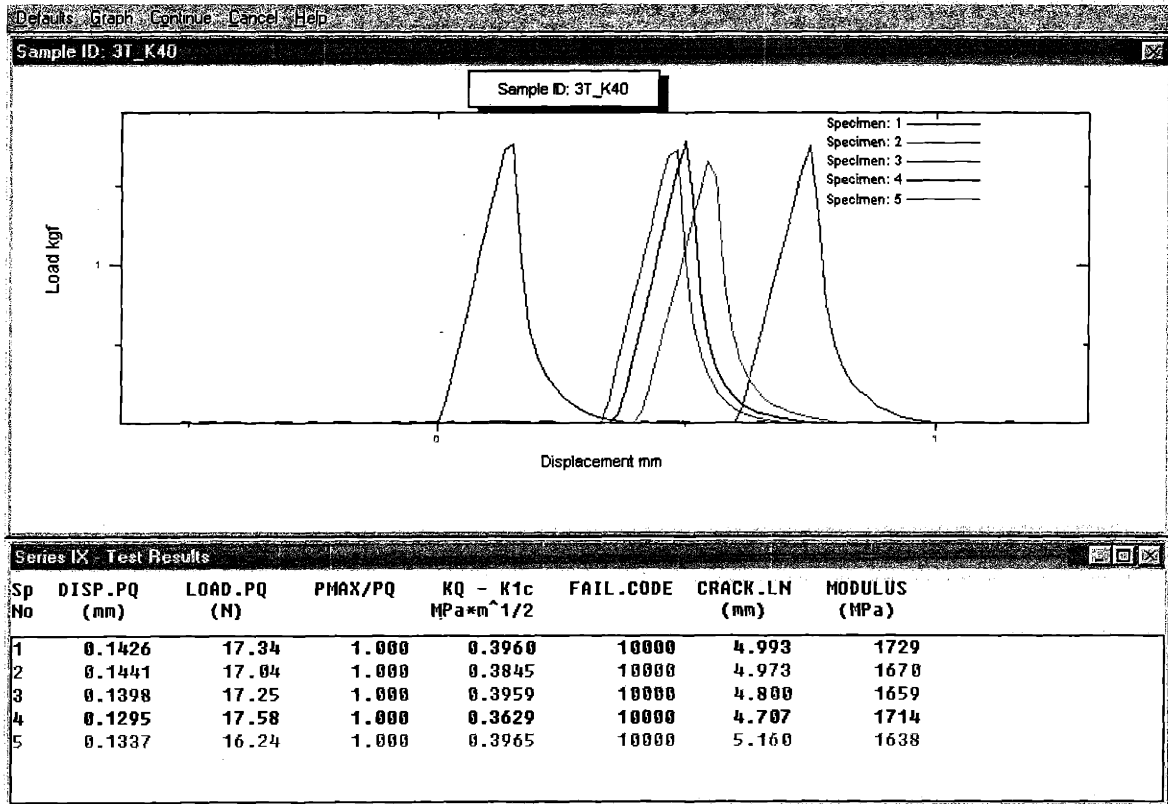


Figure A - 41 Fracture toughness test results of toughened 3136 (3136T) at 40°C.

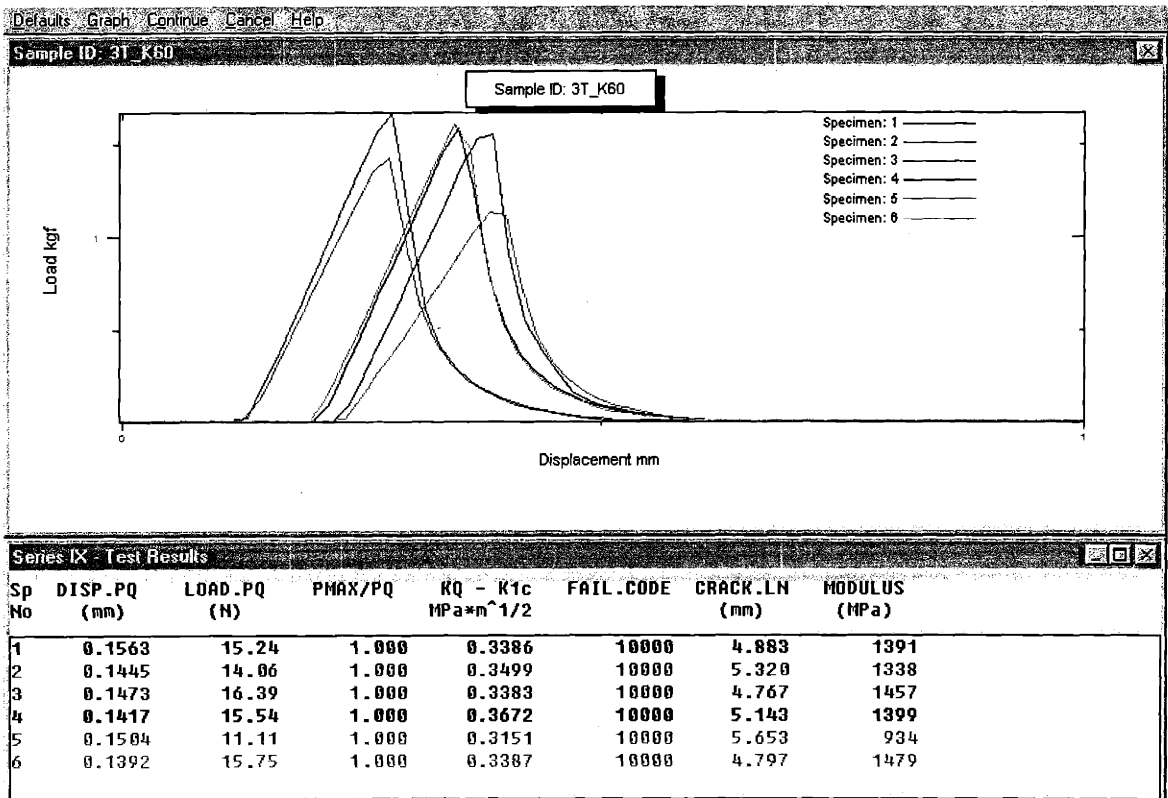


Figure A - 42 Fracture toughness test results of toughened 3136 (3136T) at 60°C.

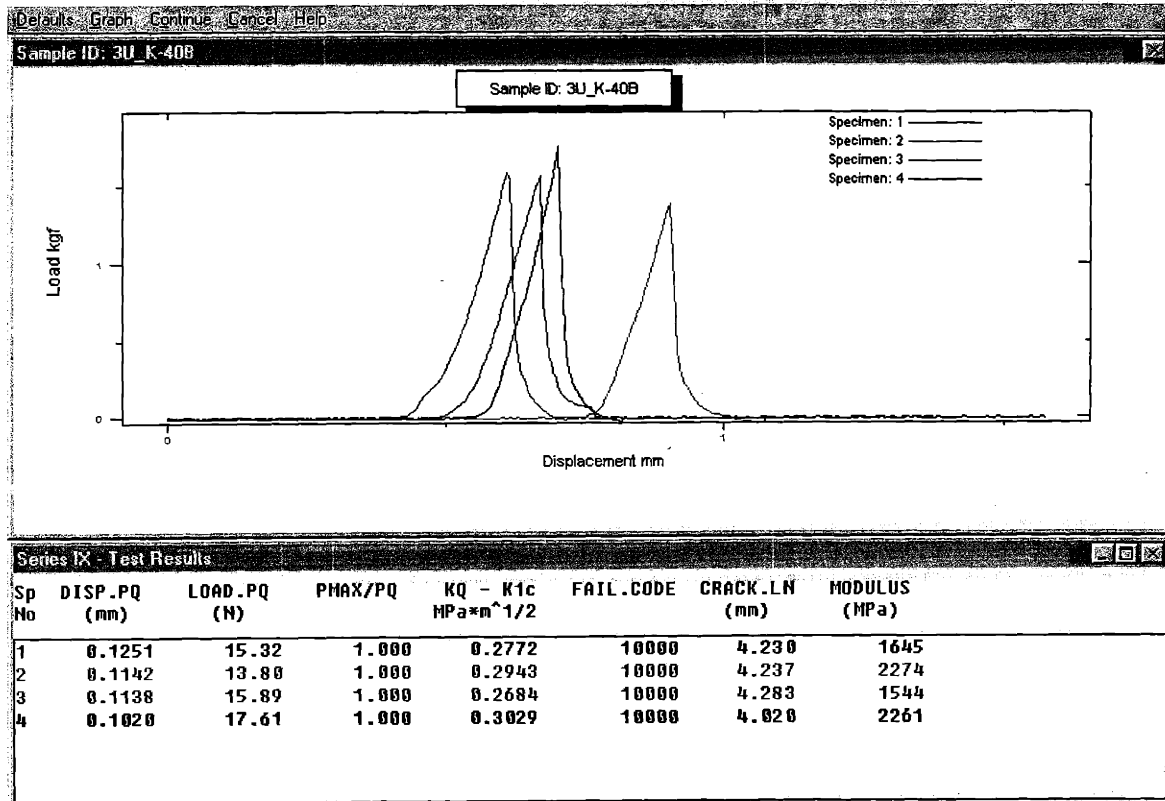


Figure A - 43 Fracture toughness test results of un-toughened 3136 (3136U) at -40°C.

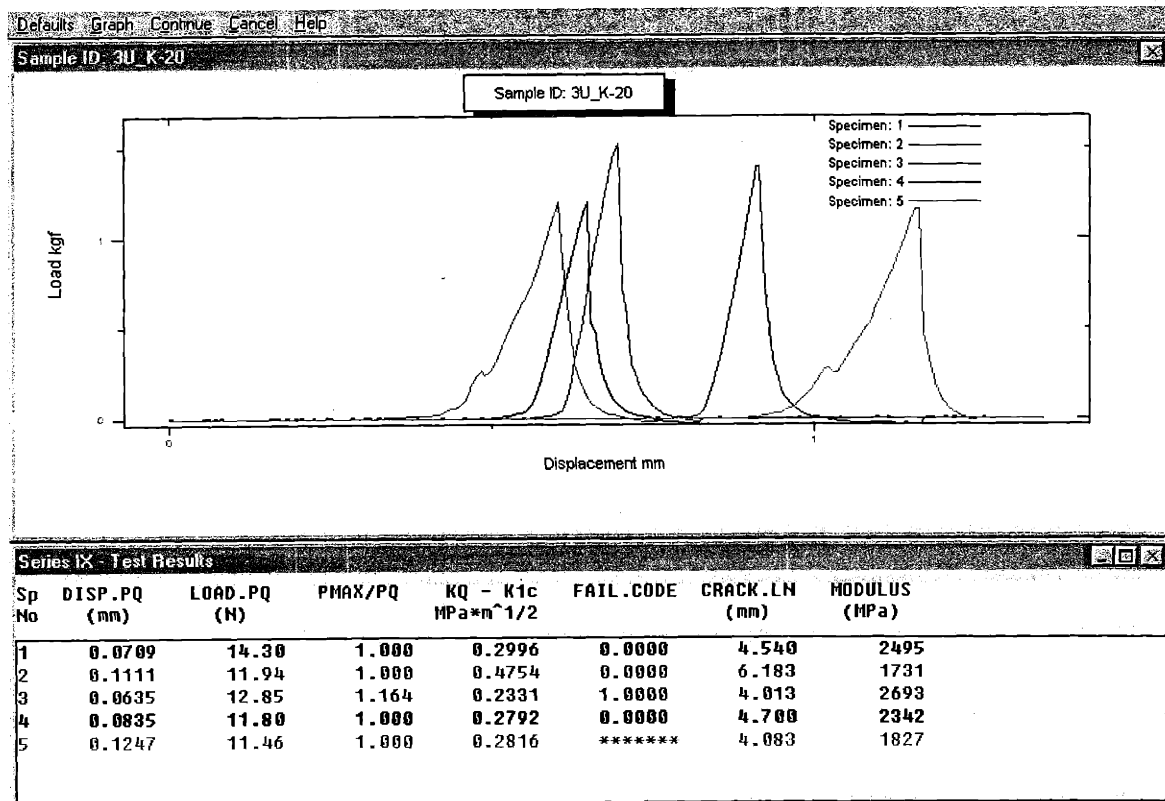


Figure A - 44 Fracture toughness test results of un-toughened 3136 (3136U) at -20°C.

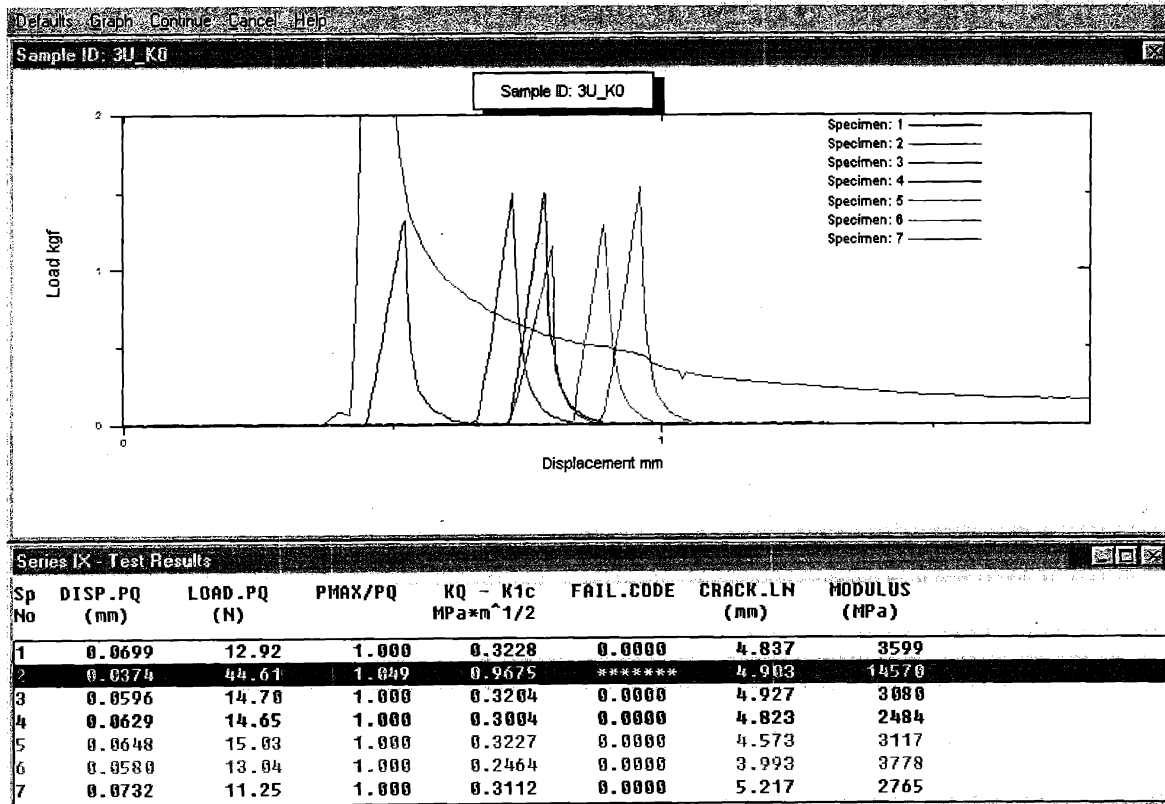


Figure A - 45 Fracture toughness test results of un-toughened 316 (3136U) at 0°C.

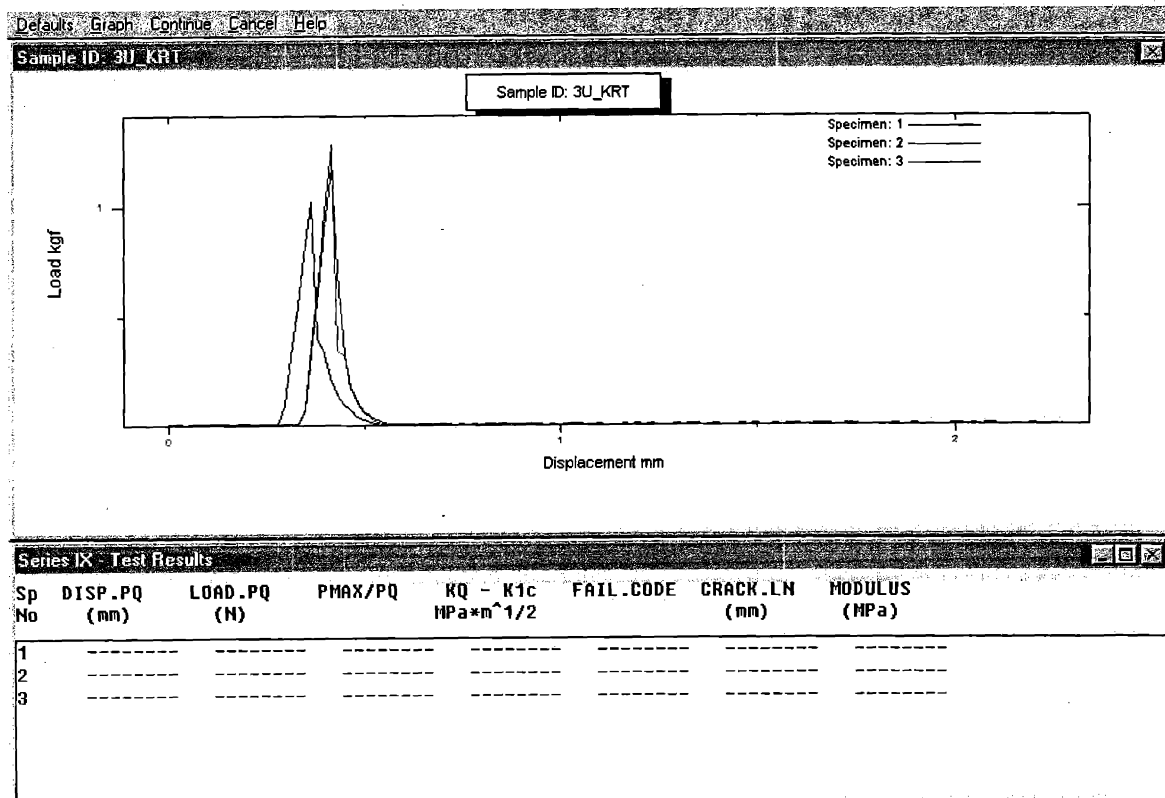


Figure A - 46 Fracture toughness test results of un-toughened 316 (3136U) at 20°C.

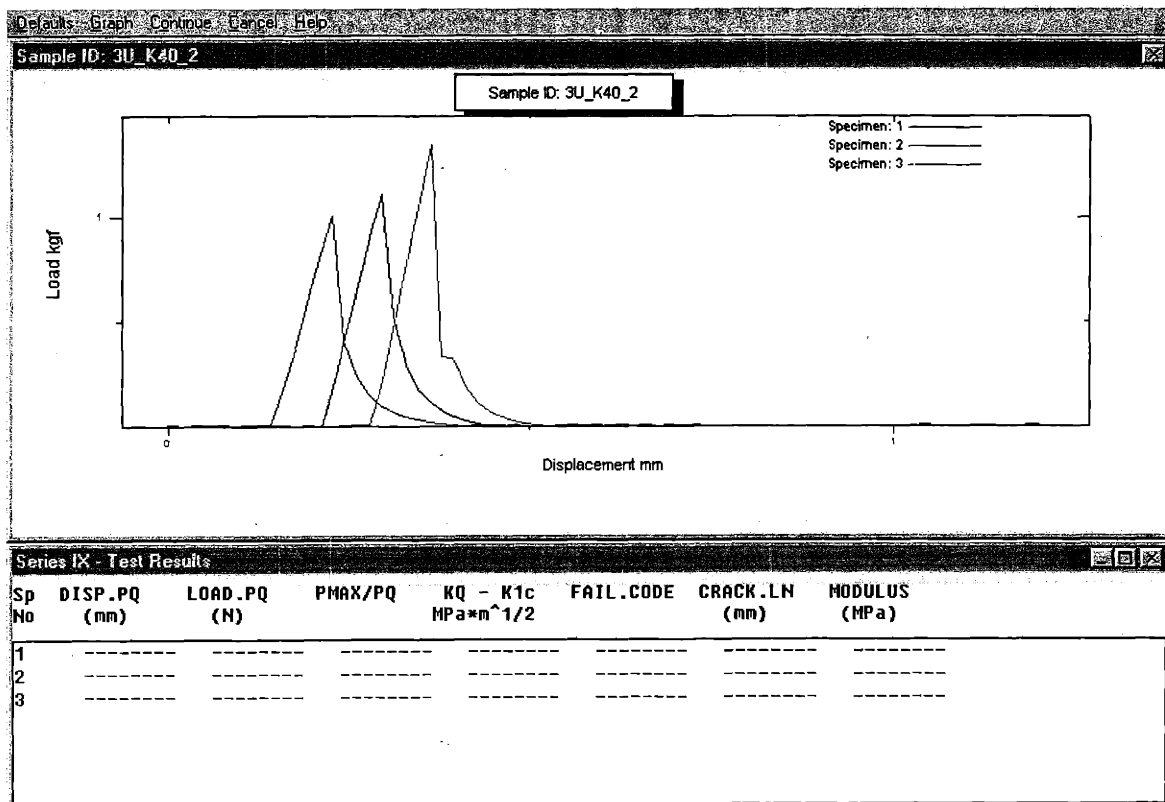


Figure A - 47 Fracture toughness test results of un-toughened 3136 (3136U) at 40°C.

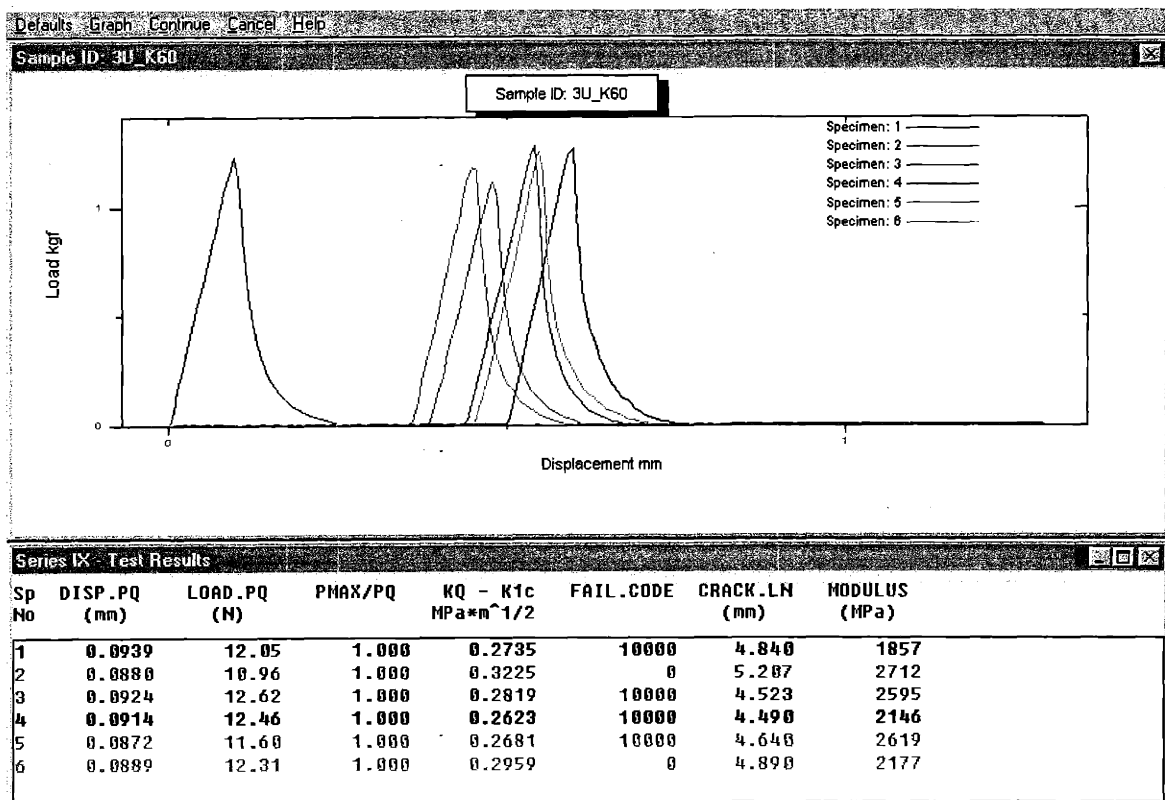


Figure A - 48 Fracture toughness test results of un-toughened 3136 (3136U) at 60°C.

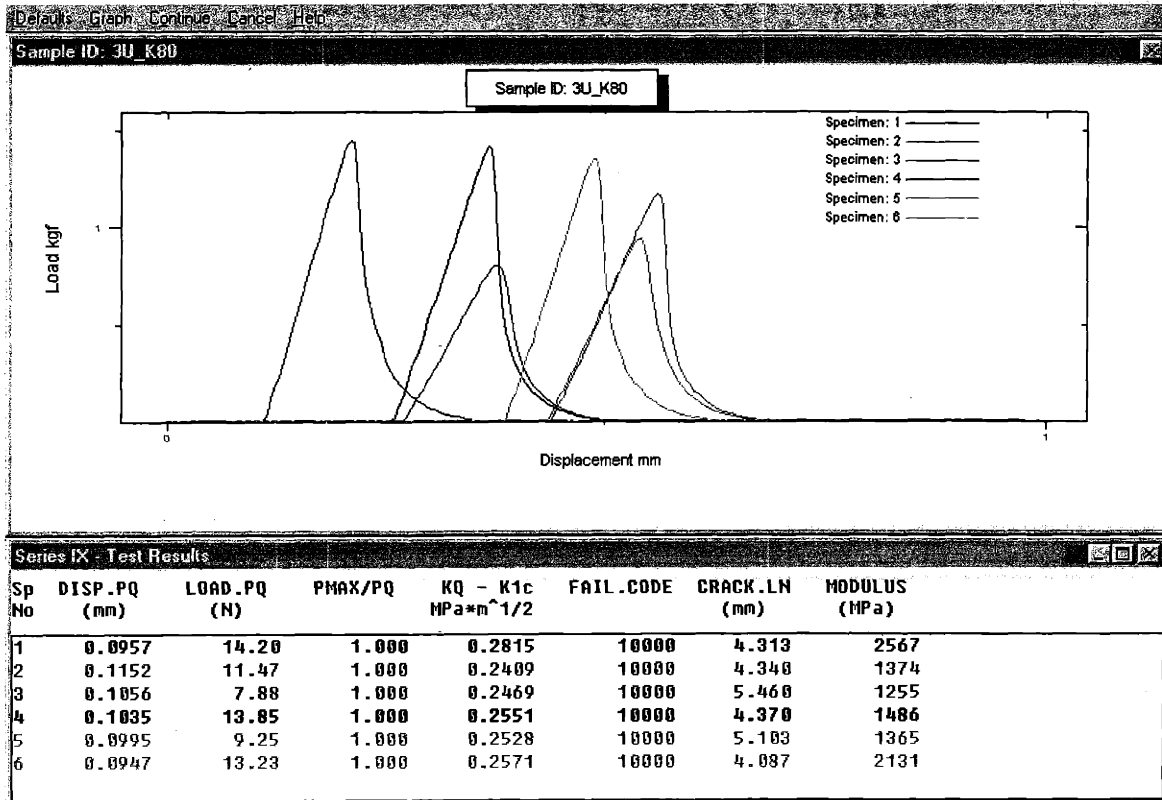


Figure A - 49 Fracture toughness test results of un-toughened 3136 (3136U) at 80°C.